INTERNATIONAL HELLENIC UNIVERSITY

Digital Fabrication of Patient Specific 3D-Printed Medical Models

Kontodina Theodora

SCHOOL OF ECONOMICS, BUSINESS ADMINISTRATION & LEGAL STUDIES
A thesis submitted for the degree of
Master of Science (MSc) in Strategic Product Design

March 2018
Thessaloniki – Greece

Student Name:	Theodora Kontodina
SID:	1106160014
Supervisor:	Dr. Dimitrios Tzetzis

I hereby declare that the work submitted is mine and that where I have made use of another's work, I have attributed the source(s) according to the Regulations set in the Student's Handbook.

March 2018
Thessaloniki - Greece

Abstract

This dissertation was written as part of the MSc in Strategic Product Design at the International Hellenic University.

Additive Manufacturing (AM) technology is currently being promoted as the spark of a new industrial revolution. The integration of 3D-printing technologies is gaining momentum into numerous emerging markets, including the medical industry. Particularly, AM technology enables the fabrication of physical parts by using initial data from medical images, such as Digital Imaging Communications in Medicine (DICOM) images. These parts can be used as customized implants or medical models, which precisely represent the patient's anatomy. The production of these models has the promising potential to affect the preoperative planning, education, and surgical simulation process, leading to various benefits regarding the surgical outcome.

The aim of the current study is to investigate the integration of AM technology in the fabrication of patient customized medical model from scanned anatomical images, acquired from Computed Tomography (CT) or Magnetic Resonance Imaging (MRI). In specific, after conducting a thorough literature review, the basic scope of this study is to demonstrate the process of the T4 vertebra (thoracic spine) production, by presenting the design, the manufacture, and the evaluation stage. With regard to the first stage, it is crucial to indicate the most appropriate open-source software program for the conversion of DICOM files to Standard Triangle Language (STL) files. After acquiring and optimizing the required medical data to the desired file format, the anatomical model is printed via Fused Deposition Modeling (FDM). Finally, the 3D-printed model is scanned via 3D-scanner and saved in STL file format, in order to measure and evaluate the results, regarding the dimensional declinations between the printed and the scanned model.

Keywords: DICOM, CT, MRI, STL, AM, RP, 3D-printing, FDM, 3D-scanning, medical models, T4 vertebra, thoracic spine

Theodora Kontodina

March 2018

Acknowledgements

It is a pleasure to acknowledge the pivotal importance of the assistance of several people in the preparation of this dissertation thesis.

I would first like to thank my thesis advisor Dr. Dimitrios Tzetzis, Academic Associate of School of Economics and Business Administration within the framework of the MSc in Strategic Product Design at International Hellenic University, for his prompting to investigate this specific field of 3D-printed medical models, which proved to be of great interest. He consistently steered me in the right direction by providing his productive advice, suggestions, and guidance for the production of this thesis.

Additionally, I would also like to acknowledge Manolis Tzimtzimis, member of the staff at International Hellenic University, responsible for the 3D-lab technical support. I appreciate his help and support, allowing me to experiment with the laboratory equipment. The door to the lab was always open for my research, facilitating the process of my survey.

I am also gratefully indebted to a great number of people, whom I would like to keep anonymous, respecting the medical confidentiality, for providing the DICOM files of their personal archive. Without their passionate participation and input, the survey could not have been successfully conducted.

Finally, I would like to express my very profound gratitude to my parents, my brother and ultimately my friends, especially Natalia, for providing me with unfailing support and continuous encouragement throughout my years of study and generally through the process of researching and finally writing this thesis. This accomplishment would not have been possible without them.

Table of Contents

Table of Illustrations

List of Figures

List of Tables

List of Graphs

List of Charts

1. Chapter One: Project Overview

1.1. Introduction

Additive Manufacturing (AM) technology is implemented in a number of applications concerning various scientific fields (Javaid *et al.*, 2017). In fact, the AM term is used to refer to a great diversity of technologies that are mainly utilized to fabricate physical models, prototypes, or functional components directly from three-dimensional (3D) Computer-Aided Design (CAD) data (Bibb *et al*., 2011). The AM process manufactures these physical objects by depositing successive layers of material on the top of each other (Bibb *et al*., 2011; Gibsion *et al.*, 2010). Especially, the most prominent technologies encompassed by the term AM are Three-Dimensional Printing (3D-Printing), Rapid Prototyping (RP) and Rapid Manufacturing (RM) (Bibb *et al*., 2011).

In the mid 1980's (Brennan, 2010), the initial use of AM mainly referred to the fabrication of conceptual and functional prototypes (Weller, 2015), which were used as inspection tools, aiming to reduce the production development steps of new parts and devices (Gibsion *et al.*, 2010; Santos, 2006). Although, since their invention AM technologies have been radically developed, providing a range of new processes, materials and applications (Brennan, 2010; Wang *et al.*, 2017). 3D-printing technology has penetrated into various fields, such as automotive, aerospace, architectural, fashion and more recently was introduced in medical industry (Chua *et al.*, 2017; Javaid *et al.*, 2017).

With reference to the medical filed, the increasing demand for quick fabrication of physical parts, like customized implants or medical models in case of pre-organizing an actual surgery, have conducted to the growth of these unconventional methods of manufacturing with regard to this specific field (Kumar *et al.*, 2017). Formerly, the analysis of the anatomy of a patient was based on two-dimensional (2D) data obtained by radiography and photography (Kumar *et al.*, 2017; Petzold *et al.*, 1999). Nowadays, due to technological improvements, we have to our disposition an arsenal of methods for acquiring 3D-images of better resolution, as being the identical replica of the anatomy of a patient (Gibson *et al.*, 2006; Kumar *et al.*, 2017). In particular, raw data acquired from the Computed Tomography (CT) and the Magnetic Resonance Imaging (MRI) is commonly reconstructed and stored as a Digital Imaging and Communication in Medicine (DICOM) file (Eijnatten *et al.*, 2018; Kumar *et al.*, 2017; Lim *et al.*, 2006). These images are supposed to be utilized as the main source for medical software's three-dimensional Computer Aided Design, in order to produce AM medical models (Eijnatten *et al.*, Kumar *et al.*, 2017; Lim *et al.*, 2006).

Furthermore, the production of patient customized physical models has the promising potential to affect the preoperative planning, education and surgical simulation process, leading to numerous advantages (Gibson *et al.*, 2006; Petzold *et al.*, 1999; Salmi *et al.*, 2013). More precisely, these benefits refer to the pre-planning of a surgery, which subsequently can lead to the reduction of the operating time, the predictability in the surgical outcome, the decreased level of risk to patient, the faster patient's recovery, the improved accuracy, no geometrical restrictions and ultimately better aesthetic and functional results (Brennan, 2010; Gibson *et al*., 2006; Huotilainen *et al.*, 2014; Petzold *et al.*, 1999; Salmi *et al*., 2013).

1.2. Project Aim

The aim of the current study is to acquire a profound understanding of the integration of Additive Manufacturing and Rapid Prototyping technologies in the fabrication of patient customized medical model from scanned anatomical images (DICOM), obtained with the help of Computed Tomography (CT) or Magnetic Resonance Imaging (MRI) scanning techniques. In particular, after conducting a thorough literature review, regarding the applications of produced medical models via Rapid Prototyping, the main objective of this study is to present the fabrication process of a real case scenario, namely the T4 vertebra of the thoracic spine of a patient, by demonstrating the three fundamental stages of this process: the design, the manufacture, and the evaluation stage. Moreover, regarding the first stage, it is essential to indicate the most appropriate open-source software program for the conversion of DICOM files to Standard Triangle Language (STL) files for the specific case study. For this purpose, four different open-source software programs (i.e. Seg3D, ImageVis3D, 3DSlicer, and ITK-SNAP) are selected to be demonstrated in a step-by-step approach. Consequently, after identifying the appropriate software solution for the current project, the required medical data is converted to the desired file format via ITK-SNAP software. Subsequently, the Meshmixer software program is utilized for the optimization of the STL file, in order to proceed to the fabrication of the medical model via 3D-printing technology. With reference to the second stage, Fused Deposition Modeling (FDM) technology is used, by utilizing the BCN3D Cura 1.0.3. software and the BCN3D Sigma R17 printer, for the creation and for the 3D-printing of the anatomical model. Finally, the 3D-printed model is scanned and edited via Next Engine 3D-scanner and ScanStudio HD software, respectively. The scanned model is saved in STL file format, in order to measure and evaluate the results, regarding the dimensional declinations between the printed and the scanned model. These measurements are conducted with the help of the Artec Studio 11 Professional software. Finally, the empirical results and findings of the research are discussed thoroughly.

1.3. Project Stages

- Literature research
- Identification of areas for further application
- Investigation and Research of available open-source software programs for the conversion of DICOM files from CT or MRI to STL files.
- Description of the basic functions of each software
    - *Seg3D Software*
    - *ImageVis3D Software*
    - *3DSlicer Software*
    - *ITK-SNAP Software*
- Identification and Selection of a specific medical case study
- Identification of the appropriate software solution
- Systematic approach of the case study

- *Design Stage*
  - Acquisition of DICOM files
  - Conversion of DICOM files to STL file format
  - Optimization of STL file
  - Acquisition of final STL file ready for RP machine
- *Manufacture Stage*
  - Creation of RP model
  - Printing of medical model via 3D-printing technology
- *Evaluation stage*
  - Scanning of the 3D-printed model via 3D-scanner
  - Measurement of the dimensions of the STL files
  - Comparison and Evaluation of the results

1.4. Structure of Thesis

With the intention of presenting the current thesis as clear, structured, and thereby, as effective as possible, the study is structured in the following manner:

The first chapter of the study provides the introduction to the general topic of the integration of Additive Manufacturing technologies in the fabrication of customized medical model of a patient from scanned anatomical images. Moreover, this chapter introduces the specific topic, by clarifying the aim, the stages and the structure of the project.

The second chapter introduces the review of the literature that comprises relevant information and theoretical issues regarding the specific field.

The third chapter describes the research methodology of the study, by presenting the steps and the analysis of the model used to approach the empirical work.

The fourth chapter comprises the results of the research in regard to the available software solutions, for the conversion of DICOM files to STL file format. Particularly, four different open-source software programs (i.e. Seg3D, ImageVis3D, 3DSlicer, and ITK-SNAP) are selected to be presented in a step-by-step approach, in order to evaluate the capabilities and the limitations of each software, and finally select the appropriate software solution for the current case study.

The fifth chapter demonstrates the process of digital fabrication of patient specific model, namely the T4 vertebra of the thoracic spine, in a step-by-step approach. More specifically, the process of fabrication is composed of three main stages: the design, the manufacture, and the evaluation stage. The first stage, is extended into four fundamental steps required for the acquisition of the desired STL file. These steps involve the acquisition of the DICOM files (via CT), the conversion of the DICOM files to STL file format (via ITK-SNAP software), the optimization of the STL file (via Meshmixer software) and finally the acquisition of the final STL file. In the second section, the manufacture stage of the final 3D-printed medical model is presented, demonstrating the required steps of the process. Hence, Fused Deposition Modeling (FDM) technology is used, by utilizing the BCN3D Cura 1.0.3. software and the BCN3D Sigma R17 printer, for the creation and the 3D-printing of the medical model, respectively. The third section, focuses on the evaluation stage. In this stage, the 3D-printed model is scanned (via Next Engine 3D-scanner), processed (via ScanStudio HD software) and saved in STL file format, in order to measure and evaluate the results (via Artec Studio 11 Professional software), regarding the dimensional declinations between the printed and the scanned model. The results of the measurements are quoted.

The sixth chapter includes the interpretation and the assessment of the results of the examined study.

The seventh chapter comprises the conclusion, the limitations of the study and the recommendations for further research.

2. Chapter Two: Literature Review

2.1. Introduction

Additive Manufacturing (AM) technology is currently being promoted as the spark of a new industrial revolution due to its huge potential in various scientific fields (Javaid *et al.*, 2017). The AM term is used to refer to a great diversity of technologies that are majorly used to construct physical models, prototypes, or functional components directly from three-dimensional (3D) Computer-Aided Design (CAD) data (Bibb *et al*., 2011). The AM process creates these physical objects by depositing consecutive thin layers of material, on top of one another, in a predetermined pattern (Bibb *et al*., 2011; Farooqi *et al.*, 2017; Gibsion *et al.*, 2010). The most prominent technologies encompassed by the term AM are Three-Dimensional (3D) Printing, Rapid Prototyping (RP) and Rapid Manufacturing (RM) (Bibb *et al*., 2011; Brennan, 2010; Owusu-Dompreh, 2013).

In the mid 1980's, the initial use of AM mainly referred to the fabrication of conceptual and functional prototypes (Brennan, 2010; Weller, 2015). In fact, these models were majorly used as inspection tools, aiming to reduce the production development steps of new parts and devices (Gibsion *et al.*, 2010; Santos, 2006). Nevertheless, in the current years the application of this technology is limitless. Actually, AM technologies, such as 3D-printing have been dramatically developed, providing various new processes, materials and applications of model fabrication in various sectors, including automotive, aerospace, architecture, fashion and more recently in medical industries (Brennan, 2010; Chua *et al.*, 2017; Wang *et al.*, 2017).

2.2. Additive Manufacturing Methods

Additive Manufacturing technology comprises a number of techniques, utilized for the fabrication of a physical part with the help of three-dimensional Computer-Aided-Design (Bibb *et al*., 2011; Hnatkova *et al.*, 2014). The majority of these techniques, regardless of applying different methods to add the material, are based on the same principle of AM layer-by-layer (Brennan, 2010; Hnatkova *et al.*, 2014; Jardini *et al.*, 2014; Javaid *et al.*, 2017; Owusu-Dompreh, 2013; Marro *et al.*, 2016).

In specific, the most fundamental AP technologies are the following: Stereo-lithography (SLA), Selective Laser Sintering (SLS), Direct Metal Laser Sintering (DMLS), Selective Laser Melting (SLM), Fused Deposition Modeling (FDM), 3D-printing (3DP) or Multi-Jet Modeling (MJM) and Electron Beam Melting (EBM), classified in accordance with the initial condition state of the material (i.e. solid, liquid or powder) (Brennan, 2010; Hnatkova *et al.*, 2014; Jardini *et al.*, 2014; Javaid *et al.*, 2017; Owusu-Dompreh, 2013; Marro *et al.*, 2016; Petzold *et al.*, 1999; Salmi *et al.*, 2013). Although, the most common used methods for medical purposes are SLA, FDM, SLS and MJM (Brennan, 2010; Hnatkova *et al.*, 2014; Owusu-Dompreh, 2013; Marro *et al.*, 2016), analysed in more detail in the following sections (Sections 2.2.1.-2.2.4.).

2.2.1. Sterolithography (SLA)

Stereolithography is considered as the first 3D-printing technology, date from the early 1980's (Brennan, 2010; Hnatkova *et al.*, 2014; Marro *et al.*, 2016). SLA generates a 3D-model by consecutively adding layers of photosensitive resin materials on the top of one another (Brennan, 2010; Hnatkova *et al.*, 2014; Marro *et al.*, 2016).

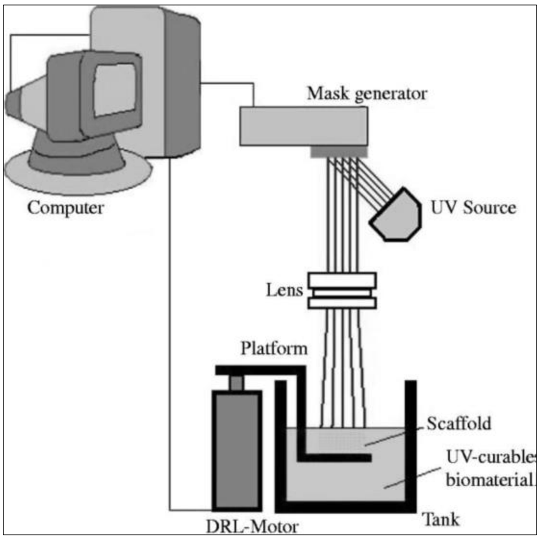

Figure 1: The principle of Stereolithography, Source: (Hnatkova *et al.*, 2014)

Subsequently, these layers are cured by ultraviolet laser (UV), as illustrated in the figure above (Figure 1) (Brennan, 2010; Hnatkova *et al.*, 2014; Marro *et al.*, 2016). The successive cross-sections, traced out be the UV laser, are submerged in a container of liquid of photoreactive polymer at specific high (Brennan, 2010; Hnatkova *et al.*, 2014;

Marro *et al.*, 2016). As the laser passes over the layer, the polymer solidifies, then the platform is lowered according to a defined distance, and afterwards a new liquid layer is added on the top of the polymerized layer (Brennan, 2010; Hnatkova *et al.*, 2014; Marro *et al.*, 2016). Thereby this process is repeated several times, until the final model is complete (Brennan, 2010; Hnatkova *et al.*, 2014; Marro *et al.*, 2016).

SLA provides a good combination of advantages, including speed, accuracy, good resolution and smooth surface finish in the created models (Brennan, 2010; Hnatkova *et al.*, 2014; Marro *et al.*, 2016). However, the main inconvenience is the limited suite of provided materials, restricted to resins (Brennan, 2010; Hnatkova *et al.*, 2014; Marro *et al.*, 2016).

2.2.2. Selective Laser Sintering (SLS)

Selective Laser Sintering is an AM technique that utilizes a high-power CO_2 laser beam to trace and subsequently fuse (or sinter) small particles of a powder material into a mass, representing the desired 3D-model (Brennan, 2010; Hnatkova *et al.*, 2014; Marro *et al.*, 2016). As presented in the following figure (Figure 2), the laser beam traces and fuses the cross-sections of the 3D-model on the surface of a platform (Brennan, 2010; Hnatkova *et al.*, 2014; Marro *et al.*, 2016). As the parts of the 3D-model are created upon the platform, the latter is lowered by one-layer thickness, and subsequently additional powder layers are deposited on the top. This process is repeated until the component is complete (Brennan, 2010; Hnatkova *et al.*, 2014; Marro *et al.*, 2016).

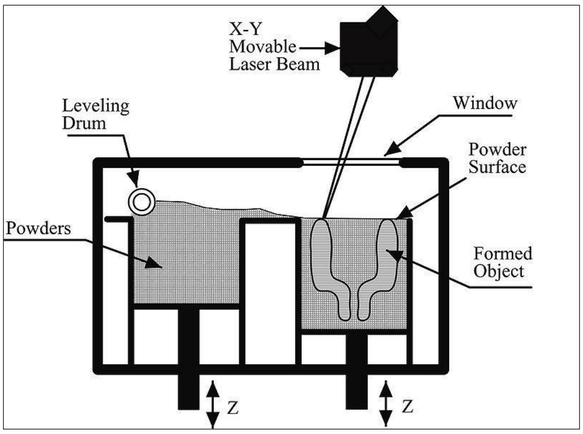

Figure 2: The principle of Selective Laser Sintering, Source: (Hnatkova *et al.*, 2014)

The main competitive superiority of SLS process is that it does not require support material during the fabrication process, as the unfused powder acts like a support material (Brennan, 2010; Hnatkova *et al.*, 2014; Marro *et al.*, 2016). This method can be utilized for the 3D-model fabrication, using a great variety of materials, including polymer, metal and ceramic (Brennan, 2010; Hnatkova *et al.*, 2014; Marro *et al.*, 2016). Though, the main drawback of this technique is the high cost and the abrasive surface of the formed models due to the sintering, requiring usually more post-processing for the smoothing of the rough surface finishes (Brennan, 2010; Hnatkova *et al.*, 2014; Marro *et al.*, 2016).

2.2.3. Fused Deposition Modeling (FDM)

Fused Deposition Modeling is an RP process using a filament of thermoplastic polymer extruded through a nozzle that forms the geometry of the part layer-by-layer (Brennan, 2010; Hnatkova *et al.*, 2014; Marro *et al.*, 2016), as demonstrated in the next figure (Figure 3). The semi-liquid material cools and hardens after being deposited in very fine layers (Brennan, 2010; Hnatkova *et al.*, 2014; Marro *et al.*, 2016). Once a layer is built, the build platform lowers, and the nozzle deposits another layer (Brennan, 2010; Hnatkova *et al.*, 2014; Marro *et al.*, 2016). This process is repeated over and over, until the final model is finished (Brennan, 2010; Hnatkova *et al.*, 2014; Marro *et al.*, 2016). A variety of materials are available, including polyester, acrylonitrile butadiene styrene (ABS), elastomers and investment casting wax (Brennan, 2010; Hnatkova *et al.*, 2014).

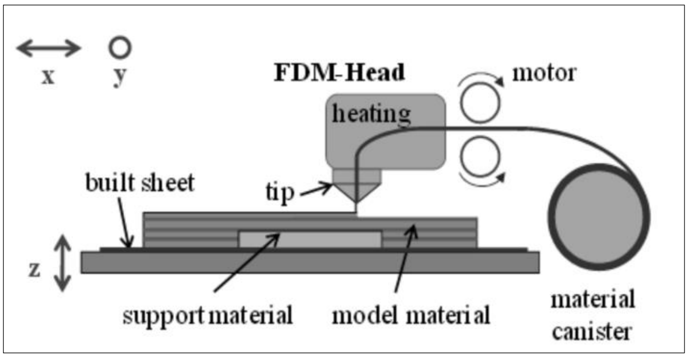

Figure 3: The principle of Fused Deposition Modeling, Source: (Hnatkova *et al.*, 2014)

FDM method is considered as an economical AM process, attributable to the inexpensive available materials (Brennan, 2010; Hnatkova *et al.*, 2014; Marro *et al.*, 2016).

The main drawbacks of FDM process are the low speed of the building time, and the low-quality level in the details of the created surfaces, in comparison with Stereolithography (Brennan, 2010; Hnatkova *et al.*, 2014; Marro *et al.*, 2016). Moreover, sometimes the created models require more post-processing in order to smooth the rough surface finishes and remove the supporting material (Brennan, 2010; Hnatkova *et al.*, 2014; Marro *et al.*, 2016).

2.2.4. Multi-Jet Modeling (MJM)

Multi-Jet Modeling or 3D-printing technology, works in similar manner with SLS method (Hnatkova *et al.*, 2014; Marro *et al.*, 2016). Though, instead of utilizing laser for the material sintering, MJM method uses an ink-jet printing head with many holes (Brennan, 2010; Hnatkova *et al.*, 2014; Marro *et al.*, 2016). This head deposits molten thermoplastic material onto a build plate, by creating one layer of the part (Brennan, 2010; Hnatkova *et al.*, 2014). After a layer is built, the platform is lowered and a new layer of material is added consecutively to the previous one (Brennan, 2010; Marro *et al.*, 2016). The process is repeated until the final model is created (Hnatkova *et al.*, 2014; Marro *et al.*, 2016). The process of MJM is illustrated in the following figure (Figure 4).

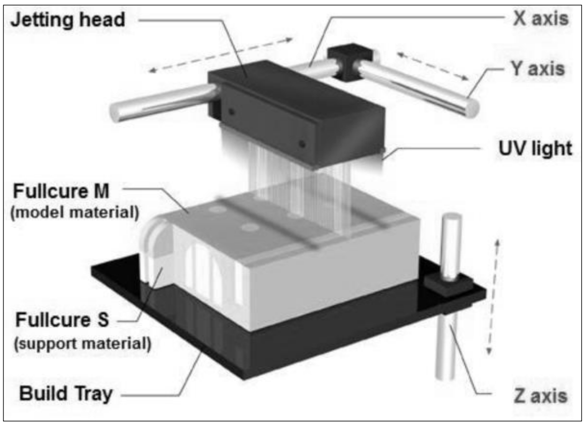

Figure 4: The principle of Multi-Jet Modeling (MJM), Source: (Hnatkova *et al.*, 2014)

Multi-Jet Modeling process provides a good combination of speed, low-cost and lack of supporting material (Brennan, 2010; Hnatkova *et al.*, 2014; Marro *et al.*, 2016). Nevertheless, the main disadvantage is the negligible mechanical properties and the low resolution of the created model (Brennan, 2010; Hnatkova *et al.*, 2014; Marro *et al.*, 2016).

2.3. Additive Manufacturing – Rapid Prototyping in Medical Field

As mentioned previously, the Additive Manufacturing technology is gaining momentum in the various scientific fields, including its penetration into the medical sector (Pucci *et al.*, 2017). In fact, the increasing demand for customized patient care has contributed to the intense use of AM technologies, providing the possibility of quick fabrication of physical parts, like customized implants or medical models (Eijnatten *et al.*, 2018; Giannatsis *et al.*, 2009; Javaid *et al.*, 2017; Kumar *et al.*, 2017; Marro *et al.*, 2016).

These medical models (mentioned as stereomodels (Cheung *et al.*, 2018; Gibson *et al.*, 2006) or biomodels (D'Urso *et al.*, 1999; Gibson *et al.*, 2006)), obtained from individual patient data, are a three-dimensional representation of the patient's anatomy, illustrating not only the bone structure, but additionally vascular structures, soft tissues, implants, foreign bodies etc. (Gibson *et al.*, 2006).

In earlier times, the fabrication of anatomical models was quite demanding and laborious process, due to the complexity of the anatomical and the geometry of the structure (Brennan, 2010; Hnatkova *et al.*, 2014). Prior to AM development, medical models were produced mainly by the use of conventional processes, such as pressing, forging, machining and casting, which proved to be time-consuming and cost a large amount of money (Hnatkova *et al.*, 2014).

Nowadays, AM plays a significant role in the production of patient customized physical models (Gibson *et al*., 2006; Hnatkova *et al.*, 2014; Javaid *et al.*, 2017). In the coming years, these medical models, optimized in design, have the promising potential to affect the preoperative planning, education and surgical simulation process, providing various benefits regarding the surgical outcome (Gibson *et al*., 2006; Hnatkova *et al.*, 2014; Javaid *et al.*, 2017; Petzold *et al.*, 1999; Salmi *et al*., 2013).

In fact, advances in biomodelling have given raise to totally additional treatment approaches and opportunities for cases regarding the preoperative planning, diagnosis of diseases, surgical simulation and medical device prototyping, aiming to restore and reconstruct the patient anatomy to its initial state after it has endured a physical trauma, disease or genetic defect (Brennan, 2010; Giannatsis *et al.*, 2009; Javaid *et al.*, 2017).

2.4. Research Status of Applications of Additive Manufacturing in Medical Field

Additive Manufacturing is one of the fastest growing markets worldwide (Weller *et al.*, 2015). Actually, the worldwide revenues of 3D-printing industry grew by 17.4% in 2016 and worth over $6 billion (Wang *et al.*, 2017). The main reason of the success of AM technologies is the combination of geometric flexibility, low-cost production, high-speed and accuracy (Giannatsis *et al.*, 2009), leading additionally to the rapid growth of the applications regarding the medical field.

Furthermore, a great number of researchers and scientists investigated the integration of AM technologies in medicine and healthcare sector, by launching various research programs (e.g. Phidias – European Commission (EC) Funded Network Project on Rapid Prototyping in Medicine) with respect to this scientific field (Brennan, 2010; Giannatsis *et al.*, 2009).

According to latest research data (Javaid *et al.*, 2017), the publications of articles regarding the applications of Additive Manufacturing technologies in medical field have been dramatically increased the last decade. Moreover, the total number of the research articles and papers in this sector are 428 from 2004 to 2016 (Javaid *et al.*, 2017). The following graph (Graph 1) presents the number of published articles in relation to the year (Javaid *et al.*, 2017).

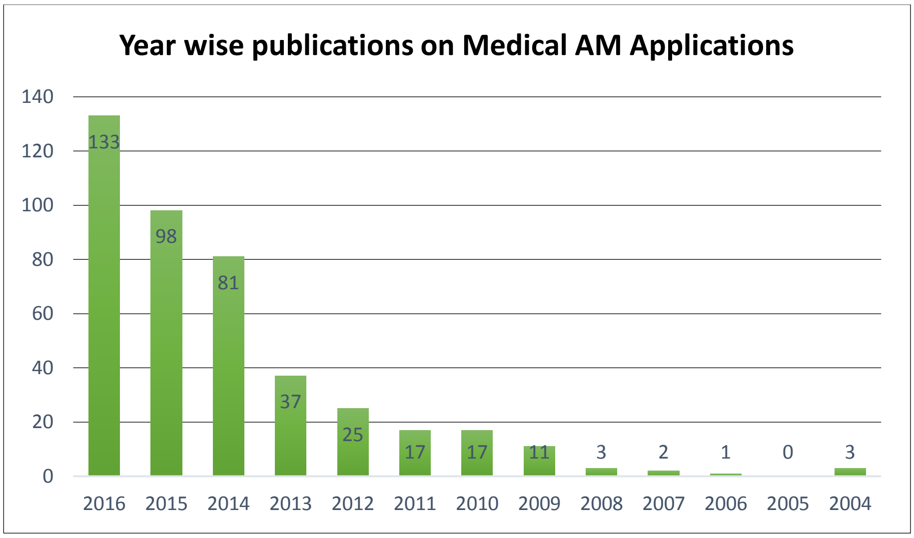

Graph 1: Year wise list of publications in journals regarding the medical applications of Additive Manufacturing, Source: (Javaid *et al.*, 2017)

The next graph (Graph 2) demonstrates the top five journals with the highest publications on AM medical applications (Javaid *et al.*, 2017). In particular, Rapid Prototyping Journal is in the first position.

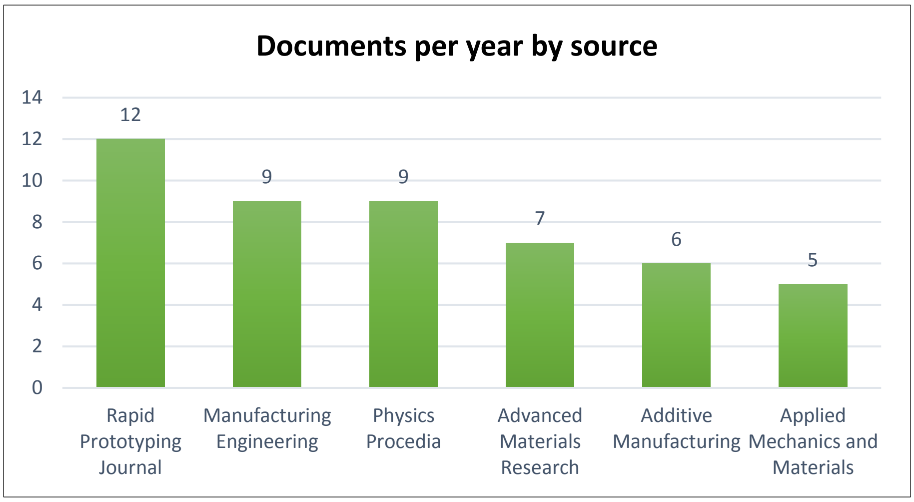

Graph 2: Top five journals of published papers regarding the medical applications of Additive Manufacturing, Source: (Javaid *et al.*, 2017)

The next graph (Graph 3) presents the area wise contribution on AM applications (Javaid *et al.*, 2017). In particular, Engineering and Materials are in the first position, presenting the 56% of the AM applications (Javaid *et al.*, 2017). While, Medicine, Dentistry and Biotechnology have significant contribution in this AM field, presenting the third highest percentage of 17% (Javaid *et al.*, 2017). Basic Science and Computer Science present 21% and Other Fields present 6% (Javaid *et al.*, 2017).

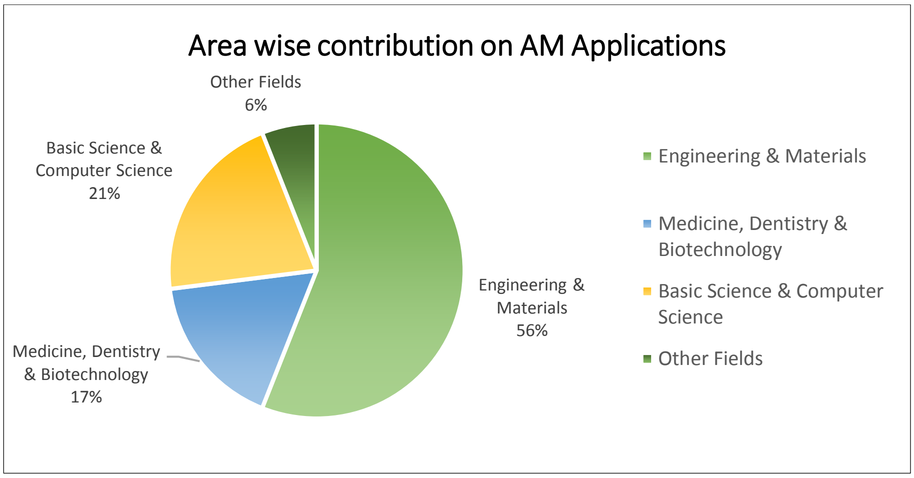

Graph 3: Area wise contribution on Additive Manufacturing applications, Source: (Javaid *et al.*, 2017)

2.5. Applications of Additive Manufacturing in Medical Field

As presented in the previous section (Section 2.4.), the number of applications in medical field, regarding the Additive Manufacturing technologies, has been radically increased (Javaid *et al.*, 2017; Marro *et al.*, 2016). Actually, AM applications in medical sector can be classified into the following major categories (Giannatsis *et al.*, 2009; Javaid *et al.*, 2017):

- *Biomedical modelling*
- *Fabrication of customized implants*
- *Fabrication of porous implants (scaffolds) and tissue engineering*
- *Design and development of devices and instrumentation used in medical sector*
- *Surgical planning*
- *Medical education and training*
- *Forensics*
- *Drug delivery and micro-scale medical devices*

2.5.1. Biomedical modelling

Biomedical modelling refers to the fabrication of physical models representing the patient's anatomy or biological structures, mainly used for preoperative planning or testing of a surgery (Giannatsis *et al.*, 2009; Javaid *et al.*, 2017). In particular, successful implant surgery requires the fabrication of accurate medical models, manufactured by biocompatible materials (Bibb *et al.*, 2011; Brennan, 2010; Giannatsis *et al.*, 2009; Javaid *et al.*, 2017). The main categories of the classified biomaterials are: metals, ceramics and polymers, presented in the next table (Table 1) (Brennan, 2010).

Table 1: Classification of biocompatible materials, Source: (Brennan, 2010)

Metals	Ceramics	Polymers
316L Stainless steel	Alumina (Al_2O_3)	Ultra-high molecular weight polyethylene
Co-Cr Alloys	Zirconia	Polyurethane
Titanium	Carbon	
Ti6A14V	Hydroxyapatite	

2.5.2. Fabrication of customized implants

The major application of AM technologies in medical sector is the design and fabrication of customized implants and fixtures which present the exact patient anatomy and comfortably fit the patient (Bibb *et al.*, 2011; Brennan, 2010; Giannatsis *et al.*, 2009; Javaid *et al.*, 2017). These medical models can be used for prosthetic operations, including maxillofacial, dental, craniofacial, orthopedic, or spinal surgery, for rehabilitation, or even for plastic surgery, in order to increase both functionality and aesthetic appearance (Bibb *et al.*, 2011; Brennan, 2010; Giannatsis *et al.*, 2009; Javaid *et al.*, 2017). In the following figures (Figures 5-6) are illustrated the 3D-model of a patient with cranial defect in the right frontal bone and the preoperative 3D-biomodel of a skull and a customized medical implant made from titanium for the operation of craniofacial surgery (Jardini *et al*., 2014).

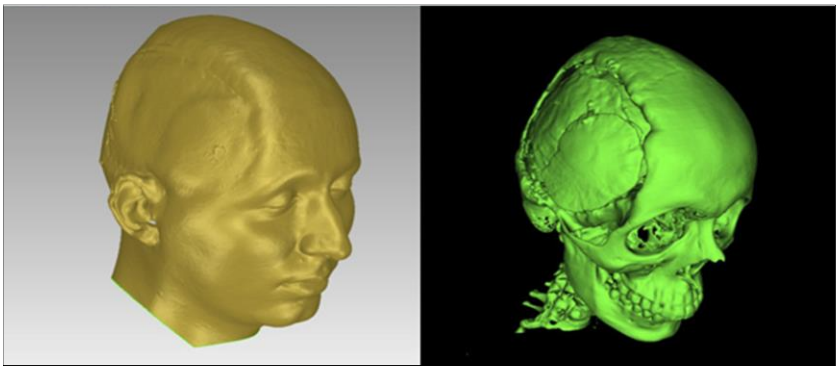

Figure 5: 3D-model of the patient with cranial defect in the right frontal bone, Source: (Jardini *et al*., 2014)

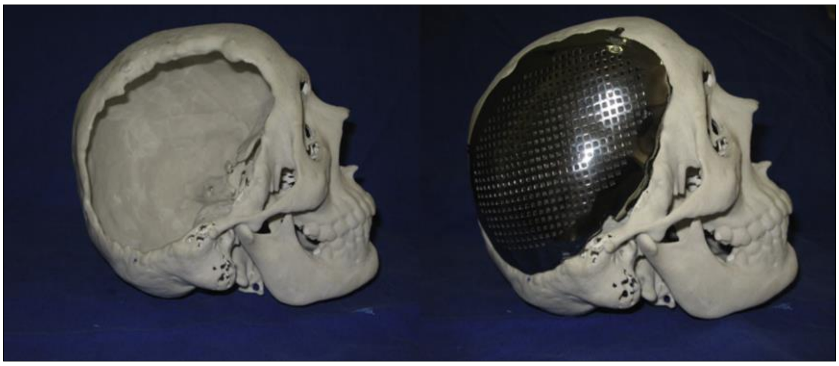

Figure 6: 3D-biomodel and customized implant for craniofacial surgery of a patient with cranial defect in the right frontal bone, Source: (Jardini *et al*., 2014)

2.5.3. Fabrication of porous implants (scaffolds) and tissue engineering

AM technolgy has increased the ability to fabricate complex geometry medical models with high accuracy (Brennan, 2010; Giannatsis *et al.*, 2009; Javaid *et al.*, 2017). Consequently, AM techniques such as FDM, SLS and 3D-printing are suitable for the fabrication of controlled porous structures with special geometrical features, by utilizing biocompatible materials in the field of sccaffolding and tissue engineering (Brennan, 2010; Giannatsis *et al.*, 2009; Javaid *et al.*, 2017). Actually, scaffolds are customized permeable implants used as a vessel for supporting tissue regeneration or restoration, by providing support and guidance to defective bone or growing tissue which was damaged (Brennan, 2010; Giannatsis *et al.*, 2009; Javaid *et al.*, 2017). The following figure (Figure 7) demonstrates the fabrication of customized porous implants made from titanium via EBM technique (Moiduddin *et al.*, 2016).

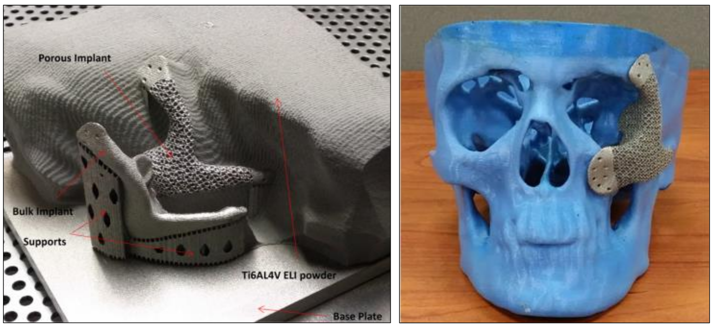

Figure 7: EBM produced titanium porous implants and FDM produced polymer skull model, Source: (Moiduddin *et al.*, 2016)

2.5.4. Design and development of devices and instrumentation used in medical sector

Furthermore, AM technogy is used not only for the pre-surgical phase, but also for the actual surgery (Brennan, 2010; Giannatsis *et al.*, 2009; Javaid *et al.*, 2017). In specific, AM technology is utilized for the design and development of medical equipment, devices and instrumentation, including hearing aid, dental devices and surgical tools used as guides during the operation process (Brennan, 2010; Giannatsis *et al.*, 2009; Javaid *et al.*, 2017). The next figure (Figure 8) presents a range of 3D-printed customized implants and surgical guides utilized for non-human primates (Chen *et al.*, 2017).

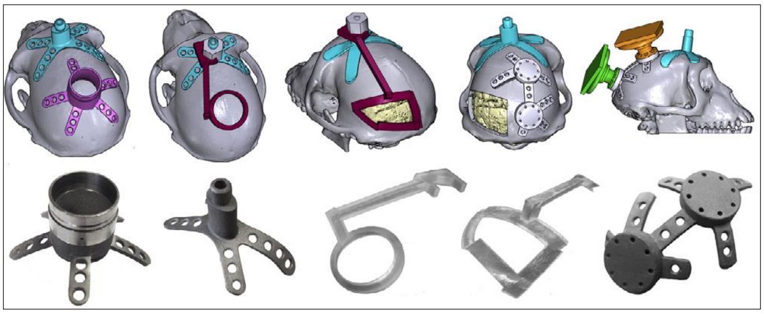

Figure 8: 3D-printed customized implants and surgical guides for non-human primates, Source: (Chen *et al*., 2017)

2.5.5. Surgical planning

As mentioned previously, the most fundamental application of AM technology in medical field is the fabrication of biomodels that can be utilized as an aiding tool for preplanning of a surgery and rehearsal, leading to numerous benefits (Brennan, 2010; Giannatsis *et al.*, 2009; Javaid *et al.*, 2017). More specifically, these benefits refer to the reduction of the operating time, the predictability in the surgical outcome, the decreased level of risk to patient, the faster patient's recovery, the improved accuracy, no geometrical restrictions and ultimately better aesthetic and functional results (Brennan, 2010; Giannatsis *et al.*, 2009; Gibson *et al*., 2006; Hnatkova *et al.*, 2014; Huotilainen *et al.*, 2014; Javaid *et al.*, 2017; Petzold *et al.*, 1999; Salmi *et al*., 2013).

The following figures (Figures 9-13) demonstrate a variety of different cases for preplanning a surgery. More precisely, in Figure 9 is presented the case of a fabricated 3D-model of patient pulmonary artery for the preplanning of thoracic surgery (Kurenov *et al*., 2015).

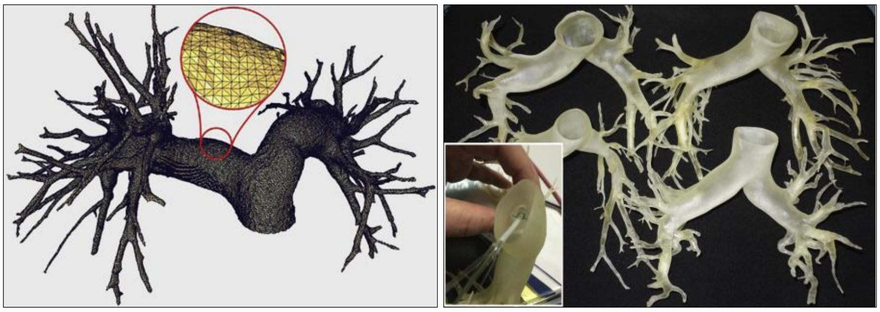

Figure 9: Preplanning in thoracic surgery, Rendered triangular surface and 3D-model of the pulmonary artery, Source: (Kurenov *et al*., 2015)

The next figures (Figures 10-11) illustrate the case of preplanning a complex surgery of a patient born with defect in joint of maxilla and mandible (Kumar *et al*., 2017). In Figure 11 is shown the comparison of aesthetic view of the patient before and after surgery (Kumar *et al*., 2017).

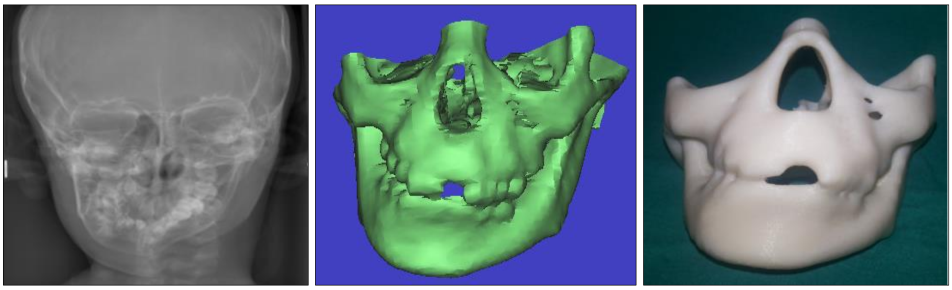

Figure 10: Manufacturing of patient specific AM model for preplanning of complex surgery, (CT scan, 3D CAD Model, AM Model), Source: (Kumar *et al*., 2017)

Figure 11: Preplanning of complex surgery, Patient born with defect in joint of maxilla and mandible, Comparison of aesthetic view of the patient before and after surgery, Source: (Kumar *et al*., 2017)

The following figure (Figure 12) presents the 3D-printed medical model for a patient after simulation of 2-jaw orthognathic surgery (Lin *et al*., 2018).

Figure 12: 3D-printed model for a patient after simulation of 2-jaw orthognathic surgery, Source: (Lin *et al*., 2018)

The next figure (Figure 13) illustrates the 3D-model of aortic aneurysm with complex geometry, created via FDM technique from the medical data acquired from Computed Tomography (CT) (Marro *et al*., 2016).

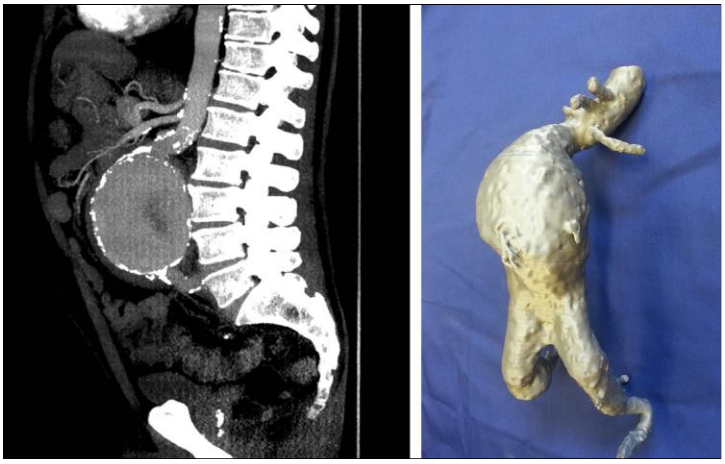

Figure 13: CT sagittal reconstruction of aortic aneurism with challenging anatomy, 3D-model of the aneurysm created via FDM, Source: (Marro *et al*., 2006)

2.5.6. Medical education and training

Additionally, AM technology can be used for purposes of medical education and training (Brennan, 2010; Giannatsis *et al.*, 2009; Javaid *et al.*, 2017). The created medical models can be utilized from medical students or young doctors in order to understand the internal or external human anatomy structure (Brennan, 2010; Giannatsis *et al.*, 2009; Javaid *et al.*, 2017). The following figure (Figure 14) presents the case of 3D-printed medical model of cervical spine, made from ABS using FDM technique (Marro *et al*., 2016).

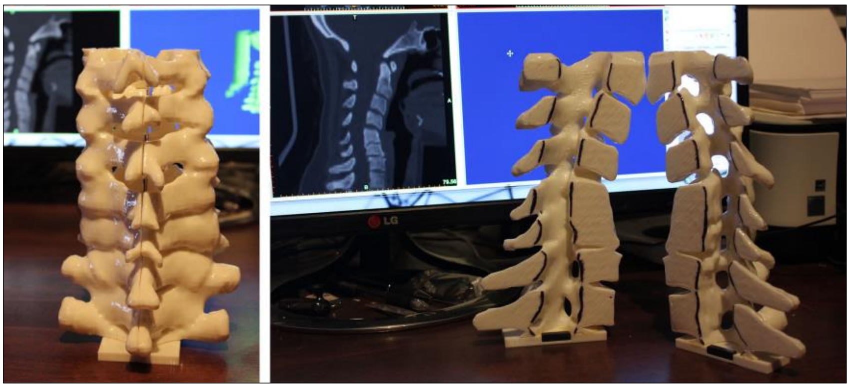

Figure 14: 3D-printed model of cervical spine, Source: (Marro *et al*., 2016)

2.5.7. Forensics

Moreover, another application of AM technology is for investigation of criminal profile (Brennan, 2010; Giannatsis *et al.*, 2009; Javaid *et al.*, 2017). In many case, the models can be used for the creation of crime scenes, in order to facilitate the process of solving cases regarding the forensic field (Brennan, 2010; Giannatsis *et al.*, 2009; Javaid *et al.*, 2017). The following figure (Figure 15) depicts the case of created skull replicas used in forensics (Gibson *et al*., 2006).

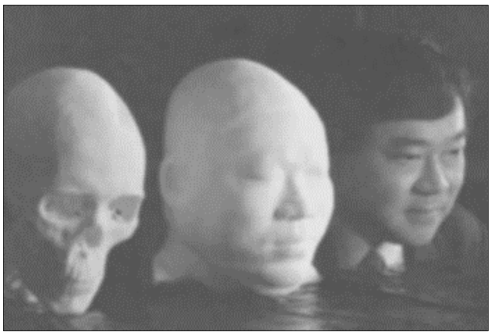

Figure 15: Forensics, Skull replicas, Source: (Gibson *et al*., 2006)

2.5.8. Drug delivery and micro-scale medical devices

Finally, another application of AM technologies is the fabrication of customized microsystems and therapeutic devices used to control drug delivery for certain cases (Giannatsis *et al.*, 2009). In specific, these devices may involve networks of fluidic and electronic components that operate in an specific manner (Giannatsis *et al.*, 2009). The basic groups of these devices involve the following: bio-capsules and microparticles for controlled and site-specific drug release, microneedles for transdermal and intravenous delivery (Figure 16) and implantable microsystems (Giannatsis *et al.*, 2009).

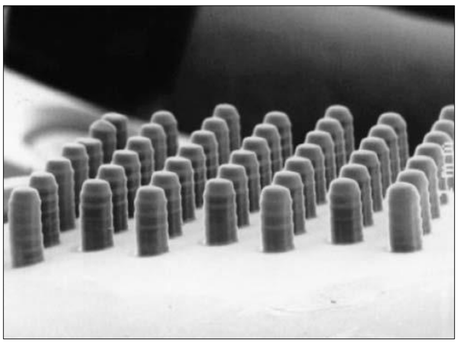

Figure 16: Microneedle array fabricated via micro-SLA, Source: (Giannatsis *et al.*, 2009)

2.6. Additive Manufacturing Criteria for Medical Models

In general, Additive Manufacturing technologies have great potential and flexibility in solving complex surgical problems (Giannatsis *et al.*, 2009; Gibson *et al*., 2006; Javaid *et al.*, 2017; Pucci *et al.*, 2017). Nevertheless, they have not been adopted to a large extent in medical and healthcare sectors, due to a number of technological issues and deficiencies (Giannatsis *et al.*, 2009; Gibson *et al*., 2006; Javaid *et al.*, 2017). Actually, the main five criteria influencing this perspective include (Giannatsis *et al.*, 2009; Gibson *et al*., 2006; Javaid *et al.*, 2017; Pucci *et al.*, 2017):

- *Speed:* One of the main competitive advantages of AM technology is the speed of production (Giannatsis *et al.*, 2009; Gibson *et al*., 2006; Javaid *et al.*, 2017; Pucci *et al.*, 2017). Though, in case of batch production of medical models the AM technologies are not suitable, due to the fact that the medical data preparation can be more time consuming than the RP building process (Giannatsis *et al.*, 2009; Gibson *et al*., 2006; Javaid *et al.*, 2017; Pucci *et al.*, 2017). Consequently, medical models can be fabricated for pre-organized surgeries and on the contrary cannot be utilized for emergency operations (Giannatsis *et al.*, 2009; Gibson *et al*., 2006; Javaid *et al.*, 2017; Pucci *et al.*, 2017).
- *Cost:* AM technologies are majorly utilized for low-cost production applications (Giannatsis *et al.*, 2009; Gibson *et al*., 2006; Javaid *et al.*, 2017; Pucci *et al.*, 2017). However, the fabrication of customized medical models requires to be of improved quality, effectiveness and efficiency, leading to the increase of the cost (Giannatsis *et al.*, 2009; Gibson *et al*., 2006; Javaid *et al.*, 2017; Pucci *et al.*, 2017).
- *Accuracy:* The AM processes provide models with high accuracy (Giannatsis *et al.*, 2009; Gibson *et al*., 2006; Javaid *et al.*, 2017; Pucci *et al.*, 2017). Nevertheless, the issue of accuracy is characterized as insufficient for numerous medical applications, due to poor or inaccurate medical data, obtained from 3D-imaging software programs (Giannatsis *et al.*, 2009; Gibson *et al*., 2006; Javaid *et al.*, 2017; Pucci *et al.*, 2017).
- *Materials:* The availability of appropriate bio-compatible materials for medical applications via AM technology are limited (Giannatsis *et al.*, 2009; Gibson *et al*., 2006; Javaid *et al.*, 2017; Pucci *et al.*, 2017; Singh *et al.*, 2017). Additionally, the AP machines

providing the most suitable material properties for medical purposes are very expensive, leading to the general increase of the cost (Giannatsis *et al.*, 2009; Gibson *et al*., 2006; Javaid *et al.*, 2017; Pucci *et al.*, 2017; Singh *et al.*, 2017).

- *Ease of use:* The fabrication of medical models requires highly-skilled and trained personnel in order to achieve accurate and good quality models, implying additional investment for training (Giannatsis *et al.*, 2009; Gibson *et al*., 2006; Javaid *et al.*, 2017).

2.7. Process of Medical Model Fabrication

The process used for the fabrication of medical models via AM technologies, is divided into two fundamental stages, namely the *design stage* and the *manufacture stage* (Brennan, 2010; Eijnatten *et al.*, 2018; Hnatkova *et al.*, 2014; Huotilainen *et al.*, 2014; Javaid *et al.*, 2017). Specifically, the design stage comprises of the following steps: acquisition of medical data (or medical imaging) and image processing via Computer-Aided Design. And finally, the manufacture stage is composed of the required steps for the creation and the fabrication of the model via AM technologies (Brennan, 2010; Eijnatten *et al.*, 2018; Hnatkova *et al.*, 2014; Huotilainen *et al.*, 2014; Javaid *et al.*, 2017).

Each of these steps, (from medical data acquisition to image processing and to the manufacturing stage and finishing process), can introduce geometric deviations, leading to distortions in the final AM medical model (Eijnatten *et al.*, 2018; Huotilainen *et al.*, 2014). Nevertheless, the main percentage of these inaccuracies in AM medical models is introduced during the process of medical imaging or during image processing, rather than during the manufacturing stage, (for example during 3D-printing process), which is considered as more accurate procedure (Eijnatten *et al.*, 2018; Huotilainen *et al.*, 2014). Consequently, further investigation regarding the accuracy of the AM in medical applications is indisputably required (Eijnatten *et al.*, 2018; Huotilainen *et al.*, 2014).

2.8. Medical Imaging

Therefore, one of the most fundamental issues, regarding the Rapid Prototyping applications in medical sector, is the accurate acquisition of three-dimensional anatomical models (Hnatkova *et al.*, 2014). In former times, the analysis of the anatomy of a patient was based on two-dimensional (2D) data obtained by radiography and photography (Kumar *et al.*, 2017; Petzold *et al.*, 1999). In the current days, the technological improvements resulted in the 3D-image acquisition of better resolution, providing the identical replica of the anatomy of a patient (Gibson *et al.*, 2006; Kumar *et al.*, 2017).

In particular, medical imaging techniques facilitate the storage of the data in Digital Imaging and Communication in Medicine (DICOM) images (Kumar *et al.*, 2017; Lim *et al.*, 2006). These images are supposed to be utilized as the main source for medical software's three-dimensional Computer Aided Design, in order to produce AM medical models (Kumar *et al.*, 2017; Lim *et al.*, 2006).

As regards the medical imaging techniques, they are used for the visualization of internal structures of the patient's anatomy, including organs, bones, or vessels (Hnatkova *et al.*, 2014). Namely, the Computed Tomography (CT), the Magnetic Resonance Imaging (MRI) and the Ultrasonography are the most common used techniques (Brennan, 2010; Hnatkova *et al.*, 2014; Owusu-Dompreh, 2013), which are analyzed briefly in the following sections (Sections 2.8.1.-2.8.3.).

2.8.1. Computed Tomography (CT)

Computed Tomography scan, (sometimes referred to as Computed Axial Tomography (CAT) scan (Brennan, 2010), is a non-invasive medical imaging technique (Brennan, 2010; Hnatkova *et al.*, 2014; Owusu-Dompreh, 2013). A CT scan utilizes X-ray technology for the geometric data acquisition of the patient's body, by generating cross-sectional slices of the scanned part obtained from different angular positions (Brennan, 2010; Hnatkova *et al.*, 2014; Owusu-Dompreh, 2013).

The following figures (Figures 17-18), illustrate the principle of the CT scanning process. More specifically, the CT operates by using an X-ray generator that rotates around the patient body, while the emitted radiation penetrates the object of examination at diverse rates, according to the tissue density positions (Brennan, 2010; Hnatkova *et al.*, 2014; Owusu-Dompreh, 2013). A digital X-ray detector visualizes the 2D-projections from different angles, as illustrated in Figure 17. Subsequently, the acquired data must be processed into cross-sectional images, by using a computed based tomographic reconstruction form (Brennan, 2010; Hnatkova *et al.*, 2014).

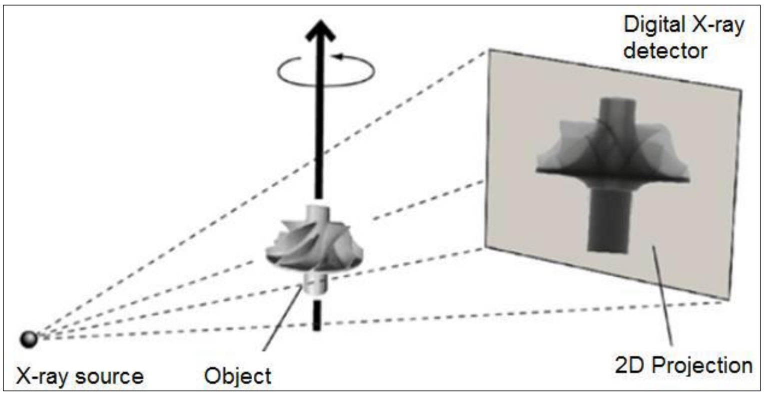

Figure 17: Principle of CT scanning technology, Source: (Hnatkova *et al.*, 2014)

The main advantage of CT scanning is the accuracy and the production of high-quality images of the generated anatomical structure (Brennan, 2010; Hnatkova *et al.*, 2014). Furthermore, it is considered as more tolerant to patient movement than MRI scanning (Brennan, 2010; Hnatkova *et al.*, 2014). Though, the patient radiation exposure is the main disadvantage of this method, that could possibly lead to a potential allergy reaction (Brennan, 2010; Hnatkova *et al.*, 2014).

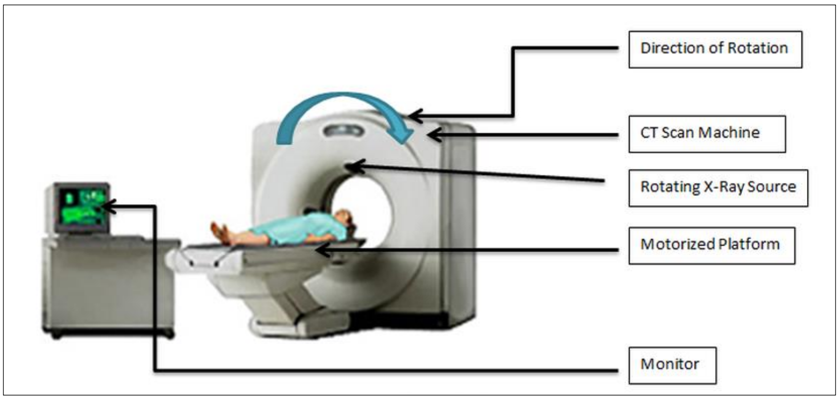

Figure 18: CT scanning machine, Source: [1]

2.8.2. Magnetic Resonance Imaging (MRI)

Magnetic Resonance Imaging (MRI) is also a medical imaging method, used for the detailed visualisation of internal structures in the human body (Brennan, 2010; Hnatkova *et al.*, 2014; Owusu-Dompreh, 2013). In opposition to CT scan, MRI scanner does not emit X-ray radiation. On the contrary, MRI scanners utiilize magnetic fields and radio waves for the medical data aquisition.

Additionally, the following figure (Figure 19) presents an MRI scanning machine, illustrating its basic parts.

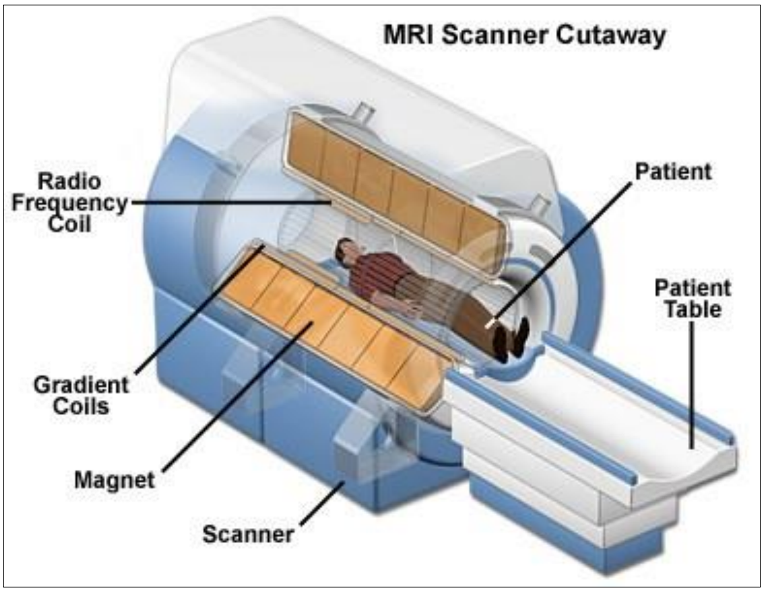

Figure 19: MRI scanning machine, Source: [2]

Actually, when specific atomic nuclei (e.g. hydrogen atoms) are located in an external magnetic field, they can absorb and emit radio frequency energy (Brennan, 2010; Hnatkova *et al.*, 2014; Owusu-Dompreh, 2013). In MRI process, the hydrogen molecules of water, contained within the human body, are used for the generation of detectable radio-frequency signal, received by antennas, and then transmitted to computer system, which subsequenlty proceesses the aquired data and generates an image of the examined area (Brennan, 2010; Hnatkova *et al.*, 2014; Owusu-Dompreh, 2013).

As mentioned above, the most prominent advantage of MRI scanning method is the lack of radiation exposure (Brennan, 2010; Hnatkova *et al.*, 2014). Moreover, the MRI scanning facilitates the visualization of soft tissues (e.g. cartilage) and can generate accurate images of parts encapsulated by bone tissue (e.g. brain, spinal cord etc.) (Brennan, 2010; Hnatkova *et al.*, 2014). On the other hand, MRI scanning method is intolerant to patient movement contrary to CT scan (Hnatkova *et al.*, 2014).

2.8.3. Ultrasonography

Ultrasonography or Medical Ultrasound is a non-invasive procedure that utilizes high frequency waves (>20kHz), mainly used as diagnostic imaging technique (Brennan, 2010; Hnatkova *et al.*, 2014). In fact, the ultrasound device sends sound waves into the examined area of the human body (Brennan, 2010; Hnatkova *et al.*, 2014;). These sound echoes are received by a sensor, which subsequently generates a digital image (Brennan, 2010; Hnatkova *et al.*, 2014;). The Ultrasonography process and machine are displayed in the next figure (Figure 20).

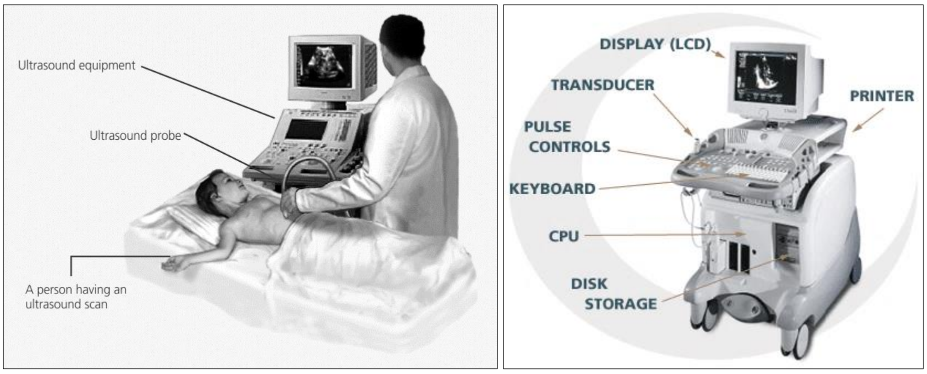

Figure 20: MRI scanning machine, Source: [3], [4]

In comparison with the other two medical imaging techniques, Ultrasonography presents several advantages (Brennan, 2010; Hnatkova *et al.*, 2014;). Mainly, the competitive superiority of this method, is the direct visualization of the examined area (Brennan, 2010; Hnatkova *et al.*, 2014;). Additionally, Ultrasonography does not use harmful ionizing radiation, similar to the MRI scanning technique (Brennan, 2010; Hnatkova *et al.*, 2014;). As regards the drawbacks of this method, it is worth mentioning that the resolution of the images is usually mid to low level, depending on the field of view and patient cooperation (Brennan, 2010; Hnatkova *et al.*, 2014).

2.8.4. Digital Imaging and Communications in Medicine (DICOM)

As a matter of fact, the growth of medical imaging techniques in the past decade, has enabled the visualisation of internal structures in the human body, by generating two-dimensional cross-sectional images of high fidelity and accuracy (Hnatkova *et al.*, 2014; Wang *et al.*, 2017). In particular, these images are stored in Digital Imaging and

Communication in Medicine (DICOM) data format, utilized as the main source for medical software's three-dimensional Computer Aided Design (CAD), in order to produce AM medical models (Hnatkova *et al.*, 2014; Kumar *et al.*, 2017; Lim *et al.*, 2006).

Especially, DICOM is a worldwide information standard, under the aegis of the National Electrical Manufacturers Association (NEMA), designed to ensure the storage and the transmission of medical images (Lim *et al.*, 2006). Actually, the basic scope of the current DICOM standards is the accomplishment of the compatibility and the improvement of workflow efficiency between imaging systems and other information systems, regarding the healthcare sector (Lim *et al.*, 2006).

Briefly, the DICOM Network, illustrated in the following figure (Figure 21), represents the typical example of the process conducted for the acquisition of the DICOM files (Brennan, 2010; Whitby J., 2007). Specifically, the process is composed of the five following steps (Brennan, 2010; Whitby J., 2007):

- Performance of CT scan.
- Generation of a set of images (study) from the raw data via scanner console.
- Distribution of the study to a Picture Archiving and Communication System (PACS) via CT console.
- Query of the PACS and retrieval of the study conducted by a workstation.
- Reconstruction and reformat of the study.

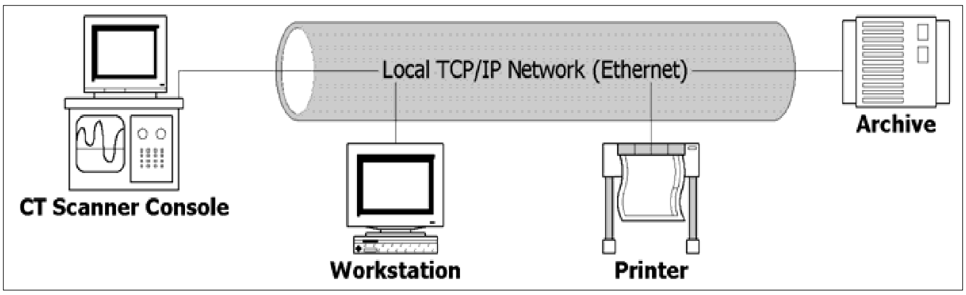

Figure 21: Typical DICOM Network, Source: (Whitby J., 2007)

2.8.4.1. *Software Programs for the Convertion of DICOM Files*

The aquired medical data (DICOM files), obtained by medical imaging techniques (i.e. CT, MRI, or Ultraphonography), can be subsequenlty processed, with the help of various medical image segmentation software programs, in order to create a three-dimensional visualization of a patient anatomic part (Hnatkova *et al.*, 2014).

The process of conversion of the DICOM files into compatible formats with RP machines include a number of steps, and each of these steps require different software programs (Hodgdon *et al.* 2018; Pucci *et al.* 2017). In brief, these steps comprise of the acquisition of the DICOM files, the conversion of DICOM files to Standard Triangle Language (STL) file format, the image optimization and the creation of the RP model.

According to research studies (Hodgdon *et al.* 2018; Pucci *et al.* 2017), there is a variety of software solutions, both open-source or commercially available, designed for the creation of 3D-printed models. The most commonly used software programs for the conversion of DICOM files to STL file format are the following: 3DSlicer, ITK-SNAP, Materialize (Mimics), Seg3D & ImageVis3D, and Osirix (Hodgdon *et al.* 2018; Pucci *et al.* 2017) [5]. Particularly, Materialise is considered as the market standard, providing Materialize Mimics for the direct creation of accurate 3D-models, which is designed for medical applications (Pucci *et al.* 2017). Although, the other solutions are free and open-source applications, that can be easily utilized from non-specialized users.

2.9. Manipulation of 3D-models

After acquiring the required medical data, obtained from CT, MRI, or Ultrasonography scans in DICOM file format, a software program can be utilized in order to create a 3D-model representing the patient anatomy (Brennan, 2010; Eijnatten *et al.*, 2018; Hnatkova *et al.*, 2014; Javaid *et al.*, 2017). This model can be exported into STL file format for further processing and optimization, before proceeding to the manufacture stage (Brennan, 2010; Eijnatten *et al.*, 2018; Hnatkova *et al.*, 2014; Javaid *et al.*, 2017).

Subsequently, the model can be exported to CAD programs for further processing, by using the provided editing tools, such as smoothing, merging, rescaling etc. (Brennan, 2010; Eijnatten *et al.*, 2018; Hnatkova *et al.*, 2014; Javaid *et al.*, 2017).

Ultimately, the creation of the RP model according to the created STL file, is used for the 3D-printing process and finally for the fabrication of the customized anatomical model (Brennan, 2010; Eijnatten *et al.*, 2018; Hnatkova *et al.*, 2014; Javaid *et al.*, 2017).

2.10. Summary of Literature Review

Briefly, in order to acquire a profound understanding of the integration of Additive Manufacturing technologies in medical sector, a thorough literature review is conducted. The main fields examined in this chapter are the following: Additive Manufacturing Methods, including the four main techniques of Stereolithography, Selective Laser Sintering, Fused Deposition Modeling and Multi-Jet Modeling. Subsequently, the research status of the applications of AM in medical field are examined, providing specific data obtained from recent research studies.

Additionally, the applications of AM in medical sector, are categorized and analyzed in detail, by demonstrating the eight major applications, including: biomedical modelling, fabrication of customized implants, fabrication of porous implants (scaffolds) and tissue engineering, design and development of devices and instrumentation used in medical sector, surgical planning, medical education and training, forensics, and finally drug delivery and micro-scale medical devices, by providing various examples.

Furthermore, the AM criteria for medical models, including speed, cost, accuracy, materials, and ease of use are examined, in order to understand the limitations of AM technology with regard to the medical applications.

Afterwards, it is crucial to demonstrate the process of medical model fabrication, considered as the main subject of the current study. This process is divided into two basic stages, the design and the manufacture stage. Regarding the design stage, the most fundamental steps is the acquisition of medical data (medical imaging) and the imaging processing for the acquisition of the medical model. In particular, the medical imaging process is analyzed thoroughly, providing the basic methods for acquiring the medical data (i.e. Computed Tomography, Magnetic Resonance Imaging and Ultrasonography) in DICOM file format. After acquiring the required medical data to the desired STL file format, the manufacture stage follows, including the creation of the RP model ready for to be fabricated via 3D-printing technology.

Consequently, aim of the current study is to present the fabrication process of a real case scenario, namely the T4 vertebra of the thoracic spine of a patient, by demonstrating the three fundamental stages of this process: the design, the manufacture, and the evaluation stage. Each step is analyzed in a step-by-step approach, providing all the necessary details for the fabrication of the medical model.

Initially, for the first stage, this study focuses on the presentation of the available open-source software programs for the conversion of DICOM files to STL file format, as this step is considered as the most determinant. Different software programs are selected to be presented in order to understand the limitations and the capabilities of each software and finally select the most appropriate one for the specific case study of the T4 vertebra.

In specific, ITK-SNAP software is selected to be utilized for the conversion of the DICOM files to STL file format, and subsequently Meshmixer software is used for the optimization of the model. Fused Deposition Modeling (FDM) technology is used, by utilizing the BCN3D Cura 1.0.3. software and the BCN3D Sigma R17 printer, for the creation and for the 3D-printing of the medical model. Finally, the 3D-printed model is scanned and edited via Next Engine 3D-scanner and ScanStudio HD software, respectively. The scanned model is saved in STL file format, in order to measure and evaluate the results, regarding the dimensional declinations between the printed and the scanned model. These measurements are conducted with the help of the Artec Studio 11 Professional software. Finally, the empirical results and findings of the research are discussed thoroughly.

With regard to the scientific contribution, the current study provides the basic theoretical review concerning the field of Additive Manufacturing technologies, and additionally the applications of these technologies in the medical field. In addition, the basic scope of the study is to present the fabrication process of a real case scenario, including all the required steps, from the design, the manufacture and finally the evaluation procedure, by providing the limitations of the process for each step.

3. Chapter Three: Methodology

3.1. Introduction

The current chapter comprises the research methodology followed, by providing the steps and the analysis of the model used to approach the empirical work. This attempt to define the basic steps needed for the development of this work, will contribute to establish a basis of the structure, leading to a profound understanding of the results obtained.

3.2. Methodology

In specific, after conducting a thorough literature review, concerning the field of Additive Manufacturing technologies with reference to the fabricated medical models (Chapter 2), the main objective of the current study is to demonstrate the process from the acquisition of medical data to the final 3D-printed anatomical model, in order to evaluate the final outcome, concerning the dimensional declinations between the printed and the scanned model.

For the purpose of acquiring the desired medical data, it is critical to select the most suitable software among a variety of open-source software tools, utilized for the conversion of DICOM files from CT or MRI to STL file format. Therefore, a comprehensive research of the available open-source software programs has been conducted in the literature review (Section 2.8.4.1.). According to this research, four different open-source software programs (i.e. Seg3D, ImageVis3D, 3DSlicer, and ITK-SNAP) are selected to be presented, in order to examine the most appropriate one for a specific case study.

Firstly, a thorough analysis of the software programs utilized for the acquisition of STL files is introduced, in order to evaluate the capabilities and the limitations of each software program. In fact, a step by step approach is conducted, by providing a modest user manual that comprises the basic functions of each program for converting the DICOM file from CT or MRI to STL file. This part of the study is extended into four different sections describing the following open-source software tools: the Seg3D, the ImageVis3D, the 3DSlicer and finally the ITK-SNAP software programs.

Subsequently, the most appropriate software (i.e. ITK-SNAP) is selected for the presentation of the process of the digital fabrication of the T4 vertebra of the patient's thoracic spine. More precisely, the systematic approach of this process is classified into three main sections: the *"Design"*, the *"Manufacture"*, and the *"Evaluation"* stage.

With regard to the first section, the design stage is described in a step-by-step approach, comprising four main steps required for the acquisition of the STL file. In particular, these steps of the design study are as follows: *"Acquisition of DICOM files"* (via CT), *"Conversion of DICOM files to STL file format"* (via ITK-SNAP software), *"Optimization of the STL file"* (via Meshmixer software) and finally *"Acquisition of the final STL file ready for the RP machine"*.

In the second section, the manufacture stage of the final 3D-printed medical model is presented. This stage is composed of the two following steps: the *"Creation of the RP model"* (via BCN3D Cura 1.0.3. software) and the *"Printing of the medical model via 3D-printing technology"* (via Fused Deposition Modeling technology – BCN3D Sigma R17 printer).

The third section focuses on the evaluation stage, composed of three principal steps. Actually, these steps consist of the above procedures: *"Scanning of the 3D-printed model via 3D-scanner"* (via Next Engine 3D-scanner and ScanStudio HD software), *"Measurement of the dimensions of the STL files"* (via Artec Studio 11 Professional software), and ultimately *"Comparison and Evaluation of the results"*.

Finally, the last two chapters constitute the summary of the empirical work of the current thesis. Specifically, the conclusions of the current case study are discussed and analyzed thoroughly. Additionally, the limitations of this project are quoted, in order to indicate potential areas for further research and investigation.

The flow chart of the methodology followed in the current study, is presented in the following flow chart (Chart 1), illustrating the most fundamental steps. At this point, it is worth mentioning that the methodology illustrated in the current chapter (Chapter 3), comprises the basic steps of the three stages of the fabrication process. Each of these stages is analyzed and described in more detail in the corresponding section of the examined case study (Chapter 5).

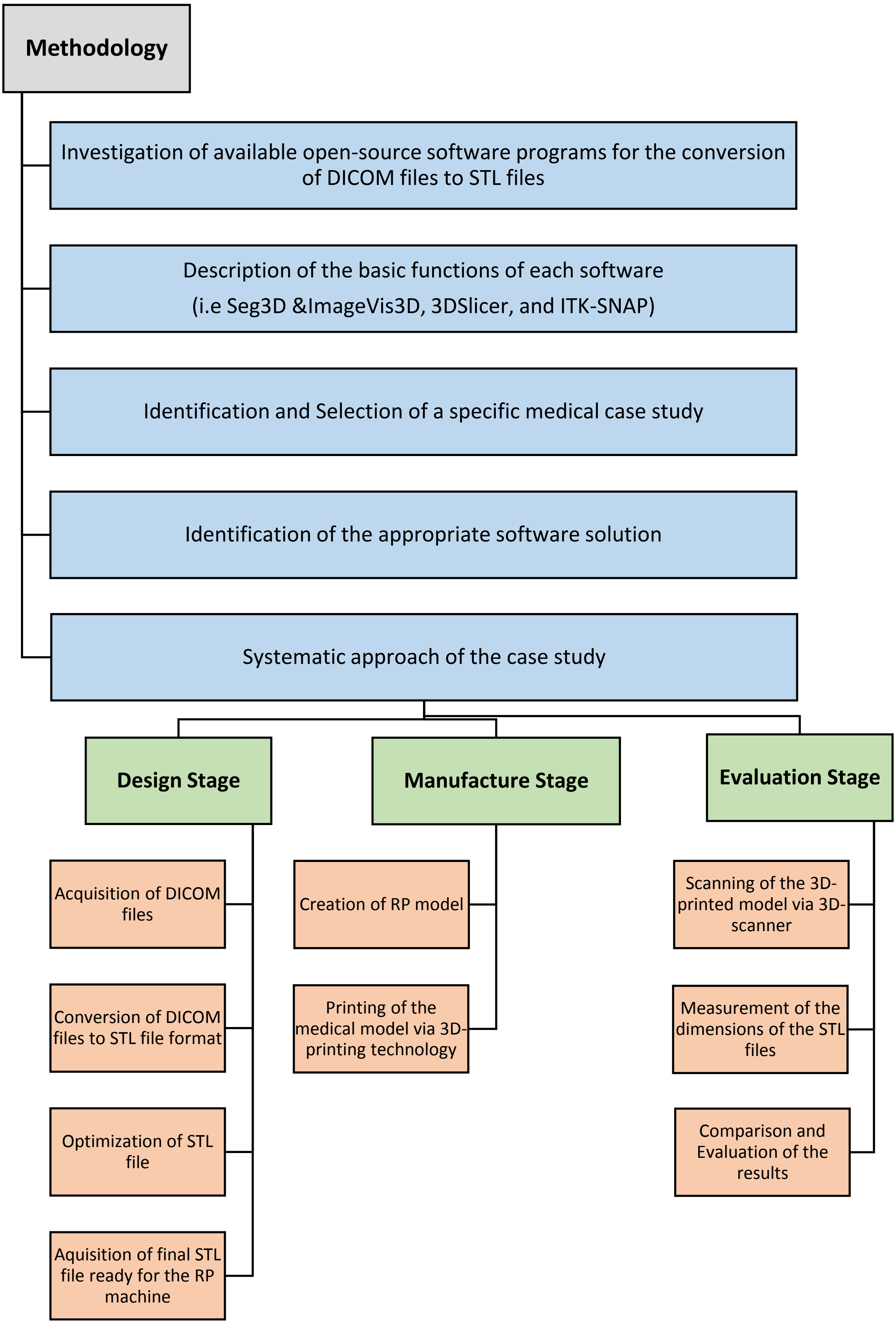

Chart 1: Flow chart of the methodology of the study

4. Chapter Four: Data Analysis

4.1. Introduction

This chapter consists of the description of the basic functions of the available open-source software tools utilized for the conversion of medical data (i.e. series of DICOM files) to STL file format. The main objective of this chapter is the exposition of four different open-source software programs, in consideration of getting familiarized with them and finally evaluating the capabilities and the limitations of each software.

Particularly, this chapter refers to the identification of the available open-source software programs, by providing a modest user manual that comprises the basic functions of each program. This section of the study is classified into four different sections describing the following open-source software tools: the Seg3D, the ImageVis3D, the 3DSlicer and finally the ITK-SNAP software programs.

4.2. Description of Software Programs

For the purpose of acquiring the desired STL files, it is essential to select the most suitable software among a variety of open-source software tools. Therefore, a comprehensive research of the procurable open-source software programs has been conducted (see Section 2.8.4.1.). According to the research findings, four different open-source software programs (i.e. Seg3D, ImageVis3D, 3DSlicer, and ITK-SNAP) are selected to be presented, in order to examine the most appropriate one for a specific case study.

In the following sections, a demonstration of the steps required to be undertaken for the conversion of a series of DICOM files to STL file format is introduced in a structured and interpretative way. The series of DICOM files utilized for the demonstration of the process is identical for the four occasions. Specifically, the DICOM files are downloaded from ITK-SNAP's official site, from the available data archive [6]. The file can be found on: *"Thorax_1CTA_THORACIC_AORTA_GATED (Adult)"* file [6].

4.2.1. Seg3D Software

Introduction to Seg3D Software

The Center for Integrative Biomedical Computing (CIBC) (Figure 22) is devoted to the development and production of open-source software tools for biomedical image-based modeling, simulation and estimation, and additionally to the visualization of bio-medical data [7]. Seg3D is a volume segmentation and processing tool, produced by the National Institutes of Health (NIH) and the CIBC at the University of Utah Scientific Computing and Imaging (SCI) Institute [7].

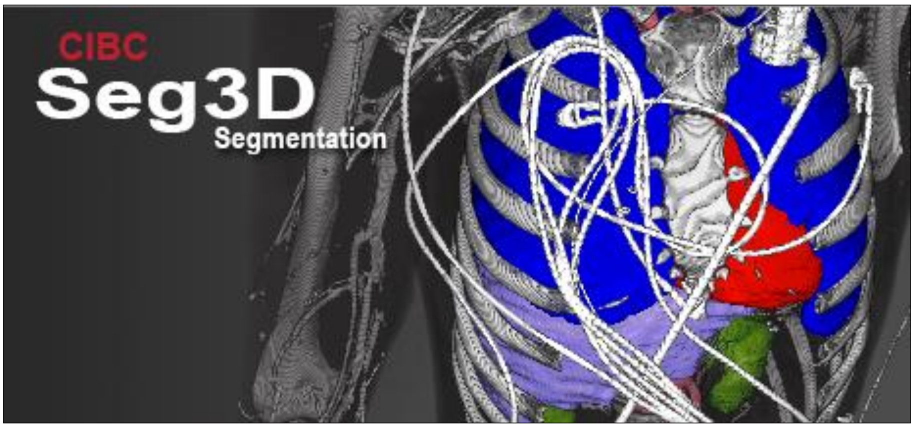

Figure 22: Seg3D Software produced by the NIH CIBC at the University of Utah Scientific Computing and Imaging Institute, Source: [7]

Seg3D combines a flexible manual segmentation interface with powerful higher-dimensional image processing and segmentation algorithms from the Insight Toolkit (ITK) [7]. According to the official site of the SCI Institute [7], the main characteristics of Seg3D needed to be mentioned are the above:

- *Fully 3D-interface with multiple volumes managed as layers* [7].
- *Automatic segmentation integrated with manual contouring* [7].
- *Volume rendering with 2D transfer function manipulation in real-time* [7].
- *Image processing and segmentation from the Insight Toolkit* [7].
- *Real time display of Insight Toolkit filtering output allows for computational steering* [7].

- *64-bit enabled for handling large volumes on large memory machines* [7].
- *Supports many common biomedical image formats* [7].
- *Open-source with BSD-style license* [7].
- *Cross platform: Windows, MacOSX, and Linux* [7].

Basic Program Functions

Particularly, in consideration of getting familiarized with the fundamental functions of Seg3D software, it is essential to demonstrate an analytical description of the steps of the utilization of the software for a specific case study. For the current case, a series of DICOM files of a thorax is used, downloaded from ITK-SNAP's official site, from the available data archive [6]. The file can be found on: *"Thorax_1CTA_THORACIC_AORTA_GATED (Adult)"* file [6].

Welcome Screen

In the following figure (Figure 23), is illustrated the *"Welcome Screen"* of Seg3D, which provides the user with a menu that displays the main available options [8]. The provided options, in order to start and continue a segmentation in Seg3D, are the following: *"Quit"*, *"Load Recent Project"*, *"Open Existing Project"*, *"Start New Project"*, *"Quick Open File"* and *"Cancel"* [8]. The same options can be found on the *"File"* drop-down menu [8].

Figure 23: Seg3D, Welcome Screen

Starting a New Project

In order to start a new project, the user should select this option from the menu on the left, or from the drop-down menu, *File → New Project* [8]. The *"New Project Wizard Window"*, presented in the figure below (Figure 24), prompts the user to specify basic information of the current project, mainly concerning the *"Project Name"* and the *"Project Path"*, so that it can be saved [8]. The user should press the *"Continue"* button (Figure 24), in order to proceed to the next page of the wizard [8].

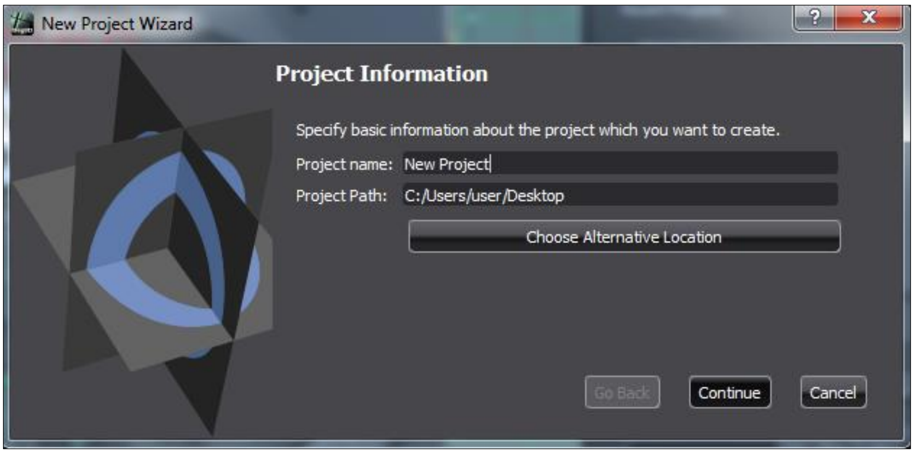

Figure 24: Seg3D, New Project Wizard, Project Information Window

Subsequently, a *"Summary"* window appears on the screen, displaying the preselected settings, as demonstrated in the following figure (Figure 25) [8]. The user should press the *"Done"* button (Figure 25), in order to proceed to the next step [8].

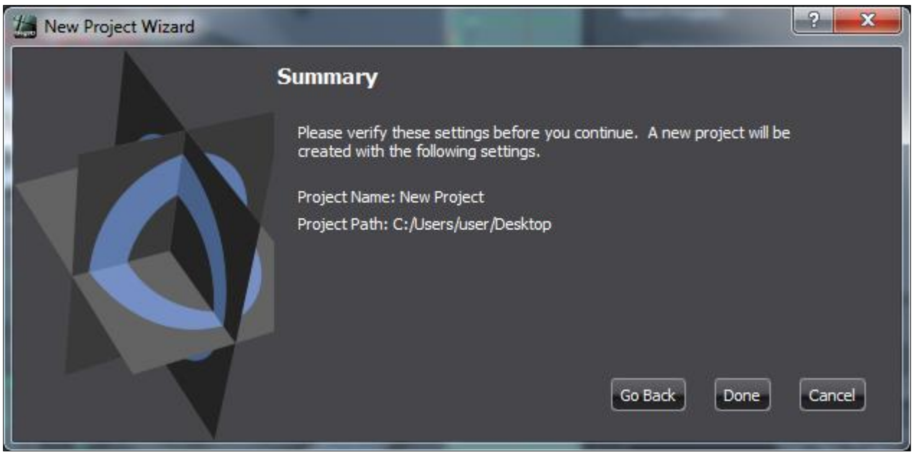

Figure 25: Seg3D, New Project Wizard, Summary, Verification of the preselected settings

Importing Layer from Single File

Additionally, the next step, for the purpose of creating a new project, is to import the appropriate files [8-9]. In this specific project, a series of DICOM files of a thorax is used [6], for the creation of the current project, as mentioned previously. From the drop-down menu on the top, the user selects *File → Import Layer from Image Series*, as presented below (Figure 26) [8-9].

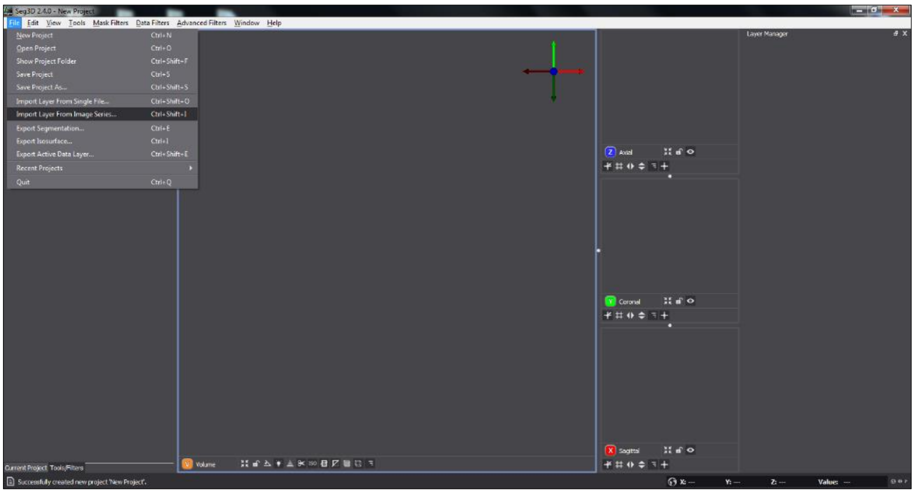

Figure 26: Seg3D, Importing Layer from Image Series

Once the user selects the suitable files to be read, the *"Layer Importer Widget"* window appears (Figure 27), displaying the selected type of the data [8-9]. In the current case, the data are displayed as *"Volume Data"*, more specifically, as solid volume of gray scale values.

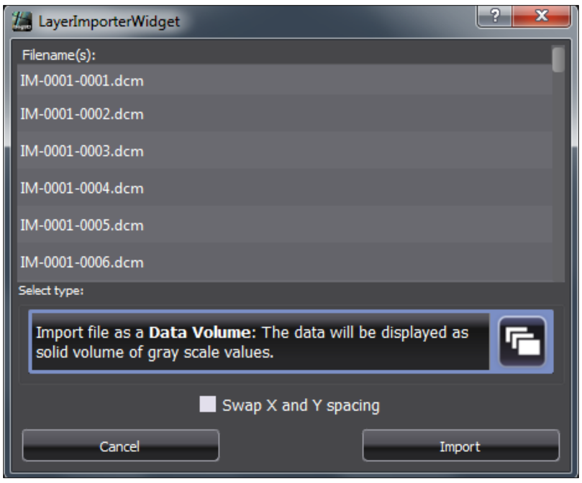

Figure 27: Seg3D, Layer Importer Widget, Importing Layer from Image Series

Interface of Seg3D

The Seg3D viewer, as being the main interface of the software, provides the user with a combination of mouse functions, keyboard shortcuts and visual buttons in order to facilitate the process of visualization and segmentation of data in a highly intuitive way [8].

In particular, in the figure presented below (Figure 28) is displayed the layout of the new project, created by using the DICOM files of a thorax [6]. The interface of Seg3D consists of various controlling windows, different viewer panels (2D Slice Viewer and 3D Volume Viewer) and a toolbar located at the bottom of the window, containing a number of useful functions [8].

Furthermore, the viewer panels provide the user with four main options of view: *"Volume"*, *"Axial"*, *"Sagittal"*, and *"Coronal"*. There are several icons in each view panel providing different functions [8].

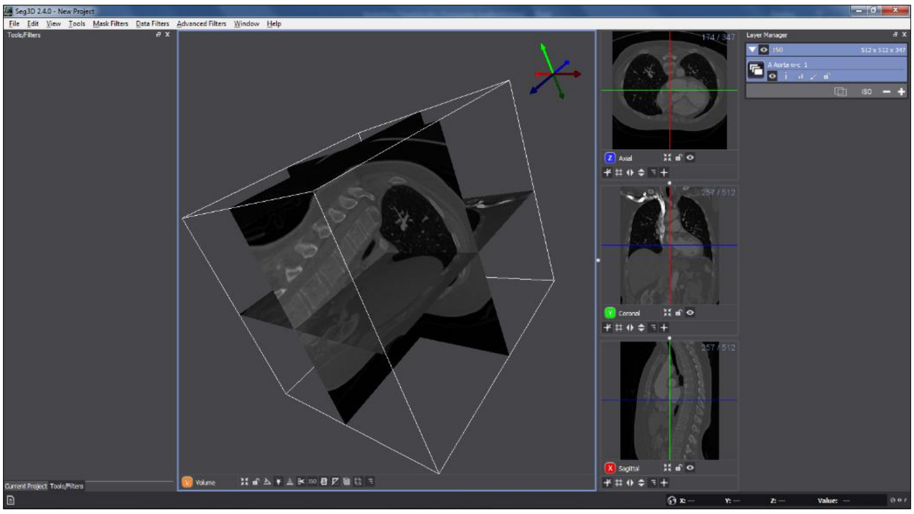

Figure 28: Seg3D, The Interface of the Created Project

Windows of Seg3D

Additionally, apart from the viewer windows mentioned before, there are several windows, appearing by default in specific positions, improving the functionality of the software. Namely, these windows are the following: *"Project"*, *"Tools"*, *"Layer Manager"*, *"Volume Viewer"* and *"Provenance Windows"* [8].

➢ *Project Window*

The *"Project Window"* opens by default when the user launches the software and it is positioned to the left side of the screen panel, as demonstrated in the following figure (Figure 29) [8].

The user is supposed to click the tab *"Current Project"* at the bottom of the left side or to select the option *"Project Window"* from the drop-down menu, for the purpose of accessing this window [8]. This window furnishes the user with information concerning the *"Project Settings"* (*"Project Name"*, *"Autosave"*, *"Project File Size"*), *"Project Sessions"* and *"Project Notes"* (Figure 29) [8].

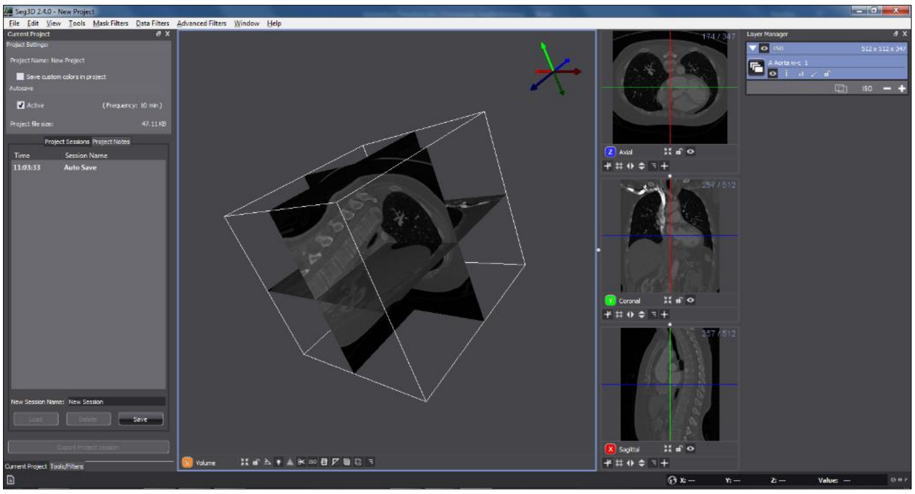

Figure 29: Seg3D, Project Window

➢ *Tools Window*

The second window, i.e. the *"Tools Window"*, is displayed by default when the Seg3D software opens. In specific, it is positioned to the left side of the screen panel as well as the *"Project Window"*, as presented in the following figure (Figure 30) [8].

Furthermore, there is a great variety of different tools and filters implemented in Seg3D software for diverse tasks [8]. The user can select from the *"Tools"* drop-down menu a number of diverse tools, in order to attempt several tasks. Mainly, these tasks pertain to reformatting original data, smoothing and de-noising image data, and additionally to automatic or manual segmenting [8-9]. In Figure 30, a *"Threshold Layer"* is created, appearing on the *"Project Window"*.

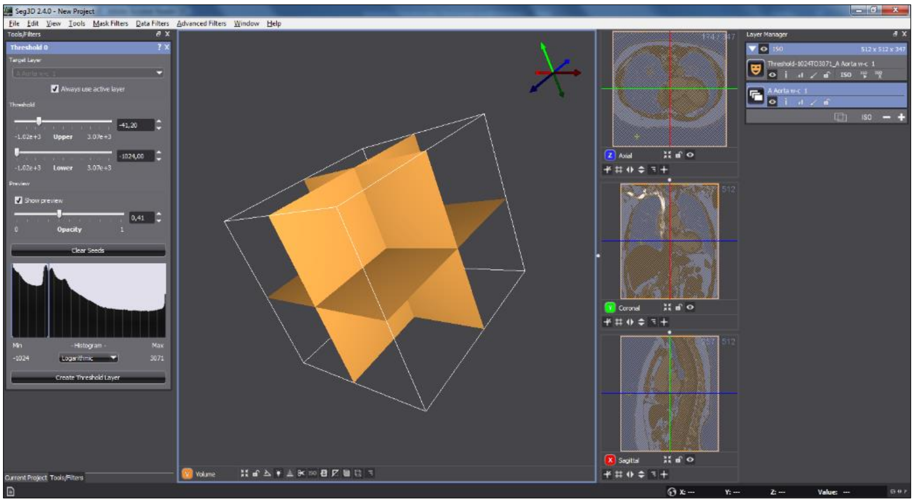

Figure 30: Seg3D, Tools/ Filters Window on the left side of the screen

- *Layer Manager Window*

The *“Layer Manager Window”*, located on the right side of the window, opens by default when Seg3D launches. Principally, it is composed of all the mask and volume files, as presented in the next figure (Figure 31) [8]. The volume file is represented by a gray icon with multiple stacked planes [8]. In this specific case, the name of the file is *“A Aorta w-c 1”*, created automatically. Although, the user can change manually the current name, by clicking and typing the intended name of the file [8]. The label masks are represented by a colored image with a mask, depicted with orange color in the following image (Figure 31) [8]. Each volume or mask labels contain separate icons associated to different tools and functions [8].

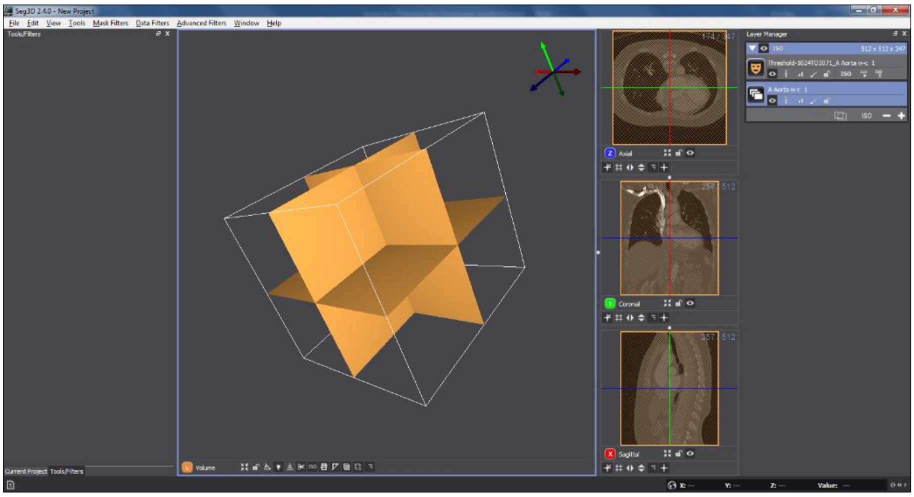

Figure 31: Seg3D, Layer Manager Window on the right side of the screen

➤ *Volume View Window*

In order to activate the *"Volume View Window"*, the user should select from the *"Window"* drop-down menu the corresponding option (Figure 32) [8]. This window is located on the right side of the Seg3D panel, replacing the *"Layer Mask Window"*, as presented in the figure below (Figure 32) [8]. This window consists of three different options for volume displaying: *"Fog"*, *"Clipping Planes"*, and *"Volume Rendering"* [8].

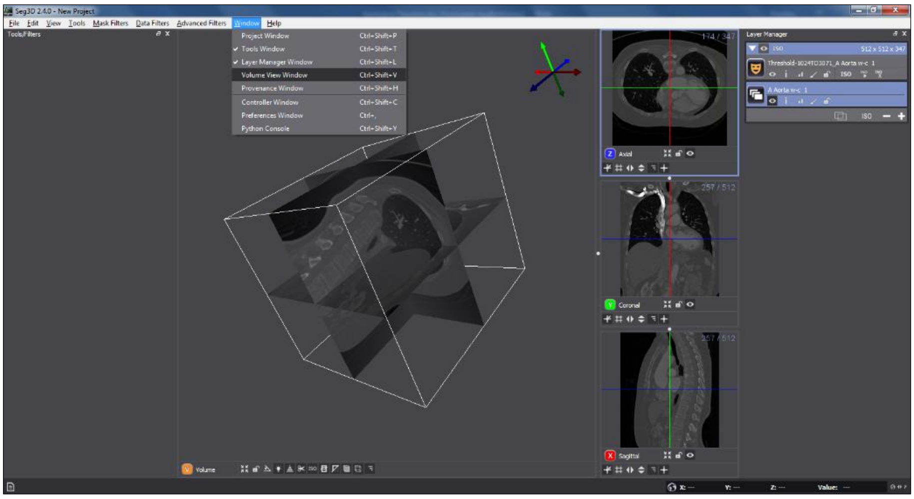

Figure 32: Seg3D, Activating Volume View Window from the drop-down menu

More specifically, the user can control the fog density from the *"Fog"* panel (Figure 33) by using the slider in the *"Volume View Window"*, and by activating at the same time the *"Show fog"* icon, illustrated with red framework in Figure 34 [8].

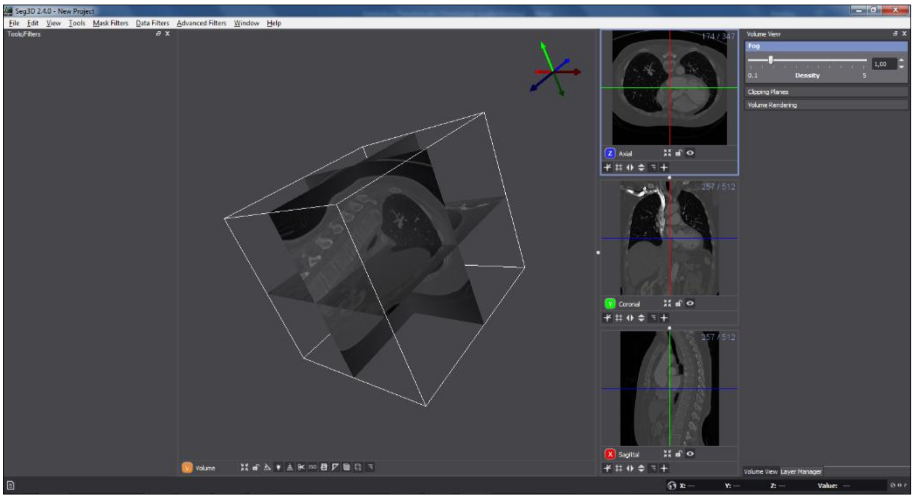

Figure 33: Seg3D, Volume View Window, Fog Panel

Figure 34: Seg3D, Volume Viewer, Show Fog Icon

Furthermore, the second available option is the *"Clipping Planes"* panel appears in the following image (Figure 35). More specifically, this option enables the user to set the limits of numerous clipping planes for the purpose of clipping the volume [8]. Respectively to the previous option (*"Fog"* panel), the user must activate the corresponding icon, representing a scissor, named *"Enable clipping"* (Figure 36) at the bottom of the 3D-viewer window [8].

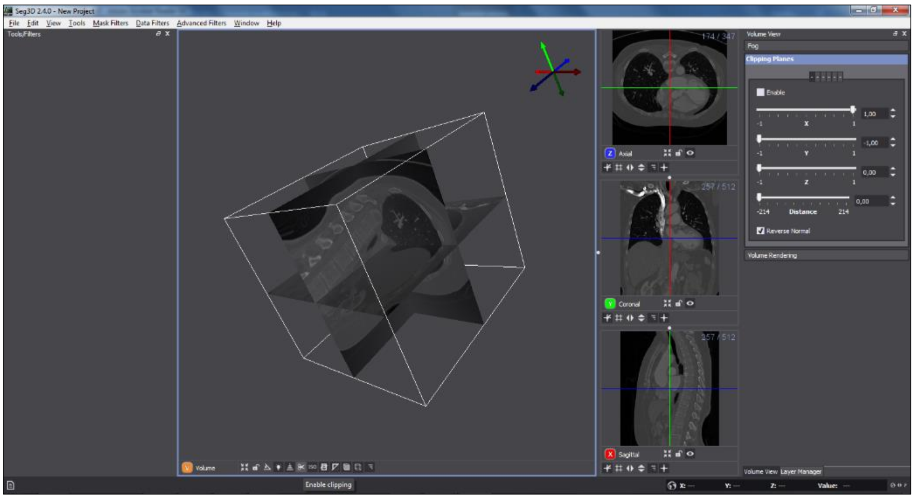

Figure 35: Seg3D, Volume View Window, Clipping Planes Panel

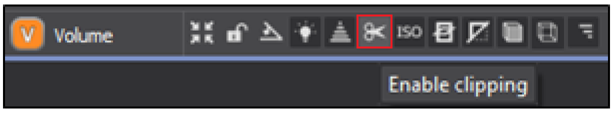

Figure 36: Seg3D, Volume Viewer, Enable Clipping Icon

The last option is the *"Volume Rendering"* panel, giving the opportunity to the user to attempt creating a volume from the volume file (Figure 37) [8]. As demonstrated in Figure 38, the user must activate the corresponding icon (Figure 38), representing a cube, named *"Show Volume Rendering"* at the bottom of the 3D-viewer window. In particular, the volume representations are generated by extracting specific values from the transfer functions [8].

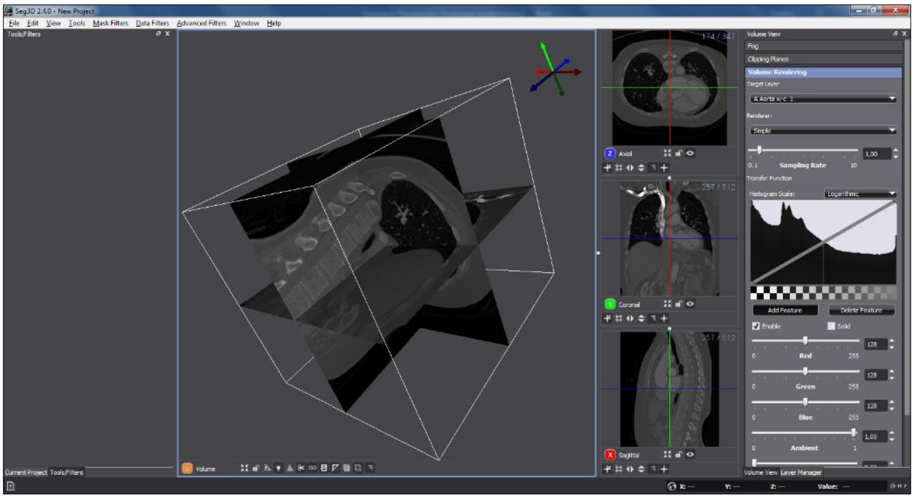

Figure 37: Seg3D, Volume View Window, Volume Rendering Panel

Figure 38: Seg3D, Volume Viewer, Show Volume Rendering

Additionally, the user must select the *"Target Layer"*, in order to obtain the desirable results. In the current case, as illustrated in the next figure (Figure 39), the selected target layer is *"A Aorta w-c 1"*. After adjusting the specifications of the *"Volume View"* and selecting the appropriate *"Target Layer"*, the user has at his disposal three options concerning the *"Renderer"* [8]. These rendering options are *"Simple"*, *"Faux Shading"*, and *"Ambient Occlusion"* [8]. In this case, the rendering option is selected to be *"Simple"*, as presented in the image below (Figure 39).

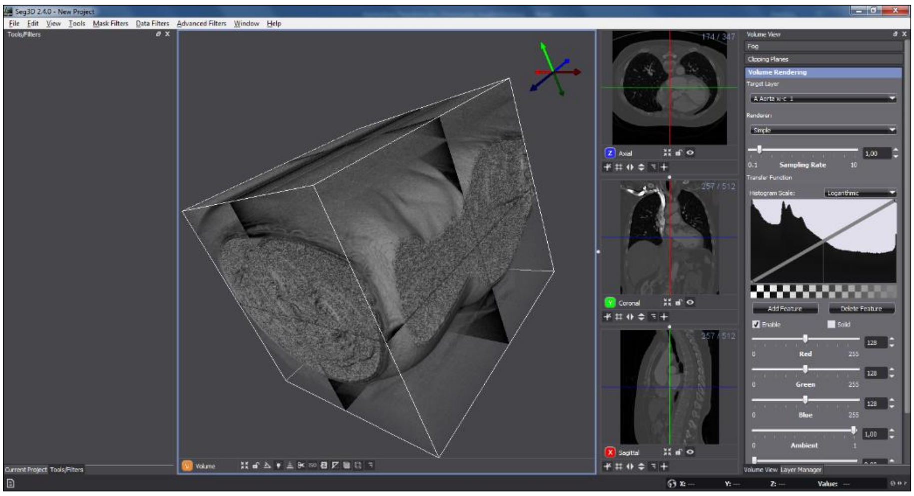

Figure 39: Seg3D, Volume View Window, Volume Rendering Panel, Adding a Feature

Finally, the last option from the *"Volume View Window"* regards the *"Transfer Function"*. As illustrated in the next figure (Figure 40), a *"Histogram Scale"* is provided to the user in order to determine the volumetric image, by selecting to *"Add a Feature"*, displayed on a *"Linear"* or on a *"Logarithmic"* scale [8]. In case of adding a feature, this appears as a line by default [8]. Though, the user can adjust this line by clicking and dragging it to the desirable position, or even by adding more points in the histogram panel [8].

Moreover, the user can choose to *"Enable"* or *"Disable"* each of the added features, and also view them as *"Solid"* or *"Graded"* slice [8]. In the current case, the *"Histogram Scale"* is selected to be *"Logarithmic"*, by adding a feature viewed as blue solid (Figure 40). Additionally, the user can define different regions, by adding more features or by adjusting the provided colors, *"Red"*, *"Green"*, and *"Blue"* [8].

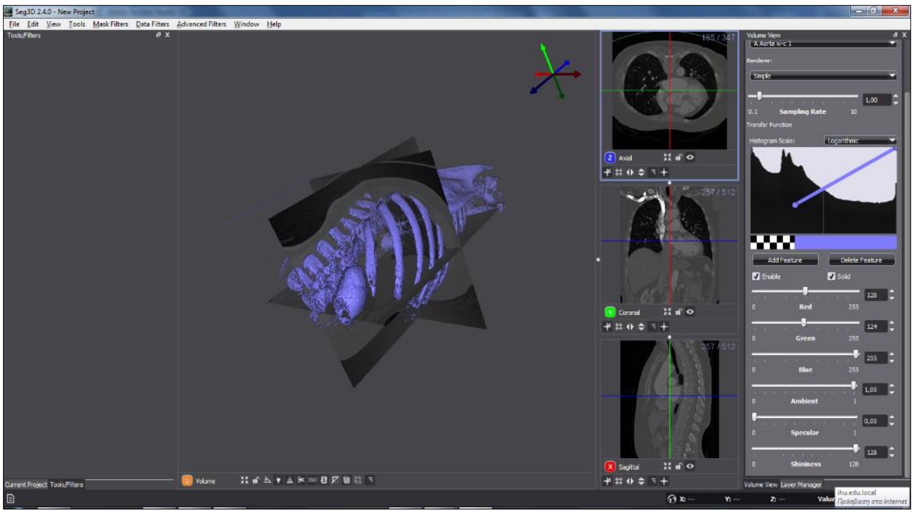

Figure 40: Seg3D, Volume View Window, Volume Rendering Panel, Adding a Feature displayed as blue

Saving a Project

After conducting the fundamental steps, as described previously, the user is supposed to save and export the final project. If the user has already defined the name and the location of the project, he can select from the drop-down menu *File → Save Project*, as illustrated in the following image (Figure 41) [8].

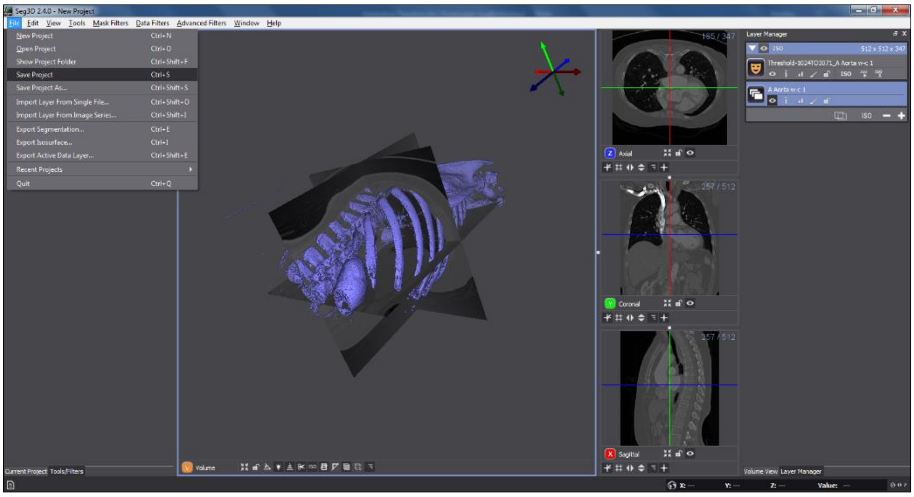

Figure 41: Seg3D, Saving a Project

Exporting Data

At last, the user can export his project. The software provides three options of exportation, namely *“Export Segmentation”*, *“Export Isosurface”*, *“Export Active Data Layer”*, appearing in the *“File”* panel from the drop-down menu [8]. With regard to this project, the third option is selected to be conducted, as demonstrated in the following figure (Figure 42). The software opens by default a window asking the user to define the location, the name and the format of the file. Various formats can be chosen, from the list presented in Figure 43, included: (nii.gz), (dcm), (mha), (mrc), (mat), (nii), (nrrd), (png), and (tiff) files [8].

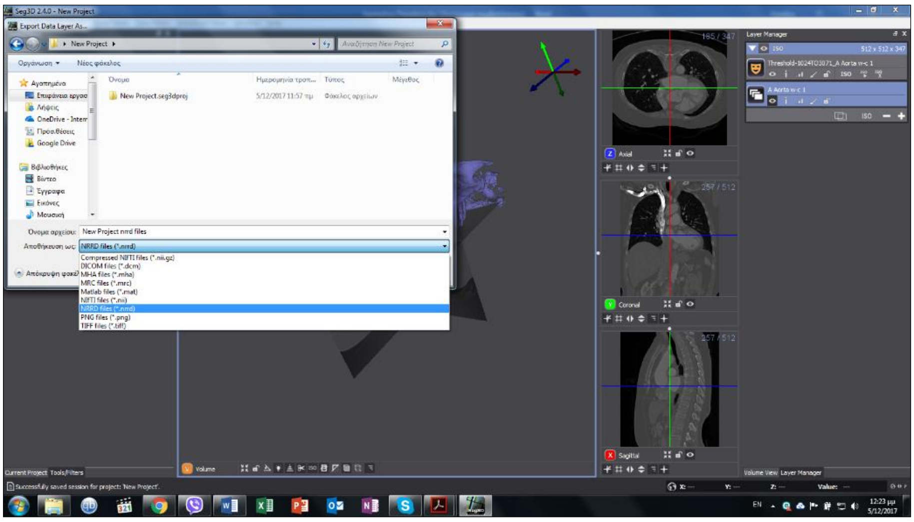

Figure 42: Seg3D, Export Active Data Layer, Selecting Format of the File

Alternatively, the user can select form the *"Layer Manager"* panel the desirable layer to be exported. The user right-clicks on the proper layer, presses the option *"Export Data As"*, and then selects the most suitable file format from the provided list illustrated below (Figure 43). For the purpose of creating an STL file, the NRRD format of the project is selected, in order to be imported in another software, named *"ImageVis3D"*. The process of utilizing this software is introduced as follows (Section 4.2.2.).

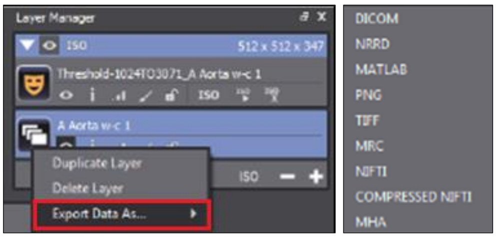

Figure 43: Seg3D, Export Active Data Layer, Selecting Format of the File

4.2.2. ImageVis3D Software

Introduction to ImageVis3D Software

The ImageVis3D software has been developed by the NIH CIBC at the University of Utah Scientific Computing and Imaging Institute [9], in addition to Seg3D, as described previously (Section 4.2.1.). Similarly, the ImageVis3D is an open-source volume rendering program, that furnishes several functions of unprecedented level of simplicity, scalability and interactivity [9].

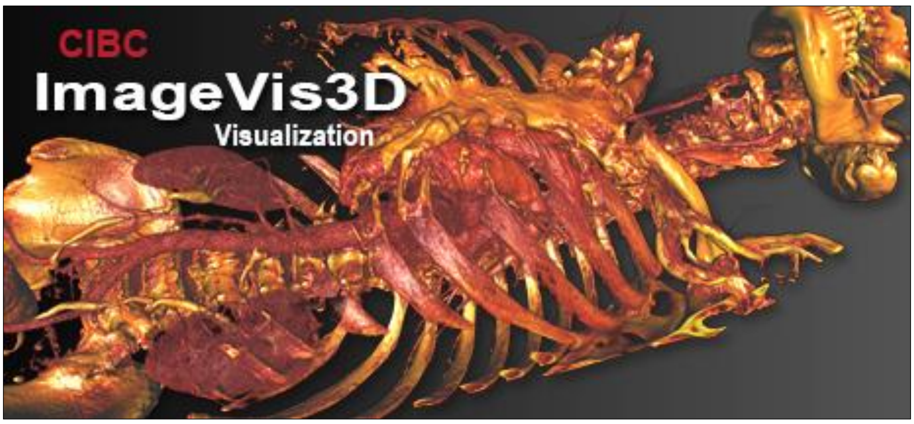

Figure 44: Image3D Software developed by the NIH CIBC at the University of Utah SCI Institute, Source: [9]

Basic Program Functions

Specifically, in order to acquaint the basic functions of ImageVis3D software, it is crucial to present a step-by-step approach of the process of the utilization of the specific software. As mentioned previously (Section 4.2.1.), a series of DICOM files of a thorax [6] has been used in order to generate a NRRD format file, by importing them to Seg3D software. The created file is used for the current case in order to examine the use of ImageVis3D software.

Welcome Screen

In the next figure (Figure 45), the *"Welcome Screen"* of ImageVis3D is demonstrated. This screen opens-up by default, displaying the principal available options [10]. The provided options, for the purpose of starting and continuing a project in ImageVis3D, are divided into two categories: *"Open a File"* and *"Get Help"*.

As regards the first category of opening a file, the software displays on the left side of the screen the following options, *"Open Data Set from File"* and *"Open Data Set from a Directory"*, or a list of the names of recently accessed projects (Figure 45, left side, on the bottom) [11]. On the right side of the screen, appear the following options: *"Open Local Manual"*, *"Go to Online Help"*, *"Go to Online Video Tutorials"*, and *"Download Example Data Sets"* [11]. The same options can be found on the *"File"* drop-down menu [11].

Figure 45: ImageVis3D, Welcome Screen

Loading Dataset from a File

In order to launch a project, the user should select the appropriate option from the *"Welcome Screen"*, or alternatively from *"File"* panel of the drop-down menu [11]. Generally, the ImageVis3D enables the user to convert and store all the data sets in Universal Volume Format (UVF) [11]. In case the user has already created a UVF file, it is recommended to go to the drop-down menu and select *File → Load Dataset from File*, as displayed in the next figure (Figure 46) [11].

Nevertheless, very frequently the data set is not saved in this type of format (UVF) [11]. For this reason, the ImageVis3D prompts the user to convert it in first place to UVF format and then continue processing the next steps [11].

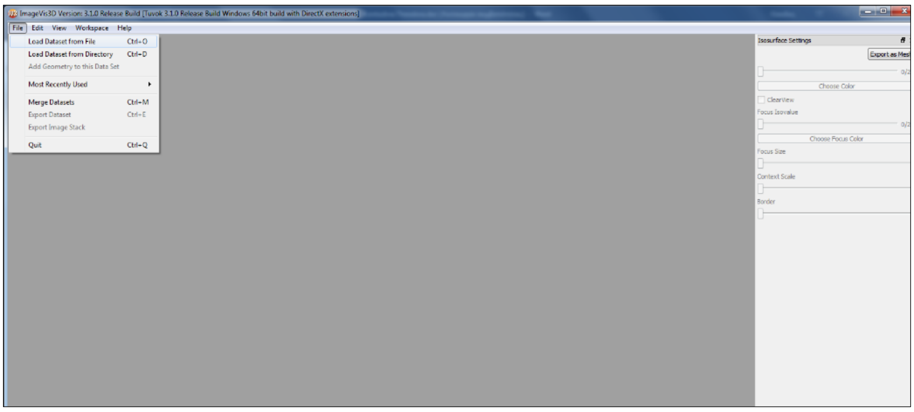

Figure 46: ImageVis3D, Loading Dataset from File, drop-down menu

Importing Data from a Single File (or from a Stack of Files)

In the following images (Figures 47-50), is demonstrated the process of loading dataset from a foreign file format. ImageVis3D software detects by default if the selected file is not a UVF [11]. In that case, the software automatically selects the most suitable converter to import the file formats described in detail in the following table (Table 2) [11].

Furthermore, ImageVis3D software supports two main types of conversion, *"From a Single-file Dataset"* (e.g. NRRD of RAW files) and *"From a Stack of Files"* (e.g. DICOM files or set of slice images) [11]. The user is supposed to select the appropriate option and proceed to the next step of the procedure [11].

Table 2: List of File Formats compatible with ImageVis3D Software, Source: [11]

File Formats	
***.dat**	QVis Data (including RGBA and float extensions)
***.nrrd & *.nhdr**	Nearly Raw Raster Data
***.stk**	Metamorph STK Volumes
***.tiff & *.tif**	TIFF Stack Volumes
***vff**	Visualization File Format
***.bov**	VisIt Brick of Values
***.rek**	Fraunhofer EZRT
.	Any Raw Data (text & binary encoding, zipped, bzipped

After selecting the desirable file (Figure 47), the software opens by default a window (Figure 48) asking for a file name, in order to convert the target dataset to UVF file and subsequently save it to a selected location. Next ImageVis3D processes the file (Figure 49), by pre-computing derived quantities of data and by storing the converted data into the UVF file and finally loads the created UVF file (Figure 50) [11].

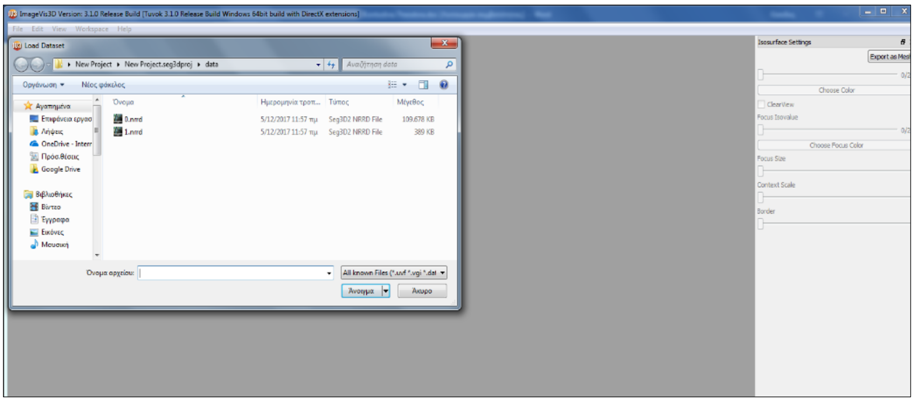

Figure 47: ImageVis3D, Loading Dataset from File, Selecting a NRRD File Dataset

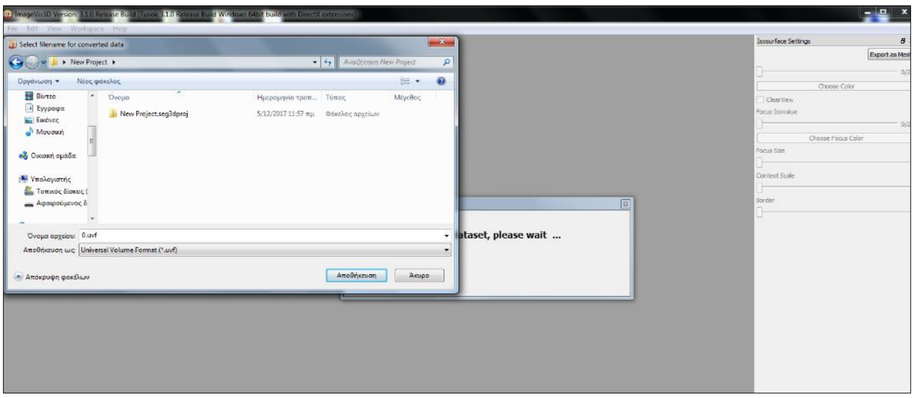

Figure 48: ImageVis3D, Converting the Target Dataset to UVF File

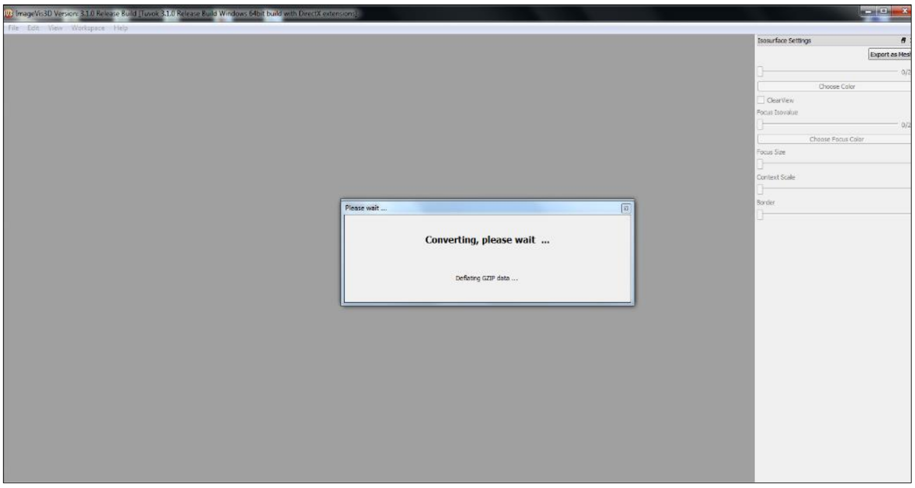

Figure 49: ImageVis3D, Converting and Storing the Target Dataset to UVF File

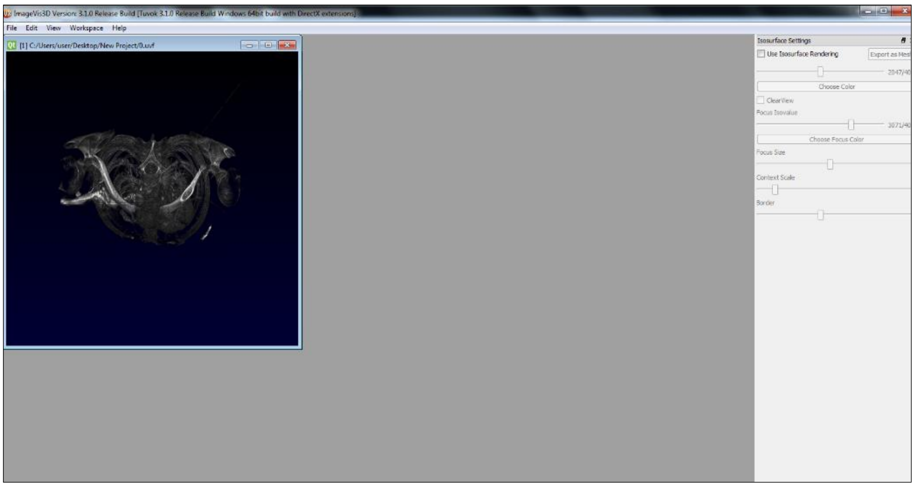

Figure 50: ImageVis3D, Loading the Created UVF File

ImageVis3D enables the user to interact with the created file. Particularly, the user can adjust the view parameters (e.g. rotation, zooming etc.) or the rendering parameters (e.g. transfer function or isosurface settings) [11]. The principal interacting tool is the mouse [11]. The user can click and drag the left mouse button, in order to rotate the generated dataset [11]. Secondly, by dragging the right mouse button the created dataset moves within the render window to the desired location [11]. At last, the rotation of mouse wheel forwards and backwards is convenient for the zooming [11].

In the following images (Figures 51-52) are illustrated different views of the same dataset by rotating it, using the appropriate tools as described previously.

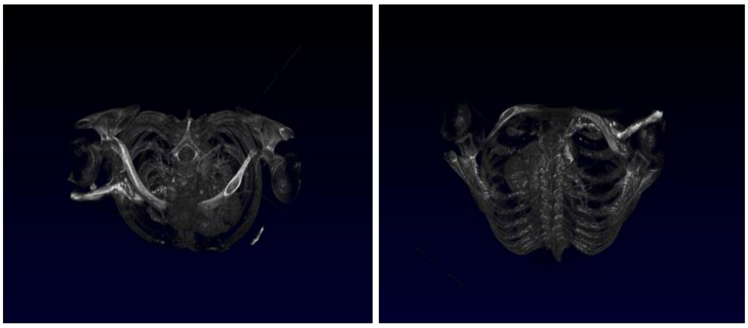

Figure 51: ImageVis3D, Loading the Created UVF File, Different Views

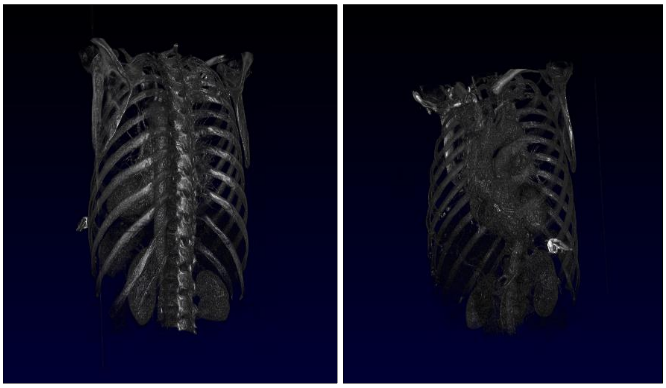

Figure 52: ImageVis3D, Loading the Created UVF File, Different Views

Exporting Data

Finally, the user is supposed to export the created UVF files into external formats. The ImageVis3D provides two different options of exportation, *“Exporting Volumetric Data”*, or *“Exporting Mesh Data from an Iso-Surface”* [11].

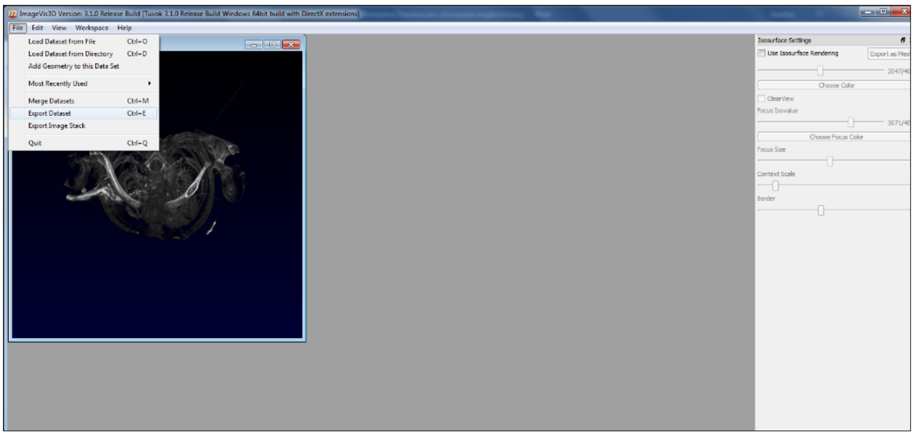

Figure 53: ImageVis3D, Exporting Volumetric Data, Exporting Dataset, drop-down menu

In more detail, as regards the first option (i.e. *"Exporting Volumetric Data"*), the user should select from the drop-down menu, *File→ Export Dataset* (Figure 53), and then select the location, the name, and the file type of the target file (Figure 54) [11]. The software provides a remarkable amount of file types, as displayed on the list below (Figure 54) [11]. In case the dataset is small enough, the software will export it instantaneously [11]. Otherwise, a *"LOD Level"* dialog window appears (Figure 55) requesting to select among the recommended types of resolution [11].

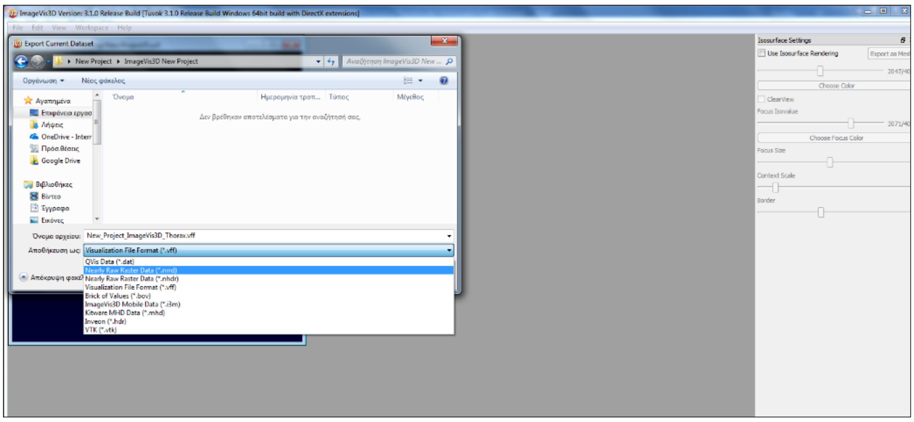

Figure 54: ImageVis3D, Exporting Volumetric Data, Selecting the Target Filename, the Location to be saved, and the File Type

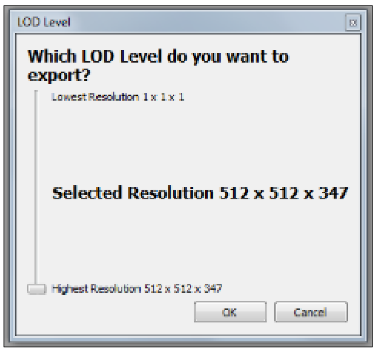

Figure 55: ImageVis3D, Exporting Volumetric Data, LOD Level Window, Selecting the desirable Resolution

Furthermore, in the matter of the second option of exportation (i.e. *"Exporting Mesh Data from an Iso-Surface"*), the user can select to export a triangle mesh representing an iso-surface, for a given iso-value [11]. The user should select from the *"Workplace"* panel, from the drop-down menu, to enable the *"Isosurface Settings"*, as presented in the following image (Figure 56) [11].

From this window, appearing on the right side of the screen (Figure 56), the user should check the option *“Use Isosurface Rendering”*, select the most suitable iso-value, and then press on the *“Export as Mesh”* button, appearing on the right side of the screen on the *“Isosurface Settings”* panel (Figure 57) [11]. At last, the software prompts the user to choose the location, the name, and the file type of the target mesh [11]. Similarly to volumetric data exportation, a *“LOD Level”* dialog window appears (Figure 58), requesting to select among the recommended types of resolution [11].

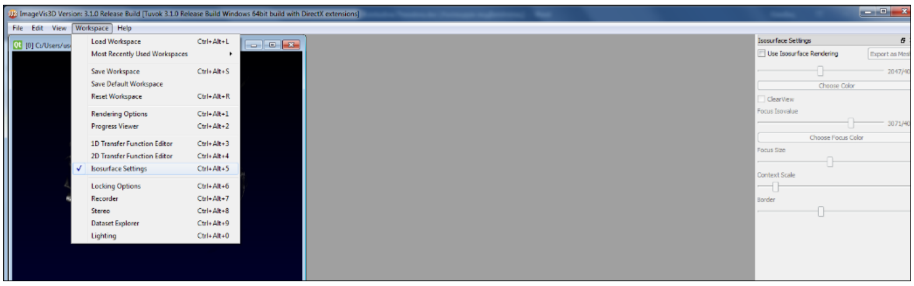

Figure 56: ImageVis3D, Enabling Isosurface Settings, drop-down menu

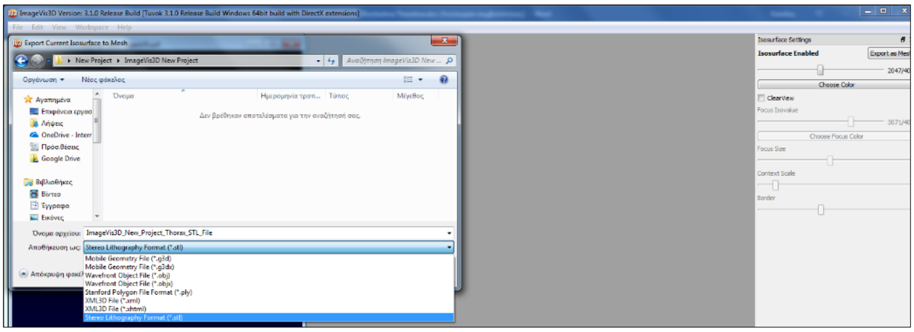

Figure 57: ImageVis3D, Exporting Mesh Data from an Iso-Surface, Selecting the Target Filename, the Location to be saved, and the File Type of the Mesh

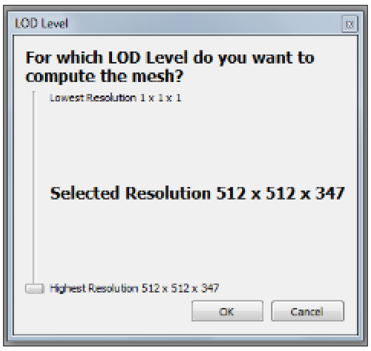

Figure 58: ImageVis3D, Exporting Mesh Data from an Iso-Surface, LOD Level Window, Selecting the desirable Resolution

4.2.3. 3DSlicer Software

Introduction to 3DSlicer Software

3DSlicer has been developed with the help of several contributions from the NIH and an international community of scientists from various scientific fields, mainly including engineering and bio-medicine (Federov *et al*., 2012) [12-13].

Notably, 3DSlicer is a multi-software platform facilitating the analysis and the visualization of medical images (Federov *et al*., 2012) [12]. In specific, it is an open-source software package for medical imaging computing, available in three different operating systems (i.e. Windows, MacOSX, and Linux) (Federov *et al*., 2012). As a medical tool, 3DSlicer provides various functions, mainly including medical image informatics, image processing and analysis (i.e. registration and segmentation), and three-dimensional visualization (i.e. volume rendering) (Federov *et al*., 2012) [12-14].

Figure 59: 3DSlicer Software, Source: [12]

Basic Program Functions

Particularly, for the acquaintance of the basic functions of 3DSlicer software, it is critical to present a step-by-step demonstration of the process of the utilization of this software. As mentioned in the two previous sections (Sections 4.2.1.-4.2.2.), a series of DICOM files of a thorax [6] is used in order to create a new project, likewise for the current case, the same series of DICOM files are used as well.

Welcome Screen

In the next figure (Figure 60) is illustrated the *"Welcome Screen"* of 3DSlicer software, providing the user with various tools and features on the left side of the screen [15]. Depending on the tools needed to be used, the user can select the appropriate module from the top toolbar. The provided options for the initial (*"Welcome to Slicer"* module) are: *"Load DICOM Data"*, *"Load Data"*, *"Install Slicer Extensions"*, *"Download Sample Data"*, *"Customize Slicer"*, and *"Explore Loaded Data"* [15].

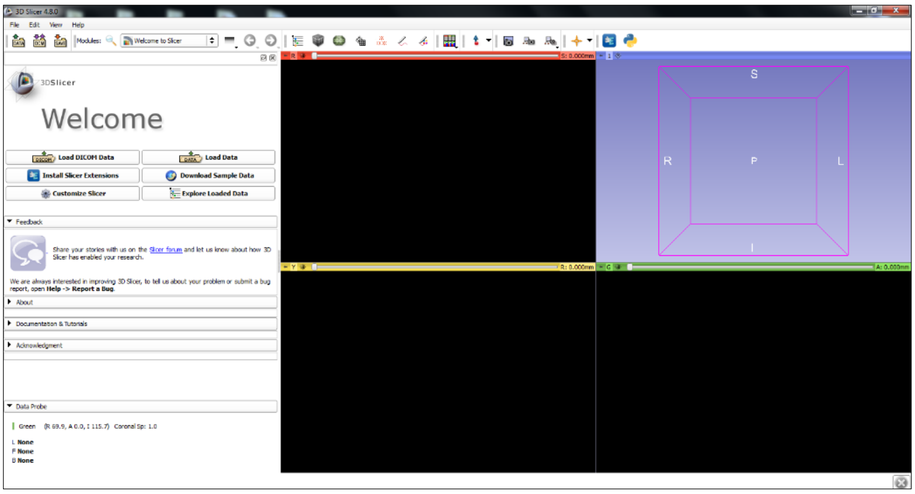

Figure 60: 3DSlicer, Welcome Screen

Loading Data

In order to launch a project, the user should select the option *"Load DICOM Data"* from the welcome screen, as presented in the figure above (Figure 60) [15]. Subsequently, the software opens a dialog box by default asking the user to select the DICOM files from a specific directory and press the *"Import"* button (Figure 61) [15]. Alternatively, the user can drag-and-drop the folder of DICOM files into the window of the software. After importing the suitable files, the module automatically changes to the *"DICOM"* module, as illustrated in the following image (Figure 61) [15]. The *"DICOM Browser"* window opens-up, demonstrating initially the process of uploading the data into the software. Once this upload is complete, another dialog box appears giving a summary of the information of the loaded data (Figure 62) [15].

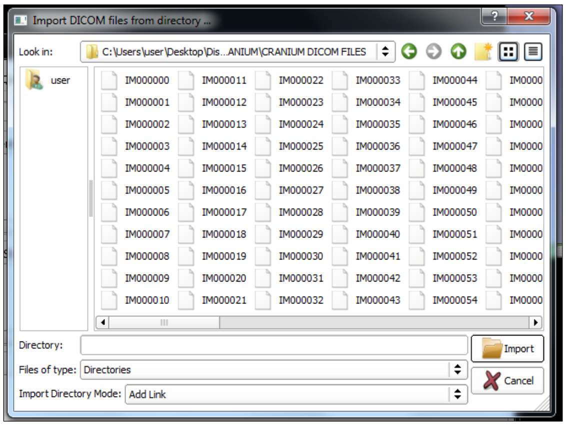

Figure 61: 3DSlicer, Importing DICOM Data from Directory

In particular, Figure 62 demonstrates the information, appearing on the *"DICOM Browser"*, concerning the new case study of a specific patient (Patient, Study, Series) [16]. The user should click on this case study, and then press the *"Load"* button on the left-down corner (Figure 62) [16].

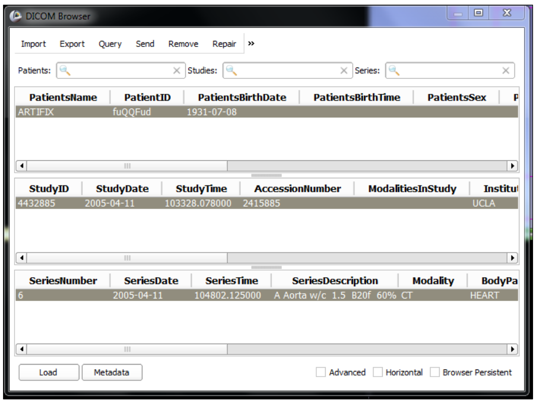

Figure 62: 3DSlicer, Importing DICOM Data, DICOM Browser

After loading the desirable data into 3DSlicer software, the user is able to see, on the right side of the interface (Figure 63), the results of the loaded data in various views [17]. Mainly, the loaded data are depicted in four different windows (i.e. Axial, Sagittal, Coronal and Volume) [17].

In this specific case, the layout is selected to be *"Four-Up"* from the toolbar, as presented in the next figure (Figure 63) [17]. For the purpose of seeing the data more conveniently, the user can interfere by changing the window leveling, regarding the brightness or the contrast of the data, or by zooming in or out [17].

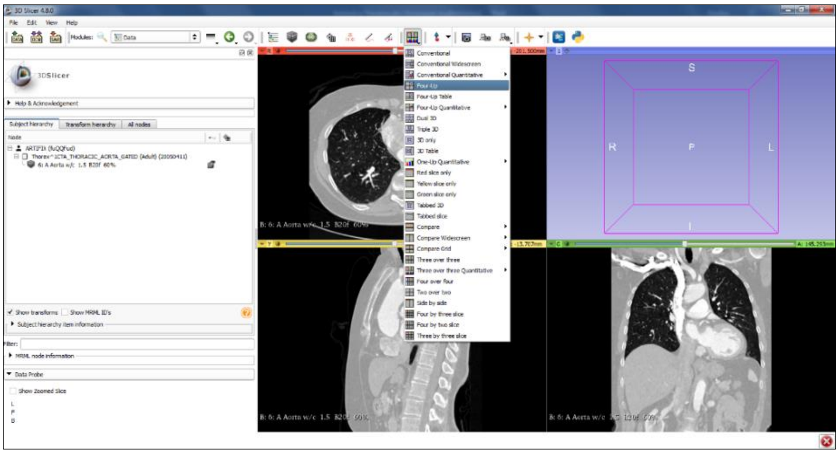

Figure 63: 3DSlicer, DICOM, Four-Up View

Crop and Volume Rendering

➢ *Volume Rendering Module*

Additionally, from the list of modules the user can choose the *"Volume Rendering"*, as being on the core modules in the drop-down menu [18]. Otherwise, it is suggested to load the full list of the modules (*"All Modules"*) and search this module, as depicted in the next figure (Figure 64) [18].

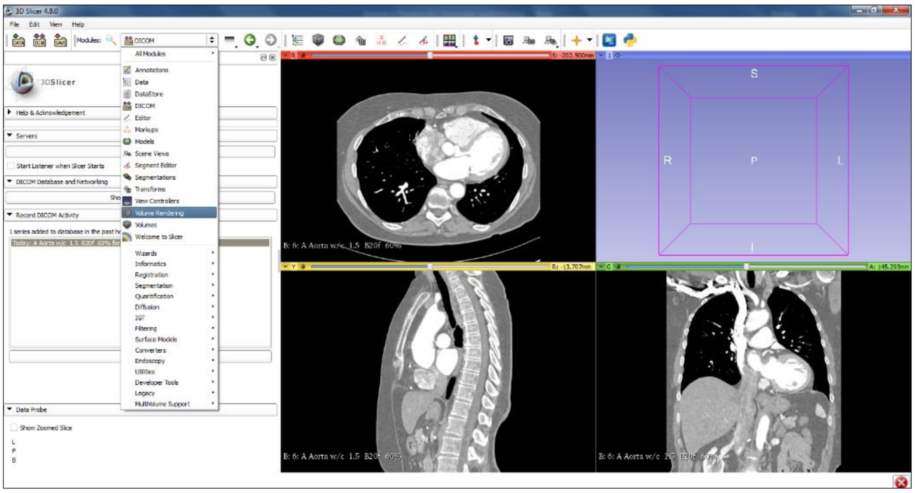

Figure 64: 3DSlicer, Volume Rendering, List of Core Modules

The left side of the interface changes, demonstrating the available options regarding this module [18]. As presented in the figure below (Figure 65), the first option regards the volume to be rendered.

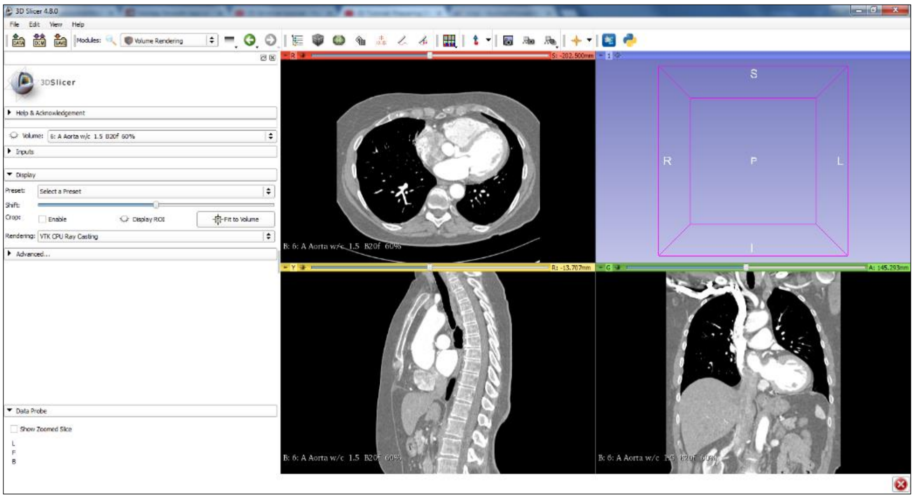

Figure 65: 3DSlicer, Volume Rendering Module

Specifically, in the current case there is only one case provided, named *"6: A Aorta w/c 1.5 B20f 60%"*. The user should turn on the *"Volume Rendering"*, by clicking the eye icon (Figure 66), in order to load the volume of the selected data [18]. The Volume Rendering appears on the left side of the interface on the left-up view of the window (Volume Window), as illustrated in Figure 67 [18].

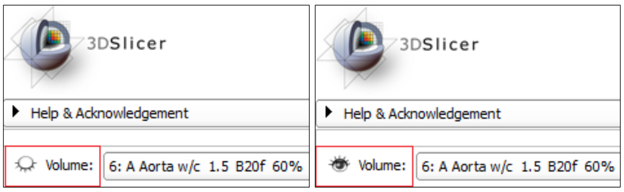

Figure 66: 3DSlicer, Volume Rendering Module, Turning on the Volume Rendering

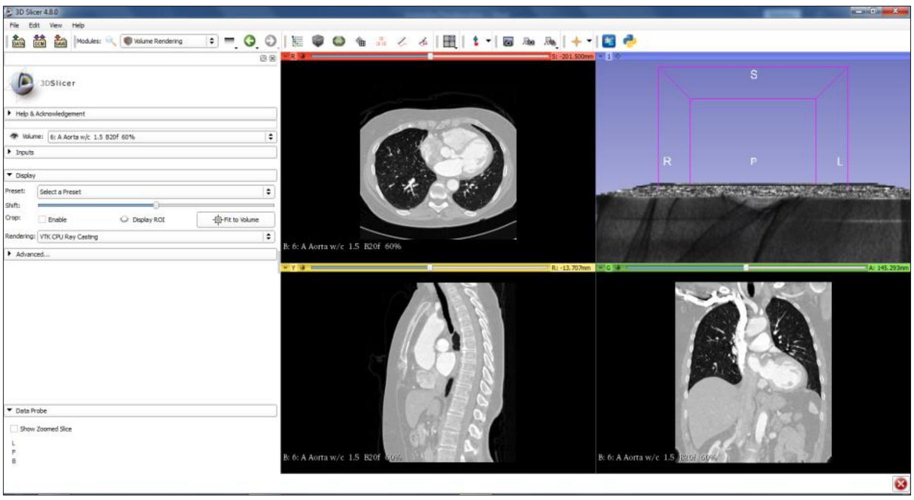

Figure 67: 3DSlicer, Volume Rendering Module, Illustration in Volume Window

Furthermore, the user should adjust the created volume on the *"Volume Window"*. In order to center the 3D-volume on the framework (depicted in magenta color in Figure 67), the user should press the corresponding button, named *"Center the 3D view on the scene"*, depicted with red framework in the next figure (Figure 68) [18]. Otherwise, there is a shortcut of this option demonstrating the same icon (Figure 68).

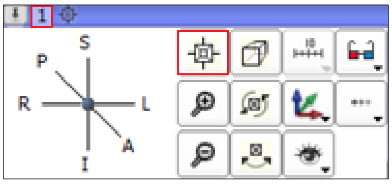

Figure 68: 3DSlicer, Volume Rendering Module, Center the 3D view on the scene

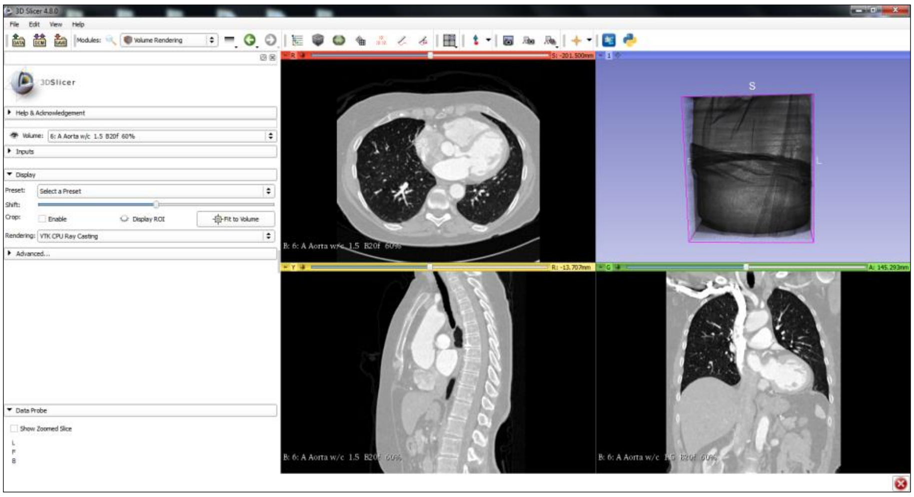

Figure 69: 3DSlicer, Volume Rendering

Afterwards, from the *"Display"* tab, the user can adjust the current volume rendering properties from the provided options [18]. Particularly, in order to see the bones in the volume rendering, the user is prompted to use one of the *"Presets"* listed in the corresponding menu (Figures 70-71), which are specifically thresholded and colorized for the convenience of visualization of different aspects of data [18]. In specific, the software provides twenty-five presets of visualization, as illustrated in the following figure (Figure 70).

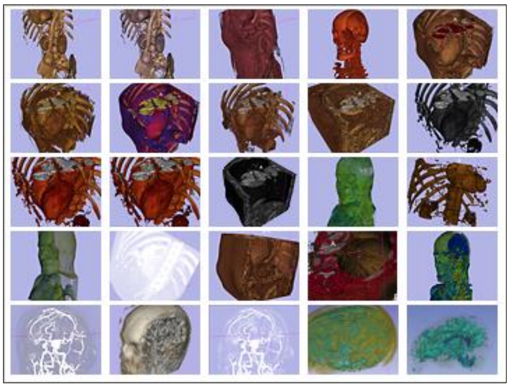

Figure 70: 3DSlicer, Volume Rendering, Display Properties, Selecting a Preset

Indicatively, in the current case, the *“CT-Bones”* preset is selected, as being the most appropriate for visualizing the bones of the volume dataset. The figure below (Figure 71) presents the result of the selected preset, demonstrating the 3D-volume on the corresponding window.

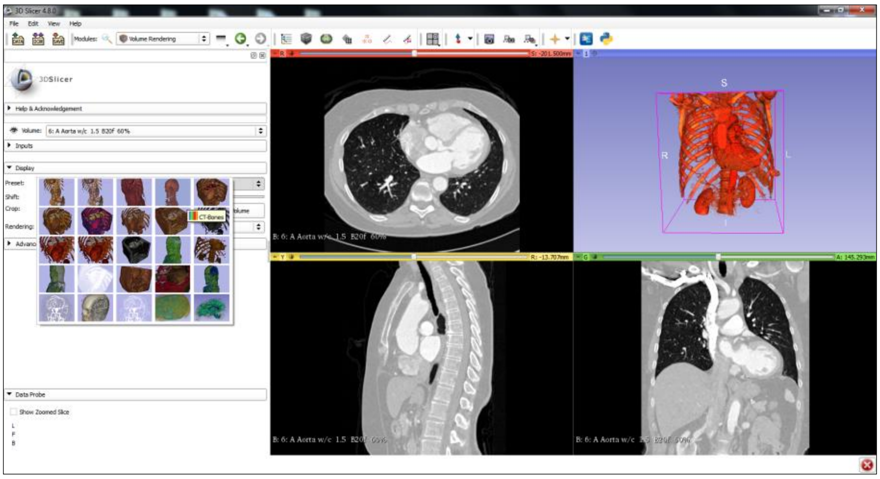

Figure 71: 3DSlicer, Volume Rendering, Display Properties, Selecting a Preset, CT-Bones

In the figure above (Figure 71), a little bit of obstruction can be observed to the volume view [18]. Therefore, from the *“Display”* tab, the *“Shift”* property enables the user to adjust the inner points, by increasing or decreasing the value of the ramp as depicted in the next figure (Figure 72) [18].

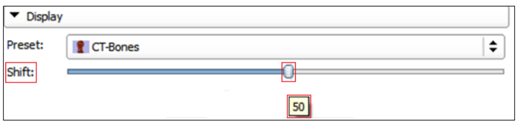

Figure 72: 3DSlicer, Volume Rendering, Display Properties, Shift Value: 50

In the current case, the result of increasing the *"Shift"* value up to 50 (Figure 72), is shown in the following figure (Figure 73), in the Volume Window.

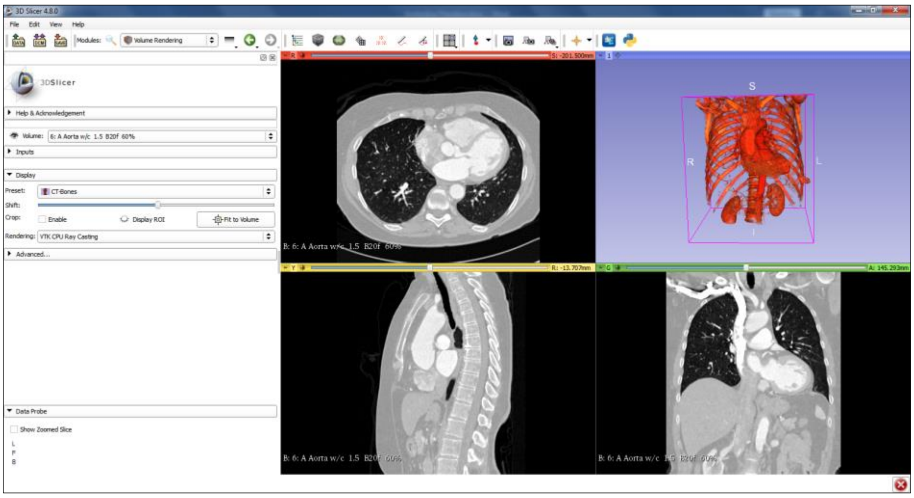

Figure 73: 3DSlicer, Volume Rendering, Display Properties, Shift Value: 50

The next property of the *"Display"* tab, regards the crop. The software provides the option of enabling or disabling the crop in the volume rendering module, by checking the corresponding option (Figure 74) [18].

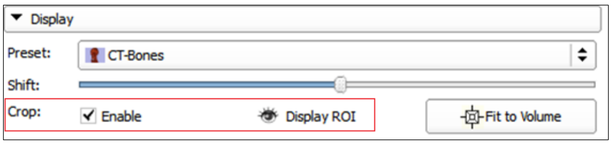

Figure 74: 3DSlicer, Volume Rendering, Display Properties, Crop and ROI framework

Additionally, the user can adjust the ROI (Region of Interest) framework, by activating the corresponding icon *"Display ROI"* (Figures 74) [18]. After activating this option, automatically, the ROI framework appears on the four views, illustrated in white framework with various colorful spots, in order to recognize and adjust the desired region of interest (Figure 75) [18].

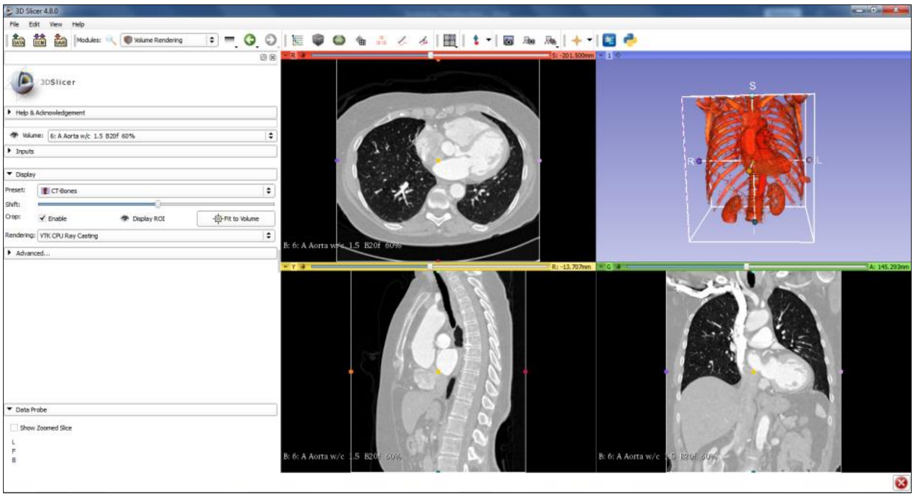

Figure 75: 3DSlicer, Volume Rendering, Display Properties, Crop and ROI Framework

In particular, the whole volume is included in the ROI framework by default (Figure 75), although as the user is shrinking the ROI framework, the crop is visible in the volume rendering in real time, illustrated in the next figure (Figure 76) [18]. In this particular case (Figure 76), the left side of the thorax is selected as the region of interest that will be examined.

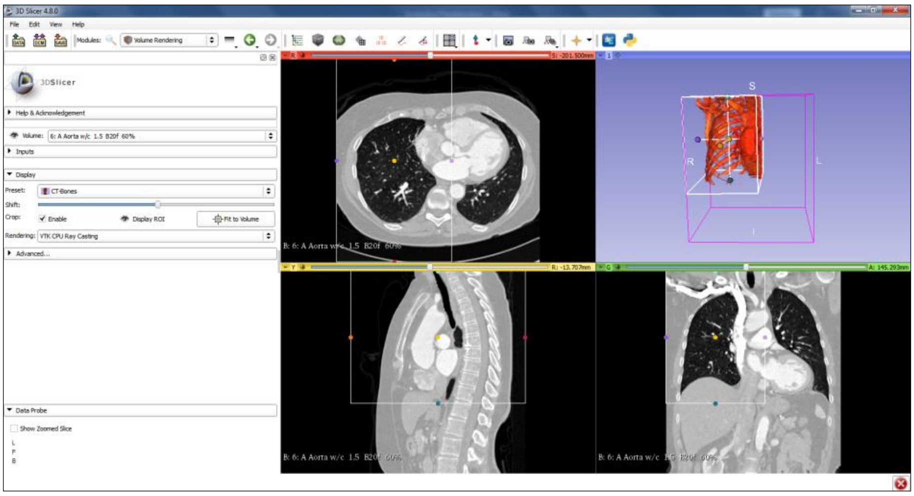

Figure 76: 3DSlicer, Volume Rendering, Display Properties, Adjusting the ROI framework

- *Crop Volume Module*

In the previous image (Figure 76), the creation of an ROI framework is demonstrated, containing the sub-volume of interest. By revealing the *"Inputs"* tab of *"Volume*

Rendering" module (Figure 77), the software allows the user to interact with a list of nodes required for *"Volume Rendering"* [18].

More precisely, this list contains the following four parameters: *"Display"*, *"ROI"*, *"Property"*, and *"View"*, shown in the figure below (Figure 77) [18].

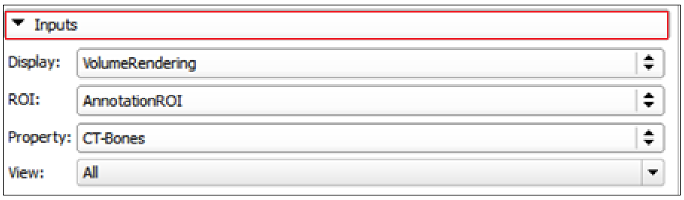

Figure 77: 3DSlicer, Volume Rendering, Inputs Parameters

Particularly, the user can select the current volume to render *("Display"* option), the created ROI (*"ROI"* option), the volume properties (i.e. opacity, color, gradient transfer functions) (*"Property"* option), and the 3D-views to be displayed respectively (*"View"* option) [18].

Regarding the current case, the selections of these parameters are depicted in the figures above (Figure 77) and below (Figure 78).

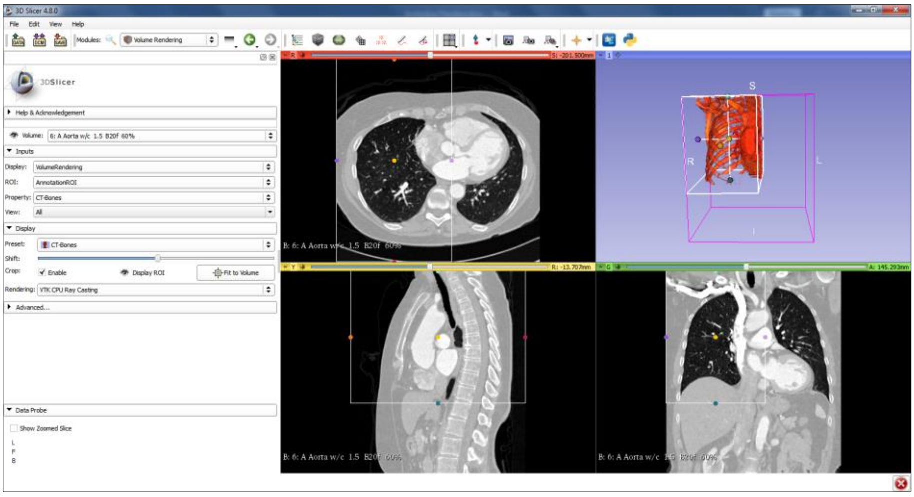

Figure 78: 3DSlicer, Volume Rendering, Inputs Parameters

Moreover, it is recommended that the user load the *"Crop Volume"* module, by activating the full list of modules from the drop-down menu, as demonstrated in the following figure (Figure 79) [18].

Figure 79: 3DSlicer, Crop Volume Module, Drop-down Menu

Furthermore, the interface of the *"Crop Volume"* module is illustrated in the following figure (Figure 80), displaying the required information of the created project [18]. In more detail, the *"Input Volume"* is selected to be the current volume and correspondingly the *"Input ROI*" is selected to be the ROI volume, as shown in Figure 81 [18].

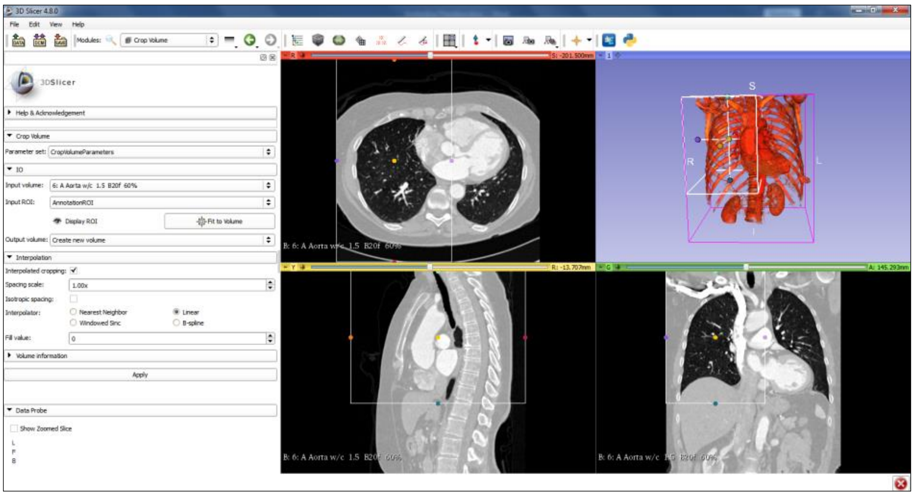

Figure 80: 3DSlicer, Crop Volume Module

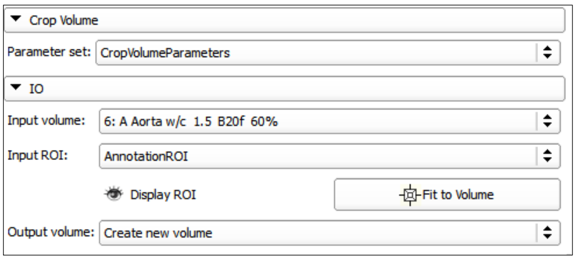

Figure 81: 3DSlicer, Crop Volume Module, Input Volume and Input ROI

In order to proceed to cropping the current volume, the user should press the *"Apply"* button, depicted with red framework in Figure 82 [18]. After applying this module, the software automatically creates a new volume, that contains only the defined region of interest (Figure 83) [18]. As it can be observed in Figure 83, the ROI volume is depicted in the four different windows (*"Axial"*, *"Sagittal"*, *"Coronal"*, and *"Volume"*).

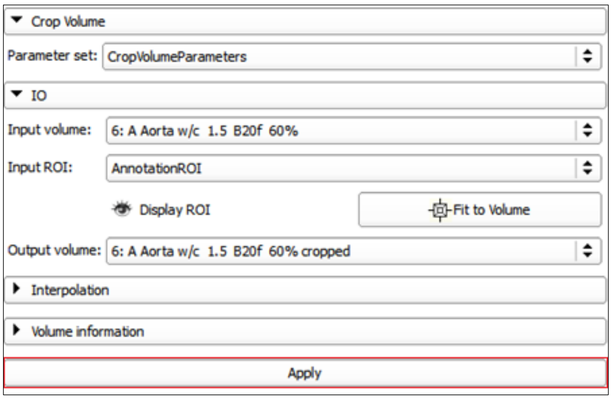

Figure 82: 3DSlicer, Crop Volume Module, Apply button

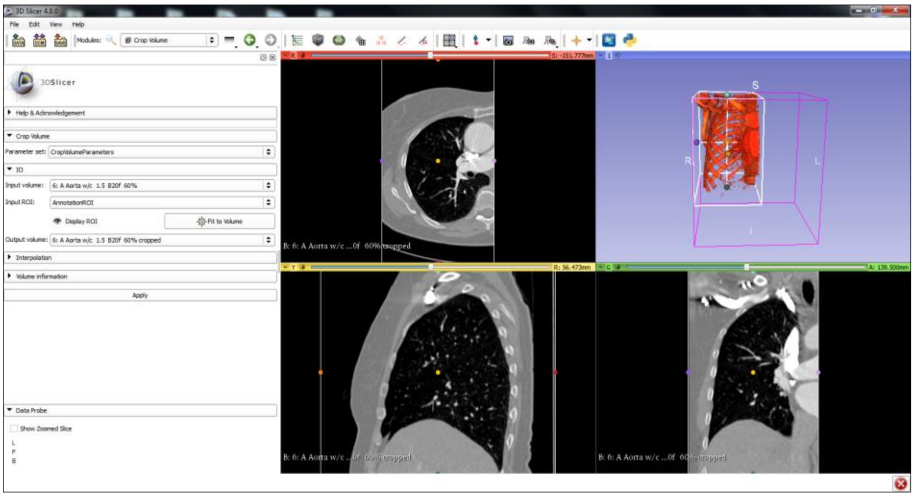

Figure 83: 3DSlicer, Crop Volume Module, ROI

Creating Label Model

- ➢ *Editor*

Before proceeding to the next step, it is advisable to disable the visibility of the data created previously, in order to deal with less information [19]. The user is prompted to turn-off the visibility of the Volume, in the *"Volume Rendering"* module (Figure 84), and of the ROI (Figure 85), in the *"Crop Volume"* module as well [19].

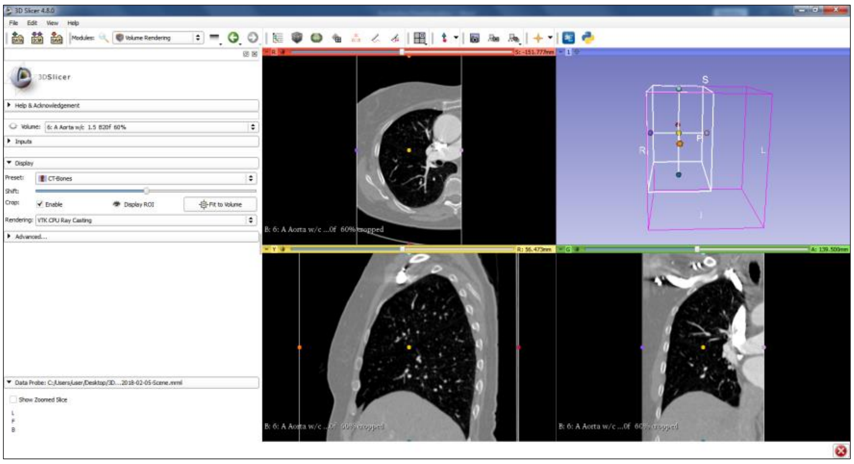

Figure 84: 3DSlicer, Volume Rendering Module, Disabling the Visibility of the Volume

Regarding the next step of creating a label model, the software enables the user to define specific structures within their volumes in a highly precise and efficient way [19].

In order to achieve this manual segmentation of volumes, the user is supposed to create a *"Label Map Volume"*, by utilizing the *"Editor"* module from the drop-down menu, as demonstrated in the Figure 86 [19]. More precisely, the *"Label Map Volume"* is a 3D-scalar volume node, in which each voxel is a number that indicates the type of tissue at that location. Additionally, the label volume is related to a color node, mapping the numbers into colors and text strings [19].

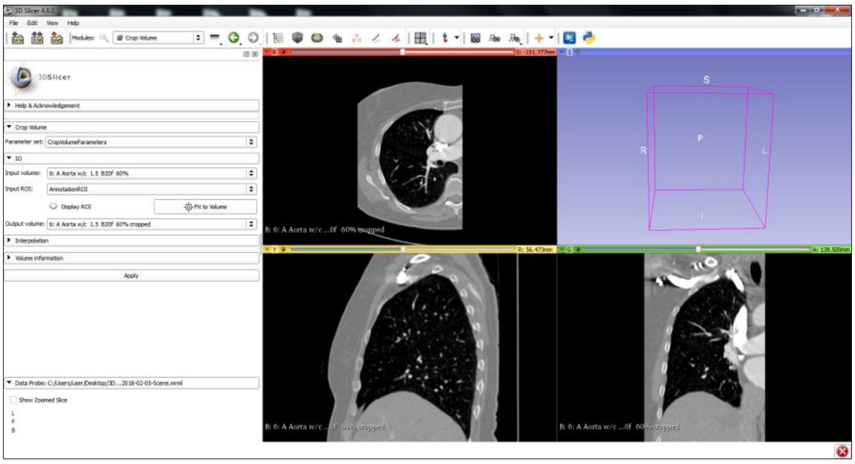

Figure 85: 3DSlicer, Crop Volume Module, Disabling the Visibility of the ROI

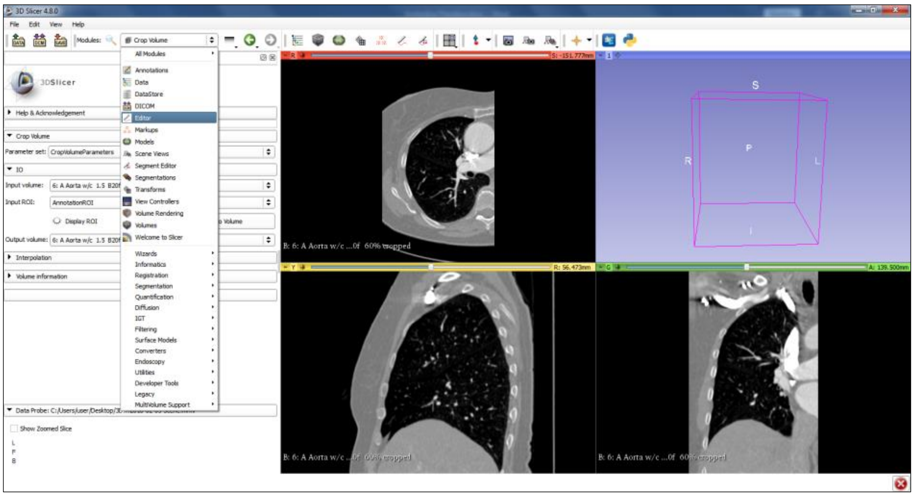

Figure 86: 3DSlicer, Creating Label Model, Editor Module, Drop-down Menu

After loading the *“Editor”* module, the software automatically opens a dialog box asking whether the user wants to create a merge label map for the selected master volume (Figure 87) [19]. As depicted in the next figure (Figure 87), the color of the table node, is selected to be *“Generic Anatomy Colors”*.

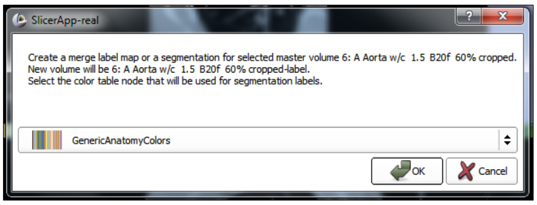

Figure 87: 3DSlicer, Creating Label Model, Editor Module, Generic Anatomy Colors

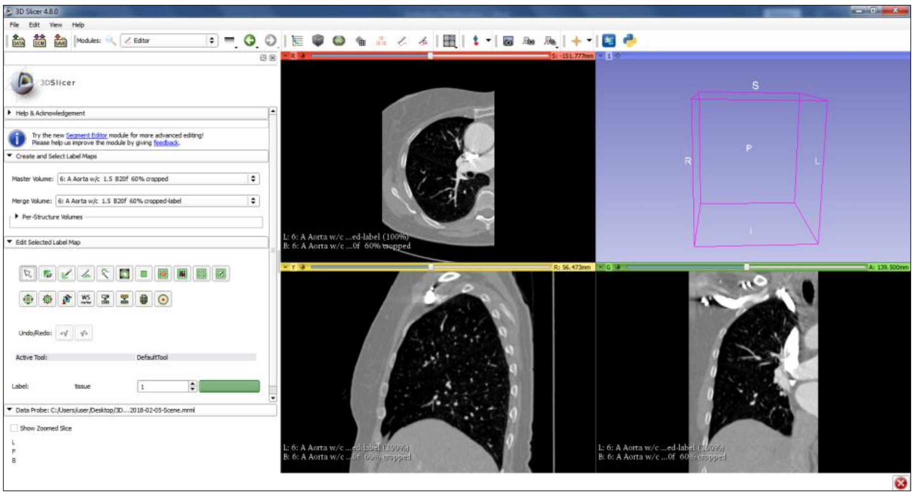

Figure 88: 3DSlicer, Creating Label Model, Editor Module

Furthermore, the *"Editor"* module provides a number of tools for manipulating a label map volume, as demonstrated in the figure above (Figure 88) [19]. The created master volume is the sub-volume created previously by cropping the initial volume (Figure 88) [19]. Subsequently, in the *"Edit Selected Label Map"* tab, the user should choose the appropriate label value, by clicking on the color swatch (depicted with red framework in Figure 89). This swatch comprises a full list of the available labels (Figure 90) [19]. Alternatively, the user can search the name of the label on the corresponding *"Search"* bar (Figure 90) [19].

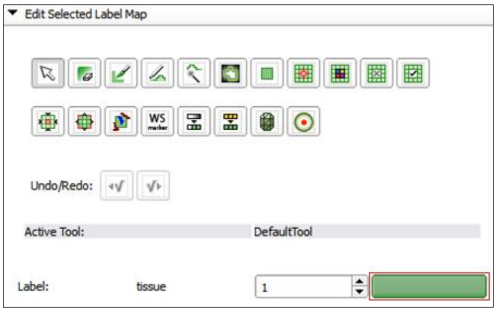

Figure 89: 3DSlicer, Creating Label Model, Editor Module, Color swatch

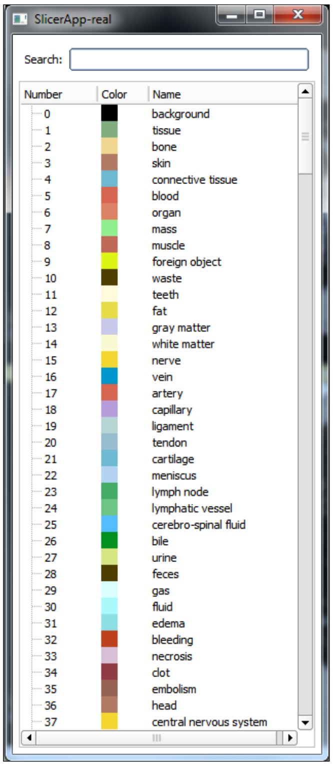

Figure 90: 3DSlicer, Creating Label Model, Editor Module, List of Labels

In the current case, the label named *"artery"* (number 17) is selected for the segmentation of the aorta of the patient's thorax, as shown in the next figure (Figure 91).

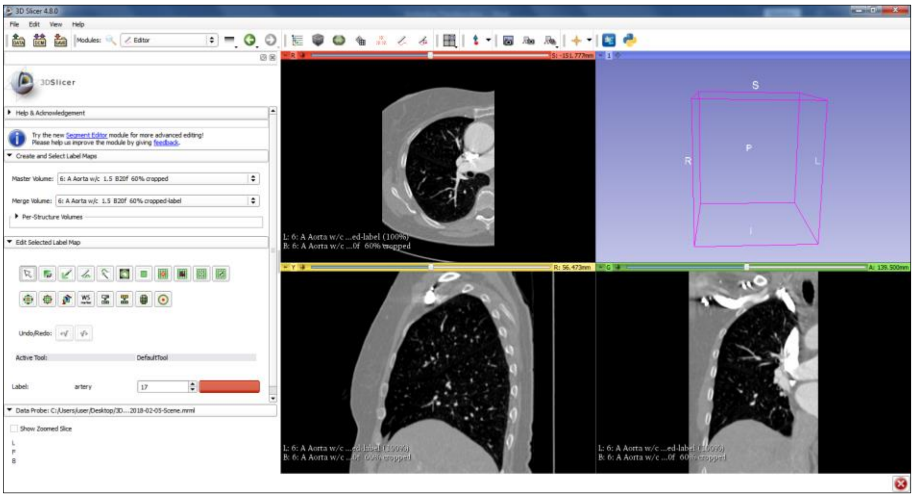

Figure 91: 3DSlicer, Creating Label Model, Editor Module, Artery Label

Hence, the result, after selecting the *"artery"* label, is presented in the following figure (Figure 92).

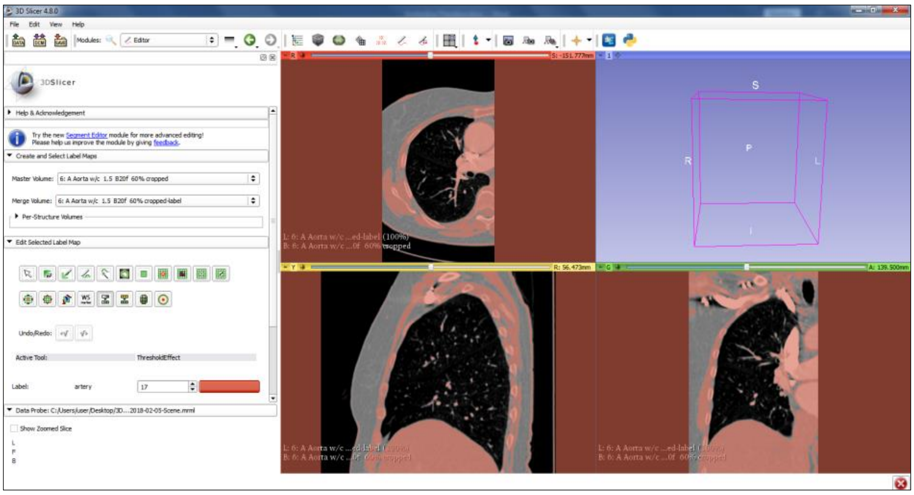

Figure 92: 3DSlicer, Creating Label Model, Editor Module, Artery Label, Result

Additionally, it is suggested that the user utilizes the *"Threshold Effect"*, by pressing the respective icon (depicted with red frame in Figure 93) [19]. This button reveals two values, the upper and the lower bound of the threshold effect, which can be adjusted according to the desired result (Figure 94) [19].

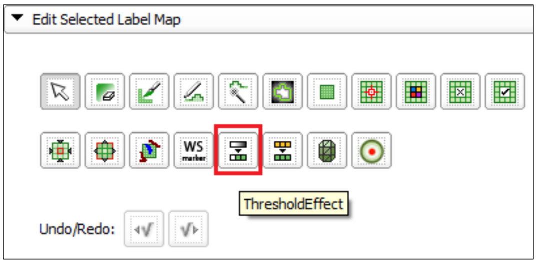

Figure 93: 3DSlicer, Creating Label Model, Editor Module, Threshold Effect Button

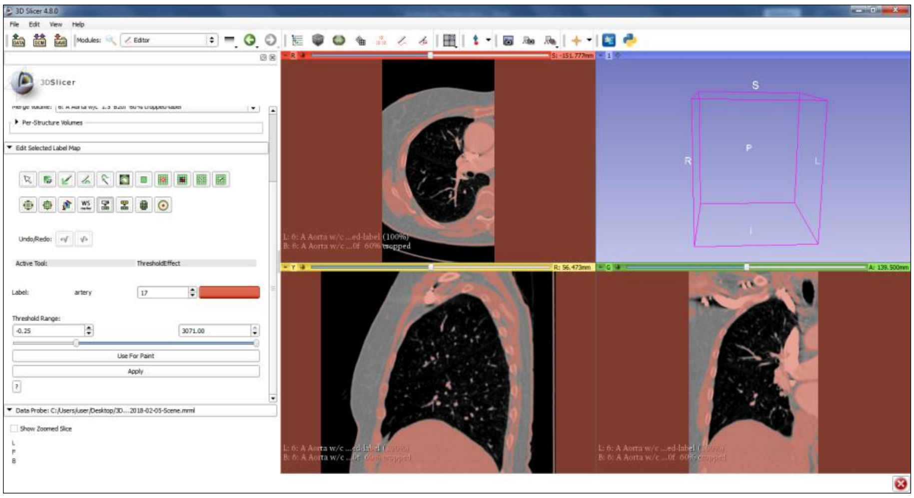

Figure 94: 3DSlicer, Creating Label Model, Editor Module, Threshold Effect

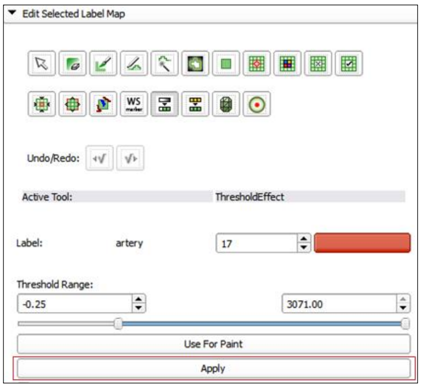

Figure 95: 3DSlicer, Creating Label Model, Editor Module, Adjusting Threshold Range

By increasing the lower bound of the threshold effect, only high-density values will be included in the segmentation [19]. According to this adjustment, the user can examine and accept the created result by pressing the *"Apply"* button, depicted with red frame (Figure 95) [19]. The result of the adjustment of the threshold effect is demonstrated in the following figure (Figure 96).

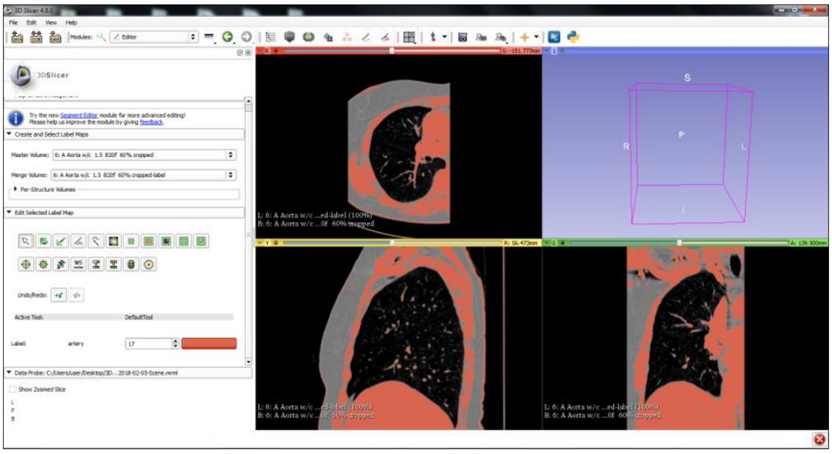

Figure 96: 3DSlicer, Creating Label Model, Editor Module, Result of Threshold Effect

Building a Model

At last, after conducting the essential steps, the user should build a model, and finaly export the final project. Therefore, the user should select the corresponding option *"Make Model Effect"*, from the *"Editor Module"*, as illustrated in the following figure (Figure 97) [19]. In particular, the available options after selecting to make a model effect are presented in Figure 98, on the left side of the screen.

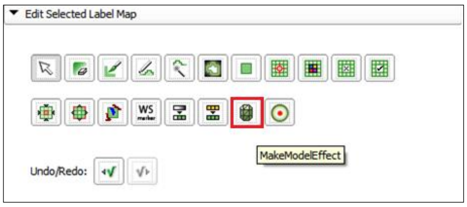

Figure 97: 3DSlicer, Building a Model, Editor Module, Make Model Effect Button

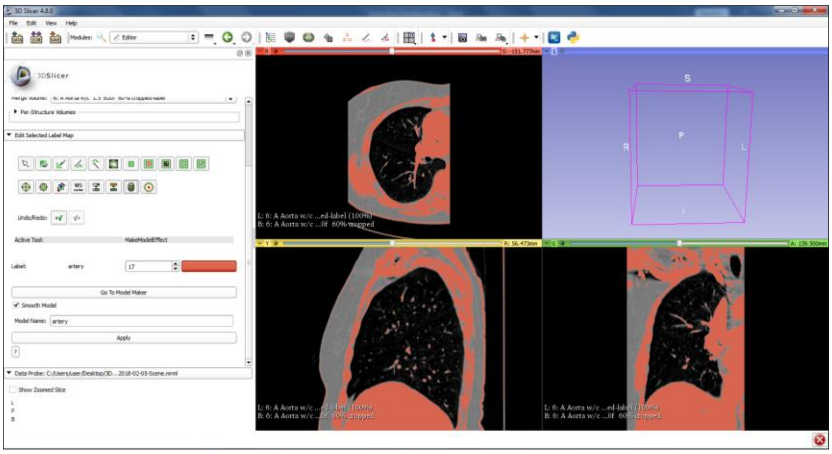

Figure 98: 3DSlicer, Building a Model, Editor Module, Make Model Effect

Afterwards, the user is supposed to fulfill the procedure by saving the created project. In order to save the data, the user should select *File→ Save*, form the drop-down menu, as demonstrated in the following figure (Figure 99) [19].

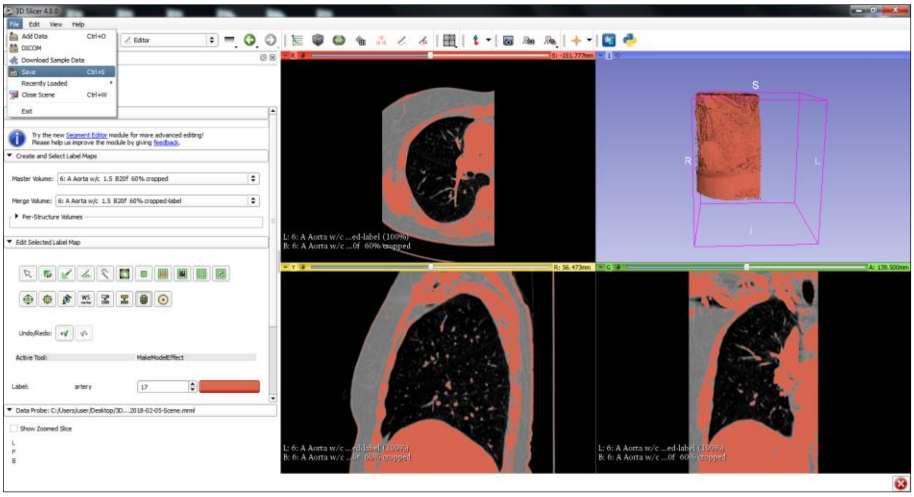

Figure 99: 3DSlicer, Saving a Project

Automatically, the software opens a window that contains all the created files (Figure 100) [19]. The user should check the desired files to be saved and also select the directory where these files will be saved (Figure 100) [19]. Additionally, the user can select file format of the segmented file from the provided options (Figure 100) [19]. In the current case, the *"artery"* file is selected to be to STL file format, as illustrated in the following figure (Figure 100) [19].

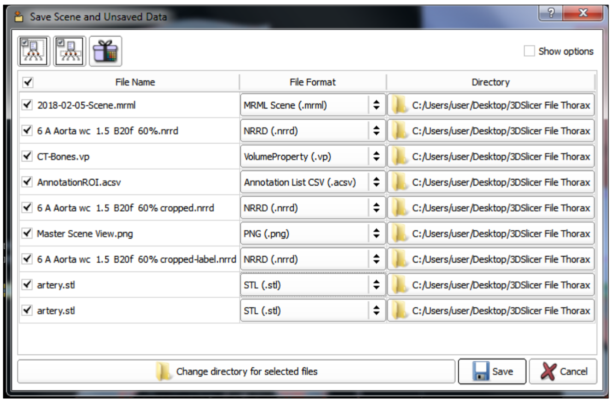

Figure 100: 3DSlicer, Saving a Project, Selecting files to be saved

4.2.4. ITK-SNAP Software

Introduction to ITK-SNAP Software

The Insight Toolkit (ITK) is a frequently encountered library of image analysis algorithms subsidized under the Visible Human Project by the United States National Library of Medicine (Ibáñez *et al.*, 2003; Yushkevich *et al*., 2006). ITK-SNAP has been developed by the efforts and the long collaboration between Yushkevich Paul, Ph. D., of the Penn Image Computing and Science Laboratory (PICSL) at the University of Pennsylvania, and Gerig Guido, Ph. D., of the Scientific Computing Imaging Institute (SCI), at the University of Utah [20].

ITK-SNAP is an open-source software system provided on multiple operating systems (i.e. Windows, MacOSX, and Linux), utilized for performing image processing, segmentation and registration (Ibáñez *et al.*, 2003; Yushkevich *et al*., 2006). This application contributes to the accomplishment of a distinct and urgent need of biomedical imaging research by providing a variety of manual and semi-automatic tools used for segmenting structures in 3D-medical data of different modalities from various anatomical regions (Ibáñez *et al.*, 2003; Yushkevich *et al*., 2006).

Figure 101: ITK-SNAP Software, Source: [20]

Additionally, ITK-SNAP is designed with the vision of being a robust and user-friendly tool that maximizes user efficiency. Consequently, it furnishes numerous supporting utilities and functions (Ibáñez *et al.*, 2003; Yushkevich *et al*., 2006). The most fundamental advantages of this software application are presented in the following list (Ibáñez *et al.*, 2003; Yushkevich *et al*., 2006) [20]:

- *Linked cursor for seamless 3D-navigation* [20].
- *Manual segmentation in three orthogonal planes at once* [20].
- *Modern graphical user interface based on Qt (cross-platform application framework)* [20].
- *Support for numerous 3D-image formats, including NIfTI and DICOM* [20].
- *Support for color, multi-channel, and time-variant images* [20].
- *3D-cut-plane tool for fast post-processing of segmentation results* [20].
- *Extensive tutorial and video documentation* [20].

Basic Program Functions

In particular, in view of becoming familiar with the basic functions of ITK-SNAP software application, it is essential to illustrate an analytical description of the steps of the utilization of the software for a particular case study. As mentioned in the previously (Sections 4.2.1.-4.2.3.), a series of DICOM files of a thorax is utilized in order to create a new project. Similarly, for the current case study, the same series of DICOM files are used, downloaded from ITK-SNAP's official site [6].

Welcome Screen

In the following figure (Figure 102) is illustrated the *"Welcome Screen"* of ITK-SNAP software [21-22]. This screen opens-up by default displaying the most fundamental options that are available, demonstrated on the main menu [21-22].

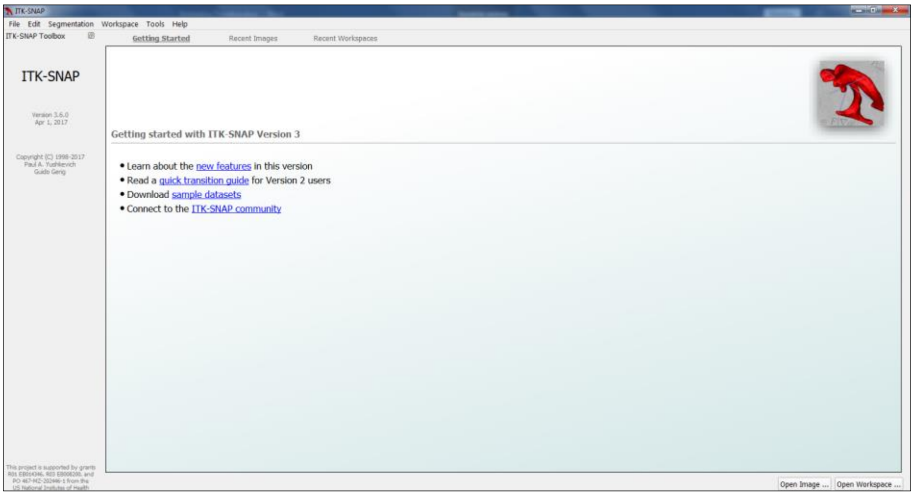

Figure 102: ITK-SNAP, Welcome Screen

Loading Data

For the purpose of creating a project, the user should select the option *“Open Main Image”* from the *“File”* panel of the drop-down menu, as presented in the next figure (Figure 103) [21-22]. Otherwise, the user should press the *“Open Image”* button at the right-down corner of the screen (Figure 103) [21-22].

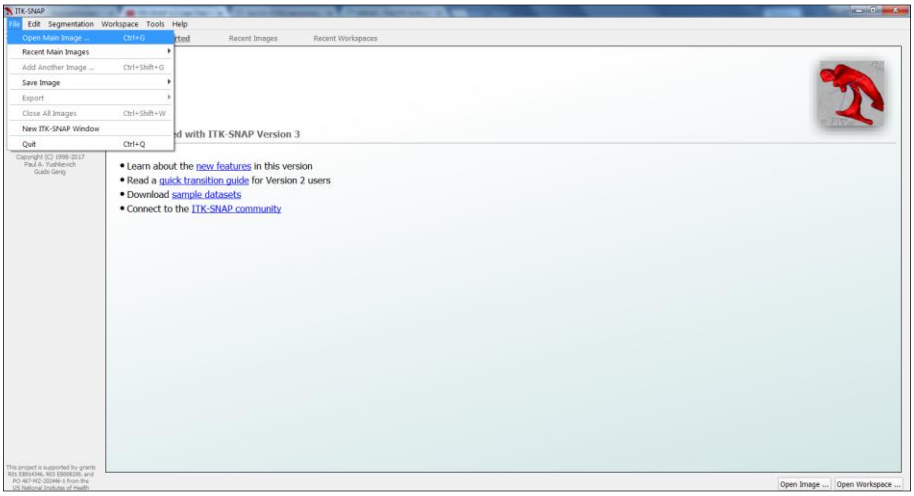

Figure 103: ITK-SNAP, Open Main Image, drop-down menu

Subsequently, the software opens by default the *“Open Main Image”* wizard (Figure 104) asking the user to browse the desired files from a specific directory [21-22]. In addition, the user is supposed to define the file format among a list, provided by the software [21-22]. In the current case, as shown in Figure 104, the file format is selected to be *“DICOM Image Series”* [21-22].

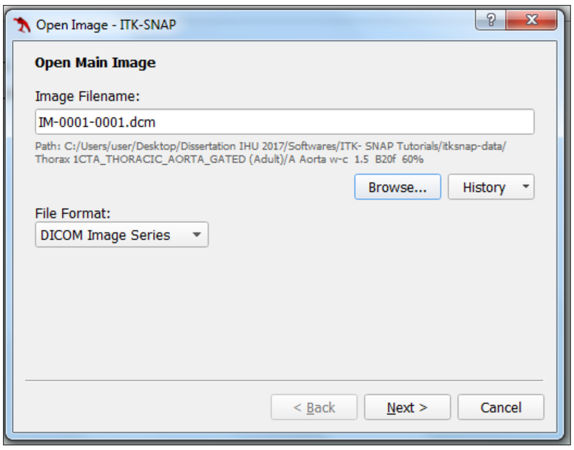

Figure 104: ITK-SNAP, Open Main Image, Importing DICOM Data from Directory

After selecting to import the desired folders, the user should press the *"Next"* button from the right-down corner of the wizard (Figure 104) [21-22]. After importing the suitable files, the procedure of uploading the data into the software is demonstrated. When this upload is complete, the wizard proceeds on the next page, prompting the user to *"Select DICOM series to open"* (Figure 105) [21-22]. The user should select the desired case study, appearing on the dialog box, and then press the *"Next"* button from the right-down corner of the wizard, as presented below (Figure 105) [21-22].

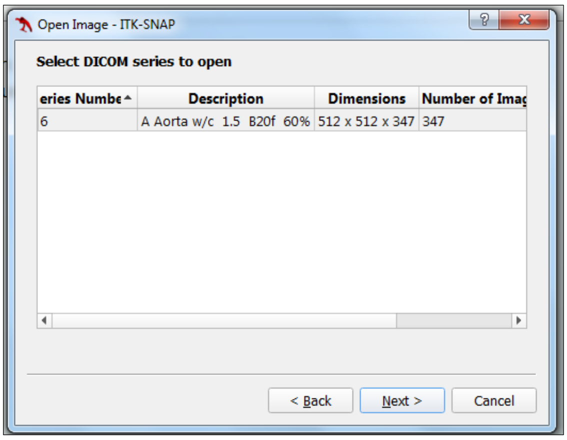

Figure 105: ITK-SNAP, Open Main Image, Selecting DICOM series to open

Afterwards, appears automatically an *"Image Summary*", concerning the basic information of loaded data (Figure 106) [21-22]. This summary contains details regarding the properties and the values of the new case study of a specific patient (Figure 106). The user should press the *"Finish"* button from the right-down corner, in order to close the wizard (Figure 106) [21-22]. Alternatively, the user can drag-and-drop the DICOM file folder over the initial interface of the ITK-SNAP software tool (Figure 102) [21-22].

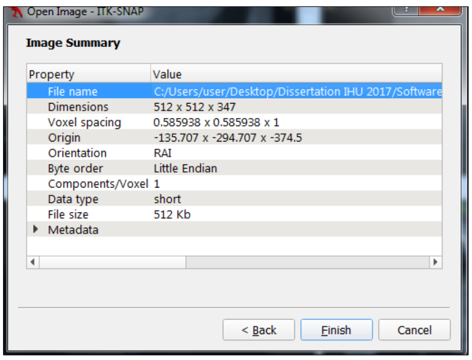

Figure 106: ITK-SNAP, Open Main Image, Image Summary

Interface of ITK-SNAP

The ITK-SNAP provides a combination of mouse functions, keyboard shortcuts and visual buttons, for maximizing the utilization efficiency [21-22]. In Figure 107, is illustrated the layout of the new created project. The main image window is composed of various controlling windows, different viewer panels (2D Slice Viewer and 3D Volume Viewer), the toolbox, and the main menu, comprising a number of functions [21-22].

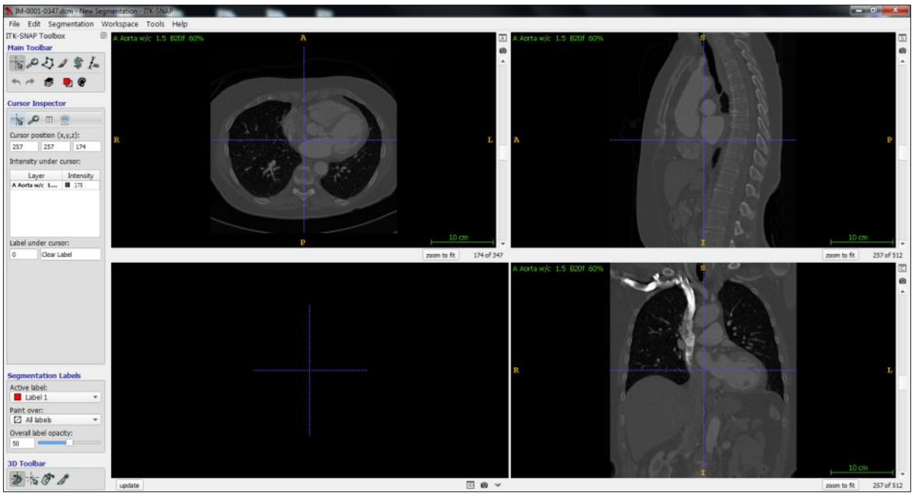

Figure 107: ITK-SNAP, The Interface of the Created Project

Viewer Panels

The viewer panels provide the user with four main options of view, as depicted in the figure above (Figure 107) [21-22]. The user can interact with the *"Slice Views"*, which are the tree orthogonal views composed of: *"Axial"*, *"Sagittal"*, and *"Coronal"*, presented in the top and the right-bottom corner [21-22]. Additionally, in the left-bottom corner is demonstrated the *"Three-dimensional View"*, in which the user can see the results of the three-dimensional surface renderings of the segmentation (Figure 107) [21-22]. The 3D-cursor, depicted with blue color (Figure 107), represents the point or the voxel in the image, where the three orthogonal view planes intersect [21-22].

ITK-SNAP Toolbox

Furthermore, on the left side appears the *"ITK-SNAP Toolbox"*, representing the control panel. In particular, it is organized into a *"Main Toolbar"*, a *"Cursor Inspector"*, *"Segmentation Labels"*, and a *"3D Toolbar"* (Figure 107) [21-22]. Initially, the *"Main*

Toolbar", provides various navigation tools facilitating the interaction with the image [21-22]. Additionally, the next panel is the *"Cursor Inspector"*, providing additional information and controls grouped by function [21-22]. Moreover, the *"Segmentation Labels"* demonstrate the created segmentations [21-22]. Finally, the last panel is the *"3D Toolbar"*, providing different options of interaction with the created 3D-object [21-22].

- *Main Toolbar*

The *"Main Toolbar"*, as mentioned previously, provides a variety of tools enabling the interaction with the image [21-22]. Especially, the most fundamental navigation tools include functions, such as navigation, cursor repositioning, zooming, panning, segmentation etc. [21-22]. The following figures (Figures 108-109), demonstrate the *"Crosshair Mode"*, the *"Zoom/ Pan Mode"* and the *"Layer Inspector"*, as being the most prominent navigation tools [21-22]. The *"Crosshair Mode"* tool, can be utilized in order to adjust the 3D-cursor in the three orthogonal image slices [21-22]. The *"Zoom/ Pan Mode"* is used for zooming into the image or panning around when zoomed in [21-22]. Alternatively, the user can utilize the mouse buttons, according with the indications of the shortcuts (Figures 108-109) [21-22].

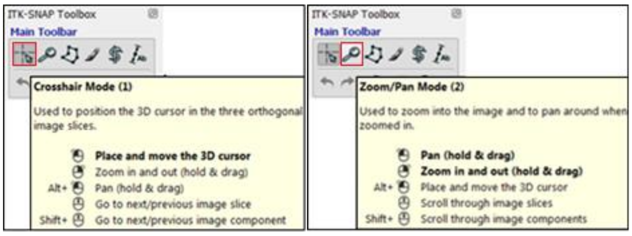

Figure 108: ITK-SNAP, Main Toolbar, Crosshair Mode (left side), Zoom/ Pan Mode (right side)

In addition, the *"Layer Inspector"* is used for the adjustment of the display properties of the images (Figure 109) [21-22]. Once the user presses this button (Figure 109) (presented in red framework), the *"Image Layer Inspector"* window opens by default, as illustrated in Figure 110 in the left side [21-22]. Otherwise, the user can select *Tools → Layer Inspector* from the main menu [21-22].

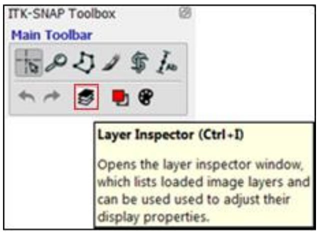

Figure 109: ITK-SNAP, Main Toolbar, Layer Inspector

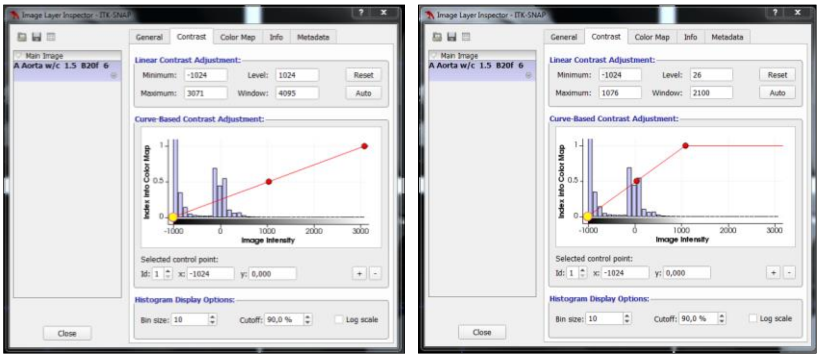

Figure 110: ITK-SNAP, Main Toolbar, Image Layer Inspector, Contrast Adjustment, before selecting Auto Mode (left), after selecting Auto Mode (right)

The *"Image Layer Inspector"* provides functions of diverse kinds, concerning notably the *"Contrast"*, the *"Color Map"*, and information about the display properties [21-22]. Basically, *"Contrast"* is described through the differentiation in brightness between tissue types in the image [21-22]. The *"Linear Contrast Adjustment"* enables the user to specify the range of image intensity [21-22]. This adjustment is supposed to be essential in case of segmentation, due to the better visual result [21-22].

In the current case, the contrast adjustment is selected to be improved automatically, by pressing the corresponding button named *"Auto"*, depicted in Figure 110 [21-22]. In particular, on the left figure (Figure 110) is illustrated the contrast adjustment before selecting *"Auto Mode"* [21-22]. Respectively, on the right figure (Figure 110) is demonstrated the contrast adjustment after selecting *"Auto Mode"* [21-22]. The results of this regulation are presented in the following images (Figure 111-112) [21-22].

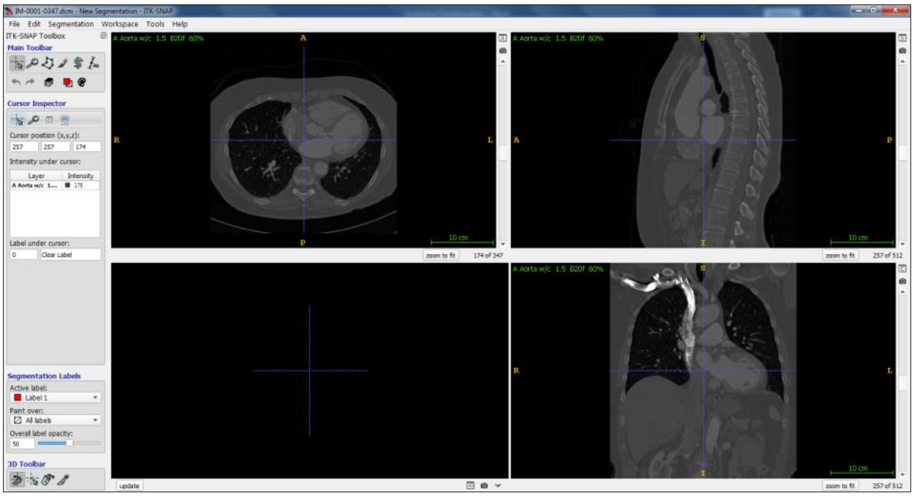

Figure 111: ITK-SNAP, Main Toolbar, Image Layer Inspector, Contrast Adjustment, before selecting Auto Mode

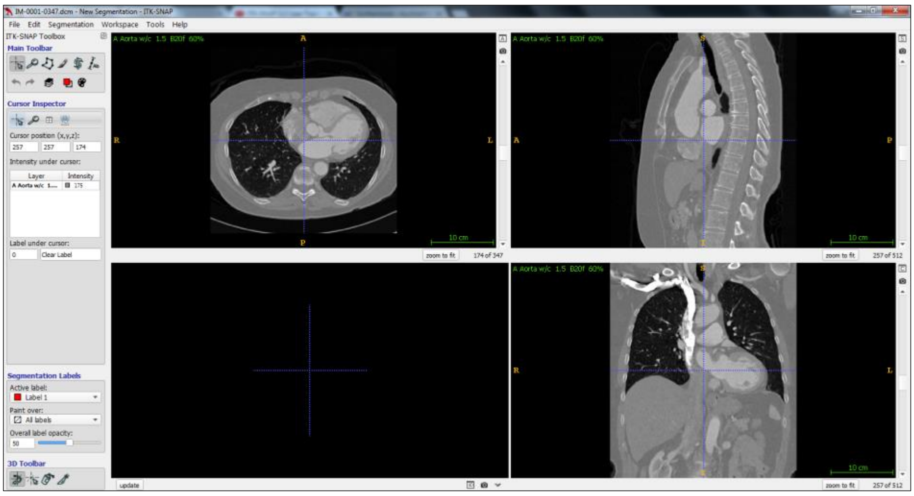

Figure 112: ITK-SNAP, Main Toolbar, Image Layer Inspector, Contrast Adjustment, after selecting Auto Mode

Furthermore, instead of adjusting the intensity of the contrast, the user can select to change the *"Color Map"* of the images from the *"Image Layer Inspector"* [21-22]. The software provides a variety of color hues, in order to achieve a better visualization [21-22]. The following figures demonstrate three different examples of color mapping: *"Grayscale"* (Figure 113), *"Jet"* (Figure 114) and *"Copper"* (Figure 115) [21-22].

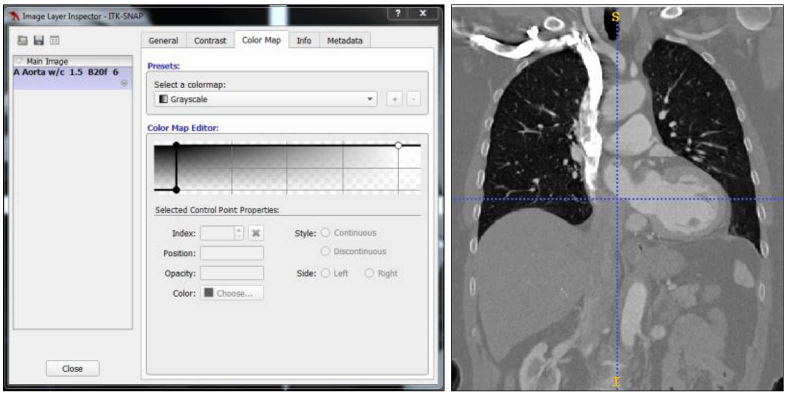

Figure 113: ITK-SNAP, Main Toolbar, Image Layer Inspector, Color Map, Grayscale

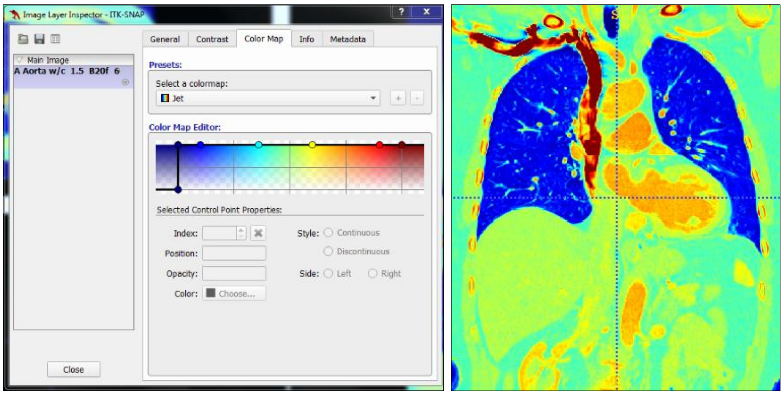

Figure 114: ITK-SNAP, Main Toolbar, Image Layer Inspector, Color Map, Jet

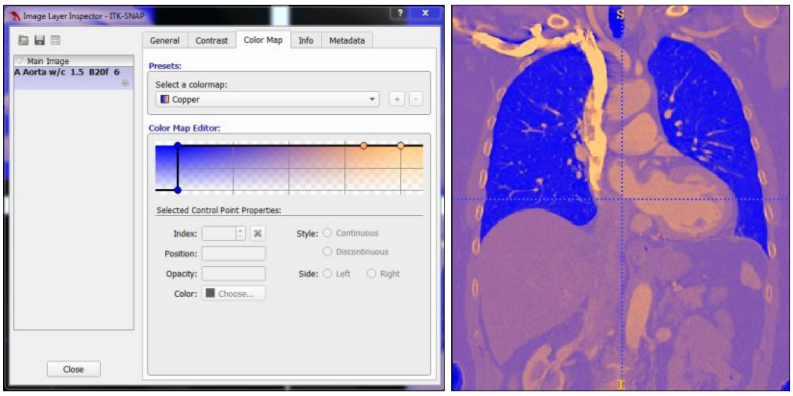

Figure 115: ITK-SNAP, Main Toolbar, Image Layer Inspector, Color Map, Copper

Segmentation

It is generally accepted that segmentation of medical images is a crucial and important function [21-22]. The ITK-SNAP software application provides the user with a set of tools that facilitate the process of segmentation of volumetric data [21-23]. More precisely, the *"Segmentation"* can be accomplished in two different modes: manually and semi-automatically [21-23]. From one point of view, by performing the *"Manual Segmentation"* the user can accomplish more accurate and precise results, although it is considered as being more time-consuming procedure [21-23]. On the contrary, the *"Automatic Segmentation"* can reduce the need for user interaction, though is weaker than *"Manual Segmentation"* [21-23]. In fact, the result of *"Automatic Segmentation"* basically relies on the quality of the input image data [21-23]. The process of performing *"Automatic Segmentation"* is demonstrated as follows, by presenting the most fundamental functions [21-23].

➢ *Automatic Segmentation*

The segmentation utilities being available in ITK-SNAP software application are based on a class of algorithms related to 3D-active contour evolution [21-25]. Basically, the segmentation of an anatomical structure is estimated by one or more evolving contours [21-25]. This methodology is named *"Snake evolution"*, due to the shape of the closed curve (or surface in 3D-model) representing the segmentation. Initially, the user starts with an initialized closed contour and over time that contour (*"snake"*) evolves from a tentative estimate of the anatomical structure of interest to an approximate structure. The main objective is to delineate the entire region of interest of the anatomical structure that will be segmented, as distinctly and precisely as possible [21-25].

Therefore, in order to perform an *"Automatic Segmentation"* the user is supposed to select the corresponding button, named *"Active Contour (aka "Snake") Segmentation Mode"*, from the main toolbar, as depicted with red framework in the following figure (Figure 116) [21-25]. Specifically, this mode is utilized for the selection of the *"Region of Interest"* (ROI) for semi-automatic active contour segmentation, providing the corresponding tools, as illustrated in the following figures (Figure 116-117).

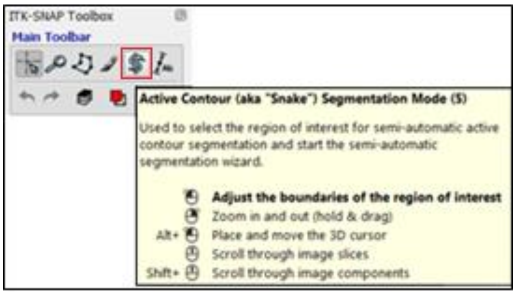

Figure 116: ITK-SNAP, Main Toolbar, Active Contour Segmentation Mode

When the user presses this button, the software application reveals a red-dotted framework in the three orthogonal views, as depicted in the following figure (Figure 117) [21-25]. After defining the *"Region of Interest"* (Figure 117) the user should press the *"Segment 3D"* button (Figure 118), demonstrated on the left side of the screen, on the *"Snake Inspector"* menu [21-25]. In the current case, the ROI is selected to be the aorta of the patient, as illustrated more clearly in the coronal view (right-down corner of the screen in Figure 117) [21-25].

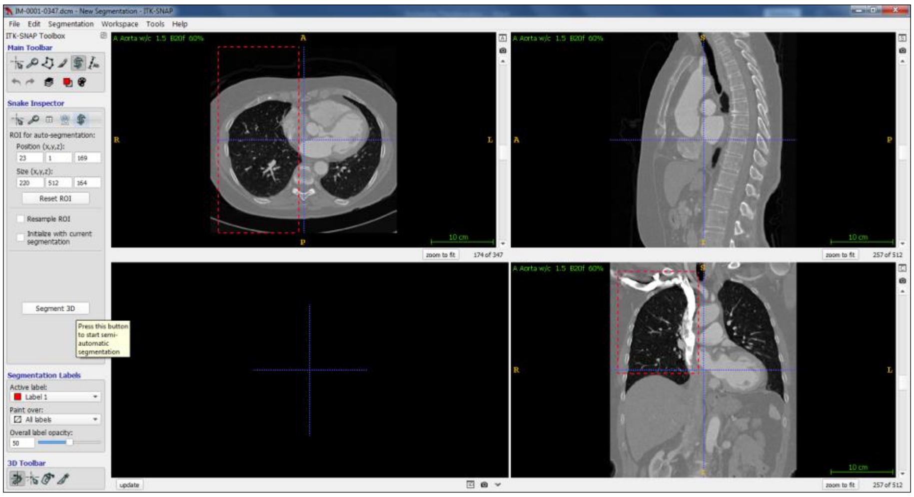

Figure 117: ITK-SNAP, Main Toolbar, Active Contour Segmentation Mode, Selecting the Region of Interest (ROI)

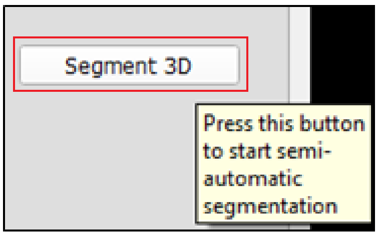

Figure 118: ITK-SNAP, Main Toolbar, Active Contour Segmentation Mode, Segment 3D

The *"Automatic Segmentation"* is divided into three different steps, which are illustrated in the right side of the screen [21-25]. The first step is called *"Pre-segmentation"*, the second is named *"Initialization"*, and the third step is called *"Evolution"* [21-25]. More specifically, the first step is related to pre-processing the image by adjusting the speed function [21-25]. The second step is relevant with the initialization of the segmentation and it is used for the placement of the initial contour [21-25]. Finally, the last step pertains to the demonstration of the evolution of the contour that will be segmented [21-25].

With reference to the first step of the *"Automatic Segmentation"*, (i.e. *"Pre-segmentation"* (Figure 119)), the software provides four pre-processing modes: *"Thresholding"*, *"Classification"*, *"Clustering"*, and *"Edge Attraction"* [21-25].

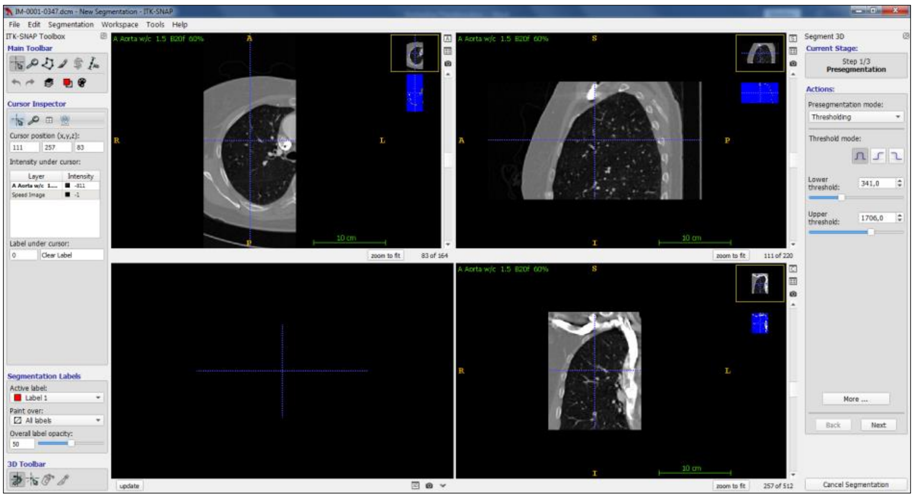

Figure 119: ITK-SNAP, Main Toolbar, Active Contour Segmentation Mode, Segment 3D, Step 1: Pre-segmentation

By pressing the *"More"* button, the software opens by default the *"Speed Image Generation"* wizard, providing more control options over the pre-processing, as presented in the next figure (Figure 120) [21-25].

Particularly, for the current case, the speed function is selected to be generated by *"Thresholding"* mode, as depicted in Figure 120 [21-25]. After adjusting the required settings, the user should press the *"Next"* button (Figure 119 – right-down corner), in order to proceed to the next step [21-25].

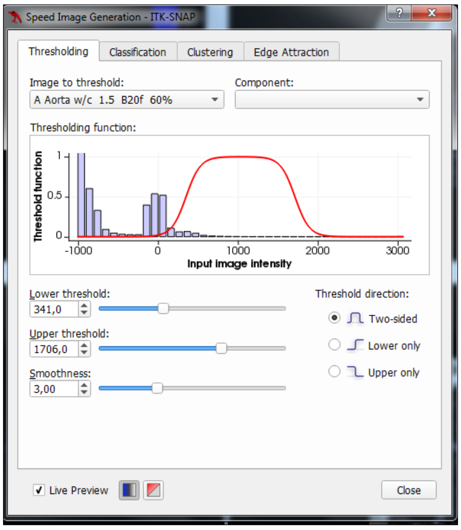

Figure 120: ITK-SNAP, Main Toolbar, Active Contour Segmentation Mode, Segment 3D, Step 1: Pre-segmentation, Speed Image Generation, Thresholding Mode

Subsequently, the user proceeds to the *"Initialization"* step (Figure 121-122). In this step, the software prompts the user to place bubbles in the image in order to initialize the contour [21-25]. The user should press the *"Add Bubble at Cursor"*, for the purpose of adding bubbles in the desired region of interest [21-25]. Additionally, the user can modify the *"Bubble radius"*, in order to be adapted to the desired region [21-25]. Furthermore, the user is enabled to go *"Back"*, or to *"Cancel Segmentation"*, by pressing the corresponding buttons (Figure 121-122) [21-25]. In Figure 122, the process is selected to be demonstrated on the second option of view, depicted with blue color.

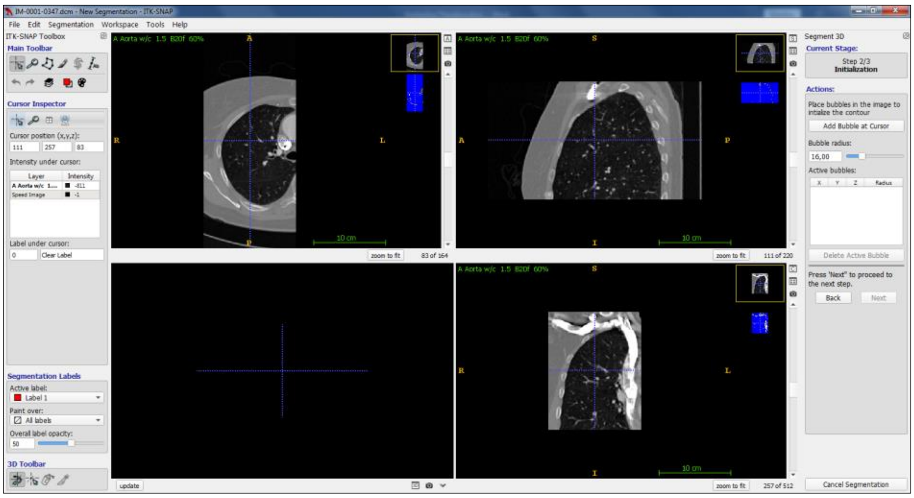

Figure 121: ITK-SNAP, Main Toolbar, Active Contour Segmentation Mode, Segment 3D, Step 2: Initialization

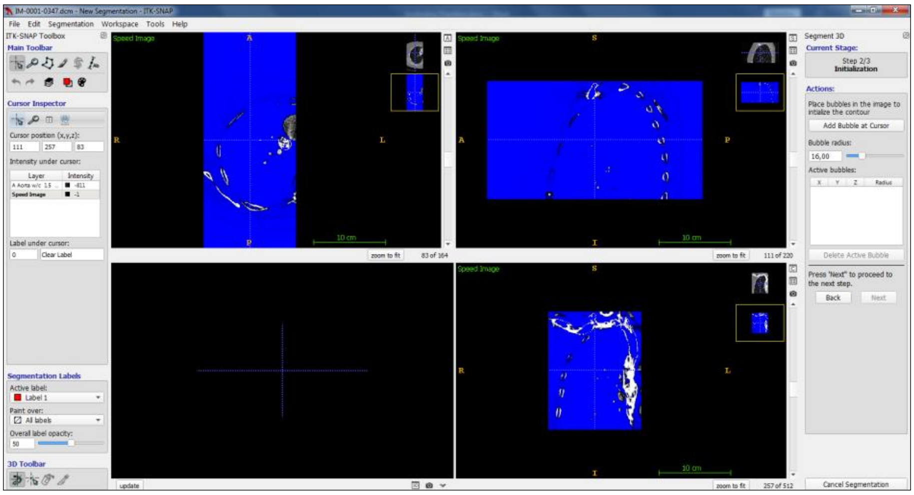

Figure 122: ITK-SNAP, Main Toolbar, Active Contour Segmentation Mode, Segment 3D, Step 2: Initialization

Additionally, the following figure (Figure 123) illustrates the process of adding multiple bubbles on the aorta. The bubbles are illustrated in red color in the three views. Additionally, the software shows a full list of the coordinates of the active bubbles, providing the option to interfere and delete the selected one in case of mistake [21-25].

Once the user has added the bubbles on the region of interest, the user should select the *"Next"* button (Figure 123), in order to proceed to the final step of segmentation [21-25]. Automatically, the software proceeds to the third step, as presented in the following figure (Figure 124) [21-25].

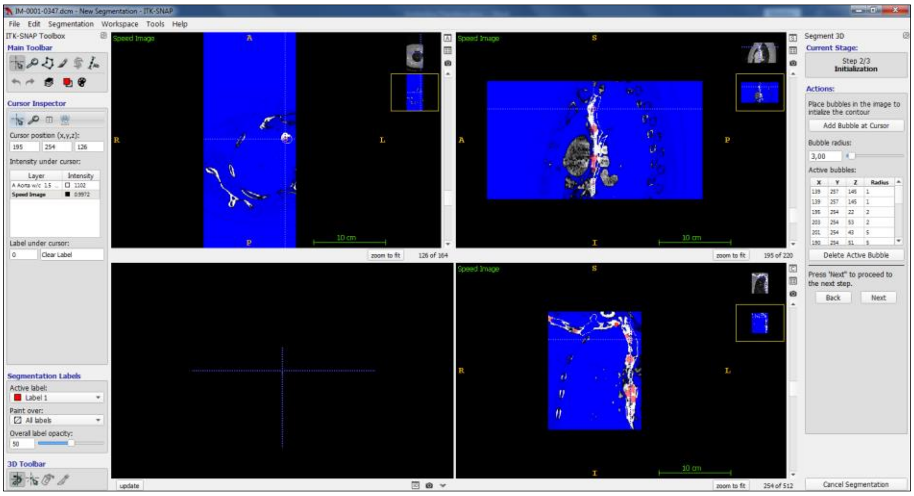

Figure 123: ITK-SNAP, Main Toolbar, Active Contour Segmentation Mode, Segment 3D, Step 2: Initialization, Adding Bubbles at Cursor

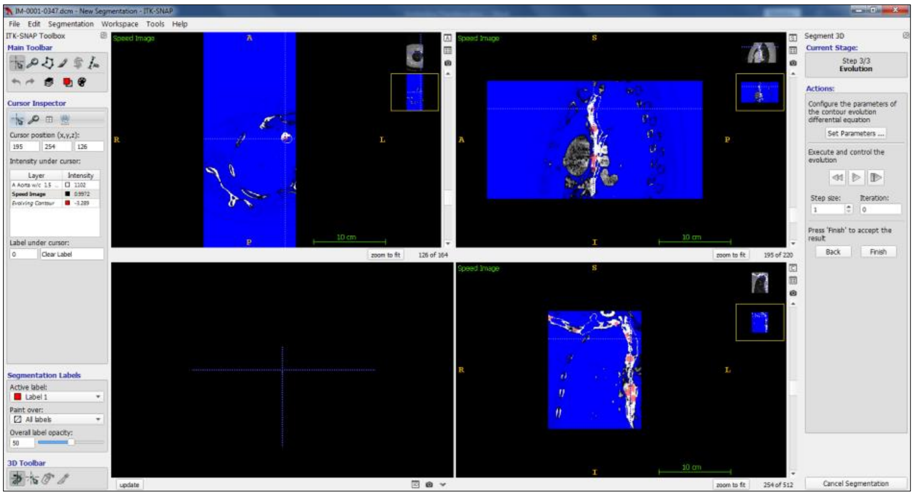

Figure 124: ITK-SNAP, Main Toolbar, Active Contour Segmentation Mode, Segment 3D, Step 3: Evolution

The user can press the *"Set Parameters"* button, on the right side of the screen (Figure 124), in order to configure the parameters of the contour evolution differential equation [21-25]. After pressing this button, the software opens be default the *"Active Contour Evolution Parameters"* wizard (Figure 125), in order to set up these parameters [21-25].

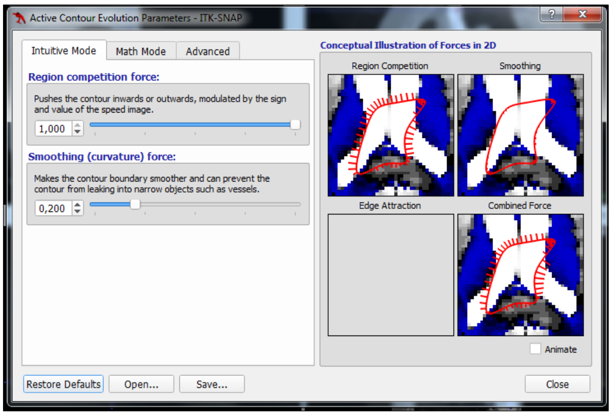

Figure 125: ITK-SNAP, Main Toolbar, Active Contour Segmentation Mode, Segment 3D, Step 3: Evolution, Set Parameters, Active Contour Evolution Parameters

At last, the user is capable of starting the contour evolution by pressing the *"Play"* button (Figure 124) [21-25]. The following figures (Figures 126-127) demonstrate the process of evolution depicted in red color [21-25]. The user is supposed to select the *"Finish"* button in order to complete the final step (Figures 126-127) [21-25].

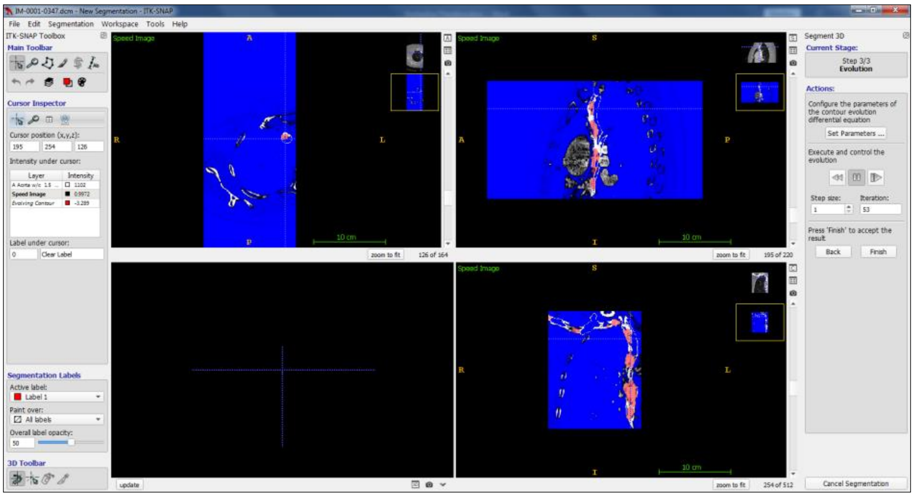

Figure 126: ITK-SNAP, Main Toolbar, Active Contour Segmentation Mode, Segment 3D, Step 3: Evolution, Process of evolution

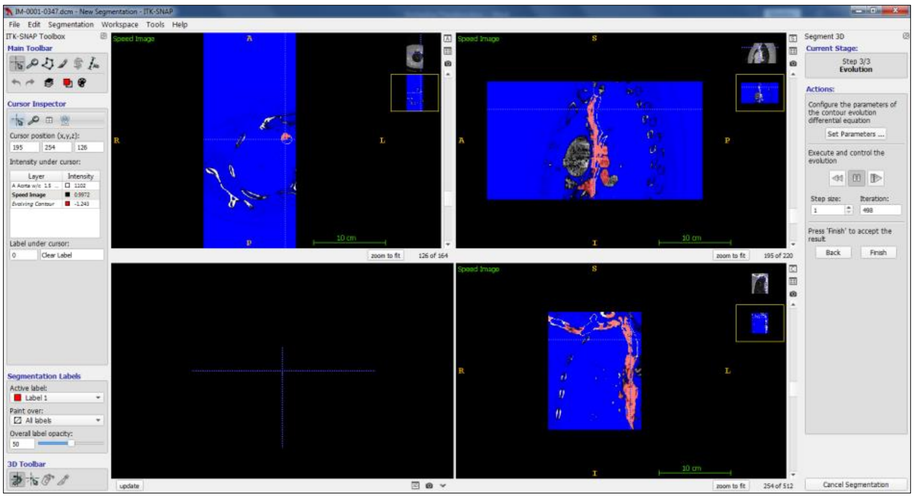

Figure 127: ITK-SNAP, Main Toolbar, Active Contour Segmentation Mode, Segment 3D, Step 3: Evolution, Final result

After completing the procedure of segmentation, the final result appears on the screen in the three views depicted in red color, as presented in the following (Figure 128) [21-25]. In case the result does not comply with the requirements of the desired region of interest, the process of segmentation must be repeated from the beginning. The user is supposed to conduct the three steps from scratch and adjust all the parameters [21-25]. In this case, the user should select for the main menu *Segmentation→ Unload Segmentation*. Alternatively, the user should press *"Cancel Segmentation"*, before pressing the *"Finish"* button on the final step (Figure 127).

Figure 128: ITK-SNAP, Main Toolbar, Active Contour Segmentation Mode, Segment 3D, Step 3: Evolution, Final result

Afterwards, in order to see the final result of the 3D-segmented model, the user should press the *"Update"* button (Figure 128), on the left-down corner of the 3D-viewer panel [21-25]. Automatically, the software reveals a 3D-image of the segmented model of the region of interest [21-25]. The result of the current case study is demonstrated in the following figure (Figure 129). Furthermore, the software enables the user to navigate through this 3D-image, by zooming or panning around.

Figure 129: ITK-SNAP, Main Toolbar, Active Contour Segmentation Mode, Segment 3D, Step 3: Evolution, Final result

The following figure (Figure 130) presents the updated 3D-model, when zoomed in [21-25].

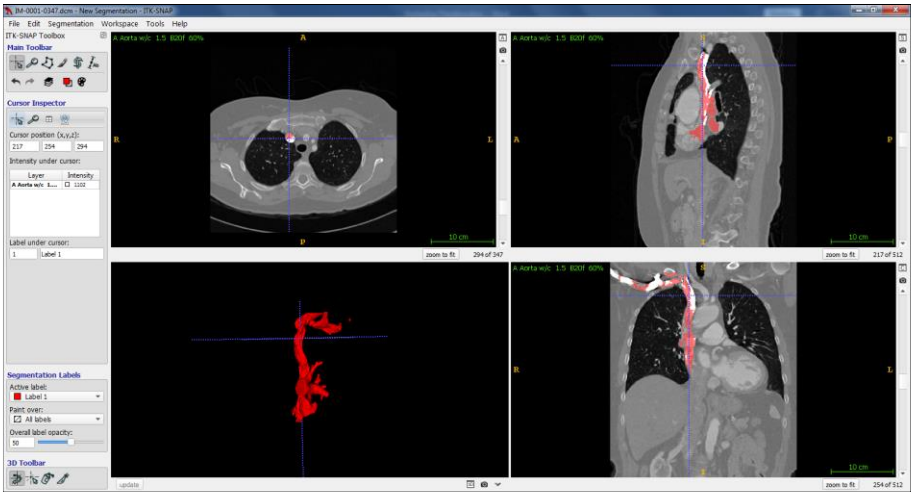

Figure 130: ITK-SNAP, Main Toolbar, Active Contour Segmentation Mode, Segment 3D, Step 3: Evolution, Final result, Zoomed

Exporting Data

Finally, the user is supposed to export the created files into external formats. In more detail, the user should select from the drop-down menu, *Segmentation→ Export as Surface Mesh*, as illustrated in the next figure (Figure 131) [22-25].

Figure 131: ITK-SNAP, Segmentation, Exporting as Surface Mesh, drop-down menu

After selecting this option, the software opens by default a wizard (Figure 132) asking the user to select *"Which labels will be exported"* [22-25]. In the current case, the first option is selected, as shown on the following figure (Figure 132). Then, the user is supposed to press the *"Next"* button, in order to proceed to the next page of the wizard.

Figure 132: ITK-SNAP, Segmentation, Exporting as Surface Mesh, Wizard, Labels to be exported

The next page of the wizard regards the destination of the exported file. In particular, the software prompts the user to select the name, the destination, the type of format of the file [22-25]. In the current case, as shown in the following figure (Figure 133), the file format is selected to be *"STL Mesh File*".

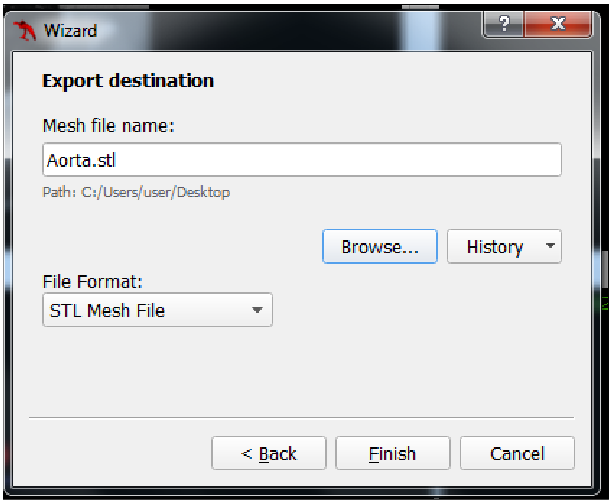

Figure 133: ITK-SNAP, Segmentation, Exporting as Surface Mesh, Wizard, Export destination

➢ *Manual Segmentation*

As described previously, the most accurate way to segment an anatomical structure by utilizing ITK-SNAP software is the *"Manual Segmentation"* [21-26].

In specific, the process of *"Manual Segmentation"* is described as follows. Optionally, the user has the potentiallity to use the *"Crosshair Mode"* tool from the *"Main Toolbar"* (Figure 134), in order to define the region of interest [21-26].

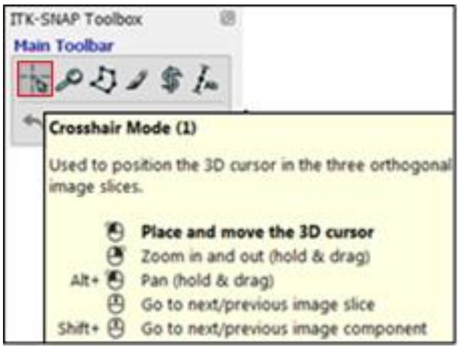

Figure 134: ITK-SNAP, Main Toolbar, Crosshair Mode

In the running case, the patient's spleen is considered as the region of interest that will be segmented. By using the *"Crosshair Mode"*, the user is able to position the 3D-cursor in the spleen, all at once in the three orthogonal image slices, as illustrated in the next figure (Figure 135) [21-26].

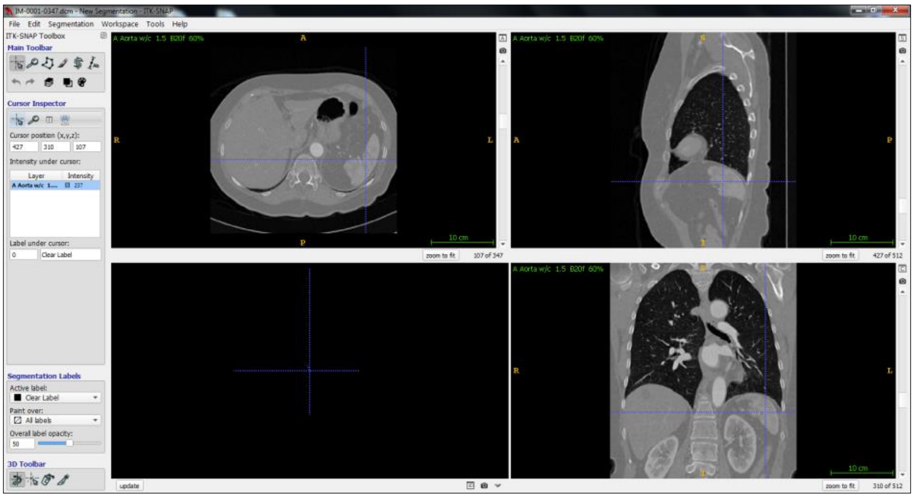

Figure 135: ITK-SNAP, Main Toolbar, Crosshair Mode, Positioning the 3D-cursor in patient's spleen

Subsequently, the user is supposed to create anatomical labels that are associated with the parts that will be segmented. In order to proceed to this step, the user should press *Segmentation→ Label Editor* from the drop-down menu, as presented in the following figure (Figure 136) [21-26].

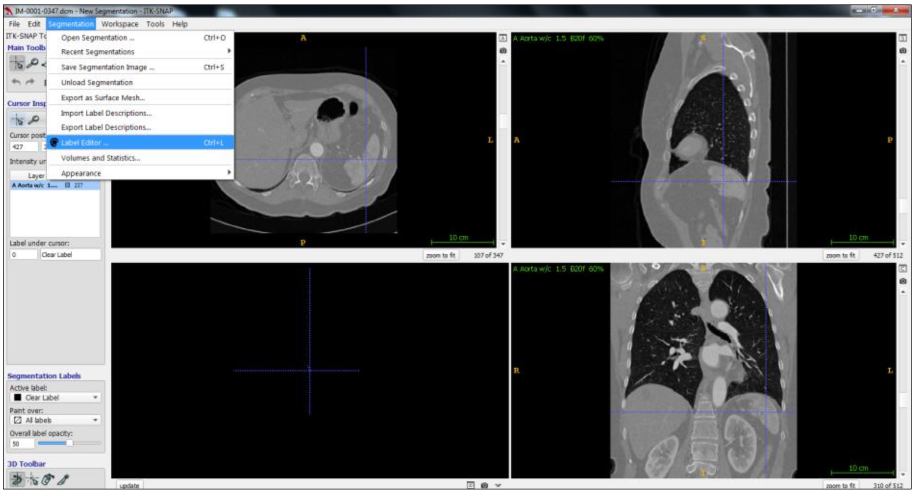

Figure 136: ITK-SNAP, Segmentation, Label Editor, drop-menu

Automatically, a *"Segmentation Label Editor"* wizard appears on the screen, furnishing several options concerning the labels, as demonstrated in Figure 137 [21-26]. Particularly, the *"Segmentation Label Editor"* should include seven available labels appearing with generic names, as depicted in Figure 137 on the left column [21-26]. With reference to the current case, the *"Label 1"* of the available list, is selected to represent the spleen of the patient. Furthermore, the user has the feasibility to change the generic name of the label, by typing the new one under the *"Description"* option [21-26]. Additionally, the *"Color"*, the *"Opacity"* and the *"Visibility"* are possible to be adjusted from the corresponding options of the wizard, as depicted in Figure 137 [21-26].

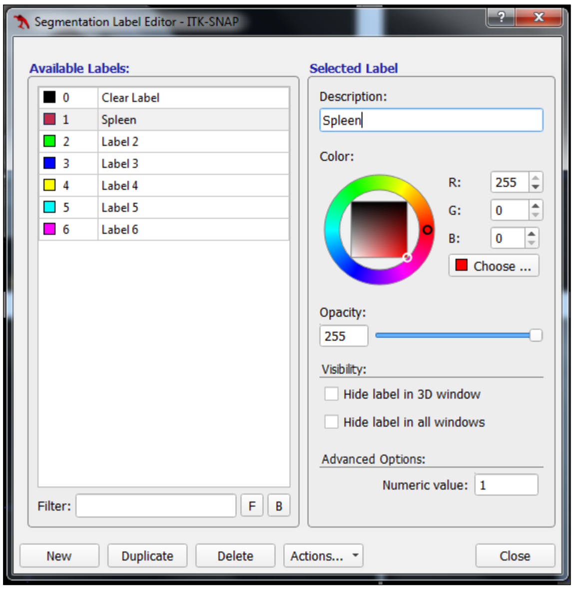

Figure 137: ITK-SNAP, Segmentation, Segmentation Label Editor, Wizard

Afterwards, the user should affirm that the created label is selected as the *"Active Label"*, in the *"Segmentation Labels"* panel, on the left side of the screen (Figure 138), in order to proceed to the next step of segmentation [21-26]. Moreover, it is crucial to guarantee that *"All Labels"* option is selected as the *"Paint over"* setting in the same panel (Figure 138) [21-26]. As illustrated in the next figure (Figure 138), in the current project, the *"Active Label"* is selected to be the *"Spleen"*, depicted with red color.

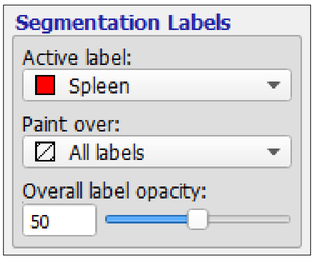

Figure 138: ITK-SNAP, Main Toolbar, Segmentation Labels

Optionally, the user is enabled to adjust the *"Zoom"* level, by pressing the *"Zoom Inspector"* button from the *"Main Toolbar"* (Figure 139) [21-26]. In the present case, the zoom factor has been set to *"2x"* and the cursor has been centered on the spleen, by selecting the respective button, named *"Center on cursor"* (Figure 140).

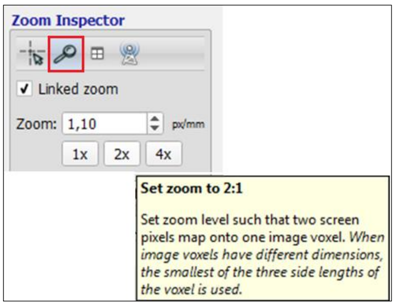

Figure 139: ITK-SNAP, Main Toolbar, Zoom Inspector

Figure 140: ITK-SNAP, Main Toolbar, Zoom Inspector

Specifically, the result after adjusting the zoom factor and the cursor on the center of the spleen is presented as follows (Figure 141). The small icon, depicted in yellow color in the three orthogonal views, demonstrates the region of interest appearing with white framework (Figure 141) [21-26].

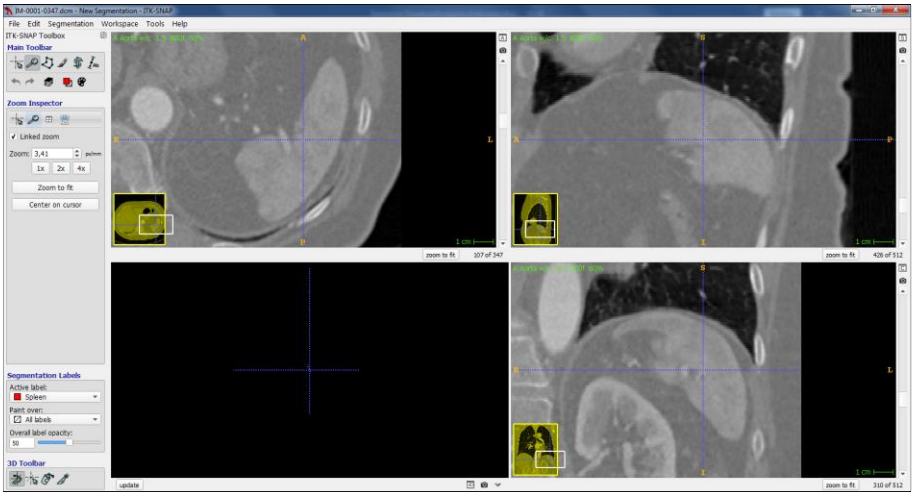

Figure 141: ITK-SNAP, Region of interest after adjusting the Zoom factor

In order to proceed to the next step of the process, the user should select the *"Polygon Mode"* from the *"Main Toolbar"*, as illustrated in the next figure (Figure 142) [21-26]. This tool is utilized for performing manual segmentation by drawing and filling polygons in the three orthogonal image slices [21-26]. The available options of the utilization of this tool by using the mouse are demonstrated in the following figure (Figure 142) [21-26].

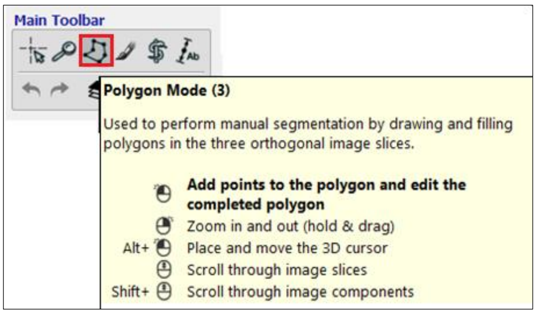

Figure 142: ITK-SNAP, Main Toolbar, Polygon Mode

Particularly, the user is supposed to create polygons in the three orthogonal views (Axial, Sagittal, and Coronal), with respect to the geometry of the illustrated organ.

Firstly, the process of adding points to the polygon of the Sagittal view is depicted in the following figures (Figures 143-144) [21-26]. Once the user has initiated the process, the software reveals three main options regarding the created polygon: *"Complete"*, *"Undo last point"*, and *"Clear"*, as presented in the next (Figure 143) [21-26].

Figure 143: ITK-SNAP, Polygon Mode, Manual Segmentation, Sagittal View

The following figure (Figure 144) presents the result of the completed polygon of the spleen in the Sagittal view, depicted with red framework [21-26]. If the result is satisfactory, the user should select the *"Accept"* button (Figure 145), and afterwards the contour will be incorporated into the segmentation [21-26].

Figure 144: ITK-SNAP, Polygon Mode, Manual Segmentation, Sagittal View, Finished Polygon of the spleen

Figure 145: ITK-SNAP, Polygon Mode, Manual Segmentation, Accept button

After pressing the *"Accept"* button, all the voxels inside the polygon are assigned to the active label, as illustrated in the following figure (Figure 146) [21-26].

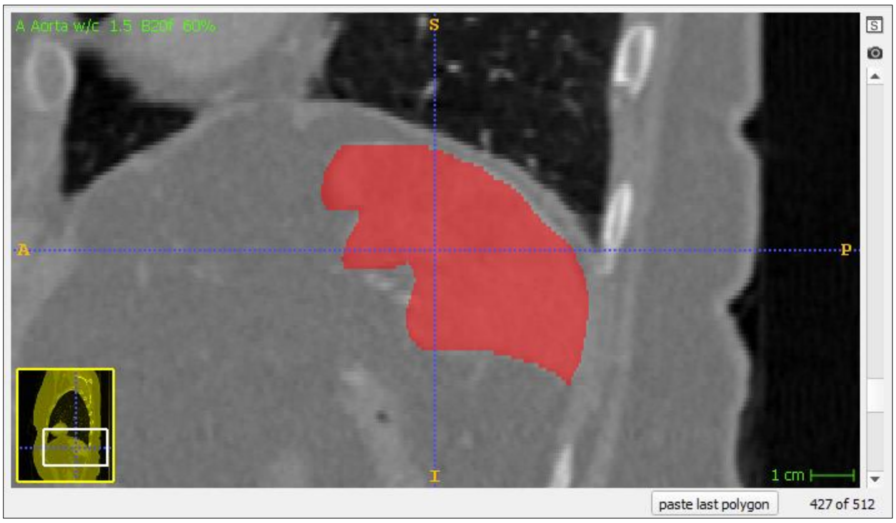

Figure 146: ITK-SNAP, Polygon Mode, Manual Segmentation, Sagittal View, Incorporated polygon into the segmentation

The user has the capacity of rendering the partial segmentation of the created model, by pressing the *"Update"* button in the 3D-view (Figure 146). Automatically, the result becomes visible in the 3D-view, as shown in the figure below (Figure 147) [21-26].

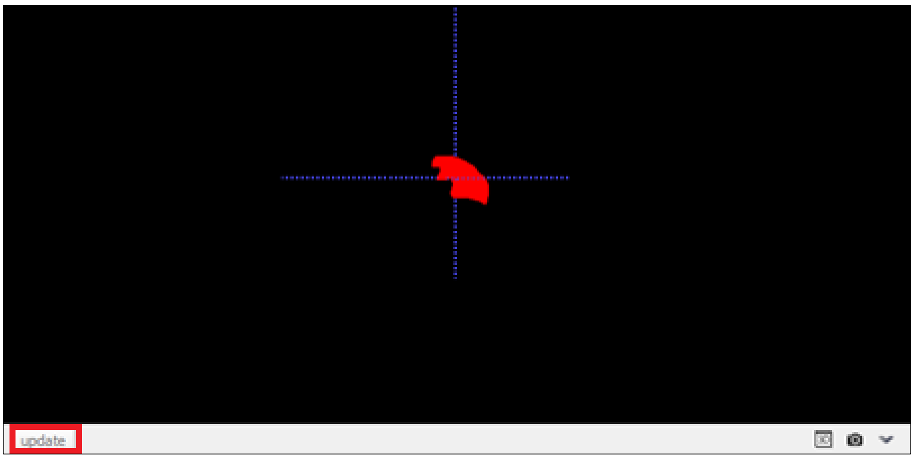

Figure 147: ITK-SNAP, Polygon Mode, Manual Segmentation, 3D-view of the polygon created in the Sagittal view, Update button

Consequently, the user should repeat the same procedure in the other two views (Axial and Coronal), presented as follows [21-26]. More specifically, the completed and the incorporated polygon of the Axial view are demonstrated in the following figures (Figures 148-149).

Figure 148: ITK-SNAP, Polygon Mode, Manual Segmentation, Axial View, Finished Polygon of the spleen

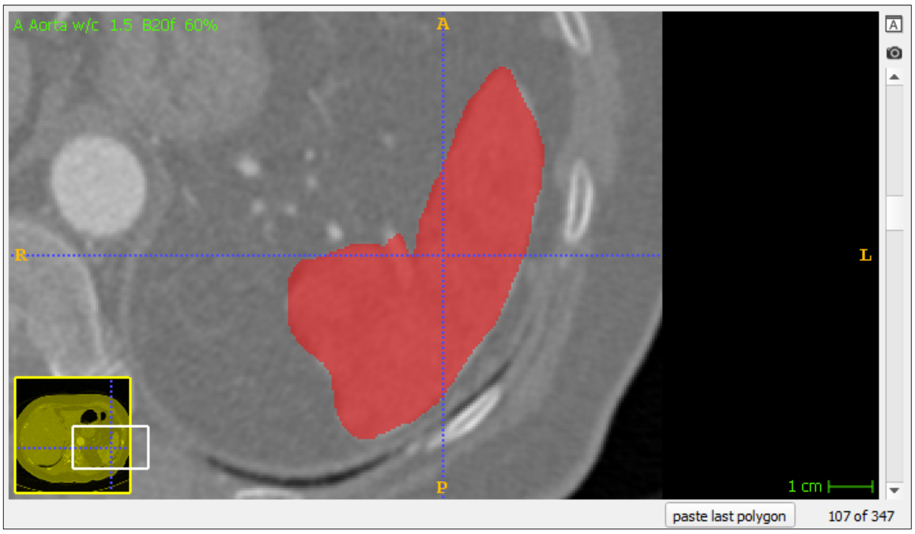

Figure 149: ITK-SNAP, Polygon Mode, Manual Segmentation, Axial View, Incorporated polygon into the segmentation

Additionally, the result of the 3D-model of the partial segmentation of the Axial view appears on the 3D-view, after pressing the *"Update"* button, as demonstrated in the next figure (Figure 150) [21-26].

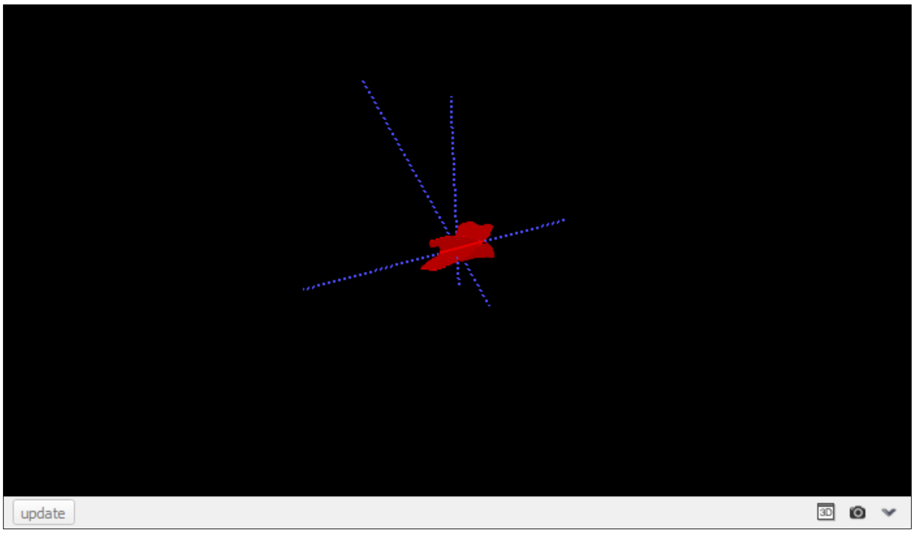

Figure 150: ITK-SNAP, Polygon Mode, Manual Segmentation, 3D-view of the polygon created in the Axial view

In similar manner, the user should proceed in creating a polygon in the Coronal view [21-26]. The completed polygon of the Coronal view is demonstrated in the following figures (Figures 151-152).

Figure 151: ITK-SNAP, Polygon Mode, Manual Segmentation, Coronal View, Finished Polygon of the spleen

Figure 152: ITK-SNAP, Polygon Mode, Manual Segmentation, Coronal View, Incorporated polygon into the segmentation

Moreover, the result of the 3D-model of the partial segmentation of the Coronal view appears on the 3D-view after pressing the *"Update"* button, as demonstrated in the next figure (Figure 153). As it can be observed in this figure, the three views created previously are visible in the 3D-view [21-26].

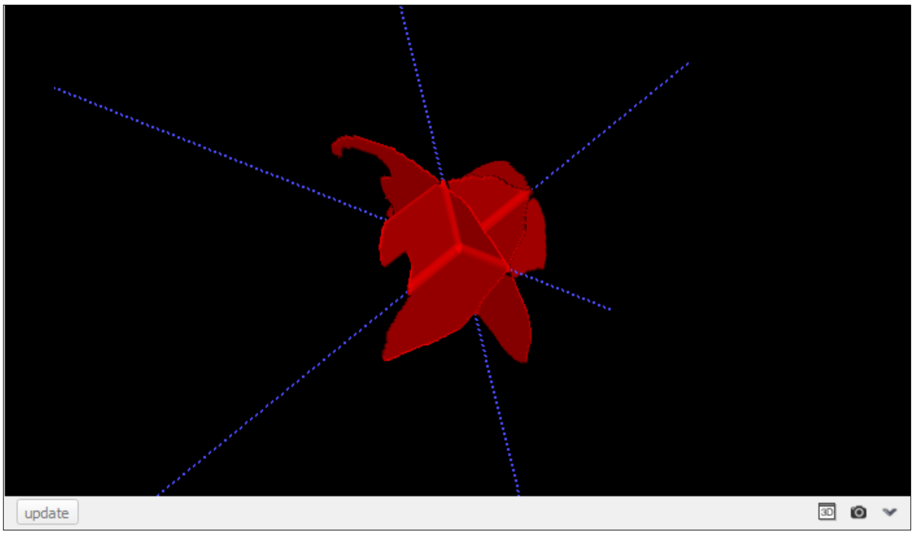

Figure 153: ITK-SNAP, Polygon Mode, Manual Segmentation, 3D-view of the polygon created in the Coronal view

Instead of using the *"Polygon Mode"* tool, as demonstrated previously, the user can select the *"Paintbrush Mode"* tool from the *"Main Toolbar"* (Figure 154), for conducting the same process [21-26]. This tool provides different brush shapes (*"Brush*

Style" and *"Brush Size"* in *"Paintbrush Inspector"* illustrated in Figure 155), in order to perform the manual segmentation [21-26].

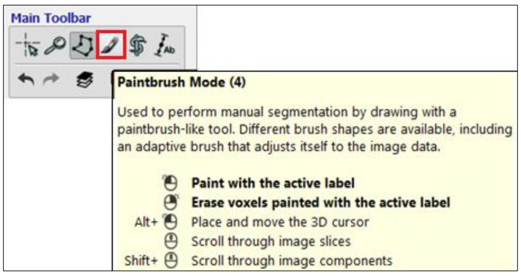

Figure 154: ITK-SNAP, Main Toolbar, Paintbrush Mode

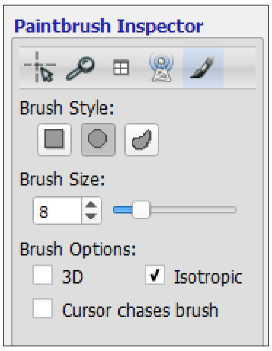

Figure 155: ITK-SNAP, Main Toolbar, Main Toolbar, Paintbrush Inspector

The final result of the manual segmentation of the spleen for the three views (i.e. Axial, Sagittal and Coronal) is presented in the following figure (Figure 156). In fact, this process must be repeated several times in the three views, until the desired geometry of the segmented part is fully captured [21-26].

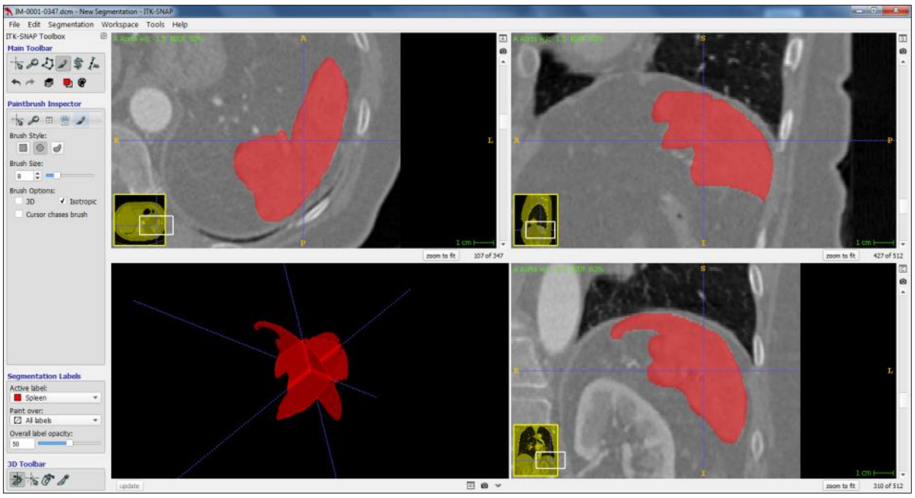

Figure 156: ITK-SNAP, Polygon Mode, Manual Segmentation, Result for the three views

Saving Segmention Image

After acquiring the desired geometry of the medical model, the user is supposed to save the created project. Therefore, in order to save the project, the user should select *Segmentation→ Save Segmentation Image*, from the drop-down menu, as illustrated in the following figure (Figure 157) [21-26].

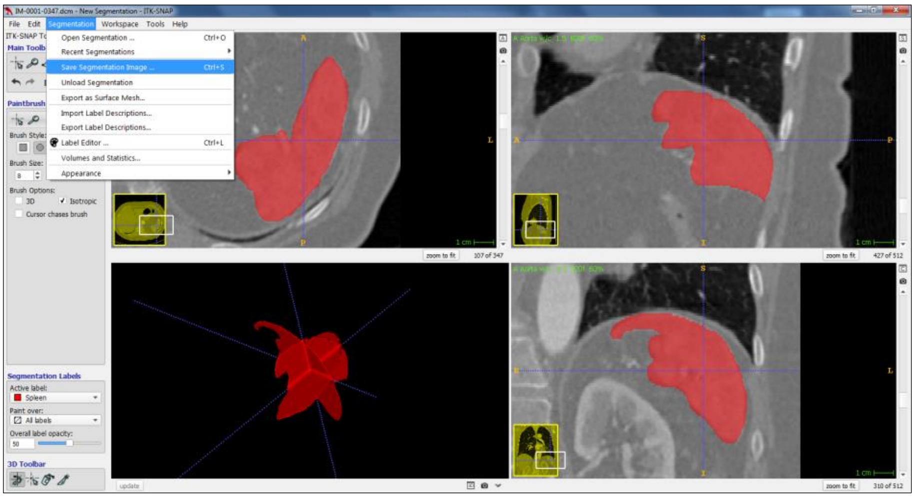

Figure 157: ITK-SNAP, Saving Segmentation Image

Automatically, the *"Save Image"* wizard reveals on the screen, asking the user to select the *"Image File name"*, the location and the *"File Format"*. For the current case, as illustrated in the next figure (Figure 158), the file format is selected to be *"NiFTI"*. Alternatively, the user has in his disposition a list of available file formats [21-26].

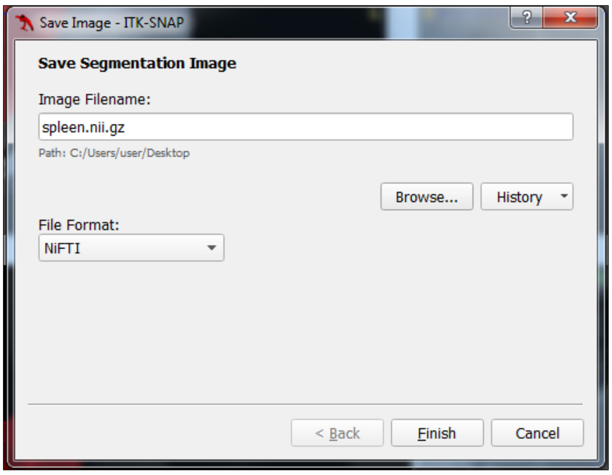

Figure 158: ITK-SNAP, Save Segmentation Image, wizard

5. Chapter Five: Case study of T4 Vertebra of Thoracic Spine

5.1. Introduction

In this chapter of the thesis, a new case study is selected to be examined. The main purpose of this chapter is the presentation of the complete process of the digital fabrication of patient specific 3D-printed medical model. Hence, the identification of a specific case scenario is crucial for the purpose of understanding the fabrication procedure. Particularly, in the current project, the T4 vertebra of the thoracic spine of a patient is selected to be examined.

5.2. Systematic Approach

In particular, the systematic approach of the process is divided into three fundamental sections: the *"Design"*, the *"Manufacture"*, and the *"Evaluation"* stage, as represented in the following flow chart (Chart 2).

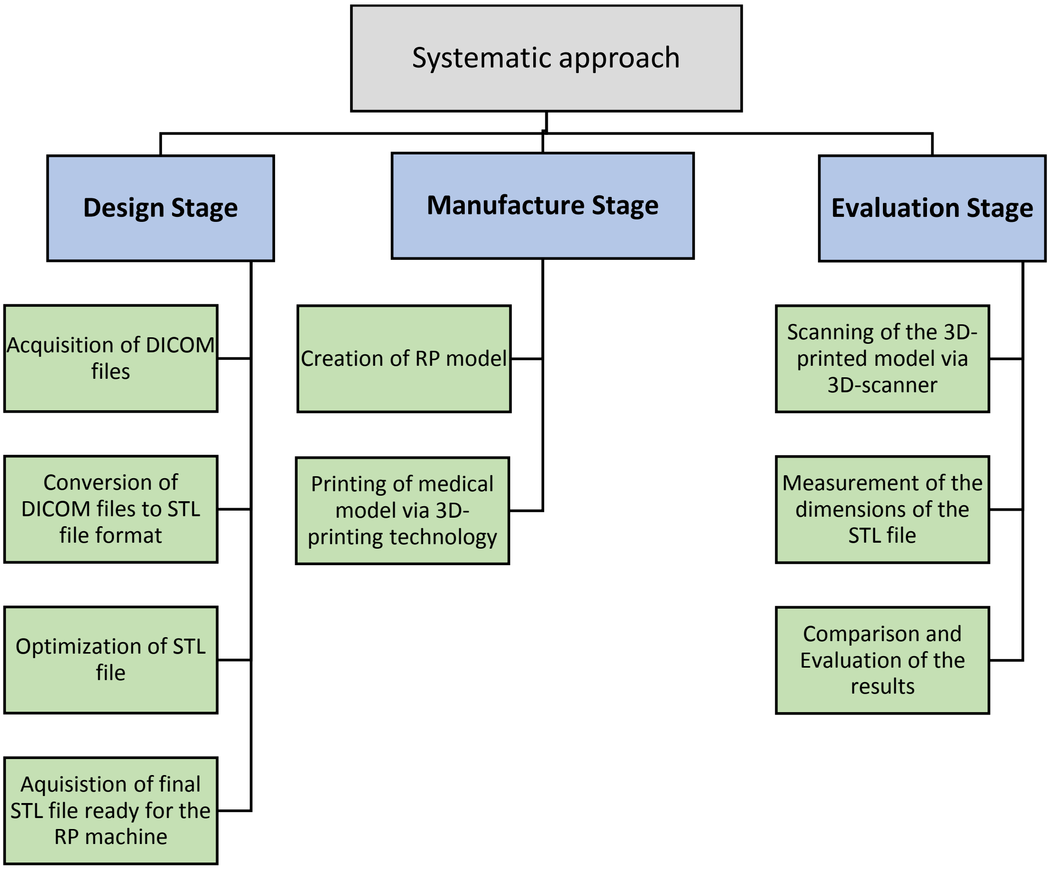

Chart 2: Flow chart of the systematic approach of the case study

5.3. Design Stage

Initially, the most fundamental step in the fabrication process of a medical part is considered to be the *"Design Stage"*. This stage is composed of four main steps, required for the acquisition of the STL file of the model. Specifically, these steps are the following: *"Acquisition of DICOM files"*, *"Conversion of DICOM files to STL file format"*, *"Optimization of the STL file"* and finally *"Acquisition of the final STL file ready for the RP machine"*, as demonstrated in the flow chart below (Chart 3). The process of this stage is described in a step-by-step approach in the following sections.

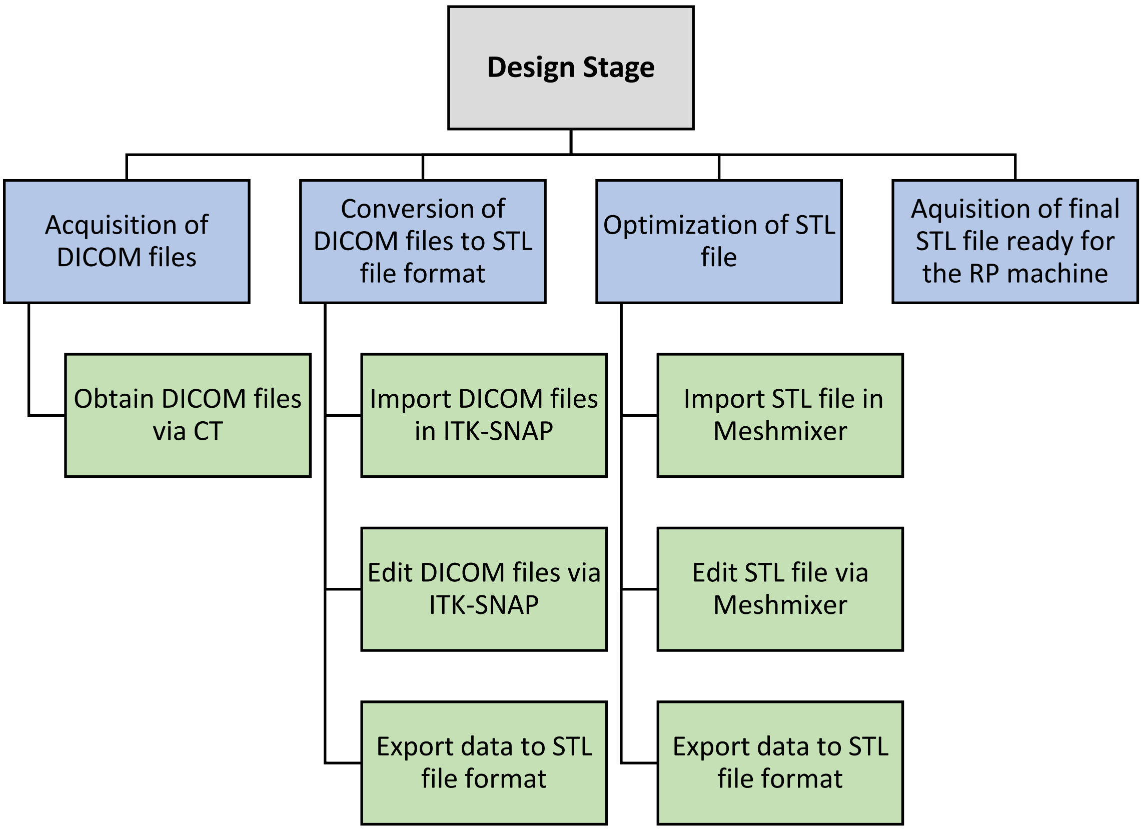

Chart 3: Flow chart of the design stage of the case study

5.3.1. Step 1: Acquisition of DICOM Files

In order to launch a new project it is essential to obtain the appropriate medical files, that provide the information about the anatomical part of the patient. In the current days, the technological improvements resulted in the 3D-image acquisition of the identical replica of the anatomy of a patient, with the help of CT (Gibson *et al.*, 2006;

Kumar *et al.*, 2017; Lim *et al.*, 2006). More specifically, the data is stored in Digital Imaging and Communication in Medicine (DICOM) images, utilized as the basic source for medical software's 3D-CAD, in order to produce AM medical models (Kumar *et al.*, 2017; Lim *et al.*, 2006), as described in the literature review (Chapter 2).

5.3.1.1. Obtain DICOM Files via CT

With respect to the current case study, a series of DICOM files of a patient's thorax is used, acquired from CT scan. More specifically, the DICOM files are downloaded from ITK-SNAP's official site, from the available data archive, found on: *"Thorax_1CTA_THORACIC_AORTA_GATED (Adult)"* file [6].

Furthermore, the output of the CT slices, saved in DICOM standardized file format, can be displayed as a two-dimensional or three-dimensional preview in various DICOM viewer software programs. In the following figures (Figures 159-161), the Radiant DICOM Viewer is selected for the display of the CT scan slices of the patient's thorax, illustrated in Axial, Coronal, and Sagittal view.

Figure 159: Radiant DICOM Viewer, 2D CT scan of the patient's thorax, Axial view

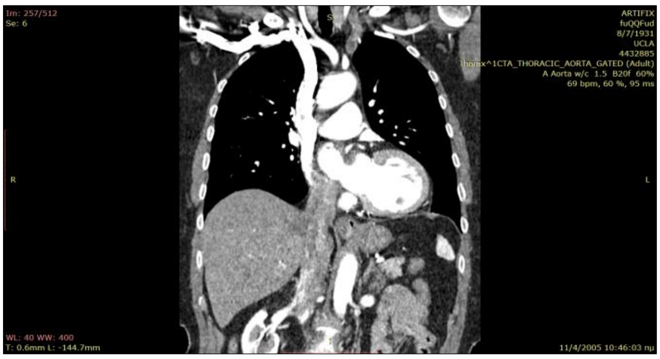

Figure 160: Radiant DICOM Viewer, 2D CT scan of the patient's thorax, Coronal view

Figure 161: Radiant DICOM Viewer, 2D CT scan of the patient’s thorax, Sagittal view

Additionally, the Radiant DICOM Viewer provides the option of 3D-volume rendering for six distinct views (i.e. Anterior (A), Posterior (P), Left (L), Right (R), Superior (S) and Inferior (I) 3D-views), as presented in the figures below (Figures 162-164).

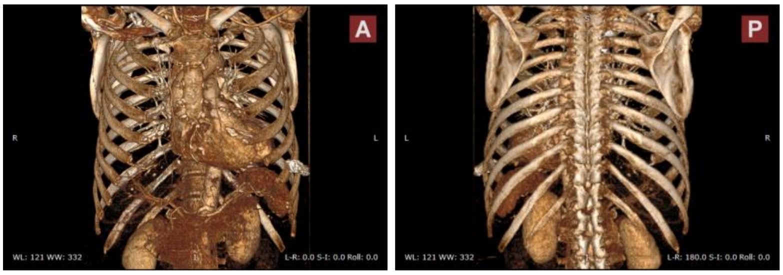

Figure 162: Radiant DICOM Viewer, 3D-volume rendering of the patient’s thorax

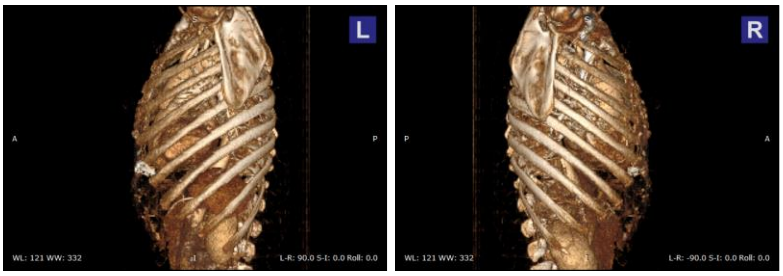

Figure 163: Radiant DICOM Viewer, 3D-volume rendering of the patient’s thorax

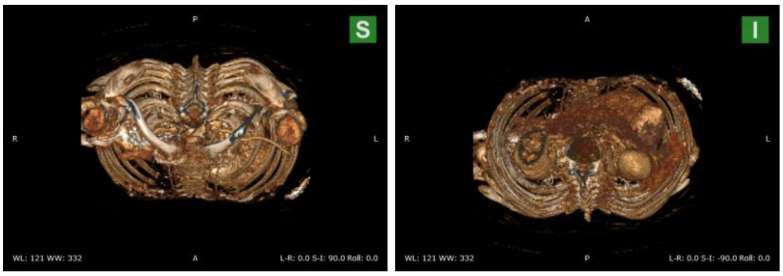

Figure 164: Radiant DICOM Viewer, 3D-volume rendering of the patient’s thorax

5.3.2. Step 2: Conversion of DICOM Files to STL File Format

After aquiring the desired DICOM files from the CT scan, the next step refers to the conversion of the DICOM files to STL file format. The following steps summarize the conversion process.

5.3.2.1. Import DICOM Files in ITK-SNAP

The first step of the conversion process refers to importing the DICOM files in the selected software. For the current case, the ITK-SNAP software program is chosen for the manipulation of the DICOM files. The importation process of the DICOM files is described in detail in the corresponding section of Chapter 4 (Section 4.2.4.).

5.3.2.2. Edit DICOM Files via ITK-SNAP

After importing the appropriate DICOM files, it is suggested that the user proceeds to the segmentation process, in order to distinguish the *"Region of Interest"* in the data set from the surroundings, by facilitating the creation of the desired geometric model (Hnatkova *et al.*, 2014). The process of *"Automatic Segmentation"* (Section 4.2.4.) for the selected region of the thoracic spine is described as follows. Particularly, the user is supposed to select the *"Active Contour (aka "Snake") Segmentation Mode"* button, from the main toolbar, as depicted with red framework in the following figure (Figure 165) [21-25].

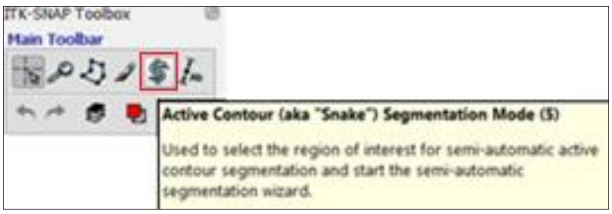

Figure 165: ITK-SNAP, Main Toolbar, Active Contour Segmentation Mode

Once the user has selected this button, the software reveals a red-dotted framework in the three orthogonal views, as depicted in the figure below (Figure 166) [21-25]. After defining the *"Region of Interest"*, the user should press the *"Segment 3D"* button (Figure 167), illustrated on the left side of the screen, on the *"Snake Inspector"* menu

[21-25]. In the current project, the ROI is selected to be the thoracic spine of the patient, as illustrated more clearly in the Sagittal view (Figure 166) [21-25].

Figure 166: ITK-SNAP, Main Toolbar, Active Contour Segmentation Mode, Selecting the Region of Interest (ROI)

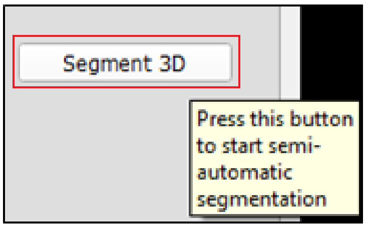

Figure 167: ITK-SNAP, Main Toolbar, Active Contour Segmentation Mode, Segment 3D

Actually, the *"Automatic Segmentation"* is divided into three different steps (*"Pre-segmentation"*, *"Initialization"*, and *"Evolution"*), illustrated in the right side of the screen [21-25], as described thoroughly in the respective section of Chapter 4 (Section 4.2.4.).

Initially, the first step is related to pre-processing the image by adjusting the speed function [21-25]. For the current case, the speed function is selected to be generated by *"Thresholding"* mode (Figures 168-169). After adjusting the required settings in the *"Pre-segmentation"* step, the user should press the *"Next"* button, in order to proceed to the second step of *"Initialization"* procedure [21-25]. In the Figure 169, the process is selected to be demonstrated on the second option of view, depicted with blue color, where the bones appear with white color.

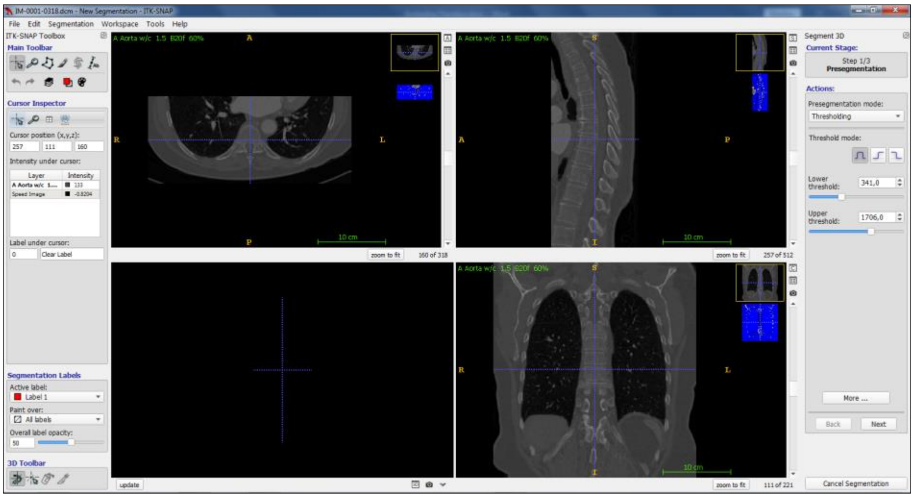

Figure 168: ITK-SNAP, Main Toolbar, Active Contour Segmentation Mode, Segment 3D, Step 1: Pre-segmentation

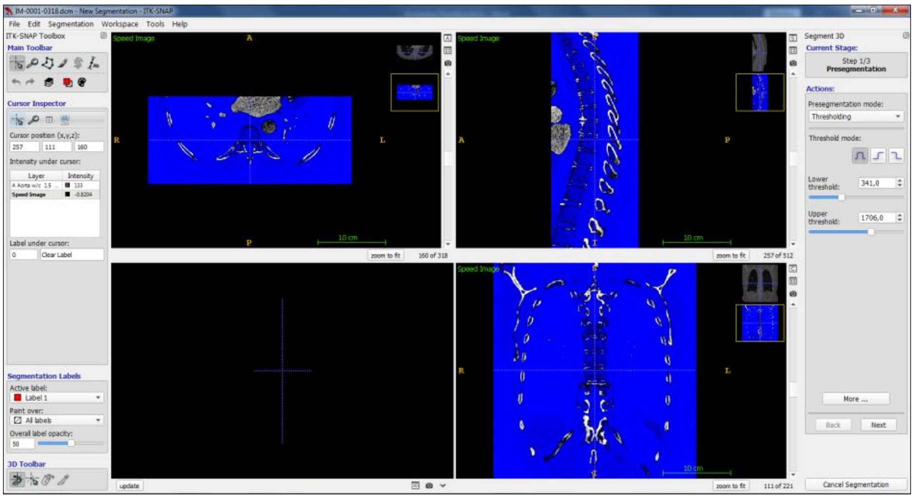

Figure 169: ITK-SNAP, Main Toolbar, Active Contour Segmentation Mode, Segment 3D, Step 1: Pre-segmentation, second option of view depicted in blue color

Secondly, the user proceeds to the *"Initialization"* step (Figure 170-172). In this step, the software prompts the user to place bubbles in the image, in order to initialize the contour [21-25].

Hence, the user should press the *"Add Bubble at Cursor"*, by adjusting the *"Bubble radius"*, in order to be adapted to the desired region of interest [21-25]. Furthermore, the user is enabled to go *"Back"*, or to *"Cancel Segmentation"*, by pressing the corresponding buttons, as illustrated in Figure 170 and Figure 172 [21-25].

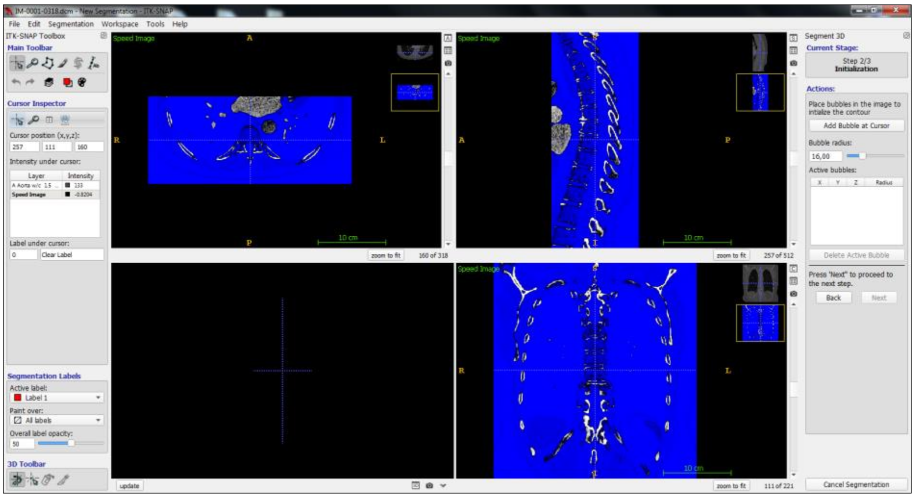

Figure 170: ITK-SNAP, Main Toolbar, Active Contour Segmentation Mode, Segment 3D, Step 2: Initialization, Adding Bubbles at Cursor

In fact, the selected bubbles for the patient's thoracic spine are illustrated in the next figure (Figure 171), for the three orthogonal views (i.e. Axial, Sagittal and Coronal).

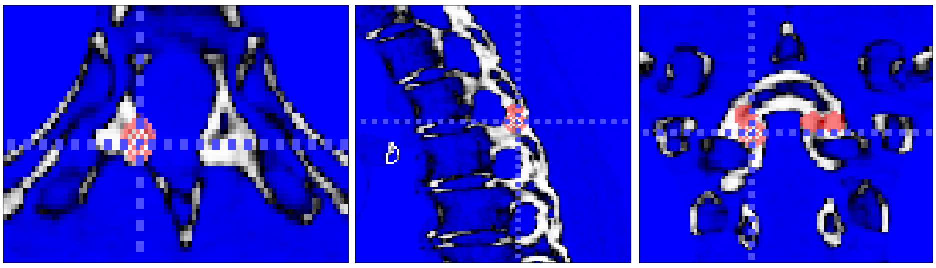

Figure 171: ITK-SNAP, Segment 3D, Step 2: Initialization, Adding Bubbles at Cursor

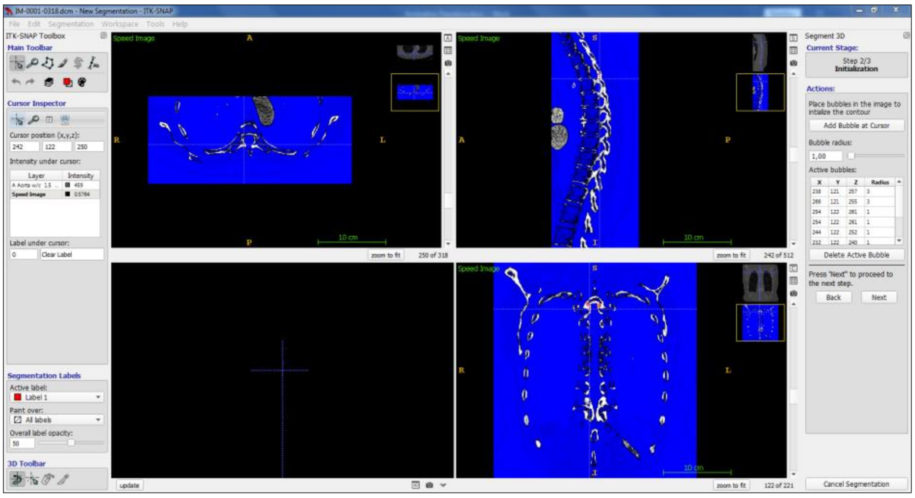

Figure 172: ITK-SNAP, Main Toolbar, Active Contour Segmentation Mode, Segment 3D, Step 2: Initialization, Adding Bubbles at Cursor

Finally, the user can start the contour evolution by pressing the *"Play"* button (Figures 173-174) [21-25]. When the result of the created region is satisfactory, the user should select the *"Finish"* button, in order to complete the final step (Figures 173-174).

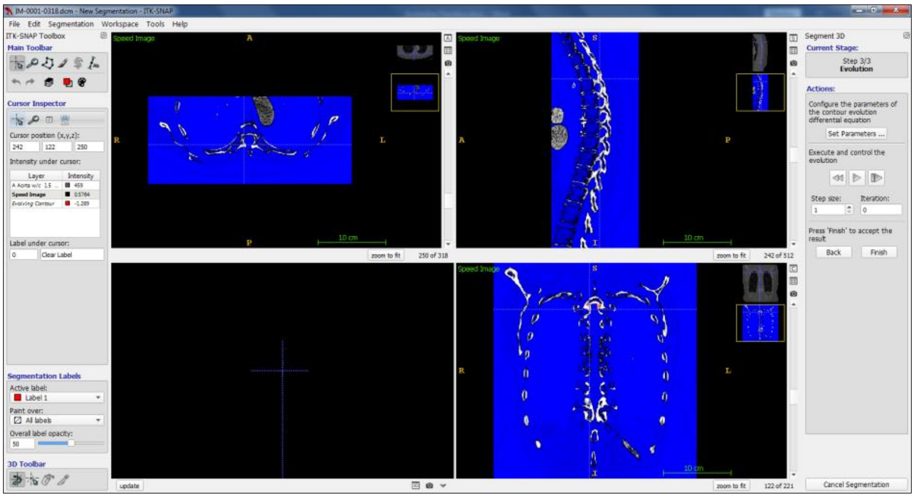

Figure 173: ITK-SNAP, Main Toolbar, Active Contour Segmentation Mode, Segment 3D, Step 3: Evolution

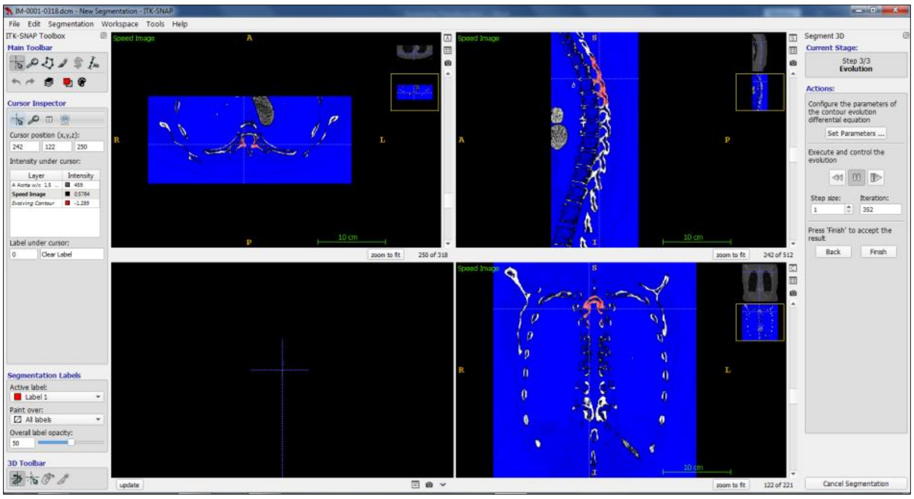

Figure 174: ITK-SNAP, Main Toolbar, Active Contour Segmentation Mode, Segment 3D, Step 3: Evolution, Process of evolution

In order to see the final result of the 3D-segmented model, the user should press the *"Update"* button (Figure 175), on the left-down corner of the 3D-viewer panel [21-25]. Automatically, the software reveals a 3D-image of the segmented model of the region of interest [21-25]. The result of the current project, is presented in the next figure (Figure 176). Additionally, the user can navigate through this 3D-image, by zooming or panning around [21-25]. In the Figure 177, the created 3D-model of the three vertebras (T3, T4, T5) of the thoracic spine, is illustrated when zoomed in.

Figure 175: ITK-SNAP, Main Toolbar, Active Contour Segmentation Mode, Segment 3D, Step 3: Evolution, Final result

Figure 176: ITK-SNAP, Main Toolbar, Active Contour Segmentation Mode, Segment 3D, Step 3: Evolution, Final result, Updated 3d-view

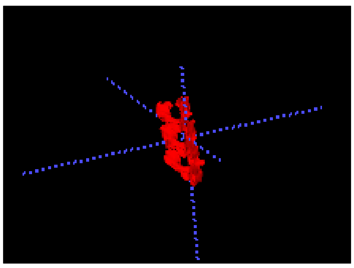

Figure 177: ITK-SNAP, Final result, Updated 3d-view of the three vertebras (T3, T4, T5) of the thoracic spine

5.3.2.3. *Export Data to STL File Format*

After completing the editing procedure, the user should export the created files into external formats. In specific, the user should select from the drop-down menu, *Segmentation→ Export as Surface Mesh*, as presented in the following figure (Figure 178) [22-25].

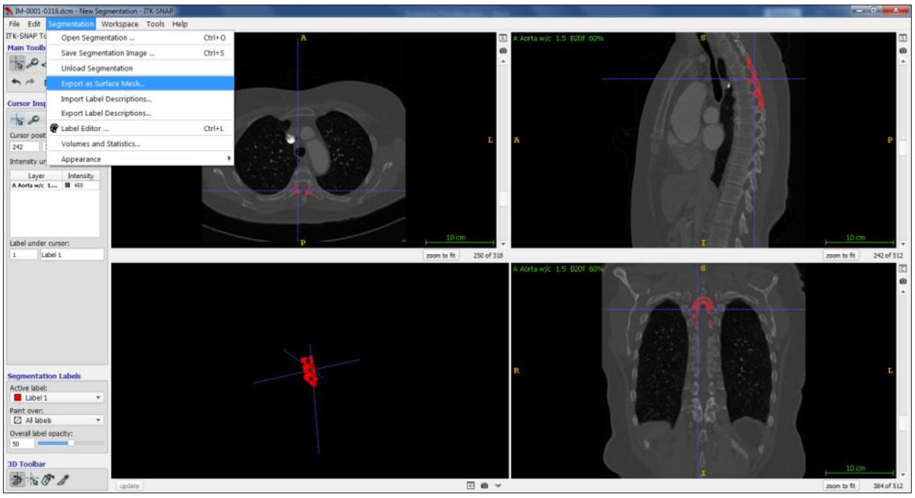

Figure 178: ITK-SNAP, Segmentation, Exporting as Surface Mesh, drop-down menu

Subsequently, the software opens by default a wizard (Figure 179) asking the user to select *"Which labels will be exported"* [22-25]. In the current project, the first option is selected, as illustrated in the following figure (Figure 179). The user should press the *"Next"* button and proceed to the next page of the wizard (Figure 180), referring to the destination of the exported file [22-25]. Actually, the software prompts the user to select the name, the destination, the type of format of the file (Figure 180).

Figure 179: ITK-SNAP, Segmentation, Exporting as Surface Mesh, Wizard, Labels to be exported

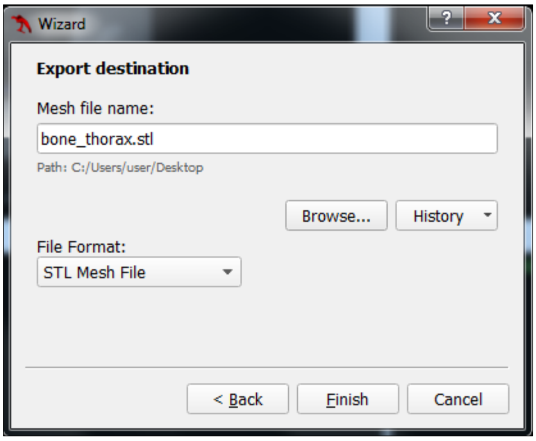

Figure 180: ITK-SNAP, Segmentation, Exporting as Surface Mesh, Wizard, Export destination

5.3.3. Step 3: Optimization of STL File

After exporting the 3D-model from the ITK-SNAP software in STL format, it is necessary to optimize this file, before procedding to the manufacture stage. The optimization process is presented in the three next sections (Sections 5.3.3.1.-5.3.3.3.), with the help of Meshmixer software.

5.3.3.1. Import STL File in Meshmixer

In the following figure (Figure 181), is illustrated the *"Welcome Screen"* of the Meshmixer software. This screen opens-up by default displaying the most fundamental options that are available, demonstrated on the main menu.

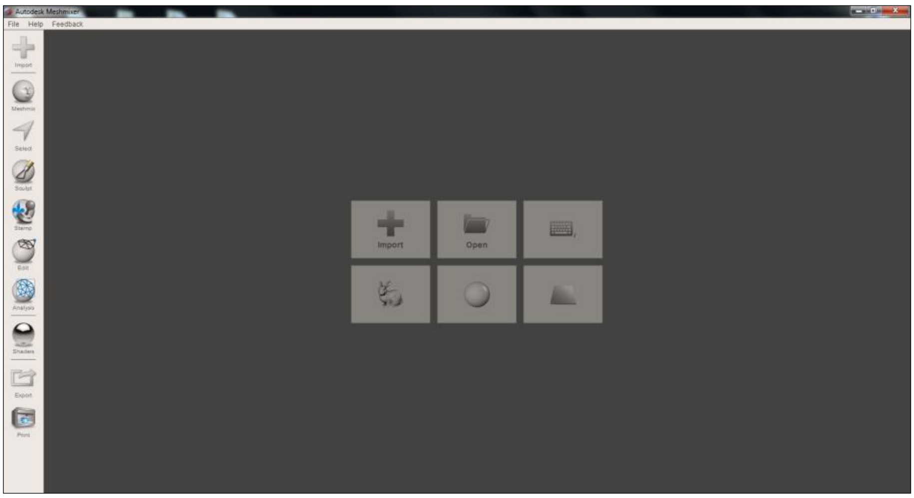

Figure 181: Meshmixer, Welcome Screen

In order to import the desired STL file, the user should press the corresponding button (*“Import”*) (Figure 181), or alternatively select *File→ Import* from the drop-down menu (Figure 182) and then select the proper STL file from the directory.

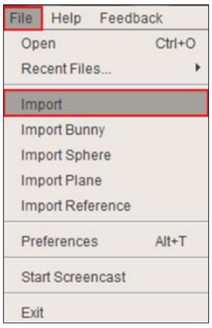

Figure 182: Meshmixer, Import file, drop-down menu

Actually, the imported STL file of the three vertebras (T3, T4, T5) of the patient’s thoracic spine is presented in the following figure (Figure 183).

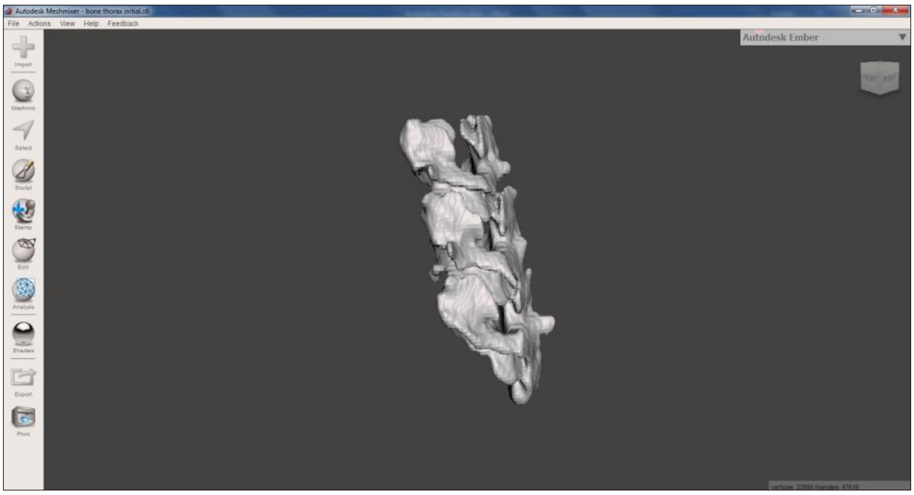

Figure 183: Meshmixer, Imported STL file, vertebras (T3, T4, T5) of the thoracic spine

5.3.3.2. *Edit STL File via Meshmixer*

For the current case, the T4 vertebra of the thoracic spine is selected to be examined. Consequently, by utilising the Meshmixer software, the T4 vertebra is isolated from the array of the thoracic vertebras. The user should press the *“Select”* button from the toolbar, then select the region that will be erased, appearing in orange color in the next figure (Figure 184), and finally press the *“Erase & Fill”* button, as illustrated below (Figure 184).

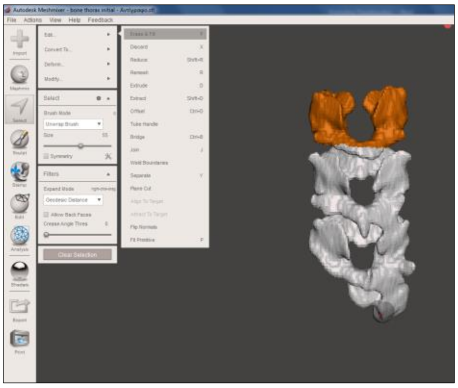

Figure 184: Meshmixer, Select option, Erase & Fill (the T3 vertebra of the thoracic spine, illustrated with orange color)

Subsequently, the user should select the *"Accept"* button, as demonstrated in the figure below (Figure 185). Additionally, the user should repeat the same process for the inferior part of the model (the T5 vertebra), as presented in Figure 186.

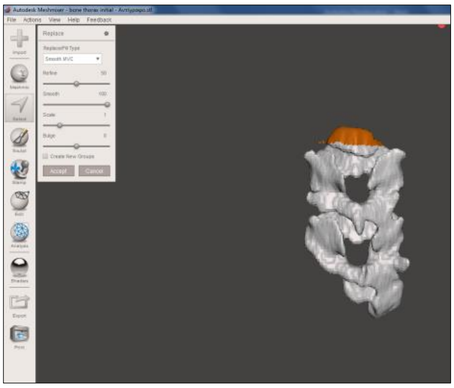

Figure 185: Meshmixer, Select option, Erase & Fill (the T3 vertebra of the thoracic spine, illustrated with orange color), Accept button

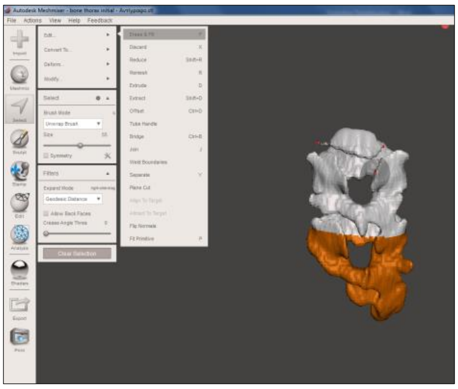

Figure 186: Meshmixer, Select option, Erase & Fill (the T5 vertebra of the thoracic spine, illustrated with orange color)

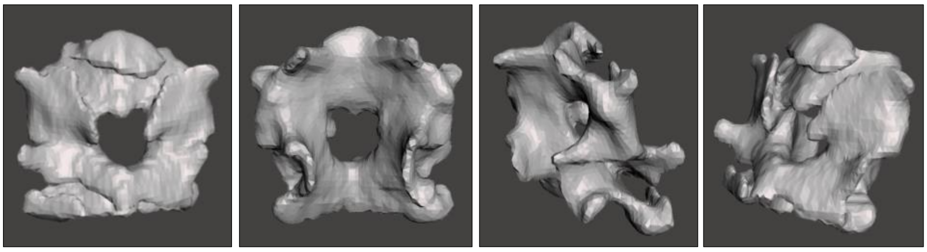

Figure 187: Meshmixer, T4 vertebra of the thoracic spine

The result of the T4 vertebra of the patient's thoracic spine, illustrated in the figures above (Figure 187), contain many imperfections. In order to optimize the created model, the user should press the *"Select"* button from the toolbar, then the *"Modify"* option and finally the *"Smooth Boundary"* option, as presented in the following figure (Figure 188). Automatically, the software opens a window that provides a number of options regarding the smoothing operation, demonstrated in the right side of the following figure (Figure 188).

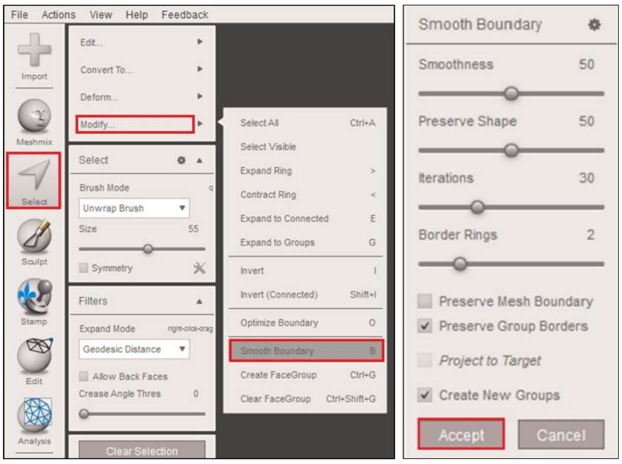

Figure 188: Meshmixer, Select option, Modify option, Smooth Boundary adjustment

The result of the 3D-model of the T4 vertebra of the patient's thoracic spine, after conducting the smoothing operations properly, is depicted in the following three figures (Figure 189). The first figure, on the left, presents the initial model before performing the smoothing operations. The second figure, in the middle, demonstrates the model after adjusting the smoothing boundaries. The third figure, on the right, presents the final model, modified in an appropriate way, by correcting and erasing the edgy points in the superior part of the volume, in order to obtain a high-quality result.

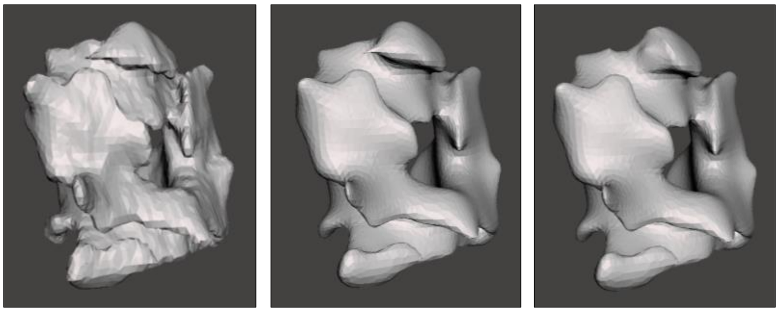

Figure 189: Meshmixer, T4 vertebra of the thoracic spine

5.3.3.3. Export Data to STL File Format

After completing the editing procedure, the user should export the created file into STL file format. Particularly, the user should select from the drop-down menu, *File→ Export*, as presented in the following figure (Figure 190).

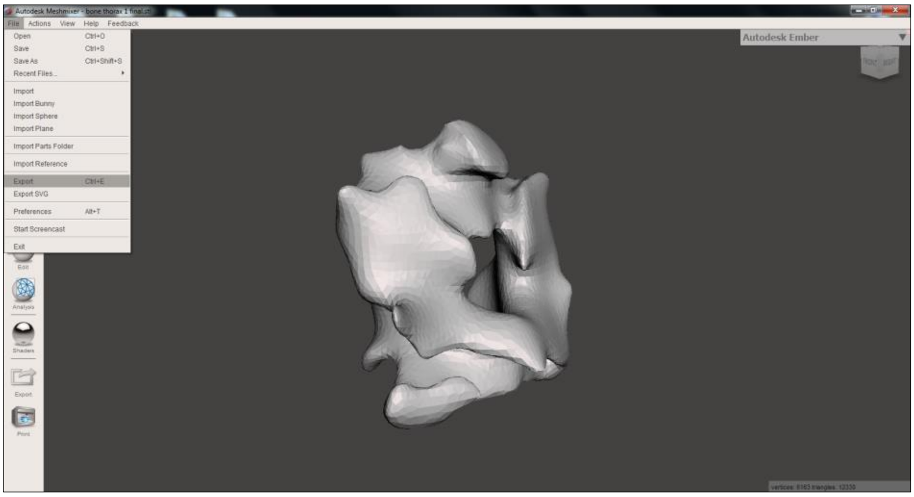

Figure 190: Meshmixer, Exporting data to STL file format, drop-down menu

5.3.4. Step 4: Aquisition of Final STL File Ready for RP Machine

At last, the design stage is completed and the final model exported into STL file format is ready for the manufacture stage, utilizing the Rapid Prototyping technology. The final result of the T4 vertebra of the patient's thoracic spine, is illustrated in the figures below (Figure 191), depicted in four different views. The first figure (from the left) presents anterior plane of model, while the second figure presents the posterior side of the model. The third and the fourth figures demonstrate the left and the right plane of the model, correspondingly.

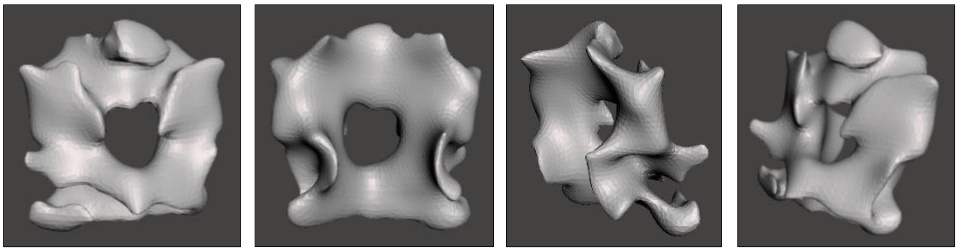

Figure 191: Final STL file of the created 3D-model of the T4 vertebra of the patient's thoracic spine, (Anterior, Posterior, Left, Right side of the model)

5.4. Manufacture Stage

Subsequently, the second stage of the fabrication process of the medical part is the *"Manufacture Stage"*. In fact, this stage is composed of two main steps, required for production of the medical model, the *"Creation of the RP model"*, and the *"Printing of medical model via 3D-printing technology"*, as demonstrated in the next flow chart (Chart 4). More precisely, for the fabrication of the T4 vertebra, the Fused Deposition Modeling (FDM) technology is used, by utilizing the BCN3D Cura 1.0.3. software and the BCN3D Sigma R17 printer, for the creation of the RP model and for the 3D-printing of the medical model respectively. As a matter of fact, the process of manufacture stage is described in a step-by-step approach in the following sections.

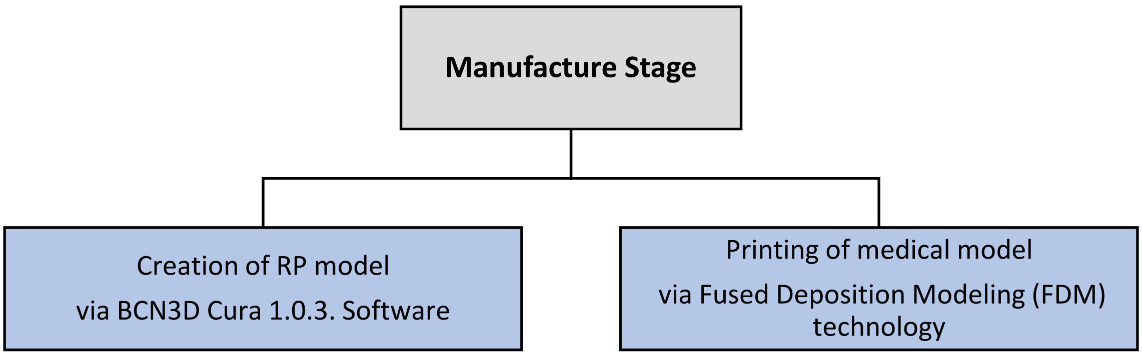

Chart 4: Flow chart of the manufacture stage of the case study

5.4.1. Step 1: Creation of RP Model

Regarding the first step of the manufacture stage, the BCN3D Cura 1.0.3. software is utilized for the creation of the RP model. The process of the RP model creation of the T4 vertebra is illustrated in the figures bellow (Figures 192-195).

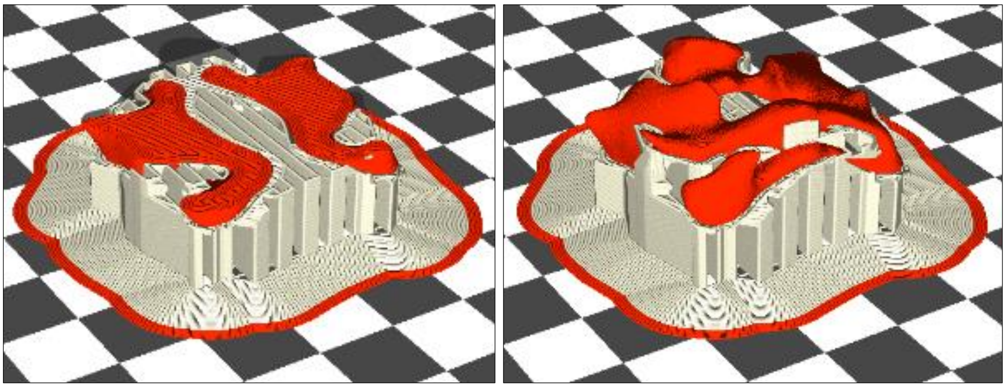

Figure 192: BCN3D Cura 1.0.3, Creating the RP model of the T4 vertebra

Actually, the next figures (Figures 193-195) demonstrate the creation of the RP model of the T4 vertebra, illustrating the environment of the software.

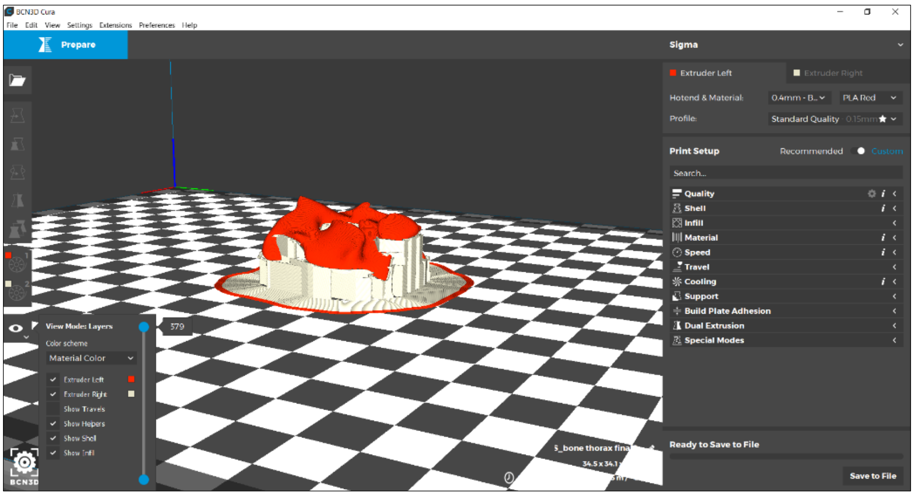

Figure 193: BCN3D Cura 1.0.3, Creating the RP model of the T4 vertebra

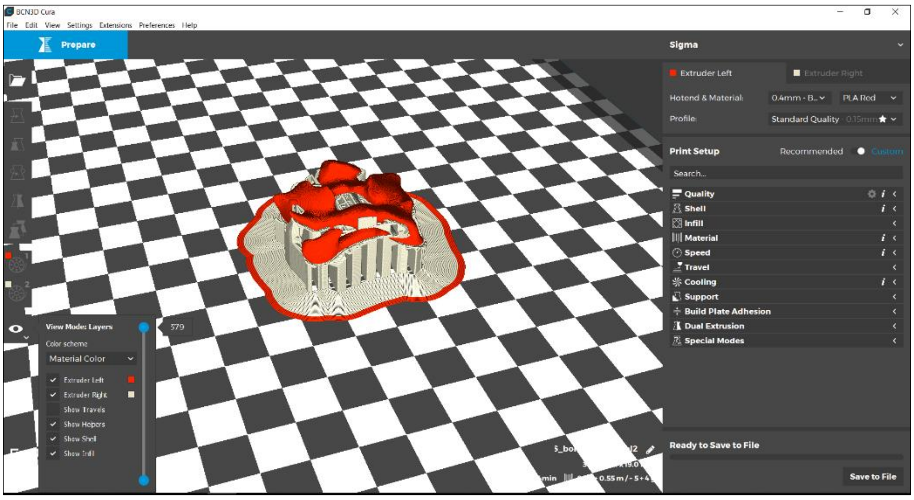

Figure 194: BCN3D Cura 1.0.3, Creating the RP model of the T4 vertebra

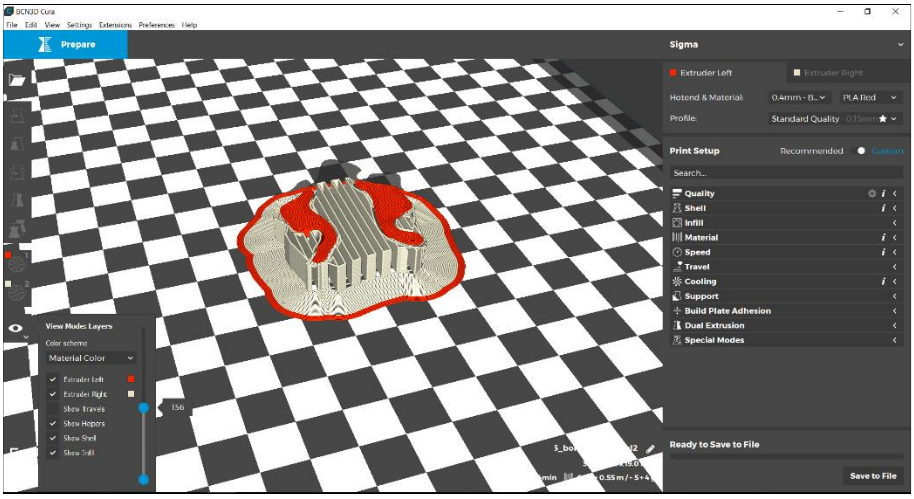

Figure 195: BCN3D Cura 1.0.3, Creating the RP model of the T4 vertebra

Moreover, the basic properties of the 3D-printing process, regarding the created medical model for the BCN3D Sigma R17 printer, are presented in the following table (Table 3).

Table 3: Printing properties of 3D-printing process for the BCN3D Sigma R17 printer

Printing Properties	
Material	PLA
Layer Thickness	0.05mm (50 microns)
Temperature	210^{o}C
Heat Bed	50^{o}C
Wall	1.6mm
Infill	100%
Speed	50mm/sec

5.4.2. Step 2: Printing of Medical Model via 3D-Printing Technology

After setting the appropriate parameters by utilizing the BCN3D Cura 1.0.3. software, the model is ready to be printed via 3D-printing technology. In particular, for the current case study of the T4 vertebra, Fused Deposition Modeling (FDM) technology is considered as a convenient method for the fabrication of the medical model, by using the BCN3D Sigma R17 printer (Figure 196) [27].

Consequently, the 3D-printing process of the T4 vertebra is illustrated in Figure 197. The medical model is printed layer-by-layer, based on FDM method.

Figure 196: The BCN3D Sigma R17 printer, Source: [27]

Figure 197: The 3D-printing process of the T4 vertebra via BCN3D Sigma R17 printer

Conclusively, the final result of the medical model, after removing the supporting material manually, is presented in the figures below (Figure 198). The first figure (on the left) depicts the anterior side of the obtained 3D-anatomical model, while the second figure (on the right) demonstrates the posterior side of the model.

Figure 198: The final 3D-printed model of the T4 vertebra, Anterior and Posterior Side

5.5. Evaluation Stage

At last, the third stage of the fabrication process of the medical model is the *"Evaluation Stage"*. Specifically, this stage is composed of three basic steps, required for evaluation of the medical model, the *"Scanning of the 3D-printed model via 3D-scanner"* (via Next Engine 3D-scanner and ScanStudio HD software), *"Measurement of the dimensions of the STL files"* (via Artec Studio 11 Professional software), and ultimately *"Comparison and Evaluation of the results"*, as illustrated in the following flow chart (Chart 5). Actually, the process of evaluation stage is presented in a step-by-step approach in the following sections.

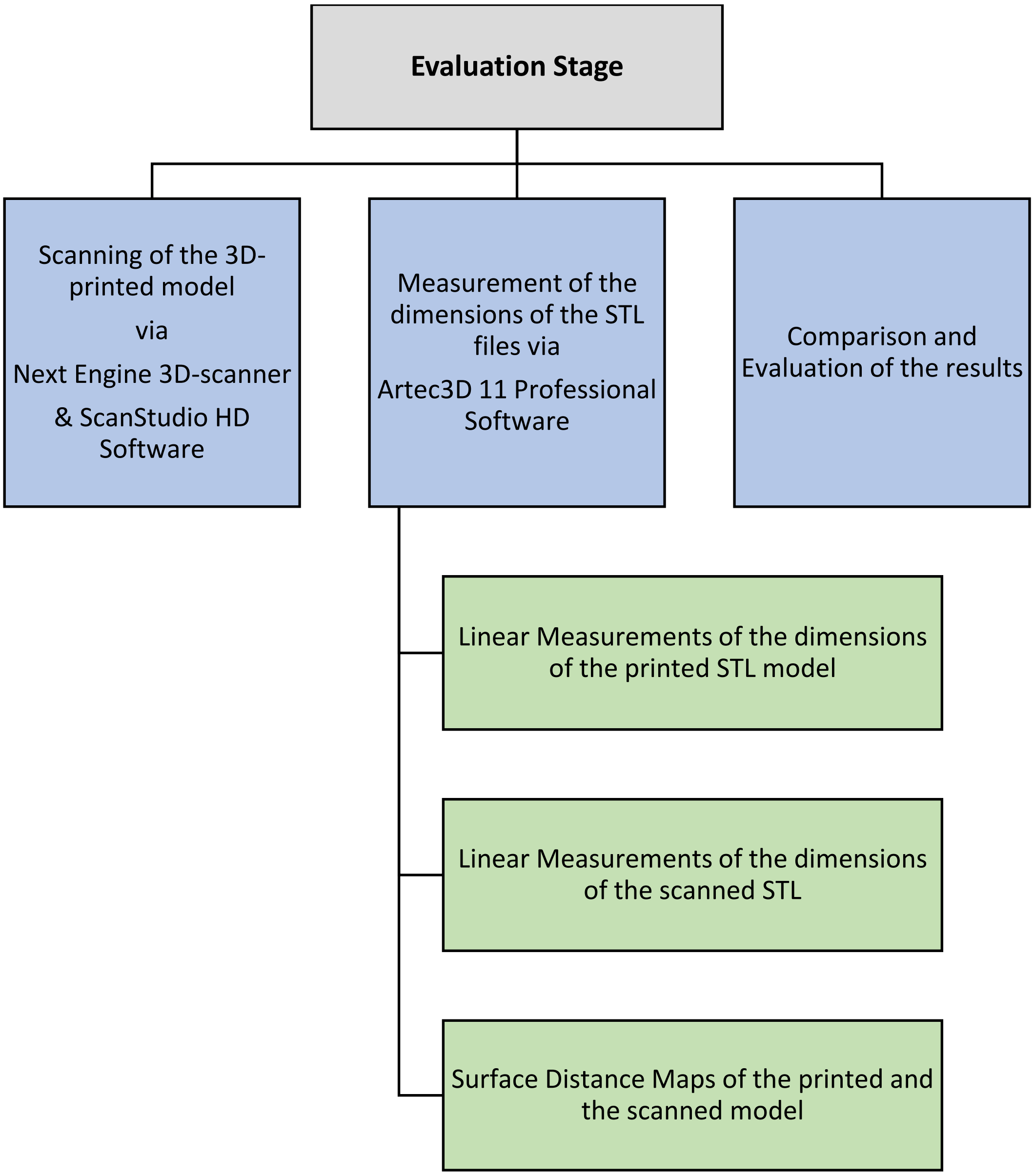

Chart 5: Flow chart of the evaluation stage of the case study

5.5.1. Step 1: Scanning of the 3D-Printed Model via 3D-Scanner

The first step of the evaluation process regards the 3D-scanning of the obtained medical model. As mentioned previously, it is essential to scan the 3D-printed model, in order to capture the entire geometry of the object and subsequently save the scanned model into STL file format, for further processing. Therefore, in the current project, the Next Engine 3D-scanner is utilized for scanning process of the 3D-printed anatomical model and the ScanStudio HD software is used for processing the scanned data.

5.5.1.1. Scanning of the 3D-Printed Medical Model via Next Engine

In fact, an analytical presentation of the steps needed to be undertaken for scanning the 3D-printed medical model are introduced as follows.

With respect to the scanning machine, the Next Engine 3D-scanner (Figure 199) is a Non-Contact Scanner that uses laser for capturing the geometry of an object and convert it to a digital format [28]. The Next Engine is a desktop 3D-scanner that measures 50,000 points per second with multi-laser precision, at 0.005 inches accuracy, providing users unprecedented ease of use to quickly create highly detailed, full color, digital models [28].

Figure 199: Next Engine 3D Scanner Source: [28], Placement of the T4 vertebra in the Auto-positioner of the scanner

Briefly, in order to achieve the most satisfactory results, concerning the geometrical features of the object, twenty-one distinct steps are conducted. Initially, the selected object is scanned, by setting the appropriate parameters in the ScanStudio HD software.

Secondly, it is crucial to understand the peculiarities and the requirements of the model, and translate them into specifications, in order to fully capture the geometry of the object. These settings regard the positioning, the number of divisions, the points/ in^2, the target and the range (Tables 4-10).

In particular, seven distinct captures (Captures A-G) are conducted by locating the object vertically and horizontally to the Auto-positioner, using additionally the provided tools (Figure 199), in order to achieve a sturdier and more stable result. Additionally, it is essential to align the object on scanning platform, by using the viewing window (Figure 200), so that the object is visible within the scanning field.

Other editing tools (trim, align, fuse, and buff) are necessary, for optimizing the captured geometry of the object. Particularly, it is mandatory to remove the noise and the overlapping surfaces from two different captures, in order to align them in a common coordinate system and get the entire geometry of the model. The alignment of the different captures (performed four times) is achieved by specifying some points in the shaded view of the object. Moreover, the fusion process is important for covering the missing geometry and gaps. In addition, the refinement of the final model is achieved by using the buffing tool. The depiction of the process is presented in detail as follows.

- *Capture A*

Figure 200: ScanStudio HD, Settings of Capture A, Viewing Window

Table 4: ScanStudio HD, Settings of Capture A

Settings	
Positioning	360
Divisions	15
Points/ in^2	160k, HD
Target	Neutral
Range	Macro
Time	51min
Memory	100%

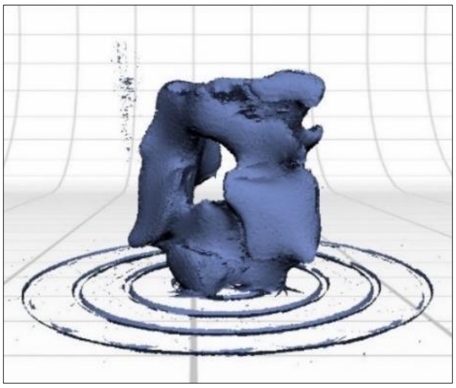

Figure 201: ScanStudio HD, Result of Capture A of T4 vertebra

- *Capture B*

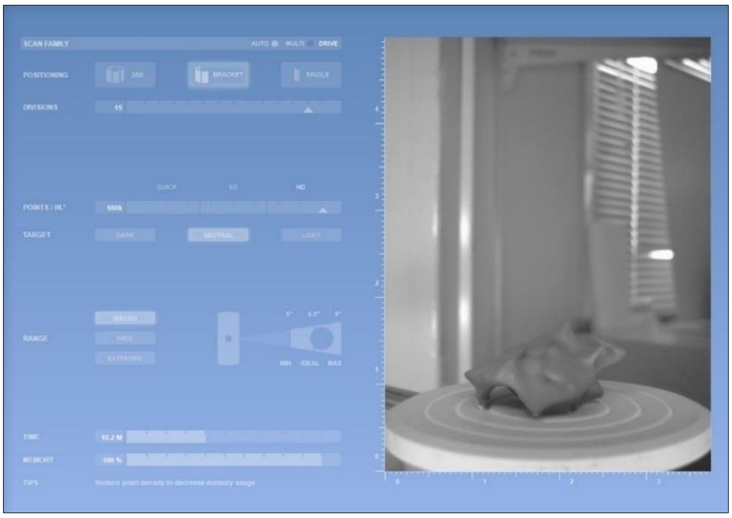

Figure 202: ScanStudio HD, Settings of Capture B, Viewing Window

Table 5: ScanStudio HD, Settings of Capture B

Settings	
Positioning	Bracket
Divisions	15
Points/ in^2	160k, HD
Target	Neutral
Range	Macro
Time	10.2min
Memory	100%

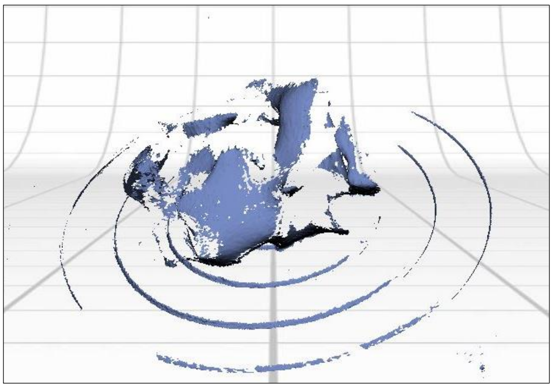

Figure 203: ScanStudio HD, Result of Capture B of T4 vertebra

➢ *Capture C*

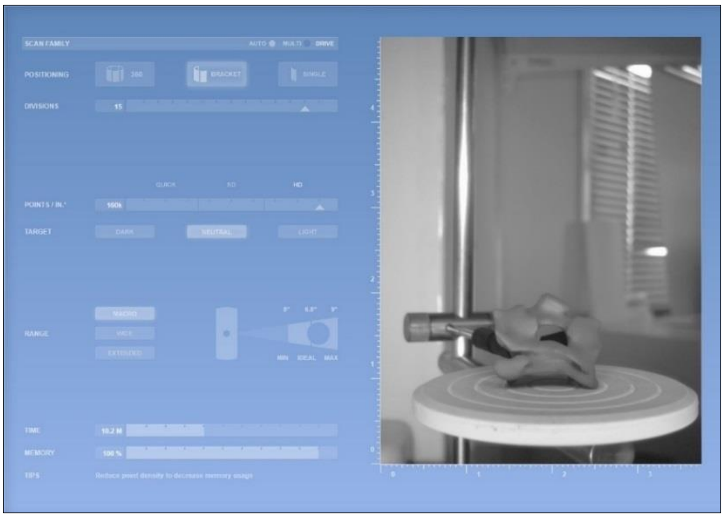

Figure 204: ScanStudio HD, Settings of Capture C, Viewing Window

Table 6: ScanStudio HD, Settings of Capture C

Settings	
Positioning	Bracket
Divisions	15
Points/ in^2	160k, HD
Target	Neutral
Range	Macro
Time	10.2min
Memory	100%

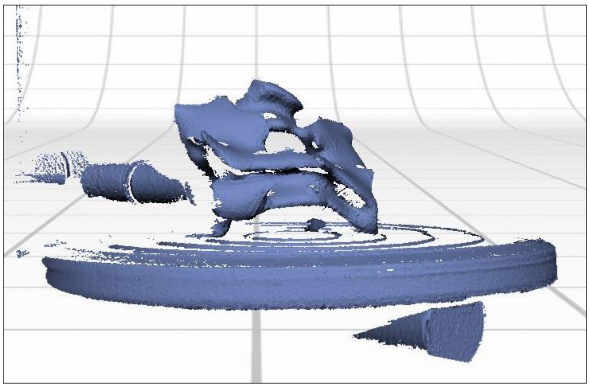

Figure 205: ScanStudio HD, Result of Capture C of T4 vertebra

- *Capture D*

Figure 206: ScanStudio HD, Settings of Capture D, Viewing Window

Table 7: ScanStudio HD, Settings of Capture D

Settings	
Positioning	Bracket
Divisions	15
Points/ in²	160k, HD
Target	Neutral
Range	Macro
Time	10.2min
Memory	100%

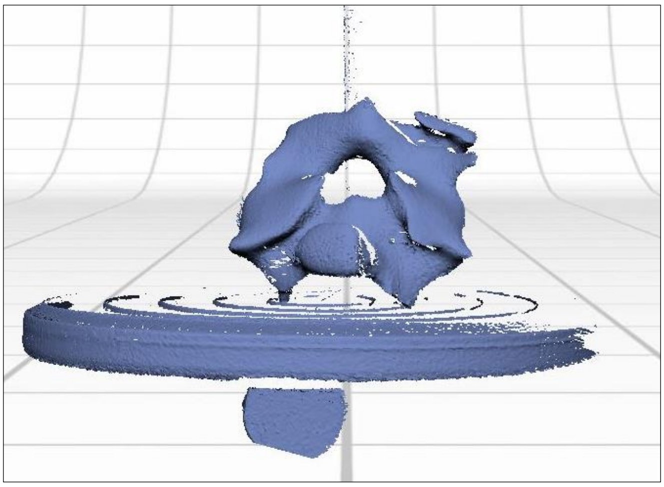

Figure 207: ScanStudio HD, Result of Capture D of T4 vertebra

- *Trimming of Capture C*

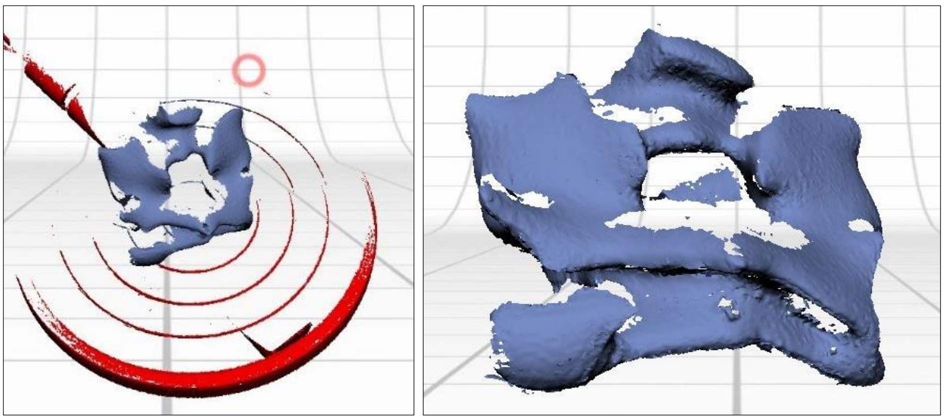

Figure 208: ScanStudio HD, Trimming of Capture C of T4 vertebra (left), Result (right)

➢ *Trimming of Capture D*

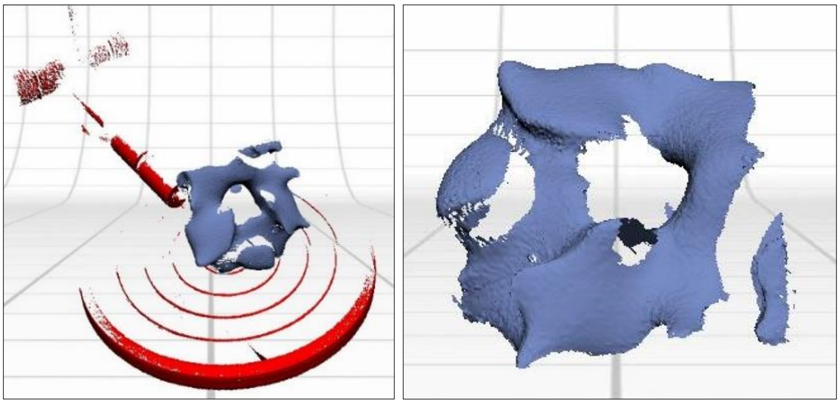

Figure 209: ScanStudio HD, Trimming of Capture D of T4 vertebra (left), Result (right)

➢ *Alignment of Captures C & D*

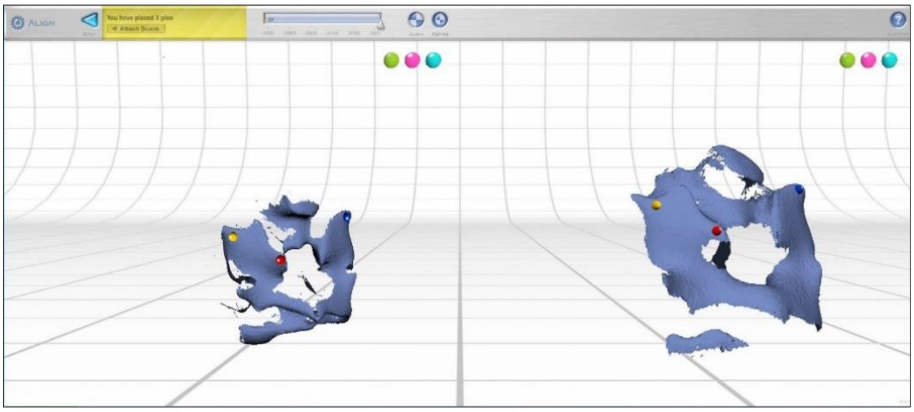

Figure 210: ScanStudio HD, Alignment of Captures C and D of T4 vertebra, adding points (red, yellow and blue)

➢ *Trimming of Capture A*

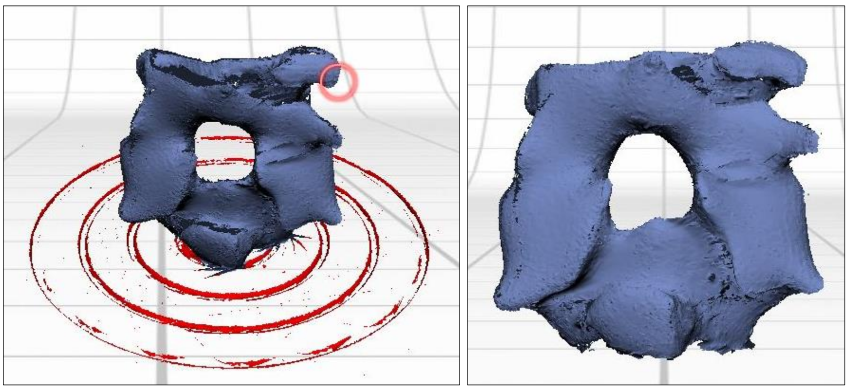

Figure 211: ScanStudio HD, Trimming of Capture A of T4 vertebra (left), Result (right)

➢ *Alignment of Capture C, D & A*

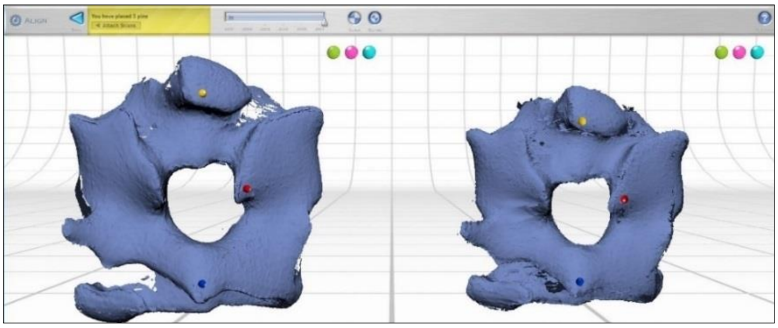

Figure 212: ScanStudio HD, Alignment of Captures C, D, and A of T4 vertebra, adding points (red, yellow and blue)

➢ *Capture E*

Figure 213: ScanStudio HD, Settings of Capture E, Viewing Window

Table 8: ScanStudio HD, Settings of Capture E

Settings	
Positioning	360
Divisions	12
Points/ in^2	160k, HD
Target	Neutral
Range	Macro
Time	40min
Memory	100%

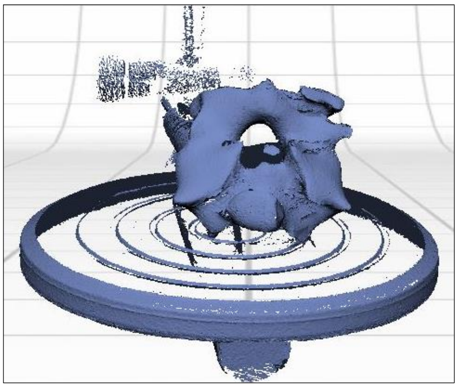

Figure 214: ScanStudio HD, Result of Capture E of T4 vertebra

- *Capture F*

Figure 215: ScanStudio HD, Settings of Capture F, Viewing Window

Table 9: ScanStudio HD, Settings of Capture F

Settings	
Positioning	360
Divisions	12
Points/ in^2	160k, HD
Target	Neutral
Range	Macro
Time	40min
Memory	100%

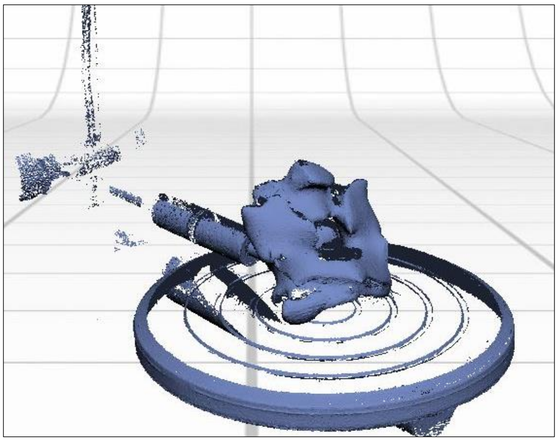

Figure 216: ScanStudio HD, Result of Capture F of T4 vertebra

- *Trimming of Capture E*

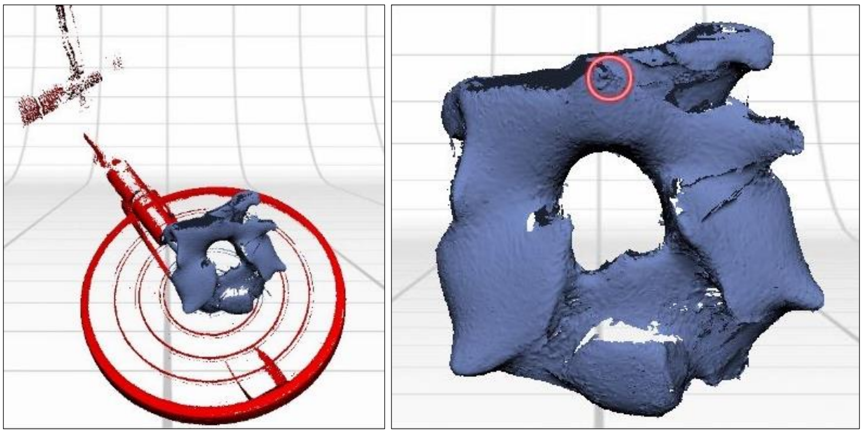

Figure 217: ScanStudio HD, Trimming of Capture E of T4 vertebra (left), Result (right)

- *Trimming of Capture F*

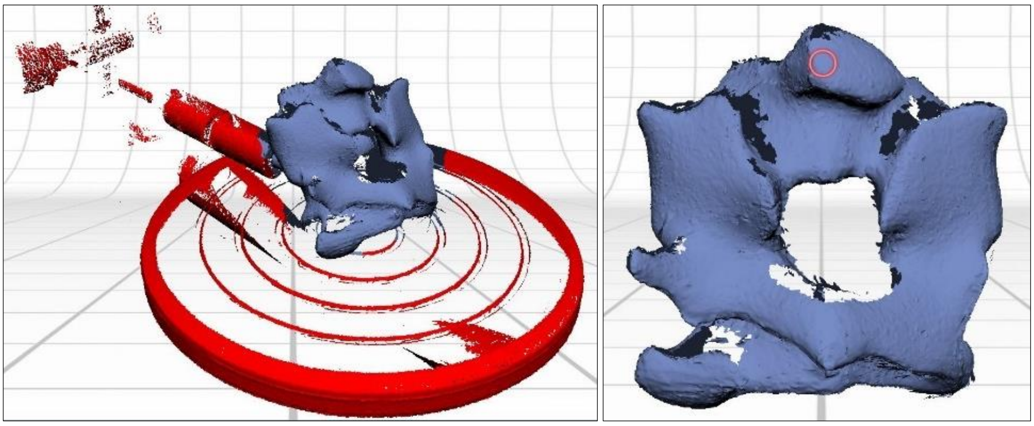

Figure 218: ScanStudio HD, Trimming of Capture F of T4 vertebra (left), Result (right)

- *Alignment of Captures C, D & E*

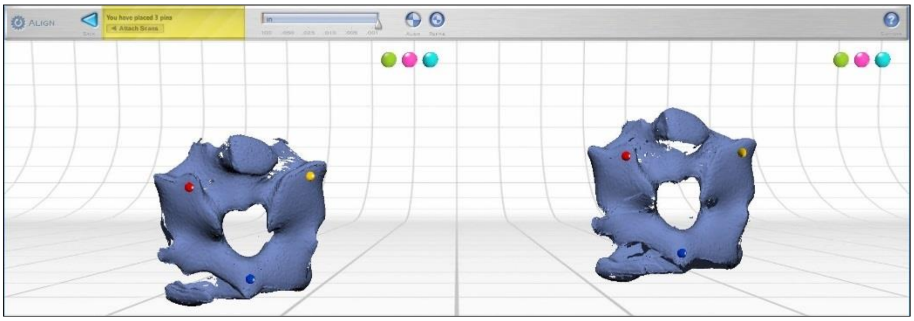

Figure 219: ScanStudio HD, Alignment of Captures C, D, and E of T4 vertebra, adding points (red, yellow and blue)

- *Alignment of Captures C, D, E & F*

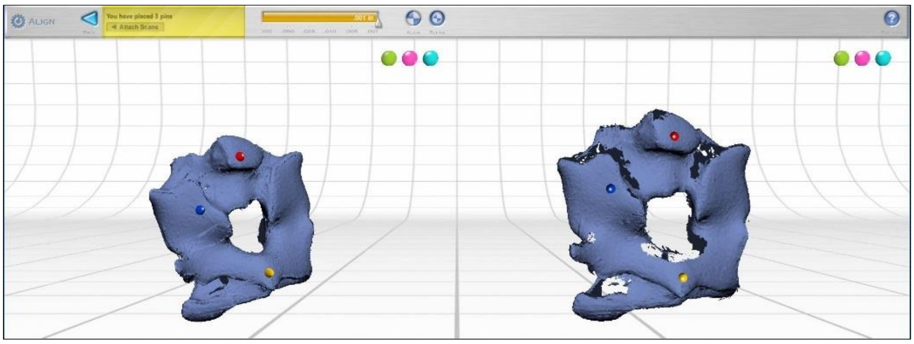

Figure 220: ScanStudio HD, Alignment of Captures C, D, E, and F of T4 vertebra, adding points (red, yellow and blue)

- *Capture G*

Figure 221: ScanStudio HD, Settings of Capture G, Viewing Window

Table 10: ScanStudio HD, Settings of Capture G

Settings	
Positioning	Bracket
Divisions	12
Points/ in^2	160k, HD
Target	Neutral
Range	Macro
Time	10.2min
Memory	100%

- *Alignment of Captures C, D, E, F & G*

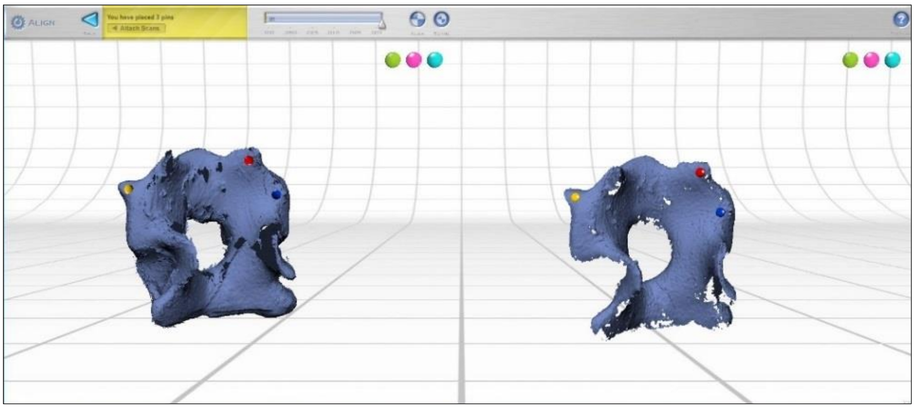

Figure 222: ScanStudio HD, Alignment of Captures C, D, E, F, and G of T4 vertebra, adding points (red, yellow and blue)

- *Trimming of Capture G after Alignment*

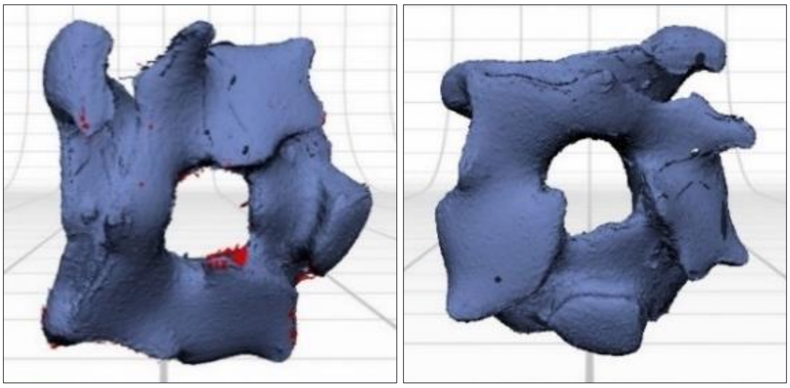

Figure 223: ScanStudio HD, Trimming of Capture G of T4 vertebra (left), Result (right)

➢ *Fusion of Capture G*

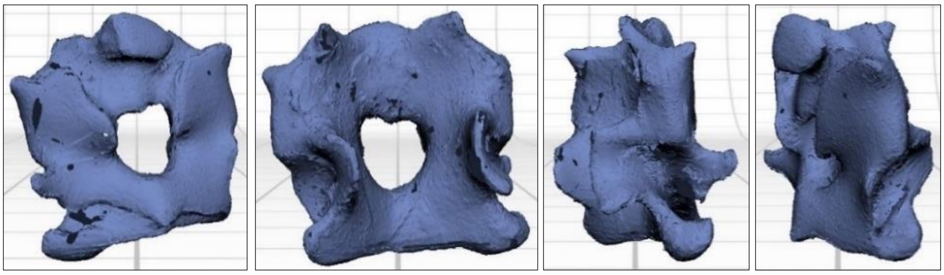

Figure 224: ScanStudio HD, Capture G of T4 vertebra before Fusion

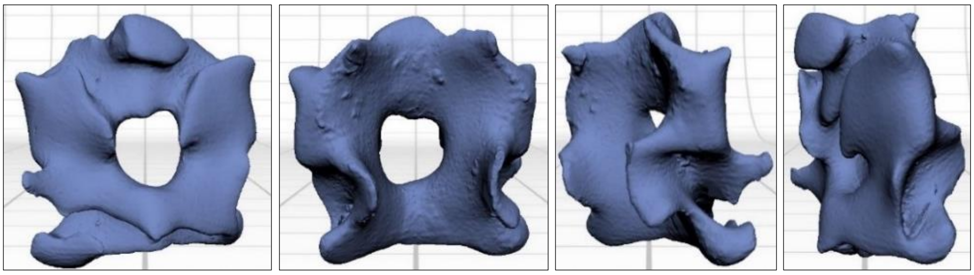

Figure 225: ScanStudio HD, Result of Capture G of T4 vertebra after Fusion

➢ *Buffing of Model on Specific Points*

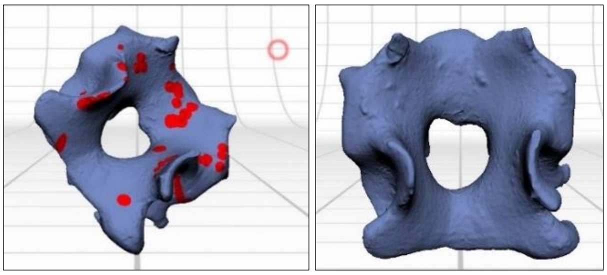

Figure 226: ScanStudio HD, Buffing of model of T4 vertebra (left), Result (right)

➢ *Buffing of the Entire Model*

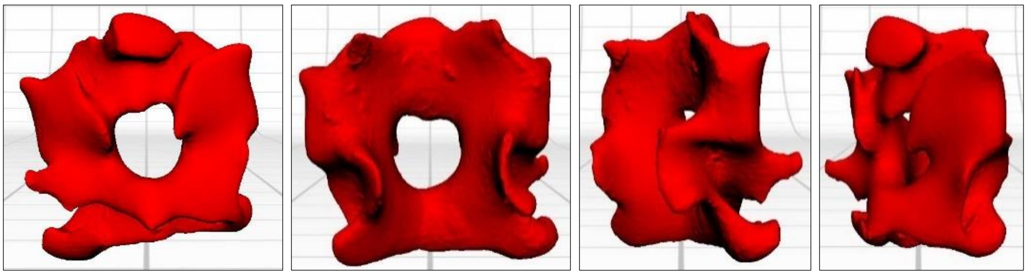

Figure 227: ScanStudio HD, Buffing of model of T4 vertebra

➢ *Final 3D-Scanned Model*

The final model obtained from the scanning process is illustrated in the following figures (Figure 228-229) in shaded and mesh view respectively.

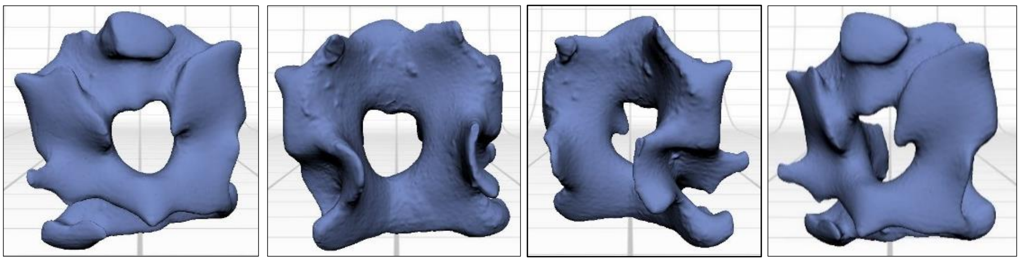

Figure 228: ScanStudio HD, Final result of the model of T4 vertebra, shaded view

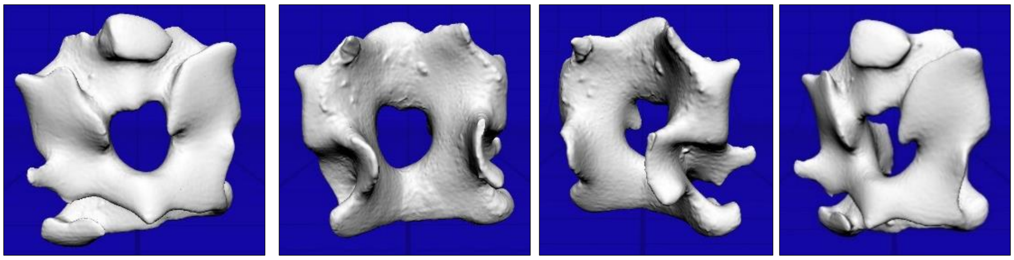

Figure 229: ScanStudio HD, Final result of the model of T4 vertebra, mesh view

5.5.1.2. Exporting Data to STL File Format

After completing the scanning procedure, the user should export the created file into STL file format. In particular, the user should select the "*Output"* button from the ScanStudio HD software, choose *"STL"* (as being the desired type of file), and then select the desired location to be saved. Alternatively, the user should select *Export→Save As* option, from the drop-down menu.

5.5.2. Step 2: Measurement of the Dimensions of the STL Files

After aquiring the desired STL files of the anatomical model of the T4 vertebra, it is fundamental to proceed to the next step of the evaluation stage. This step comprises the measurement and the evaluation of the dimensional declinations between the printed and the scanned STL models. Specifically, these measurements are conducted with the help of the Artec Studio 11 Professional software. In fact, the process of the measurements of the dimensions of the two STL models are presented as follows.

5.5.2.1. *Linear Measurement of the Printed STL Model*

The Artec Studio 11 Professional provides several measuring tools, including: *"Linear distance"*, *"Geodesic distance"*, *"Sections"*, *"Surface distance maps"*, and *"Annotations"* [29]. For the current project, the linear measuring tool is used in order to measure the distances between selected points [29]. The user should select the *"Measures"* button from the main toolbar, and then select the *"Linear distance"* tool, as illustrated in the following figure depicted with red framework (Figure 230) [29].

Figure 230: Artec Studio 11 Professional, Measures, Linear distance

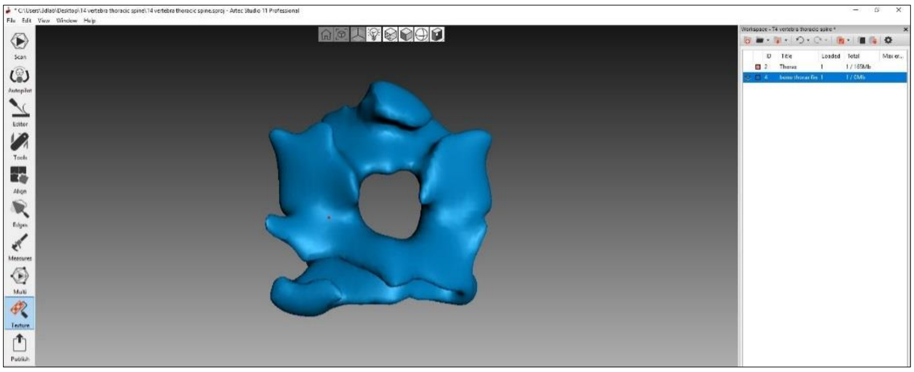

Figure 231: Artec Studio 11 Professional, Imported STL file of the printed model

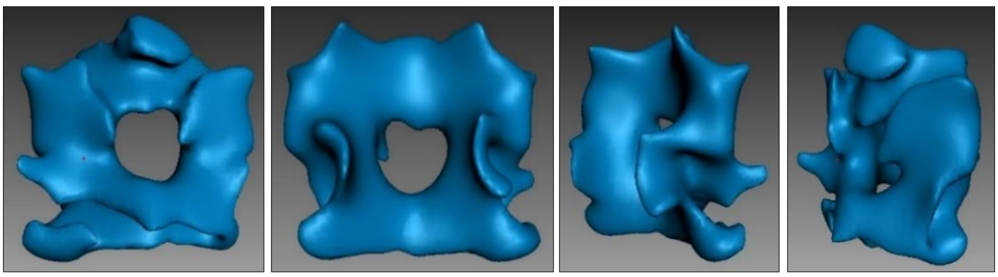

Figure 232: Artec Studio 11 Professional, Printed model of the T4 vertebra

➢ *First linear measurement of the printed model*

Initially, the linear measurements are conducted to the printed model of the T4 vertebra, depicted with blue color (Figures 231-232). In particular, three distinct measurements are made in two different parts of the model, in order to evaluate the results. Specifically, the process of the first measurement is presented in Figures 233-236, while the Table 11 demonstrates the results. The first linear measurement is defined from the distance from point 1 to point 2 (depicted with red color). The Figure 236 presents the depiction of all the linear measurements conducted for the current model, in order to examine the declinations of the arrows.

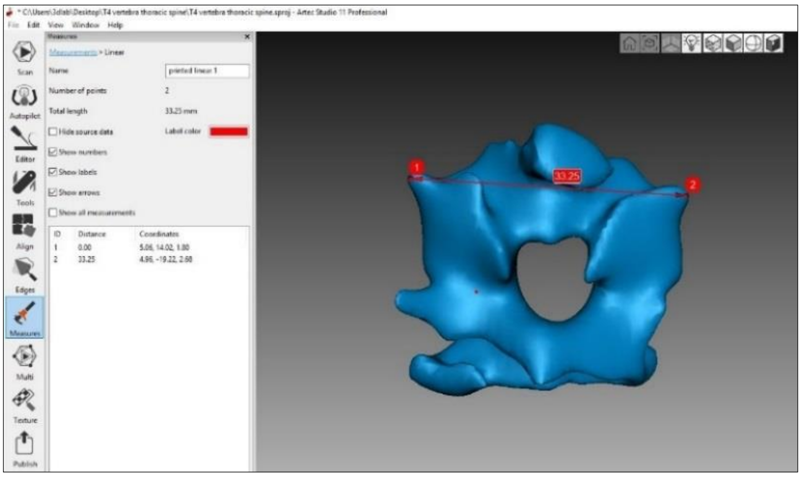

Figure 233: Artec Studio 11 Professional, Printed model of the T4 vertebra, Linear Measurement 1, Arrow from 1 to 2: 33.25mm

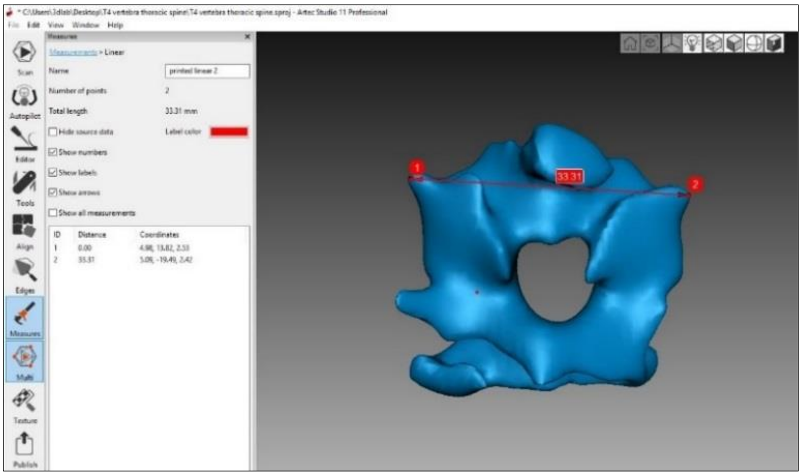

Figure 234: Artec Studio 11 Professional, Printed model of the T4 vertebra, Linear Measurement 2, Arrow from 1 to 2: 33.31mm

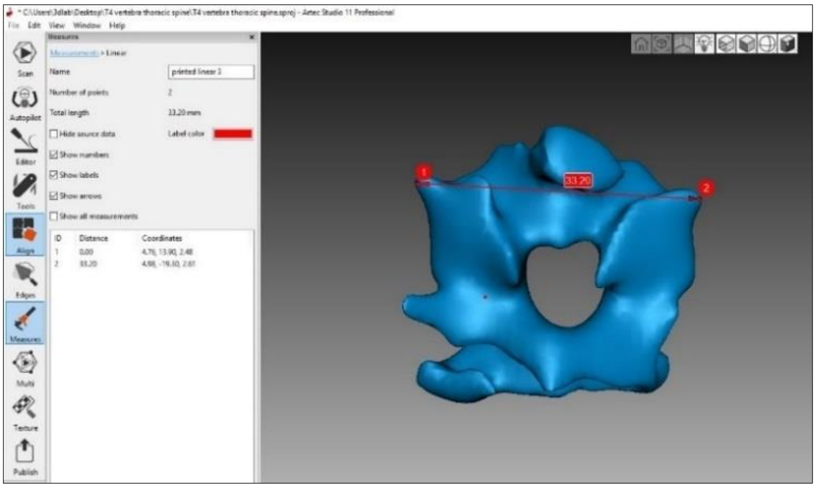

Figure 235: Artec Studio 11 Professional, Printed model of the T4 vertebra, Linear Measurement 3, Arrow from 1 to 2: 33.20mm

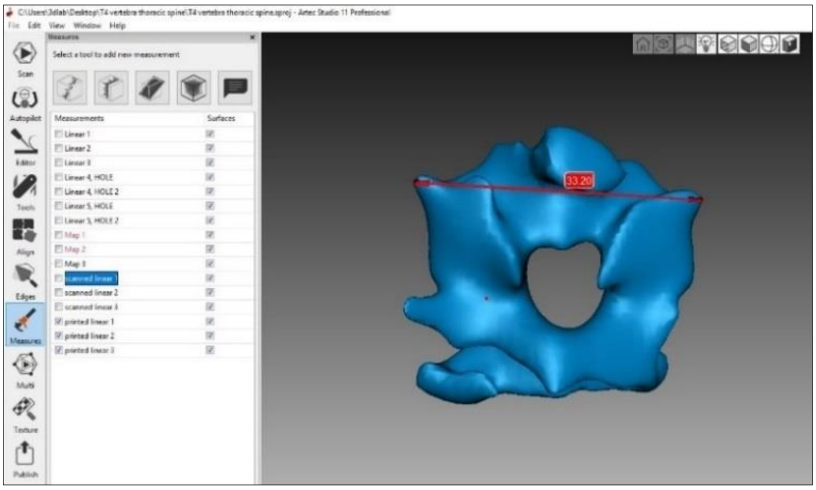

Figure 236: Artec Studio 11 Professional, Printed model of the T4 vertebra, Linear Measurement 2, Arrows of all measurements

Table 11: Results of the linear measurement for the printed model of the T4 vertebra

ID	Distance (mm)	Coordinates (x, y, z) (mm)		
1	0.00	5.06	14.02	1.80
2	33.25	4.96	-19.22	2.68
1	0.00	4.98	13.82	2.53
2	33.31	5.09	-19.49	2.45
1	00.00	4.76	13.90	2.48
2	32.20	4.98	-19.30	2.61

Additionally, it is worth mentioning that the linear measurements conducted for the case of the printed model of the T4 vertebra are made manually. In particular, the specification of the points that define the line of measurement (depicted with red color in Figures 233-236) is determined manually. Consequently, it is expected that the values of the measurements will vary from each other, raising issues of accuracy and precision.

Furthermore, in order to evaluate the results of the linear measurements (Table 11), conducted to the printed model of the T4 vertebra, it is essential to specify the average value of the final distance from point 1 to point 2. According to the results (Table 11), the average distance is estimated to be 33.253mm.

➢ *Second linear measurement of the printed model*

Subsequently, the process of the second measurement is illustrated in Figures 237-240, while the Table 12 demonstrates the results. In particular, three distinct measurements are made in the hole of the model (as presented in Figures 237-240), in order to evaluate the results. Additionally, the Figure 240 demonstrates the depiction of all the linear measurements, in order to examine the declinations of the arrows. Similar to the previous case, it is remarkable mentioning that the linear measurements are conducted manually. Consequently, it is expected that the values of the measurements will vary from each other, raising issues of accuracy and precision.

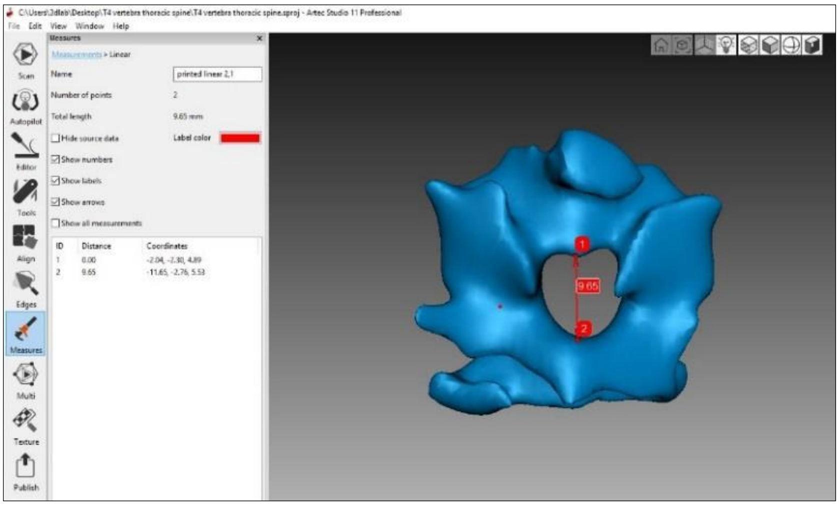

Figure 237: Artec Studio 11 Professional, Printed model of the T4 vertebra, Linear Measurement 1 of the hole, Arrow from 1 to 2: 9.65mm

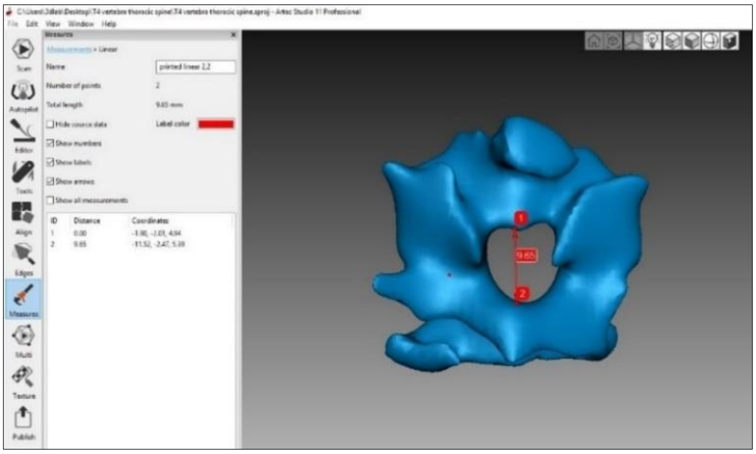

Figure 238: Artec Studio 11 Professional, Printed model of the T4 vertebra, Linear Measurement 2 of the hole, Arrow from 1 to 2: 9.65mm

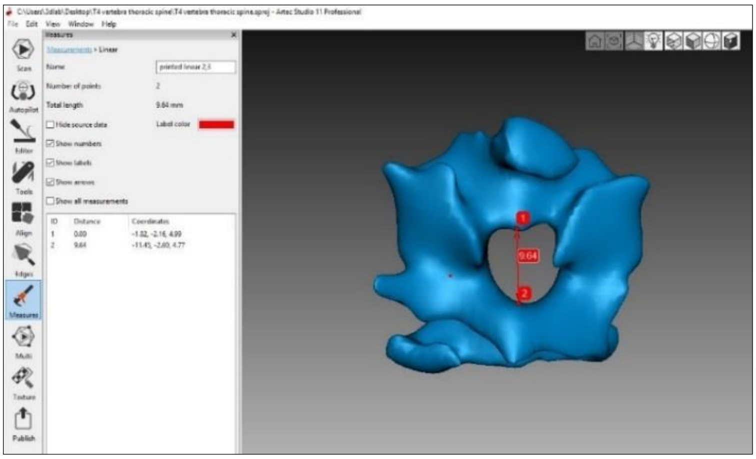

Figure 239: Artec Studio 11 Professional, Printed model of the T4 vertebra, Linear Measurement 3 of the hole, Arrow from 1 to 2: 9.64mm

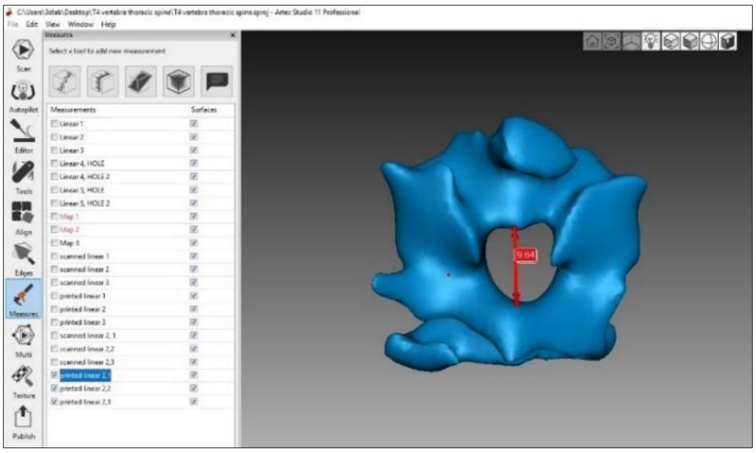

Figure 240: Artec Studio 11 Professional, Printed model of the T4 vertebra, Linear Measurement of the hole, Arrows of all measurements

Table 12: Results of the linear measurement for the printed model of the T4 vertebra

ID	Distance (mm)	Coordinates (x, y, z) (mm)		
1	0.00	-2.04	-2.30	4.89
2	9.65	-11.65	-2.76	5.53
1	0.00	-1.90	-2.01	4.94
2	9.65	-11.52	-2.47	5.39
1	00.00	-1.82	-2.16	4.99
2	9.64	-11.45	-2.60	4.77

Furthermore, in order to evaluate the results of the second linear measurement (Table 12), conducted to the printed model of the T4 vertebra, it is essential to define the average value of the final distance from point 1 to point 2. According to the results (Table 12), the average distance is estimated to be 9.646mm.

5.5.2.2. Linear Measurement of the Scanned STL Model

Secondly, the same linear measurements are conducted to the scanned model of the T4 vertebra, depicted with pink color (Figures 241-242). In particular, three distinct measurements are made in two different parts of the model, in order to evaluate the results, as conducted to the printed model previously. The linear measuring tool (Figure 230), is used in order to conduct these measurements.

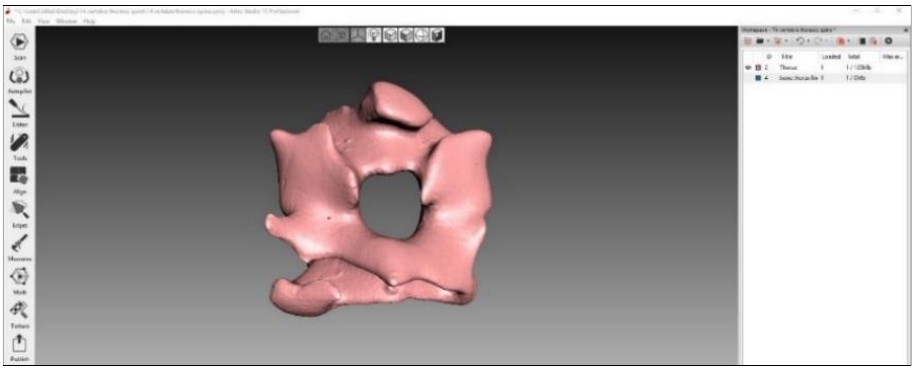

Figure 241: Artec Studio 11 Professional, Imported STL file of the scanned model

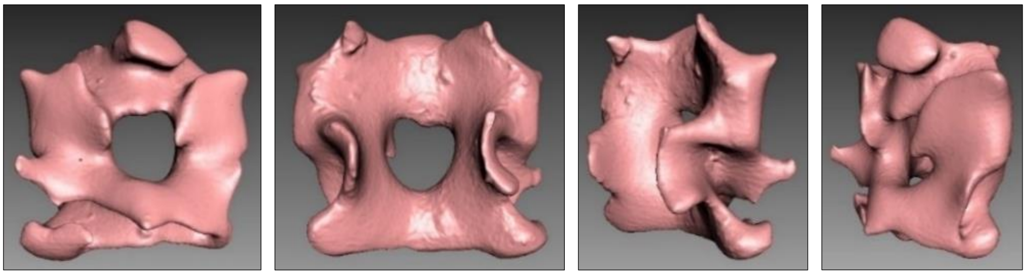

Figure 242: Artec Studio 11 Professional, Scanned model of the T4 vertebra

- *First linear measurement of the scanned model*

More specifically, the process of the first measurement is represented in Figures 243-246, while the Table 13 demonstrates the results of the measurements. The first linear measurement is defined from the distance from point 1 to point 2 (depicted with blue color in Figures 243-246). The Figure 246 presents the depiction of all the linear measurements, in order to examine the declinations of the arrows.

Similarly, it is necessary noting that the linear measurements conducted for the case of the scanned model of the T4 vertebra are made manually, likewise the measurements of the printed model. As a result, it is expected that the values of the measurements will vary from each other, raising issues of accuracy and precision.

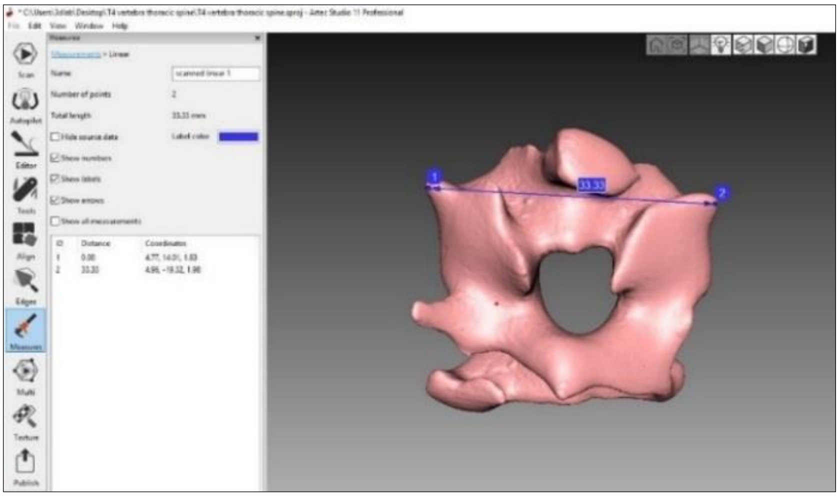

Figure 243: Artec Studio 11 Professional, Scanned model of the T4 vertebra, Linear Measurement 1, Arrow from 1 to 2: 33.33mm

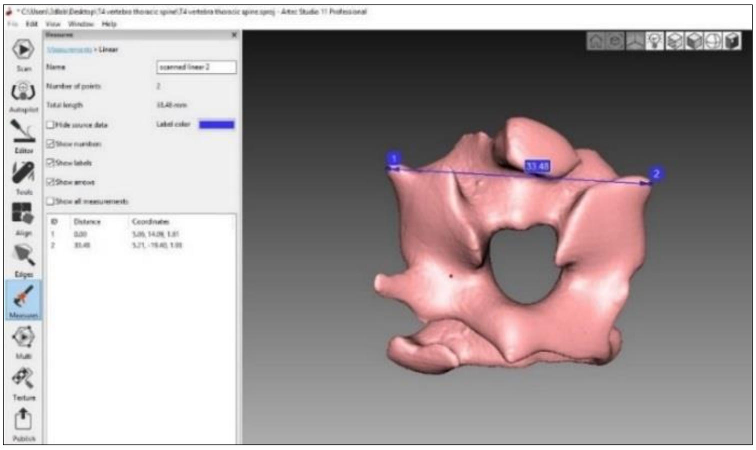

Figure 244: Artec Studio 11 Professional, Scanned model of the T4 vertebra, Linear Measurement 2, Arrow from 1 to 2: 33.48mm

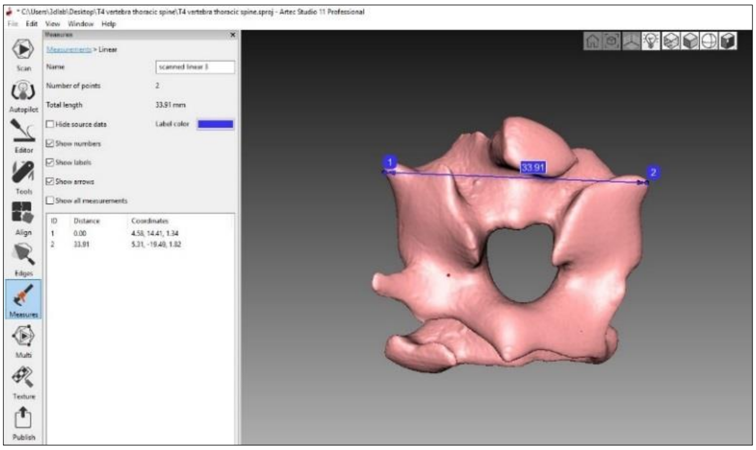

Figure 245: Artec Studio 11 Professional, Scanned model of the T4 vertebra, Linear Measurement 1, Arrow from 1 to 2: 33.91mm

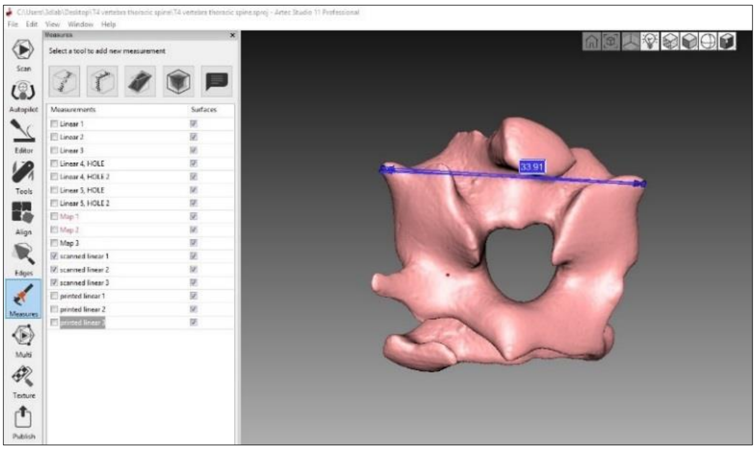

Figure 246: Artec Studio 11 Professional, Scanned model of the T4 vertebra, Linear Measurement 1, Arrows of all measurements

Table 13: Results of the linear measurement for the scanned model of the T4 vertebra

ID	Distance (mm)	Coordinates (x, y, z) (mm)		
1	0.00	4.77	14.01	1.83
2	33.33	4.96	-19.32	1.98
1	0.00	5.06	14.09	1.81
2	33.48	5.21	-19.40	1.93
1	00.00	4.58	14.41	1.34
2	33.91	5.31	-19.49	1.82

Moreover, in order to evaluate the results of the linear measurement (Table 13), conducted to the scanned model of the T4 vertebra, it is important to specify the average value of the final distance from point 1 to point 2. According to the results (Table 13), the average distance is estimated to be 33.573mm.

- *Second linear measurement of the scanned model*

The process of the second measurement for the scanned model is illustrated in Figures 247-250, while the Table 14 demonstrates the results. Three distinct measurements are made in the hole of the model (as presented in Figures 247-250). Figure 250 presents the depiction of all the linear measurements for the scanned model, in order to examine the declinations of the arrows.

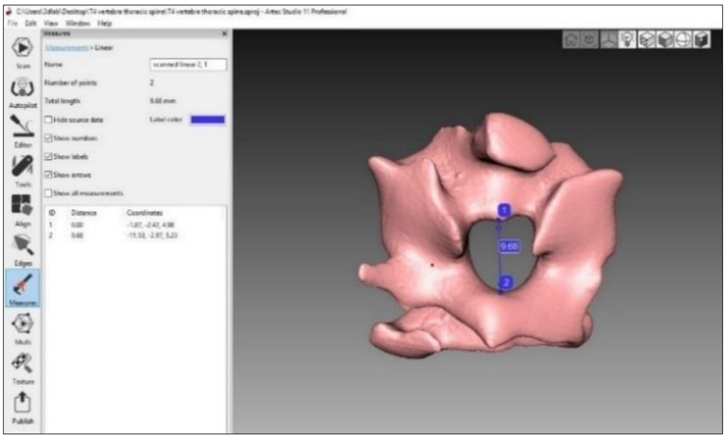

Figure 247: Artec Studio 11 Professional, Scanned model of the T4 vertebra, Linear Measurement 1 of the hole, Arrow from 1 to 2: 9.68mm

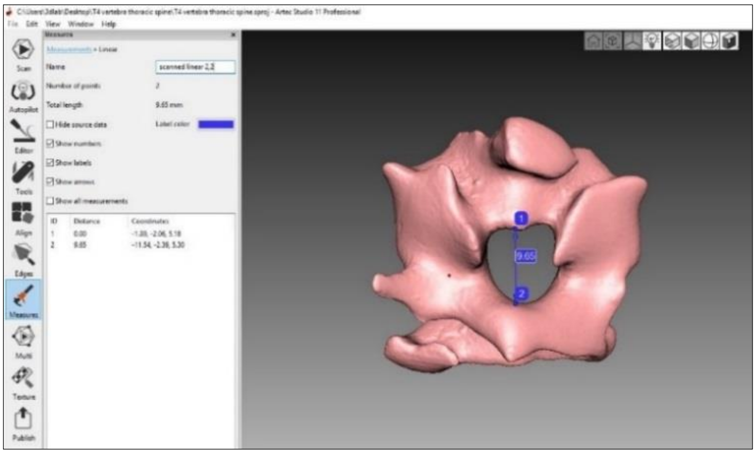

Figure 248: Artec Studio 11 Professional, Scanned model of the T4 vertebra, Linear Measurement 1 of the hole, Arrow from 1 to 2: 9.65mm

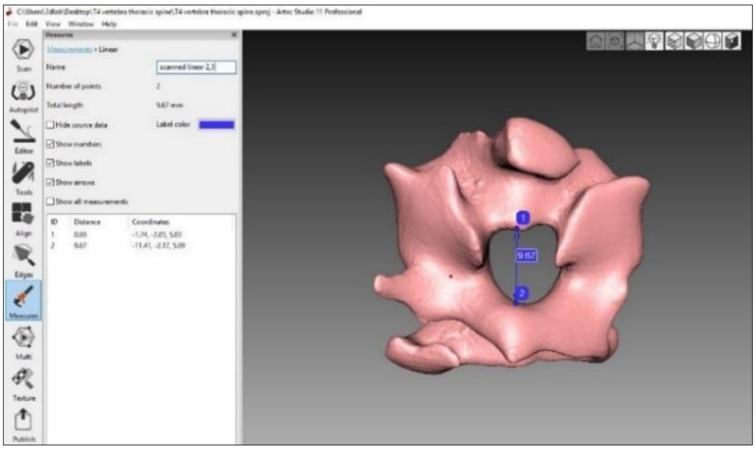

Figure 249: Artec Studio 11 Professional, Scanned model of the T4 vertebra, Linear Measurement 1 of the hole, Arrow from 1 to 2: 9.67mm

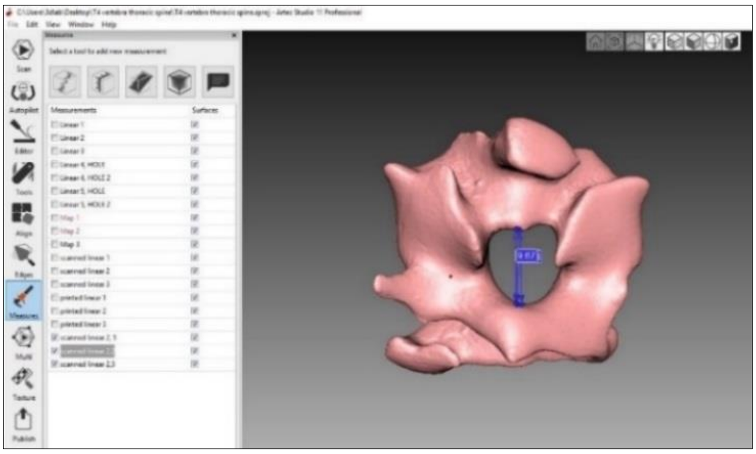

Figure 250: Artec Studio 11 Professional, Scanned model of the T4 vertebra, Linear Measurement of the hole, Arrows of all measurements

Table 14: Results of the linear measurement for the scanned model of the T4 vertebra

ID	Distance (mm)	Coordinates (x, y, z) (mm)		
1	0.00	-2.04	-2.30	4.89
2	9.65	-11.65	-2.76	5.53
1	0.00	-1.90	-2.01	4.94
2	9.65	-11.52	-2.47	5.39
1	00.00	-1.82	-2.16	4.99
2	9.64	-11.45	-2.60	4.77

Similar to the previous case, the linear measurements are conducted manually, provoking issues of accuracy and precision. In addition, in order to evaluate the results of the linear measurement (Table 14), conducted to the scanned model of the T4 vertebra, it is important to specify the average value of the final distance from point 1 to point 2. According to the results (Table 14), the average distance is estimated to be 9.646mm.

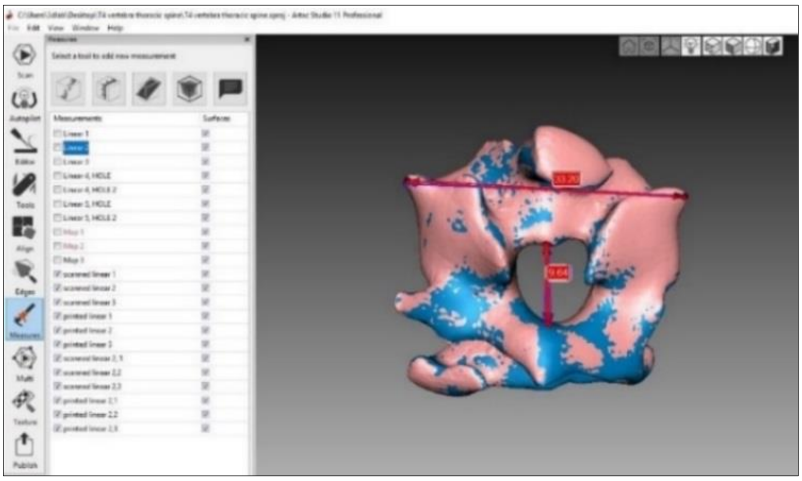

Figure 251: Artec Studio 11 Professional, Linear Measurements

The figure above (Figure 251) presents the depiction of all the linear measurements for both cases (i.e. printed and scanned model). The red arrows (Figure 251) represent the linear measurements for the printed model, while the blue arrows (Figure 251) represent the linear measurements of the scanned model. The evaluation and the comparison of the final results is examined in Step 3 (Section 5.5.3.)

5.5.2.3. *Surface Distance Maps of the Printed and the Scanned Model*

In order to compare the two models and assess form deviation, the Artec Studio 11 Professional provides the *"Surface distance maps"*, measuring tool [29]. For the current project, this tool is used in order to compare the printed model with the scanned one [29]. Actually, the user should select the *"Measures"* button from the main toolbar, and then select the *"Surface distance maps"* tool, as illustrated in the following figure (Figure 252) [29]. The user should select the two models for comparison (i.e. printed and scanned STL files) and initiate the process. This process is considered as more accurate and precise, in comparison with the linear measurements conducted previously.

Figure 252: Artec Studio 11 Professional, Measures, Surface distance maps

Subsequently, the user should define the *"Search distance value"*, considered as a maximal range in millimeters that calculated the distances between surfaces [29]. The surface distance map appears on the screen (3D-view window), while the calculation results appear in the left panel of the screen [29].

In fact, regarding the analysis of the obtained results, the software calculates three measurements according to the selected value of the search distance parameter [29]. There measurements include the following:

- *Root Mean Square (*RMS) (that is the square root of the arithmetic mean of the squares of the actual distances) [29].
- *Mean absolute deviation* [29].
- *Mean of signed distances* [29].

The created surface distance map is a rendering of particular regions of surfaces of the models, appearing with different colors [29]. Related values of distances and the distribution of them can be found in the graduated scale with histogram, located next to the model [29]. Actually, the map color can change from *"blue"* (corresponding to negative distance) to *"red"* (corresponding to positive distance) [29]. The *"green"* color indicates that the distance between surfaces of this region is zero [29]. The *"grey"* color means that the highlighted surfaces are out of the specified search distance [29]. The *"orange"* and the *"bright blue"* colors refer to the distances which are slightly below and above the limiting values of the scale, correspondingly [29]. At last, the graduated scale varies within limits of the positive to the negative value of the selected *"Error scale"* [29]. The value of the *"Error scale"* can be adjusted from the slider or the corresponding textbox, although its maximal value cannot surpass the *"Search distance value"* [29].

More specifically, for the current case study of the printed and the scanned 3D-medical model of the T4 vertebra, six distinct cases are examined by adjusting the *"Error scale"* parameter to the following values: 0.001, 0.045, 0.066, 0.141, 0.209 and 0.470. The results of the calculation of the surface distance maps are illustrated in the following figures (Figures 253-271) for different views of the model.

Furthermore, the figure below (Figure 253) demonstrates the results regarding the RMS, the Mean absolute deviation and the Mean of signed distances, when the *"Error scale"* is set to 0.001 value. According to the findings, these values are 0.089480, 0.058955, -0.023571, respectively. Though, the values of these parameters are the same for the six distinct cases.

Figure 253: Artec Studio 11 Professional, Measures, Surface distance maps, Graduated scale and results of the measurements

➢ *Surface Distance Maps, Error scale: 0.001*

The results of the surface distance map, when the *"Error scale"* is set to 0.001 value, are presented in the following figures (Figures 254-256). The analysis of the results is presented in the end of the current section (Section 5.5.2.3.).

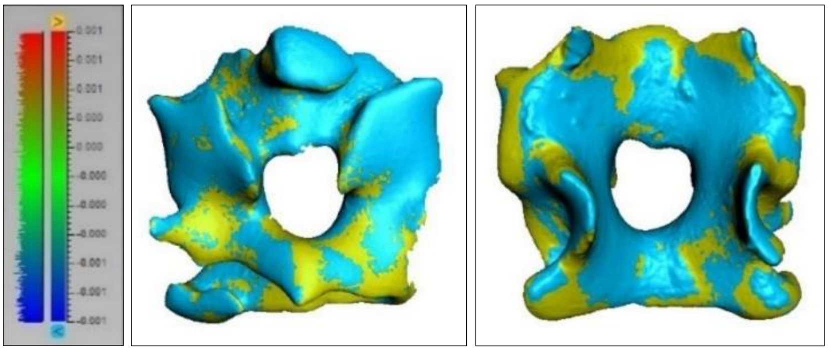

Figure 254: Artec Studio 11 Professional, Measures, Surface distance maps of the printed and the scanned model of the T4 vertebra, Error scale: 0.001

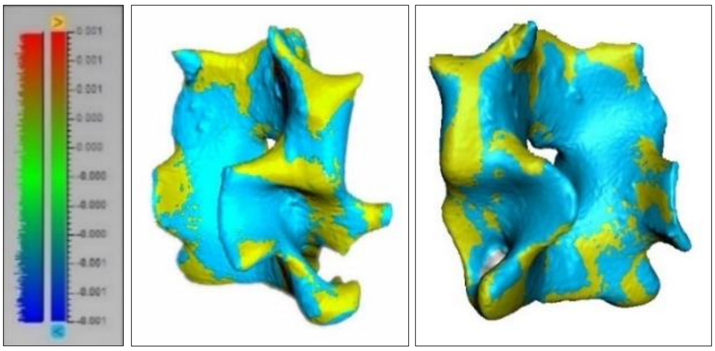

Figure 255: Artec Studio 11 Professional, Measures, Surface distance maps of the printed and the scanned model of the T4 vertebra, Error scale: 0.001

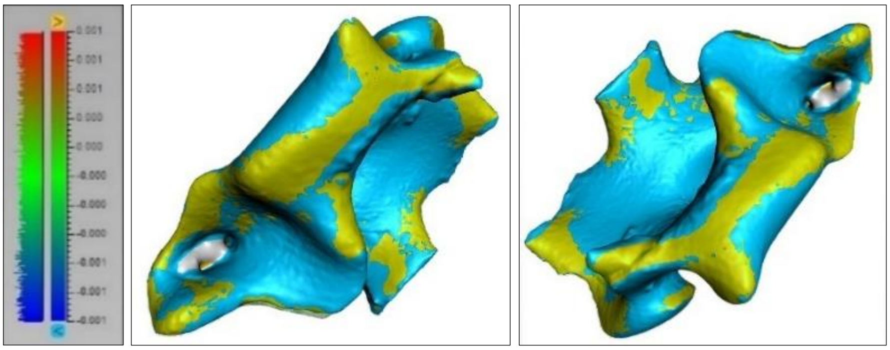

Figure 256: Artec Studio 11 Professional, Measures, Surface distance maps of the printed and the scanned model of the T4 vertebra, Error scale: 0.001

➢ *Surface Distance Maps, Error scale: 0.045*

The results of the surface distance map, when the *"Error scale"* is set to 0.045 value, are presented in the following figures (Figures 257-259). The analysis of the results is presented in the end of the current section (Section 5.5.2.3.).

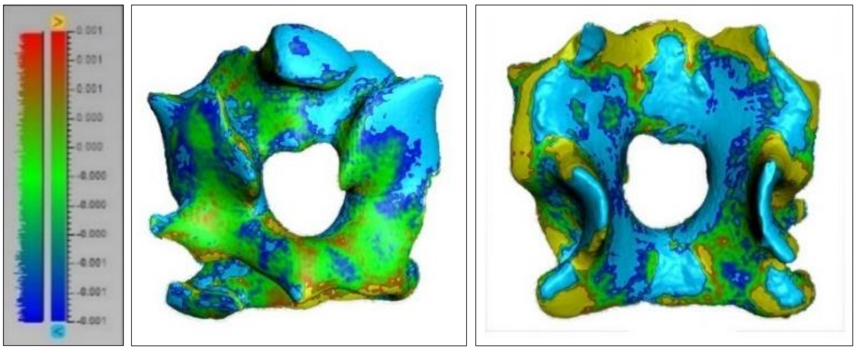

Figure 257: Artec Studio 11 Professional, Measures, Surface distance maps of the printed and the scanned model of the T4 vertebra, Error scale: 0.045

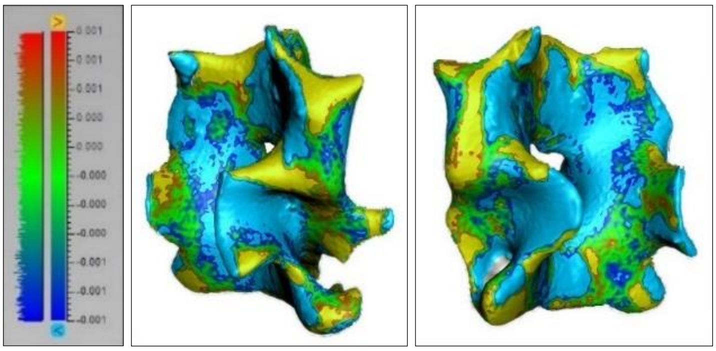

Figure 258: Artec Studio 11 Professional, Measures, Surface distance maps of the printed and the scanned model of the T4 vertebra, Error scale: 0.045

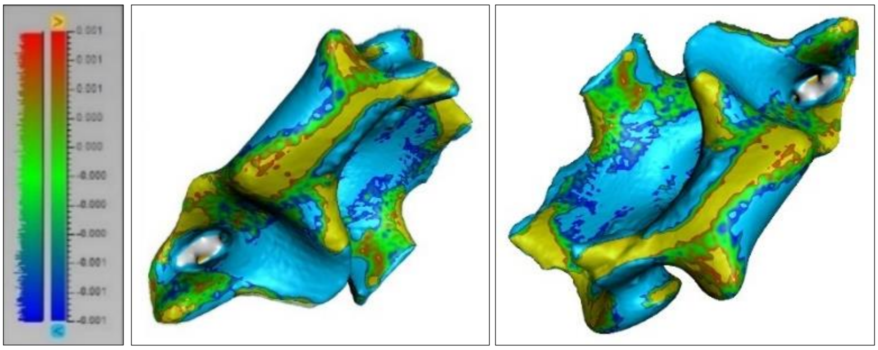

Figure 259: Artec Studio 11 Professional, Measures, Surface distance maps of the printed and the scanned model of the T4 vertebra, Error scale: 0.045

➢ *Surface Distance Maps, Error scale: 0.066*

The results of the surface distance map, when the *"Error scale"* is set to 0.066 value, are presented in the following figures (Figures 260-262). The analysis of the results is presented in the end of the current section (Section 5.5.2.3.).

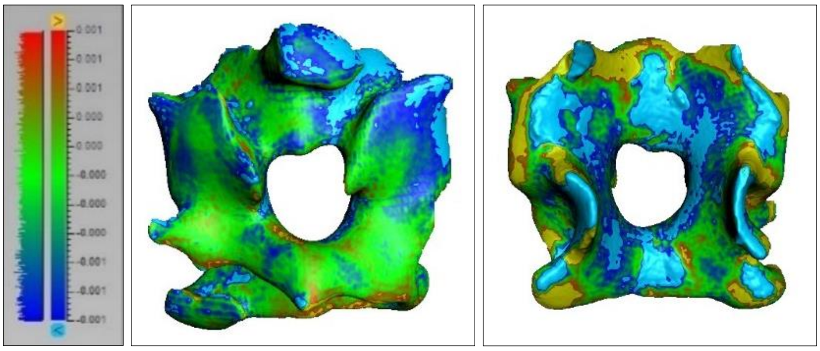

Figure 260: Artec Studio 11 Professional, Measures, Surface distance maps of the printed and the scanned model of the T4 vertebra, Error scale: 0.066

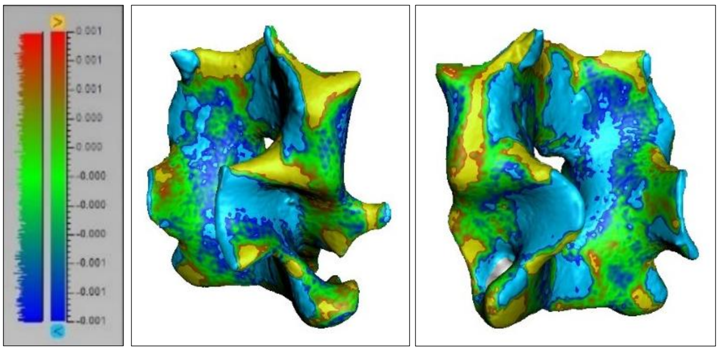

Figure 261: Artec Studio 11 Professional, Measures, Surface distance maps of the printed and the scanned model of the T4 vertebra, Error scale: 0.066

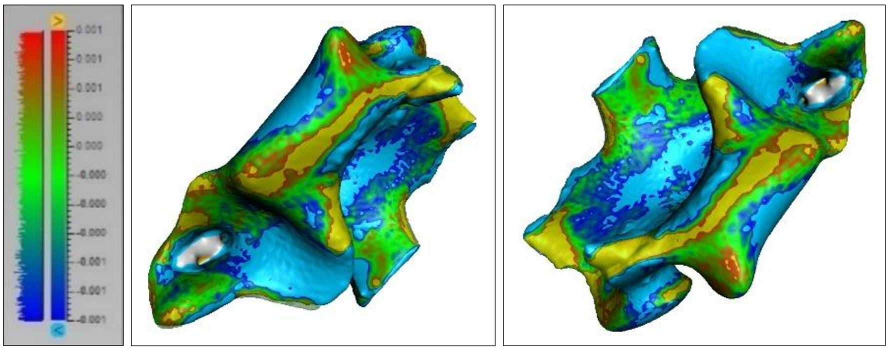

Figure 262: Artec Studio 11 Professional, Measures, Surface distance maps of the printed and the scanned model of the T4 vertebra, Error scale: 0.066

➢ *Surface Distance Maps, Error scale: 0.141*

The results of the surface distance map, when the *"Error scale"* is set to 0.141 value, are presented in the following figures (Figures 263-265). The analysis of the results is presented in the end of the current section (Section 5.5.2.3.).

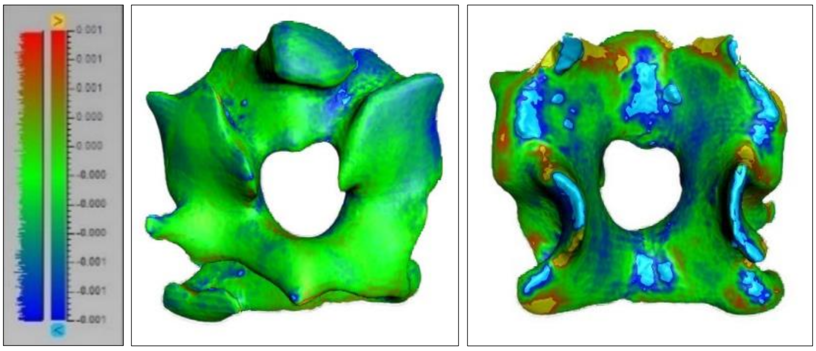

Figure 263: Artec Studio 11 Professional, Measures, Surface distance maps of the printed and the scanned model of the T4 vertebra, Error scale: 0.141

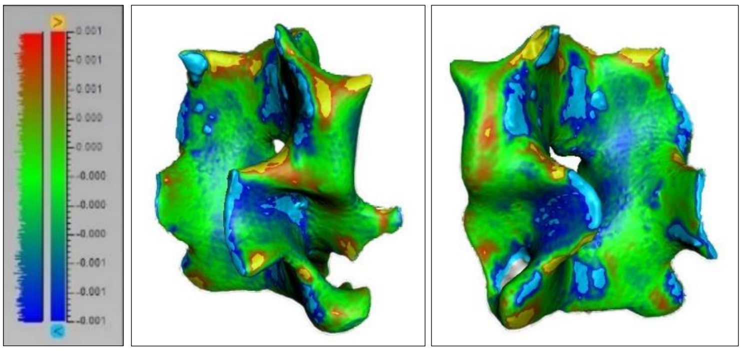

Figure 264: Artec Studio 11 Professional, Measures, Surface distance maps of the printed and the scanned model of the T4 vertebra, Error scale: 0.141

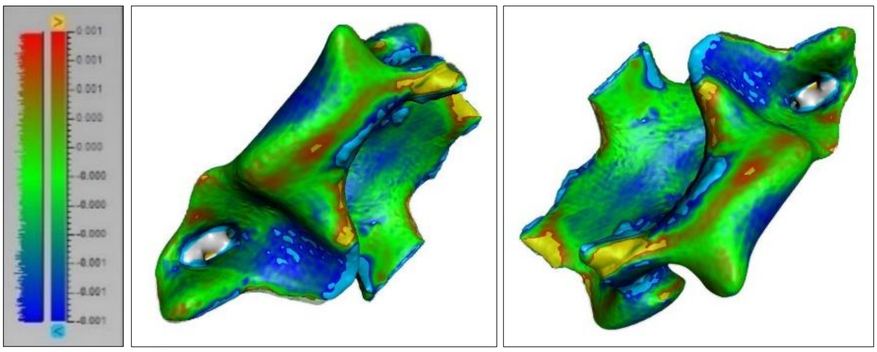

Figure 265: Artec Studio 11 Professional, Measures, Surface distance maps of the printed and the scanned model of the T4 vertebra, Error scale: 0.141

➢ *Surface Distance Maps, Error scale: 0.209*

The results of the surface distance map, when the *"Error scale"* is set to 0.209 value, are presented in the following figures (Figures 266-268). The analysis of the results is presented in the end of the current section (Section 5.5.2.3.).

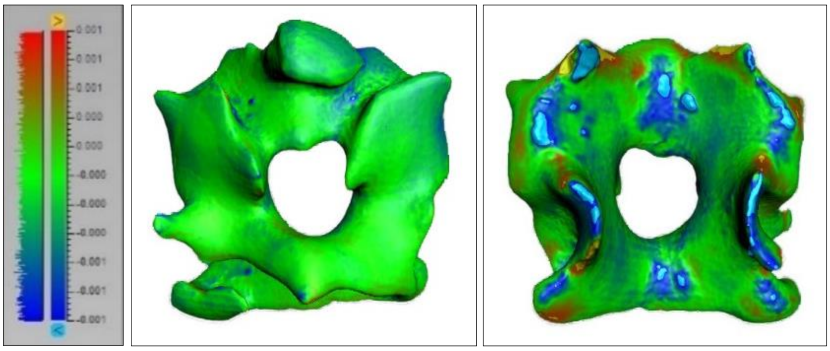

Figure 266: Artec Studio 11 Professional, Measures, Surface distance maps of the printed and the scanned model of the T4 vertebra, Error scale: 0.209

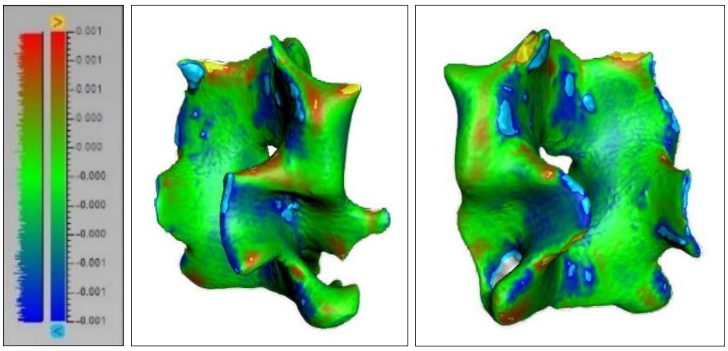

Figure 267: Artec Studio 11 Professional, Measures, Surface distance maps of the printed and the scanned model of the T4 vertebra, Error scale: 0.209

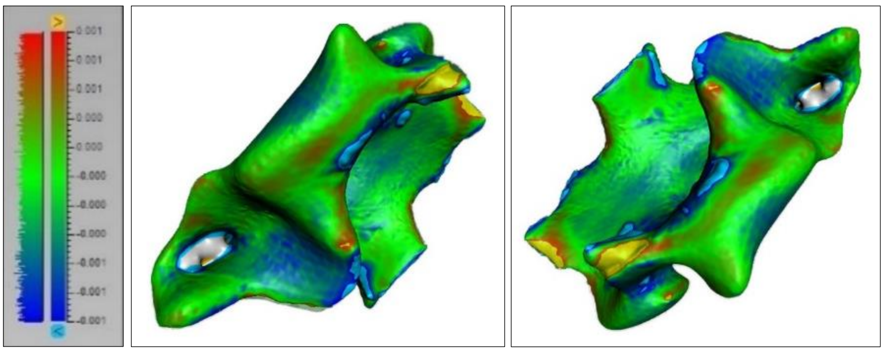

Figure 268: Artec Studio 11 Professional, Measures, Surface distance maps of the printed and the scanned model of the T4 vertebra, Error scale: 0.209

➢ *Surface Distance Maps, Error scale: 0.470*

The results of the surface distance map, when the *"Error scale"* is set to 0.470 value, are presented in the following figures (Figures 269-271). The analysis of the results is presented in the end of the current section (Section 5.5.2.3.).

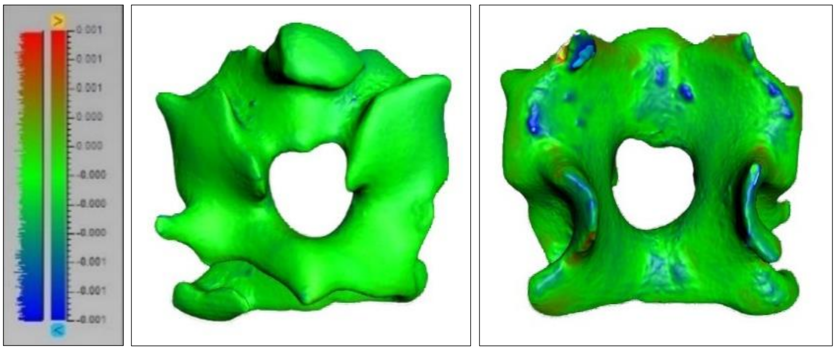

Figure 269: Artec Studio 11 Professional, Measures, Surface distance maps of the printed and the scanned model of the T4 vertebra, Error scale: 0.470

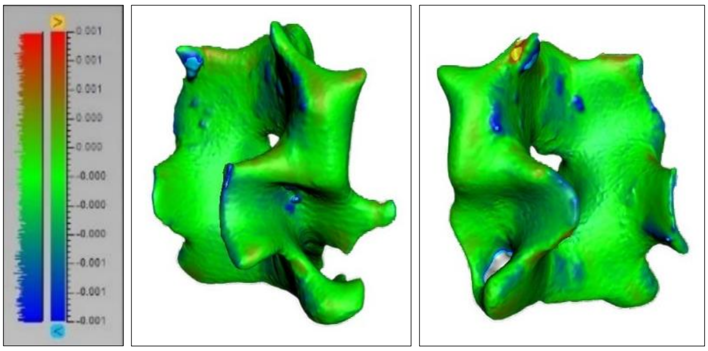

Figure 270: Artec Studio 11 Professional, Measures, Surface distance maps of the printed and the scanned model of the T4 vertebra, Error scale: 0.470

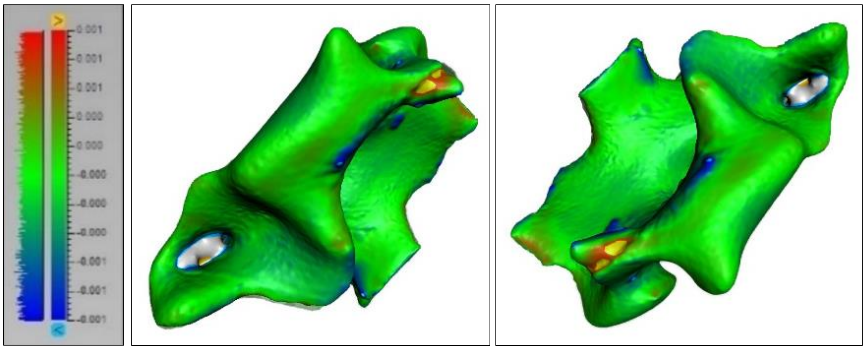

Figure 271: Artec Studio 11 Professional, Measures, Surface distance maps of the printed and the scanned model of the T4 vertebra, Error scale: 0.470

➢ *Analysis of the results*

As mentioned previously, for the current case study of the printed and the scanned 3D-medical model of the T4 vertebra, six distinct cases are examined by adjusting the *"Error scale"* parameter to the following values: 0.001, 0.045, 0.066, 0.141, 0.209 and 0.470. The results of the calculation of the surface distance maps are illustrated in the figures above (Figures 253-271) for different views of the model.

Furthermore, the results regarding the RMS, the Mean absolute deviation and the Mean of signed distances, when the *"Error scale"* is set to 0.001 value, are 0.089480, 0.058955, -0.023571, respectively (Figure 253). Though, the values of these parameters are the same for the six distinct cases.

❖ *Surface Distance Maps, Error scale: 0.001*

With reference to the first case, when the *"Error scale"* is set to 0.001 value (Figures 254-256), the following results of the surface distance map are obtained. In particular, the models present mainly *"orange"* and the *"bright blue"* colors, referring to the distances which are slightly below and above the limiting values of the scale, correspondingly. Furthermore, in Figures 255-256 it can be noticed that the models present areas of *"grey"* color, meaning that these surfaces are out of the specified search distance. Actually, these areas are holes that are not fully captured during the scanning process. In total, the overall picture revealed by these results is that the models present dimensional deviation for this error scale.

❖ *Surface Distance Maps, Error scale: 0.045*

With regard to the second case, when the *"Error scale"* is set to 0.045 value (Figures 254-256), the following results of the surface distance map are obtained. In specific, the surface distance map changes, presenting all the color ranges. Actually, the anterior part of the model is majorly *"green"* color, indicating zero distance. The posterior part of the model is mainly *"bright blue"* color, referring to the distances which are slightly above the limiting values of the scale. In general, the map presents mostly *"orange"* and the *"bright blue"* regions (referring to the distances which are slightly below and above the limiting values of the scale, correspondingly), *"red"* in slight areas (corresponding to positive distance) and sporadically *"blue"* (corresponding to negative distance). In addition, *"grey"* color appears in the same areas with the previous case (i.e. Error scale: 0.001), indicating the holes that are not fully captured during the scanning process. In general, the overall picture revealed by these results is that the models present dimensional deviation for this error scale. Though, the results are considerably improved in comparison with the previous case (i.e. Error scale: 0.001).

❖ *Surface Distance Maps, Error scale: 0.066*

Regarding the third case, when the *"Error scale"* is set to 0.066 value (Figures 260-262), the following results of the surface distance map are obtained. Particularly, the surface distance map changes, presenting all the color ranges. Actually, the anterior part of the model is majorly *"green"* color, indicating zero distance. The posterior part of the model is mainly *"bright blue"* color, referring to the distances which are slightly above the limiting values of the scale. In general, the map presents mostly *"blue"* areas (corresponding to negative distance), while there are some *"orange"* (referring to the distances which are slightly below the limiting values of the scale) and sparsely *"red"* areas (corresponding to positive distance). In addition, *"grey"* color appears in the same areas with the previous two cases (i.e. Error scale: 0.001 and 0.045), indicating the holes that are not fully captured during the scanning process. In general, the overall picture revealed by these results is that the models present dimensional deviation for this error scale. Although, the results are considerably improved in comparison with the two previous cases (i.e. Error scale: 0.001 and 0.045).

❖ *Surface Distance Maps, Error scale: 0.141*

Regarding the forth case, when the *"Error scale"* is set to 0.141 value (Figures 263-265), the following results of the surface distance map are obtained. Specifically, the surface distance map presents all the color ranges. Actually, the anterior part of the model is majorly *"green"* color (indicating zero distance) with some sparse *"blue"* regions (corresponding to negative distance). Furthermore, it is also noticed the significant decrease of *"bright blue"* and regions *"orange"* (referring to the distances which are slightly above and below the limiting values of the scale, correspondingly). Additionally, the *"red"* regions (corresponding to positive distance) are decreased and presented rarely. In addition, *"grey"* color appears in the same areas with the three previous cases (i.e. Error scale: 0.001, 0.045, 0.066), indicating the holes that are not fully captured during the scanning process. In general, the overall picture revealed by these results is that the models present dimensional deviation for this error scale. Nevertheless, the results are considerably improved in comparison with the three previous cases (i.e. Error scale: 0.001, 0.045, 0.066).

❖ *Surface Distance Maps, Error scale: 0.209*

Regarding the fifth case, when the *"Error scale"* is set to 0.209 value (Figures 266-268), the following results of the surface distance map are obtained. More precisely, the surface distance map changes, presenting all the color ranges. In fact, the anterior part of the model is majorly *"green"* (indicating zero distance) and with some areas of *"blue"* color (corresponding to negative distance). Furthermore, it is worth mentioning that the *"bright blue"*, *"orange"* (referring to the distances which are slightly above and below the limiting values of the scale, correspondingly), and *"red"* regions (corresponding to positive distance) are significantly decreased. In addition, *"grey"* color appears in the same areas with the previous four cases (i.e. Error scale: 0.001, 0.045, 0.066, 0.141), indicating the holes that are not fully captured during the scanning process. In general, the overall picture revealed by these results is that the models present slightly dimensional deviation for this error scale. In fact, the results are considerably upgraded in comparison with the previous four cases (i.e. Error scale: 0.001, 0.045, 0.066, 0.141).

❖ *Surface Distance Maps, Error scale: 0.470*

Regarding the sixth case, when the *"Error scale"* is set to 0.470 value (Figures 269-271), the following results of the surface distance map are obtained. In specific, the entire part is majorly *"green"* (indicating zero distance) and with some sparse areas of *"blue"* color (corresponding to negative distance). Furthermore, it is worth mentioning that the *"bright blue"*, *"orange"* (referring to the distances which are slightly above and below the limiting values of the scale, correspondingly), and *"red"* regions (corresponding to positive distance) are negligible. In addition, *"grey"* color appears in the same areas with the previous five cases (i.e. Error scale: 0.001, 0.045, 0.066, 0.141, 0.209), indicating the holes that are not fully captured during the scanning process. In general, the overall picture revealed by these results is that the models present slightly dimensional deviation for this error scale, presenting satisfactory results with reference to the accuracy. Actually, the results are considerably improved in comparison with the previous five cases (i.e. Error scale: 0.001, 0.045, 0.066, 0.141, 0.209).

5.5.3. Step 3: Comparison and Evaluation of the Results

After completing all the required measurements of the anatomical model of the T4 vertebra, it is crucial to proceed to the final step of the evaluation stage. In particular, this step comprises the comparison and the evaluation of the measurements conducted previously (Section 5.5.2.), regarding the dimensional declinations between the printed and the scanned STL models. The following figures (Figures 272-273) show an illustration of the printed (depicted with blue color) and of the scanned (depicted with pink color) model of the T4 vertebra. The analysis of the obtained results is presented as follows.

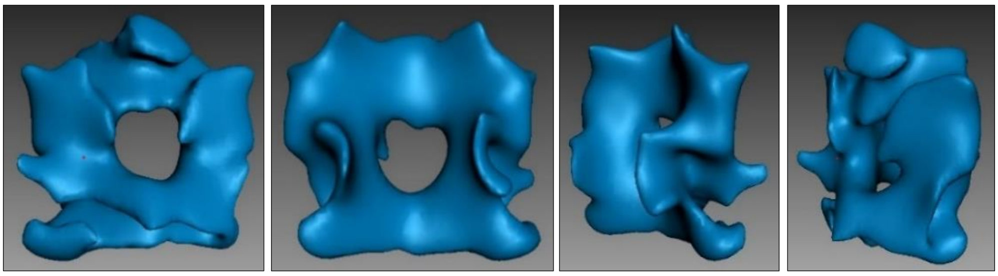

Figure 272: Printed model of the T4 vertebra

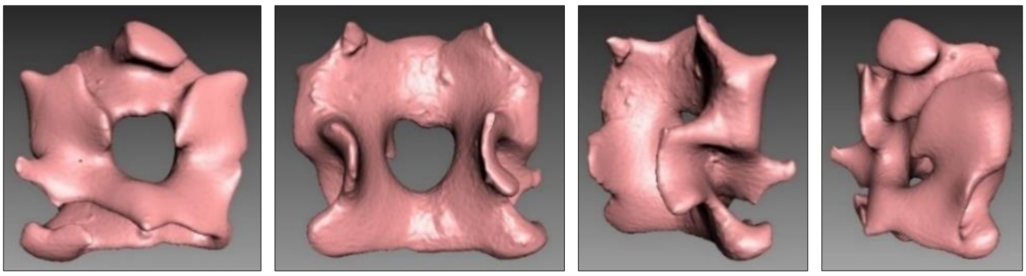

Figure 273: Scanned model of the T4 vertebra

The results are divided into three categories, including the *"Results of linear measurements regarding Case #1"* for both printed and scanned model, the *"Results of linear measurements regarding Case #2"* for both printed and scanned model, and finally the *"Results of Surface Distance Maps"* for both printed and scanned model.

5.5.3.1. Results of Linear Measurements: Case #1

Initially, three distinct linear measurements are made both in the printed and scanned model, evaluating the same distance. According to the results (Table 11 and Table 13), the average distance is estimated to be 33.253mm and 33.573mm, for the printed and the scanned model respectively. The percentage of the deviation between this measurement is estimated to 1.049%. Nevertheless, it is worth mentioning that the linear measurements are made manually. Consequently, it is expected that the values of the measurements will vary from each other, raising issues of accuracy and precision.

5.5.3.2. Results of Linear Measurements: Case #2

Secondly, three distinct linear measurements are made both in the printed and scanned model, evaluating the same distance of the hole. According to the results (Table 12 and Table 14), the average distance is estimated to be 9.646mm and 9.646mm, for the printed and the scanned model respectively. The percentage of the deviation between this measurement is estimated to zero. Nevertheless, it is worth mentioning that the linear measurements are made manually, provoking issues of accuracy and precision, similar to the previous case. For this reason, it is considered that in this case the models do not present dimensional declinations, accounting for the factor of chance.

5.5.3.3. Results of Surface Distance Maps

Hence, the Surface Distance Maps are considered as more accurate and precise process, in comparison with the linear measurements for the evaluation of the dimensional declinations between the printed and the scanned models.

In particular, six distinct cases are examined by adjusting the *"Error scale"* parameter to the following values: 0.001, 0.045, 0.066, 0.141, 0.209 and 0.470. The results of the calculation of the surface distance maps are presented in Figures 274-279 for different views of the model. In addition, the results regarding the RMS, the Mean absolute deviation and the Mean of signed distances, are 0.089480, 0.058955, -0.023571, respectively (Figure 253). In fact, the values of these parameters are the same for the six distinct cases.

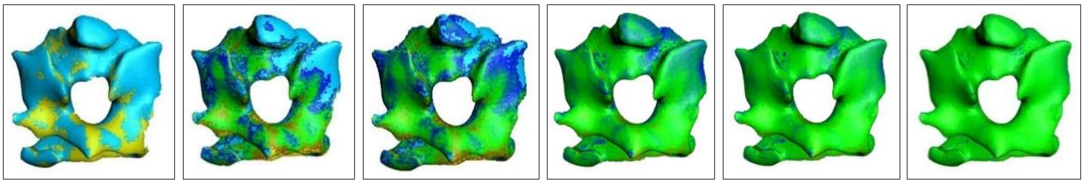

Figure 274: Surface distance maps, Error scale: 0.001, 0.045, 0.066, 0.141, 0.209, 0.470

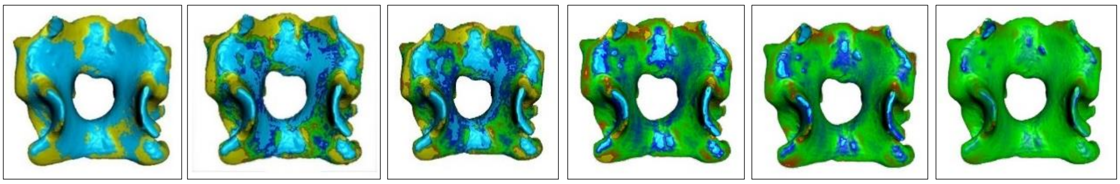

Figure 275: Surface distance maps, Error scale: 0.001, 0.045, 0.066, 0.141, 0.209, 0.470

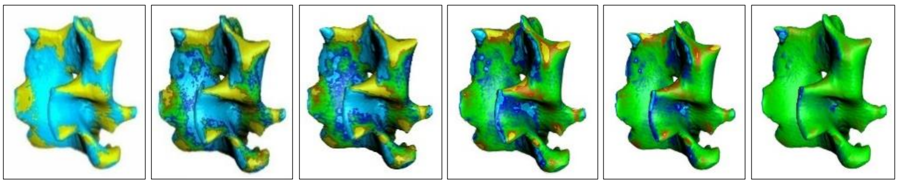

Figure 276: Surface distance maps, Error scale: 0.001, 0.045, 0.066, 0.141, 0.209, 0.470

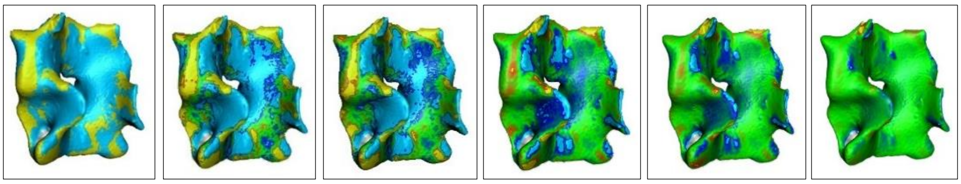

Figure 277: Surface distance maps, Error scale: 0.001, 0.045, 0.066, 0.141, 0.209, 0.470

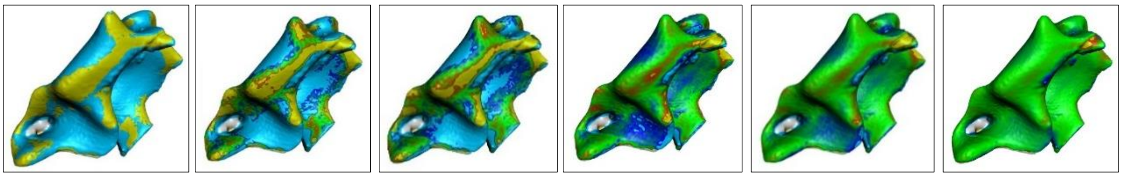

Figure 278: Surface distance maps, Error scale: 0.001, 0.045, 0.066, 0.141, 0.209, 0.470

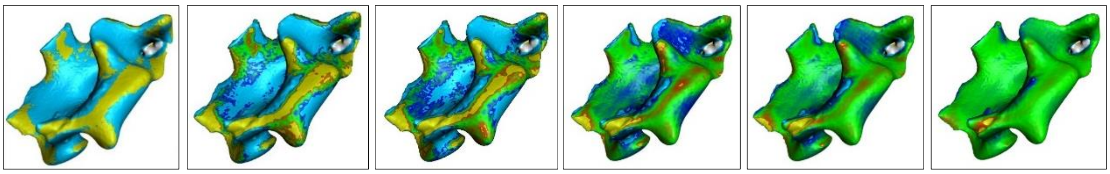

Figure 279: Surface distance maps, Error scale: 0.001, 0.045, 0.066, 0.141, 0.209, 0.470

The following Table (Table 15) presents the results, obtained from Surface Distance maps for the six different cases of Error scale. Related values of distances and the distribution of them can be found in the graduated scale with histogram. The map color can change from *"blue"* (corresponding to negative distance) to *"red"* (corresponding to positive distance) [29]. The *"green"* color indicates that the distance between surfaces of this region is zero [29]. The *"grey"* color means that the highlighted surfaces are out of the specified search distance [29]. The *"orange"* and the *"bright blue"* colors refer to the distances which are slightly below and above the limiting values of the scale, correspondingly [29]. The scale from 0 to 5 number indicates the rate of the distribution of each color for the six different cases. Furthermore, it is worth mentioning that this is an approximate estimation.

Table 15: Comparison of Surface Distance Maps results

		E.s.: 0.001	E.s.: 0.045	E.s.: 0.066	E.s.: 0.141	E.s.: 0.209	E.s.: 0.470
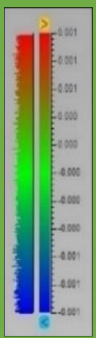	red	0	0	1	3	5	1
	orange	2	2	3	3	4	1
	green	2	4	3	2	3	1
	blue	2	3	4	1	2	1
	bright blue	2	3	5	1	1	1
	grey	1	2	5	1	1	1

In total, according to the results of the surface distance deviation, it can be noticed that the printed and the scanned models do present remarkable dimensional deviation, especially when the Error scale is from 0.001-0.066. When the value of Error scale is from 0.141-0.470, the models present slightly dimensional declination. The regions depicted with grey color in Figures 278-279, indicate holes of the printed model that are not fully captured during the scanning process. In general, the overall picture revealed by these results is that the models present remarkable dimensional deviation. Though, the results are satisfactory with reference to the pilot approach of the case study.

6. Chapter Six: Discussion & Interpretation of Findings

On the completion of the current study it became apparent that the integration of Additive Manufacturing technologies has contributed in a meaningful and substantive way to the medical sector. In fact, the most fundamental factors determining the success and the rapid growth of Rapid Prototyping technologies are the combination of geometric flexibility, relatively high-speed, accuracy, low-cost production, and ease of use. Nowadays, the most common used methods of AM for medical purposes are Stereolithography (SLA), Selective Laser Sintering (SLS), Fused Deposition Modeling (FDM), 3D-Printing (3DP) or Multi-Jet Modeling (MJM).

Actually, AM technology enables the fabrication of physical parts by using initial data from medical images, such as Digital Imaging and Communications in Medicine (DICOM) images, obtained with the help of Computed Tomography (CT), Magnetic Resonance Imaging (MRI) or Ultrasonography scanning processes. These parts can be used as customized implants, bio-models, or scaffolds for tissue engineering, representing precisely the patient anatomy. Hence, biomedical modelling has the promising potential to create improved prerequisites for preoperative planning, education, and surgical simulation process, leading to various benefits.

According to the results of the majority of the studies, AM technologies, as being utilized in medical and healthcare sector, provide various benefits along-with contemporary and future applications. In reality, biomedical modelling plays a significant role in diagnosis, preplanning, prediction and communication of disease or defect, by reducing at the same time the operation time and the level of patient risk and by improving the surgical outcome. Additionally, the design and development of multiple devices, instrumentation or aid tools used for medical purposes and drug delivery proved beneficial for the medical sector, by facilitating the medical profession.

The process used for the medical model fabrication via AM technologies, is divided into two fundamental stages, the design stage and the manufacture stage. Specifically, the design stage comprises of the acquisition of medical data and image processing via Computer-Aided Design (CAD) systems. Subsequently, the manufacture stage is composed of the required steps for the creation and finally the fabrication of the model via Rapid Prototyping technologies.

After acquiring the required medical data, obtained from CT, MRI, or Ultrasonography scans saved in DICOM file format, a software program can be utilized in order to create a 3D-model representing the anatomy of the patient. The most important step in image processing is the segmentation method, used for the creation of a model corresponding to a specific region of interest. This model can be exported into CAD or STL file format, which is supported mostly by all the AM systems, before proceeding to the manufacture stage.

Subsequently, the model can be exported to CAD programs for further processing and optimization, by using the available editing tools, such as smoothing, merging, rescaling etc. Ultimately, the creation of the RP model according to the created STL file, is used for the 3D-printing process and finally for the fabrication of the customized anatomical model.

Furthermore, it should be taken into consideration that each of these steps can introduce geometric deviations, leading to distortions in the final AM medical model. Though, the largest percentage of these inaccuracies in AM medical models is introduced during the process of medical imaging or during image processing, rather than during the manufacturing stage (e.g. during 3D-printing process), which is considered as more accurate procedure. For this reason, the medical imaging process is considered as the major source of inaccuracies, requiring indisputable investigation.

According to the findings with respect to literature review, there is a great variety of software program solutions, both open-source or commercially available, designed for the creation of 3D-printed models. The most commonly used software tools for the conversion of DICOM files to STL file format are the following: 3DSlicer, ITK-SNAP, Materialize (Mimics), Seg3D & ImageVis3D, and Osirix. Particularly, Materialise is considered as the market standard, providing an extra application tool (i.e. Mimics) for the direct creation of accurate 3D-models, designed for medical applications. Nevertheless, the other solutions are free and open-source applications and consequently can be easily utilized from non-specialized users.

7. Chapter Seven: Conclusions, Recommendations

7.1. Conclusions

The aim of presented study is to acquire a profound understanding of the integration of Additive Manufacturing and Rapid Prototyping technologies in the fabrication of patient customized medical model from scanned anatomical images (i.e. DICOM), obtained with the help of Computed Tomography. In particular, the basic scope of the current study is to demonstrate the process of fabrication for a real case scenario, namely the T4 vertebra of patient's thoracic spine, in a step-by-step approach by illustrating the three fundamental stages: the design, the manufacture, and the evaluation stage.

The first stage, is extended into four fundamental steps required for the acquisition of the desired STL file. These steps involve the acquisition of the DICOM files (for the current project via CT), the conversion of the DICOM files to STL file format, the optimization of the STL file and finally the acquisition of the final STL file.

Initially, for this stage, this study focused on the exposition of the available open-source software programs for the conversion of DICOM files to STL file format, as this step is considered as the most determinant. Particularly, four different open-source software programs (i.e. Seg3D, ImageVis3D, 3DSlicer, and ITK-SNAP) are selected to be presented in a step-by-step approach, in order to evaluate the capabilities and the limitations of each software, and finally select the appropriate software solution for a real case scenario.

Consequently, ITK-SNAP software is selected to be utilized for the conversion of the medical data, mainly due to the satisfactory results regarding the segmentation process. The specific region of interest of the T4 vertebra is isolated from the patient's thoracic spine by using the available segmentation tools for semi-automatic procedure. Additionally, the optimization of the STL file is conducted via Meshmixer software, as being necessary for the correction of the model's imperfections. The model is isolated again, by using the erasing and filling tool, in order to obtain the desired result. Furthermore, smoothing operation is essential for adjusting the surface and guarantee the quality of the model. Finally, the model is saved in STL file format for further processing.

In the second section, the manufacture stage of the final 3D-printed medical model is presented, demonstrating the required steps of the process. Hence, Fused Deposition Modeling (FDM) technology is used, by utilizing the BCN3D Cura 1.0.3. software and the BCN3D Sigma R17 printer, for the creation and the 3D-printing of the medical model, respectively. After completing the 3D-printing procedure, the model required more processing, in order to remove manually the supporting material.

The third section, focuses on the most important stage of the process, specifically the evaluation stage. In this stage, the 3D-printed model is scanned via Next Engine 3D-scanner and processed via ScanStudio HD software, in order to optimize the final result. Seven distinct captures (Captures A-G) are conducted by locating the object vertically and horizontally to the Auto-positioner, by using additionally the provided tools. Other editing tools, (such as trimming, alignment, fusion, and buffing), are necessary for optimizing the captured geometry of the object. Particularly, it is mandatory to remove the noise and the overlapping surfaces from two different captures, in order to align them in a common coordinate system and get the entire geometry of the model. The alignment of the different captures, performed four times, is achieved by specifying some points in the shaded view of the object. Moreover, the fusion process is important for covering the missing geometry and gaps. At last, the refinement of the final model is achieved by using the buffing tool.

Afterwards, the model is saved in STL file format, in order to measure and evaluate the results, regarding the dimensional declinations between the printed and the scanned model. Specifically, the measurements are conducted with the help of the Artec Studio 11 Professional software, by utilizing the created STL files.

Initially, three distinct linear measurements are made both in the printed and scanned model, evaluating the same distance. According to the results, the average distance is estimated to be 33.253mm and 33.573mm, for the printed and the scanned model respectively. The percentage of the deviation between this measurement is estimated to 1.049%. Though, it is worth mentioning that the linear measurements are made manually. Consequently, it is expected that the values of the measurements will vary from each other, raising issues of accuracy and precision.

Secondly, three distinct linear measurements are made both in the printed and scanned model, evaluating the same distance of the hole of the medical model. According to the results, the average distance is estimated to be 9.646mm and 9.646mm, for the printed and the scanned model respectively. The percentage of the deviation between this measurement is estimated to zero. Nevertheless, it is remarkable that the linear measurements are made manually, provoking issues of accuracy and precision, similar to the previous case. For this reason, it is considered that in this case the models do not present dimensional declinations, accounting for the factor of chance.

Hence, the measurement via Surface Distance Maps method is required, considered as more accurate and precise process, in comparison with the linear measurements. For the comparison and the evaluation of dimensional declinations between the printed and the scanned models, six distinct cases are examined by adjusting the *"Error scale"* parameter to the following values: 0.001, 0.045, 0.066, 0.141, 0.209 and 0.470. The results of the calculation of the surface distance maps, regarding the Root Mean Square (RMS), the Mean absolute deviation and the Mean of signed distances, are 0.089480, 0.058955, -0.023571, respectively. Furthermore, it is noteworthy mentioning that the values of these parameters are the same for the six distinct cases.

In total, according to these results, it can be noticed that the printed and the scanned models do present remarkable dimensional deviation, especially when the Error scale is from 0.001-0.066. When the value of Error scale is from 0.141-0.470, the models present slightly dimensional declination. The regions depicted with grey color indicate holes of the printed model that are not fully captured during the scanning process, due to the complexity of the structure. In general, the overall picture revealed by these results is that the models present remarkable dimensional deviation, although the results are satisfactory with reference to the pilot approach of the case study.

7.2. Limitations

Despite the fact that the current study is conducted in accordance with the methods proposed by the related literature, the matter of accuracy should be highlighted. The conversion of DICOM files into the final 3D-model is identified as the major source of inaccuracies, leading to distortions and geometric deviations in the final AM medical model. Though, the largest percentage of these inaccuracies is introduced during the process of medical imaging or during image processing, rather than during the 3D-printing process. The semi-automatic segmentation, provided by ITK-SNAP software application, provides satisfactory results, although the improvement of process parameters need to be further investigated before medical models are used in a real surgery or in the clinical practise.

Furthermore, the process involved a significant number of software programs for conducting distinct steps. Nevertheless, the majority of these programs are open-source and not require specialized manipulation knowledge. Especially as regards the medical imaging processing, the ascertainment by a professional medical opinion is crucial for the more adequate and precise outcome.

In addition, this study is conducted in the framework of a pilot demonstration of the fabrication of patient specific 3D-printed medical models, utilizing Fused Deposition Modeling method. Though, other Rapid Prototyping techniques can be utilized for the manufacture process. Similarly, there is a great variety of 3D-scanning methods that present more accurate results. Nevertheless, the overall picture revealed by the obtained results is quite satisfactory and adequate.

7.3. Recommendations & Further investigation

The current study is an interpretative research, mainly focused on the direction of profound understanding, regarding the integration of Additive Manufacturing and Rapid Prototyping technologies in medical sector. The obtained results indicated the capabilities of the AM application in terms of fabrication of customized medical models.

In the current years, despite the fact that AM technologies offer a great potential regarding the field of medical applications, although they have not been adopted yet in a large extent, mainly due to the high cost and fabrication time involved. Nevertheless, it is a common fact that AM technologies are more flexible, efficient and less-time consuming in comparison with conventional manufacturing methods for designing and manufacturing customized anatomical models. In future, AM technologies can persist to improve if the medical implant technology will be offered in a reasonable cost.

Additionally, one of the most important limitations of AM technologies in medical applications is the excessive use of classical materials, in relation to biomaterials. Future research studies should investigate and expand the knowledge in this field, by incorporating new biocompatible materials in the fabrication of medical models via Rapid Prototyping technologies.

Furthermore, suggested future research should include the investigation of materials for customized medical models that are not only biocompatible, but also materials that fulfil all the appropriate requirements and specifications, as regards the mechanical properties, such as stiffness, tensile strength and certainly the proper geometrical accuracy.

According to literature review, there is a great plethora of software packages utilized for the conversion of DICOM files to CAD or STL file formats. The majority of them provide a variety of distinct CT image segmentation methods, for the creation of a 3D-model, representing the anatomy of a patient. Though, the accuracy of the final model depends on the user's familiarization with the software or on the profound medical knowledge. Automatic image segmentation methods do not present highly accurate results, while manual image segmentation techniques demand excessive manual post-processing, effort and time in order to isolate the region of interest and obtain a satisfactory result. In fact, this factor limits the growth of AM technologies. For this reason, it is highly recommended for future research to broaden and examine the development of fully automatic and adaptive image segmentation software programs that improve not only the quality, but also the overall accuracy of the result.

Moreover, the process of creating 3D-models for medical purposes is a collaborative issue that integrates the expertise from various scientific fields. Consequently, the investigation of a possible collaboration of AM researchers with medical professions (e.g. doctors, radiologists etc.) is indisputably required, in order to enhance the capabilities of AM technologies in medical purposes. Actually, the verification by a professional medical opinion is crucial during the image acquisition and image processing phase, for the determination of the optimal parameters that best delineate the region of interest and provide adequate resolution and accuracy.

List of References

Articles & Papers

Ahn J., Shnorhavorian M., Amies Oelschlager A.M. E., Ripley B., Shivaram G. M., Avansino J. R., Merguerian P. A. (2017) Use of 3D reconstruction cloacagrams and 3D printing in cloacal malformations, *Journal of Pediatric Urology, Vol. 13, Issue: 395, pp. 1-6.*

Bibb R., Thompson D., Winder J. (2011) Computed tomography characterization of additive manufacturing materials, *Medical Engineering & Physics, Vol. 33, pp. 590-596.*

Cai T., Rybicki F. J., Giannopoulos A. A., Schultz K., Kumamaru K. K., Liacouras P., Demehri S., Shu Small K. M., Mitsouras D. (2015) The residual STL volume as a metric to evaluate accuracy and reproducibility of anatomic models for 3D printing: application in the validation of 3D-printintable models of maxillofacial bone from reduced radiation dose CT images, *3D Printing in Medicine, Vol. 1, pp. 1-9.*

Chen X., Possel J. K., Wacongne C., van Ham A. F., Klink P. C., Roelfsema P. R. (2017) 3D printing and modelling of customized implants and surgical guides for non-human primates, *Journal of Neuroscience Methods, Vol. 286, pp. 38-55.*

Cheung L.K., Wong M.C.M., Wong L.L.S. (2002) Refinement of facial reconstructive surgery by stereomodel planning, *Annals of the Royal Australian College of Dental Surgeons, pp. 129-132.*

Chougule V. N., Mulay A.V., Ahuja B. B. (2014) Development of patient specific implants for Minimum Invasive Spine Surgeries (MISS) from non-invasive imaging techniques by reverse engineering and additive manufacturing techniques, *Procedia Engineering, Vol. 97, pp. 212-219.*

Choy W. J., Mobbs R. J., Wilcox B., Phan S., Phan K., Sutterlin C. E. (2017) Reconstruction of thoracic spine using a personalized 3D-printed vertebral body in adolescent with T9 primary bone tumor, *World Neurosurgery, Vol. 105, pp. 1032.e13-1032.e17*.

Ciocca L., De Crescenzio F., Fantini M., Scotti R. (2009) CAD/CAM and rapid prototyped scaffold construction for bone regenerative medicine and surgical transfer of virtual planning: A pilot study, *Computerized Medical Imaging and Graphics, Vol. 33, pp. 58-62.*

Cromeens B. P., Ray W. C., Hoehne B., Abayneh F., Adler B., Besner G. (2017) Facilitating surgeon understanding of complex anatomy using a three-dimensional printed model, *Journal of Surgical Research, Vol. 216, pp. 18-25.*

Dupret-Bories A., Vergez S., Meresse T., Brouillet F., Bertrand G. (2017) Contribution of 3D printing to mandibular reconstruction after cancer, *European Annals of Otorhinolaryngology, Head and Neck diseases, Vol. xxx, pp. xxx-xxx.*

D'Urso P.S., Barker T.M., Earwaker W.J., Bruce L.J., Atkinson R.L., Langian M.W., Arvier J.F., Effeney D.J. (1999) Stereolithographic biomodelling in craniomaxillofacial surgery: a prospective trial, *Journal of Cranio-Maxillo-Facial Surgery: Official Publication of the European Association for Cranio-Maxillo-Facial Surgery, Vol. 27, No. 1, pp. 30-37.*

Eijnatten M., Dijk R., Dobbe J., Streekstra G., Koivisto J., Wolff J. (2018) CT image segmentation methods for bone used in medical additive manufacturing, *Medical Engineering and Physics, Vol. 51, pp. 6-16.*

Farooqi K. M., Mahmood F. (2017) Review Article – Innovations in preoperative planning: Insights into another dimension using 3D printing for cardiac disease, *Journal of Cardiothoracic and Vascular Anesthesia, pp. 1-9.*

Farré-Guasch E., Wolff J., Dent M., Helder M. N., Schulten E. A. J. M., Forouzanfar T., Klein-Nulend J. (2015) Application of Additive Manufacturing in Oral and Maxillofacial Surgery*, Journal of Oral and Maxillofacial Surgery, Vol. 73, pp. 2408-2418.*

Fedorov A., Beichel R., Kalpathy-Cramer J., Finet J., Fillion-Robin J.-C., Pujol S., Bauer C., Jennings D., Fennessy F., Sonka M., Buatti J., Aylward S., Miller J.V., Pieper S., Kikinis R. (2012) 3D Slicer as an image computing platform for the Quantitative Imaging Network, *Magnetic Resonance Imaging, Vol. 30, pp. 1323-1341.*

Giannatsis J., Dedoussis V. (2009) Additive fabrication technologies applied to medicine and health care: a review, *International Journal of Advanced Manufacturing Technology, Vol. 40, pp. 116-127.*

Gibson I., Cheung L. K., Chow S. P., Cheung W. L., Beh S. L., Savalani M., Lee S. H. (2006) The use of rapid prototyping to assist medical applications, *Rapid Prototyping Journal, Vol. 12, Issue: 1, pp. 53-58.*

Jardini A. L., Larosa M. A. Filho R. M., Carvalho Zavaglia C. A., Bernardes L. F., Lambert C. S., Calderoni D. R., Kharmandayan P. (2014) Cranial reconstruction: 3D biomodel and custom-built implant created using additive manufacturing, *Journal of Cranio-Maxillo-Facial Surgery, Vol. 42, pp. 1877-1884.*

Javaid M., Haleem A. (2017) Additive manufacturing applications in medical cases: A literature-based review, *Alexandria Journal of Medicine, Vol. xxx, pp. xxx-xxx.*

Hnatkova E., Kratky P. and Dvorak Z. (2014) Production of Anatomical Models via Rapid Prototyping, *International Journal of Circuits, Systems and Signal Processing, Vol. 8, pp. 479-486.*

Hodgdon T., Danrad R., Patel M. J., Smith S. E., Richardson M. L., Ballard D. H., Ali S., Trace A. P., DeBenedectis C. M., Zygmont M. E., Lenchik L., Decker S. J. (2018) Logistics of three-dimensional printing: Primer for Radiologists, *Academic Radiology, Vol. 25, No. 1, pp. 40-51*

Huotilainen E., Jaanimets R., Valásek J., Marcián P., Salmi M., Tuomi J., Mäkitie A., Wolff J. (2014) Inaccuracies in additive manufactured medical skull models caused by the DICOM to STL conversion process, *Journal of Cranio-Maxillo-Facial Surgery, Vol. 42, pp. 259-265.*

Ibáñez L., Schroeder W., Ng. L., Cates J. (2003) The ITK Software Guide, *Insight Software Consortium (ISC), Insight Toolkit Publications, Kitware, Inc.*

Kim M. P., Anderson H. T., Warrenn A., Ellsworth IV, Rex A. M., Puja G., Jordan S. M. (2015) Three-dimensional model for surgical planning in resection of thoracic tumors, *International Journal of Surgery Case Reports, Vol. 16, pp. 127-129.*

Kumar S. M., Manmadhachary A., Kumar. R. Y., Alwala A. (2017) Manufacturing of Patient specific AM medical models for Complex Surgeries, *Journal of Materials Today: Proceedings, Vol. 4, pp. 1134-1139.*

Kurenov S. N., Ionita C., Sammons D., Demmy T. L. (2015) Three-dimensional printing to facilitate anatomic study, device development, simulation, and planning in thoracic surgery, *The Journal of Thoracic and Cardiovascular Surgery, Vol. 49, No. 4, pp. 973-979.*

Laycock S. D., Hulse M., Scrase C. D. (2015) Towards the production of radiotherapy treatment shells on 3D printers using data derived from DICOM CT and MRI: preclinical feasibility studies, *Journal of Radiotherapy in Practice, Vol. 14, pp. 92-98.*

Lethaus B., Poort L., Böckmann R., Smeets R., Tolba R., Kessler P. (2012) Additive manufacturing for microvascular reconstruction of the mandible in 20 patients, *Journal of Cranio-Maxillo-Facial Surgery, Vol. 40, pp. 43-46.*

Liacouras P., Garnes J., Roman N., Petrich A., Grant G. T. (2011) Designing and manufacturing an auricular prosthesis using computed tomography, 3-dimensional photographic imaging and additive manufacturing: A clinical report, *The Journal of Prosthetic Dentistry, Vol. 105, Issue: 2, pp. 78-82.*

Lin H.-H., Lonic D., Lo L.-J. (2018) 3D printing in orthognathic surgery – A literature review, *Journal of the Formosan Medical Association, Vol. xx, pp. 1-12.*

Li J., Lin J., Xu J., Meng H., Su N., Fan Z., Li J., Yang Y., Li D., Wang B., Fei Q. (2017) A novel approach for percutaneous vertebroplasty based on preoperative computed tomography – based three-dimensional model design, *World Neurosurgery, Vol. 105, pp.20-26.*

Marro A., Bandukwala T., Mak W. (2016) Three-Dimensional Printing and Medical Imaging: A Review of the Methods and Applications, *Current Problems in Diagnostic Radiology, Vol. 45, pp. 2-9.*

Milovanović J., Trajanović M. (2007) Medical applications of Rapid Prototyping, *Mechanical Engineering Vol. 5, No. 1, pp. 79 - 85*

Moiduddin K., Al-Ahmari A., Al Kindi M., Abouel Nasr E. S., Mohammad A., Ramalingam S. (2016) Customized porous implants by additive manufacturing for zygomatic reconstruction, *Biocybernetic and Biomedical Engineering, Vol. 36, pp. 719-730.*

Moiduddin K., Darwish S., Al-Ahmari A., ElWatidy S., Mohammad A., Ameen W. (2017) Structural and mechanical characterization of custom design cranial implant created using additive manufacturing, *Electronic Journal of Biotechnology, Vol. 29, pp. 22-31.*

Otero J.J. Vijverman A., Mommaerts MY (2017) Use of fused deposition modeling for additive manufacturing in hospital facilities: European certification directives, *Journal of Cranio-Maxillofacial Surgery*, doi: 10.1016/j.jcms.2017.06.018.

Petzold R., Zeilhofer H. F., Kalender W. A. (1999) Rapid Prototyping technology in medicine – basics and applications*, Computerized Medical Imaging and Graphics, Vol. 23, pp. 277-284.*

Pucci J. U., Christophe B. R., Sisti J. A., Connolly E. S. Jr. (2017) Three-dimensional printing: technologies, applications, and limitations in Neurosurgery, *Biotechnology Advances, Vol. 35, pp. 521- 529.*

Salmi M., Paloheimo K.-S., Tuomi J., Wolff J., Mäkitie A. (2013) Accuracy of medical models made by additive manufacturing (rapid manufacturing), *Journal of Cranio-Maxillo-Facial Surgery, Vol. 41, pp. 603- 609*.

Santos E.C., Shiomi M., K. Osakada, Laoui T. (2006) Rapid manufacturing of metal components by laser forming, *International Journal of Machine Tools and Manufacture, Vol. 46, No. 12-13, pp. 1459-1468.*

Singh S., Ramakrishna S. (2017) Biomedical applications of additive manufacturing: present and future, *Current Opinion in Biomedical Engineering*, doi: 10.1016/ j.cobme.2017.05.006.

Su X.-b., Yang Y.-q., Yu P., Sun J.-f. (2012) Development of porous medical implant scaffolds via laser additive manufacturing, *Transactions of Nonferrous Metals Society of China, Vol. 22, pp. 181-187.*

Wang K., Ho C.-C., Zhang C., Wang B. (2017) A review on the 3D printing of functional structures for medical phantoms and regenerated tissue and organ applications, *Engineering, Vol. 3, pp. 653-662*.

Weller C., Kleer R., Piller F. T. (2015) Economic implications of 3D printing: Market structure models in light of additive manufacturing revisisted, *International Journal of Production Economics, Vol. 164, pp. 43-56.*

Yushkevich P. A., Piven J., Hazlett H. C., Smith R. G., Ho S., Gee J. C., Gerig G. (2006) User-guided 3D active contour segmentation of anatomical structures: Significantly improved efficiency and reliability, *NeuroImage, Vol. 31, pp. 1116-1128.*

Dissertations

Brennan J. (2010) Production of Anatomical Models from CT scan Data, *Master Dissertation, Dublin Institute of Technology, School of Manufacturing and Design Engineering, De Montfort University, Leicester, United Kingdom.*

Owusu-Dompreh F. (2013) Application of Rapid Manufacturing Technologies to Integrated Product Development in Clinics and Medical Manufacturing Industries, *Master Dissertation, Youngstown State University, School of Industrial and Systems Engineering.*

Books

Chua C. K., Leong K. F. (2017) *3D Printing and Additive Manufacturing: Principles and Applications*, 5th edition, Singapore: World Scientific.

Available: http://www.worldscientific.com/doi/abs/10.1142/9789813149274_fmatter

Date of Access: [28 December 2017]

Gibsion I., Rosen D.W., Stucker B. (2010) *Additive Manufacturing Technologies: Rapid Prototyping to Direct Digital Manufacturing*, New York, London: Springer.

Available: https://link.springer.com/book/10.1007/978-1-4419-1120-9

Date of Access: [28 December 2017]

Lim J., Zein R. (2006) *The Digital Imaging and Communications in Medicine (DICOM): Description, Structure and Applications*, In: *Rapid Prototyping: Theory and practice*, New York, USA: Springer, pp. 63-86.

Whitby J. (2007) *White Paper: The DICOM standard, Kortrijk, Belgium: BARCO*.

Available:https://mafiadoc.com/queue/white-paper-the-dicom-stand-ard_598d16821723ddcb690d84a6.html

Date of Access: [20 February 2018]

Websites

[1] https://computertomography.weebly.com/ct-scan-diagram.html

Date of Access: [20 October 2017]

[2] https://www.orthopaedics.com.sg/treatments/other-services/magnetic-resonance-imaging-mri/

Date of Access: [20 October 2017]

[3] http://www.sunshinehospital.in/diagnostics.html

Date of Access: [20 October 2017]

[4] http://letseatradiology.blogspot.gr/2014/01/pengenalan-usg.html

Date of Access: [20 October 2017]

[5] https://en.wikipedia.org/wiki/DICOM

Date of Access: [20 October 2017]

[6] http://www.itksnap.org/pmwiki/pmwiki.php?n=Train.RSNA2016

Date of Access: [10 November 2017]

[7] http://www.sci.utah.edu/cibc-software/seg3d.html

Date of Access: [10 November 2017]

[8] https://www.sci.utah.edu/devbuilds/seg3d_docs/Seg3DBasicFunctionality.pdf

Date of Access: [10 November 2017]

[9]https://www.sci.utah.edu/images/CIBC/Workshops/cibcwksp2009/seg3dtuto-rial.pdf

Date of Access: [10 November 2017]

[10] http://www.sci.utah.edu/cibc-software/imagevis3d.html

Date of Access: [12 November 2017]

[11] http://www.sci.utah.edu/releases/imagevis3d_v1.3/ImageVis3D-1.3_docs.pdf

Date of Access: [12 November 2017]

[12] https://www.slicer.org/

Date of Access: [15 November 2017]

[13] https://www.slicer.org/wiki/Documentation/4.x/Acknowledgments

Date of Access: [15 November 2017]

[14] https://www.slicer.org/wiki/Documentation/4.8/Announcements

Date of Access: [15 November 2017]

[15] https://www.slicer.org/wiki/Documentation/Nightly/Modules/Welcome

Date of Access: [15 November 2017]

[16] https://www.slicer.org/wiki/Documentation/4.8/Modules/DICOM

Date of Access: [16 November 2017]

[17] https://www.slicer.org/wiki/Documentation/4.8/Modules/Data

Date of Access: [16 November 2017]

[18] https://www.slicer.org/wiki/Documentation/4.8/Modules/VolumeRendering

Date of Access: [16 November 2017]

[19] https://www.slicer.org/wiki/Documentation/4.8/Modules/Editor

Date of Access: [17 November 2017]

[20] http://www.itksnap.org/pmwiki/pmwiki.php?n=Main.HomePage

Date of Access: [10 November 2017]

[21] http://www.itksnap.org/pmwiki/pmwiki.php?n=Videos.SNAP3

Date of Access: [20 November 2017]

[22] http://www.itksnap.org/pmwiki/pmwiki.php?n=Train.RSNA2016

Date of Access: [20 November 2017]

[23]http://www.itksnap.org/pmwiki/pmwiki.php?n=Documentation.TutorialSection-ManualSegmentation?n=Documentation.TutorialSectionIntroduction

Date of Access: [30 November 2017]

[24]http://www.itksnap.org/pmwiki/pmwiki.php?n=Documentation.TutorialSection-IntroductionToAutomatic

Date of Access: [30 November 2017]

[25]http://www.itksnap.org/pmwiki/pmwiki.php?n=Documentation.TutorialSectionRe-gionSegmentation

Date of Access: [30 November 2017]

[26]http://www.itksnap.org/pmwiki/pmwiki.php%3Fn%3DDocumentation.TutorialSec-tionManualSegmentation

Date of Access: [5 December 2017]

[27] https://www.bcn3dtechnologies.com/en/3d-printer

Date of Access: [15 February 2017]

[28] http://www.nextengine.com

Date of Access: [15 February 2017]

[29] https://www.artec3d.com/files/pdf/artec_studio_userguide_en.pdf

Date of Access: [16 February 2017]

Appendix

List of terms

i. Acrylonitrile Butadiene Styrene: (ABS)
ii. Additive Manufacturing: (AM)
iii. Center for Integrative Biomedical Computing: (CIBC)
iv. Computed Axial Tomography: (CAT)
v. Computed Tomography: (CT)
vi. Computer-Aided Design: (CAD)
vii. Digital Imaging Communications in Medicine: (DICOM)
viii. Direct Metal Laser Sintering: (DMLS)
ix. Electron Beam Melting: (EBM)
x. Fused Deposition Modeling: (FDM)
xi. Insight Toolkit: (ITK)
xii. Magnetic Resonance Imaging: (MRI)
xiii. Multi-Jet Modelling: (MJM)
xiv. National Electrical Manufacturers Association (NEMA)
xv. National Institutes of Health: (NIH)
xvi. Neuroimaging Informatics Technology Initiative: (NIfTI)
xvii. Scientific Computing and Imaging Institute: (SCI)
xviii. Selective Laser Melting: (SLM)
xix. Selective Laser Sintering: (SLS)
xx. Standard Triangle Language: (STL)
xxi. Stereolithography: (SLA)
xxii. Three-Dimensional: (3D)
xxiii. Three-Dimensional-Printing: (3DP)
xxiv. Two-Dimensional: (2D)
xxv. Rapid Manufacturing: (RM)
xxvi. Rapid Prototyping: (RP)
xxvii. Region of Interest: (ROI)
xxviii. Penn Image Computing and Science Laboratory: (PICSL)
xxix. Universal Volume Format: (UVF)
xxx. Ultraviolet Laser: (UV)